LADUNGSTRÄGERTRENNUNG IN ORGANISCHEN DONOR-AKZEPTOR SOLARZELLEN

DISSERTATION

zur Erlangung des akademischen Grades
eines Doktors der Naturwissenschaften (Dr. rer. nat.)
im Fach Physik der Fakultät für
Mathematik, Physik und Informatik der Universität Bayreuth

vorgelegt von

Christian Schwarz

geboren in Kulmbach / Deutschland

Bayreuth, 2014

Die vorliegende Arbeit wurde in der Zeit von Februar 2011 bis Januar 2014 am Lehrstuhl für Experimentalphysik II der Universität Bayreuth unter der Betreuung von Prof. Dr. Anna Köhler angefertigt.

Dissertation eingereicht am:

Prüfungsausschuss:

Prof. Dr. Anna Köhler (Erstgutachter)

Amtierender Dekan: Prof. Dr. Walter Zimmermann

„Wirkliches Neuland in einer Wissenschaft kann wohl nur gewonnen werden, wenn man an einer entscheidenden Stelle bereit ist, den Grund zu verlassen, auf dem die bisherige Wissenschaft ruht, und gewissermaßen ins Leere zu springen.“

Werner Heisenberg 1902-1976

Inhaltsverzeichnis

1. Zusammenfassung

Organische Solarzellen haben jüngst Wirkungsgrade von 12 % unter Laborbedingungen erreicht und sind damit für die industrielle Fertigung geeignet. Im Vergleich zu den weit verbreiteten Silizium-Solarzellen zeichnen sich organische Solarzellen durch große Extinktionskoeffizienten aus, wodurch das einfallende Sonnenlicht innerhalb weniger hundert Nanometer vollständig absorbiert werden kann. Dies ermöglicht die Herstellung dünner, flexibler, leichter und kostengünstiger Solarfolien durch Druck- oder Verdampfungstechnik.

Die jüngsten Effizienzsteigerungen organischer Solarzellen beruhen jedoch mehr auf Verbesserungen der Solarzellenmorphologie und der Solarzellenarchitektur, als auf einem vollständigen Verständnis der in einer Solarzelle ablaufenden Prozesse. Auf dem Weg zu leistungsstärkeren Solarzellen ist es jedoch unerlässlich, den komplexen, aber für den Erfolg entscheidenden Prozess der Ladungsträgertrennung vollständig zu verstehen. Die vorliegende Arbeit untersucht deshalb die Ladungsträgertrennung in Donor-Akzeptor-(D-A)-Solarzellen aus verschiedenen Blickwinkeln, um mit den gewonnenen Erkenntnissen die gezielte Entwicklung neuer, leistungsstärkerer Solarzellenmaterialien und Solarzellenarchitekturen zu ermöglichen.

In der vorliegenden Arbeit wird erstmalig an drei Poly(*p*-phenylen)-basierten Polymeren in Kombination mit jeweils zwei Akzeptoren die feldabhängige Quantenausbeute in einer Zweischichtsolarzelle bis zur Sättigung des Fotostroms bei hohen Feldstärken gemessen. Die Ergebnisse zeigen, dass eine große Konjugationslänge bei Polymeren mit einem gleichzeitig hohen Grad an energetischer Ordnung die Ladungsträgertrennung entscheidend unterstützt. Dieses Ergebnis ist unabhängig davon, ob ausschließlich der jeweilige Donor oder der jeweilige Akzeptor angeregt werden. Jedoch werden geringere Sättigungsfeldstärken beobachtet, wenn die Donormaterialien angeregt werden. Da die Energiedifferenz zwischen LUMO-Donor und LUMO-Akzeptor konsequent größer ist als die Energiedifferenz zwischen HOMO-Akzeptor und HOMO-Donor bei der Anregung des Akzeptors, könnte dies darauf hinweisen, dass ein größerer Energieunterschied die Ladungsträgertrennung unterstützt.

Fortführende Untersuchungen an einem erweiterten System von Donormaterialien in Zweischichtsolarzellen mit C_{60} ermöglichen dann eine Unterscheidung zwischen Auswirkungen auf die Ladungsträgertrennung, die durch Konjugation oder durch energetische Ordnung verursacht werden. Es wird deutlich, dass besonders eine ausgedehnte Konjugation des Polymers und eine damit verbundene Delokalisation des Coulomb-gebundenen Lochs entlang der Polymerkette die Ladungsträgertrennung maßgeblich begünstigt und über Effekte der energetischen Unordnung dominiert. Die experimentell gemessenen feldabhängigen Quantenausbeuten werden mit bestehenden theoretischen Modellen simuliert und verglichen, wobei Ultraviolett-Photoelektronen-Spektroskopie-

(UPS)-Messungen von Grenzflächendipolen mit berücksichtigt werden. Es zeigt sich, dass eine Kombination zweier Modelle die Messungen am besten beschreibt. Beide Modelle basieren in der Grundidee auf der Delokalisation des gebundenen Lochs, das quantenmechanische Nullpunktschwingungen auf der Polymerkette im Coulombpotential seines zugehörigen Elektrons ausführt. Die Nullpunktschwingungen sind durch eine effektive Masse charakterisiert und stellen dem dissoziierenden Loch zusätzliche kinetische Energie zur Überwindung der Coulombbarriere zur Verfügung. Daher werden diese Modelle auch als „effektive-Masse-Modelle“ bezeichnet. Bei dem einen Modell, im Folgenden als „Dipolmodell“ spezifiziert, wird der Einfluss des elektrostatischen Potentials an der D-A-Grenzfläche berücksichtigt. Bei dem anderen Modell, dem „Fehlstellenmodell“, wird eine Dissoziation an vereinzelten Defekten mit berücksichtigt. Die Kombination der beiden effektive-Masse-Modelle ermöglicht schließlich eine geschlossene und stimmige Beschreibung der Ladungsträgertrennung in D-A-Solarzellen.

Um ein breiteres Verständnis der Ladungsträgertrennung in organischen Solarzellen zu bekommen wird an einem auf Triphenylamin-basierenden D-A-Copolymer Materialsystem der Einfluss der Akzeptorstärke und –position auf die Ladungsträgertrennung anhand optischer und elektrischer Messungen untersucht. Die experimentell gemessenen feldabhängigen Quantenausbeuten der D-A-Copolymere in Zweischichtsolarzellen mit C_{60} werden mit dem Dipolmodell analysiert. Die Ergebnisse zeigen, dass ein schwächerer, innerhalb des Copolymers gut mit dem Donor auf dem Polymerrückgrad konjugierter Akzeptor die Ladungsträgertrennung mehr erleichtert, als ein stärkerer Akzeptor, der seitlich zum Polymerrückgrad lokalisiert ist. Dies wird durch ein kleineres Dipolmoment an der Copolymer-C_{60}-Grenzfläche und durch eine kleinere effektive Masse in den Fitparametern für den im Polymerrückgrad eingebundenen Akzeptor belegt.

Weitere Einblicke in die Ladungsträgertrennung liefern systematische Absorptionsmessungen an D-A-Grenzflächen. Es zeigt sich, dass die optische Dichte eines elektrisch halbleitenden Donors und eines Akzeptors bei direktem Kontakt an einer gemeinsamen Grenzfläche nicht additiv ist, sondern dass ein signifikanter Anteil der Extinktion des Donors und des Akzeptors im sichtbaren Wellenlängenbereich fehlt. Dieses Phänomen wird sowohl experimentell an mehreren D-A-Kombinationen, als auch bei theoretischen Simulationen eines übereinander liegenden Donors und Akzeptors mittels zeitabhängiger Dichtefunktionaltheorie festgestellt. Die „fehlende“ Absorption wird auf die Bildung eines Grundzustandskomplexes an der D-A-Grenzfläche zurückgeführt. Weiter beobachtet man, dass ein großer Anteil an fehlender Extinktion in den Experimenten direkt mit niedrigen Sättigungsfeldstärken der feldabhängigen Quantenausbeute zugehöriger D-A-Zweischichtsolarzellen korreliert, was im Umkehrschluss eine erleichterte Ladungsträgertrennung bescheinigt. Dadurch lässt sich auf eine aktive Beteiligung des Grundzustandskomplexes bei der Ladungstrennung schließen. Die Lichtabsorption direkt an der D-A-Grenzfläche ist stark reduziert und die D-A-Wechselwirkung führt nach Dichtefunktionaltheorie-Rechnungen zur Ausbildung eines treppenförmigen Energieniveausystems.

Bei diesem wird beim Ladungstransfer eines angeregten Donors (Akzeptors) das Elektron (Loch) über den Grundzustandskomplex auf den Akzeptor (Donor) übertragen, wodurch ein gebundenes Elektron-Loch-Paar gebildet wird. Der Grundzustandskomplex wirkt bei der Bildung des gebundenen Elektron-Loch-Paares als räumlicher Distanzhalter, der den anfänglichen Elektron-Loch-Abstand vergrößert und damit die Rekombination unterdrückt.

Summary

Organic solar cells have recently reached power conversion efficiencies of 12% and are thus ready for industrial mass production. In contrast to the widely used silicon solar cells, organic solar cells are characterized by large extinction coefficient, so that the incident sunlight can be absorbed completely within a film thickness of a few hundred nanometers. This allows for the fabrication of flexible, light weight and cheap solar foils in a printing or evaporation technique.

The recent rise of the organic solar cells efficiencies is related more to improvements of the solar cell morphologies and device architectures than to a full understanding of the processes that take place in an organic solar cell. When aiming for efficient solar cells, however, it is essential to completely understand the complex, yet crucial step of charge separation. Therefore, the work presented in this thesis is concerned with investigations in the process of charge separation in donor-acceptor-(D-A)-solar cells. This issue is addressed from several angles with the aim that the insights gained may enable the systematic development of new and more powerful solar cell materials and solar cell architectures.

In this work, the field-depended quantum efficiency of bilayer solar cells is measured as a function of the electric field strength, for the first time until the photo-current saturates at high field strengths for a wide range of materials. The material set used here comprises three poly(*p*-phenylene) based polymers, each combined with two different acceptors. The results show that a large conjugation length in the polymers, with a concomitant high degree of energetic order, facilitates charge separation. This result is independent on whether only the donor or only the acceptor is excited. Overall smaller saturation field strengths are observed when the donor material is excited. Since the energy difference between the donor's LUMO and acceptor's LUMO is consistently larger than the energy difference between the acceptor's HOMO and donor's HOMO upon exciting the acceptor, this might indicate that a larger energy difference assists charge separation.

Further studies on an extended system of donor materials in bilayer solar cells with C_{60} enable us to distinguish between effects on charge separation caused by conjugation from those caused by energetic order. It emerges that in particular an increased conjugation of the polymer and the associated delocalization of a Coulomb-bound hole along the polymer backbone facilitates charge separation significantly and that this dominates over effects caused by energetic disorder. The experimentally measured field-dependent quantum yields are simulated numerically on the basis of published theoretical models and the experimental data are compared against the published models. In this approach, possibly existing surface dipoles as measured by ultraviolet-photoelectron-spectroscopy (UPS) are taken into account. The results show that a combination of two models fits the

measurements best. Both models are based on the idea of delocalization of a bound hole that performs quantum mechanical zero point oscillations in the Coulomb potential of its sibling electron. The zero point oscillations are characterized by an effective mass that provides the dissociating hole with an additional amount of kinetic energy to overcome the Coulomb barrier. For this reason, they are also referred to as “effective mass models”. One model, in the following termed as “dipole model” accounts for the effect of the electrostatic potential at the D-A-interface. The other model, the so-called “trap-induced dissociation model” considers the dissociation on localized defects. The combination of these two effective-mass-models finally offers a complete and consistent description of the process of charge separation in D-A-solar cells.

In order to gain a deeper understanding of the charge separation in organic solar cells the influence of the strength and position of the acceptor on the charge separation is investigated in a triphenylamine based material system of D-A-copolymers using optical and electrical measurements. The experimentally measured field-dependent quantum yields of the D-A-copolymers in bilayer solar cells with C_{60} are analyzed in the framework of the dipole model. The results show that a weaker acceptor that is well conjugated within the polymer backbone facilitates charge separation more than a stronger acceptor that is localized on the side of the polymer backbone. This result is expressed in the parameterization of the simulation by a smaller dipole moment at the copolymer-C_{60}-interface and by a smaller effective mass for the acceptor that is conjugated with the polymer backbone.

Systematic absorption measurements at D-A-interfaces give further insights into charge separation. It is shown that the optical density of a semiconducting donor and an acceptor that are in direct contact at their interface is not equal to a superposition of the individual contributions. Rather, there is a significant amount of extinction missing in the visible wavelength regime when donor and acceptor are in contact. This phenomenon is observed experimentally for several combinations of donors and acceptors and also in theoretical time dependent density functional theory simulations of an acceptor lying on top of a donor. The “missing” absorption is attributed to the formation of a ground state complex at the D-A-interface. Furthermore, it is observed that a large amount of missing extinction in the experiments directly correlates with low saturation field strengths of the corresponding D-A-bilayer solar cell which implies an easier charge separation. Thus, there is evidence for an active participation of the ground state complex at the charge separation process. The absorption of light directly at the D-A-interface is strongly decreased and the D-A-interaction leads to the formation of a cascading energy level system in density functional theory calculations. In this system the electron (hole) of an excited donor (acceptor) is transferred via the ground state complex onto the acceptor (donor), thus forming a bound electron-hole-pair. Upon the formation of the electron-hole-pair the ground state complex acts like a local spacer increasing the initial electron hole distance und thus suppressing the recombination.

2. Einleitung

2.1 Motivation

Innerhalb einer Stunde strahlt die Sonne den von der gesamten Weltbevölkerung in einem Jahr benötigten Energiebedarf auf die Erde ein.[1-2] Die Umwandlung von Strahlungsenergie der Sonne in elektrisch nutzbare Energie mittels Solarzellen hat damit in der Zukunft endlicher fossiler Brennstoffe großes Potential in einer Kombination erneuerbarer Energien im Rahmen der Energiewende. Die Erforschung organischer Solarzellen als ernstzunehmende Alternative zu den etablierten Silizium-Solarzellen wurde dabei in den letzten Jahren besonders gefördert und die wirtschaftliche Massenproduktion ist mittlerweile in greifbare Nähe gerückt. So hat Heliatek im Jahr 2013 einen labortechnischen Wirkungsgrad von 12 % erreicht und damit die geforderte untere wirtschaftliche Rentabilitätsgrenze organischer Solarzellen von 10 % deutlich übertroffen.[3]

Organische Solarzellen bestehen aus wenigen hundert Nanometer dicken kohlenstoffbasierten Polymer- oder Molekülfilmen und können in großtechnischer Herstellung kostengünstig auf flexible, leichte Kunststofffolien aufgedruckt oder aufgedampft werden.[1, 4-6] Diese Eigenschaften ermöglichen aktuell bereits einen universellen Einsatz der Solarfolien als kleines „Reservekraftwerk“ in der Freizeit, etwa für die Aufladung eines Handys oder zum Betrieb kleinerer elektronischer Geräte im Freien fernab der Stromversorgung. Großflächig können bunte Solarfolien als Gestaltungselemente an Häuserfassaden mit der gleichzeitigen Nutzung als Stromlieferanten eingesetzt werden.

Leider besitzen organische Solarzellen im Vergleich zu anorganischen Solarzellen den Nachteil, dass durch die Absorption von Sonnenlicht nicht sofort aufgespaltene Ladungsträger entstehen.[7-8] Vielmehr generiert die Absorption eines Photons ein stark Coulomb-gebundenes Elektron-Loch-Paar, das über mehrere Zwischenschritte aufgespalten und aus der Solarzelle extrahiert werden muss, ohne ungenutzt zu rekombinieren.[9-12]

Die Steigerung des Wirkungsgrades wurde in den letzten Jahren besonders durch Bauteil-technische Verbesserungen erhöht.[13-15] Hierbei liegt der Fokus zum einen auf der Erhöhung der Anzahl der absorbierten Photonen und zum anderen in der Unterdrückung der Rekombination bereits gebildeter freier Ladungsträger in der Solarzelle. Ersteres wird durch die Synthese neuer Materialien[16-18] mit einem dem Sonnenlicht möglichst angepasstem Absorptionsspektrum, und dem Einsatz von Tandemsolarzellen erreicht, bei denen zwei Solarzellen mit verschiedenen Absorptionsbereichen hintereinander gebaut sind.[19-20] Die Unterdrückung der Rekombination wurde besonders durch eine Verbesserung der Filmmorphologie erreicht. [21-27]

Diese Arbeit beschäftigt sich mit dem komplexen Prozess der Ladungsträgertrennung, der im Detail noch nicht vollständig verstanden ist, aber auf dem Weg zu leistungsstarken organischen Solarzellen eine Schlüsselrolle einnimmt. An einem breiten Materialsystem wird deshalb aus verschiedenen Blickwinkeln die Ladungsträgertrennung in Donor Akzeptor (D-A)-Solarzellen mittels elektrischer und optischer Experimente genauer untersucht und durch theoretische Modelle beschrieben. Die erlangten Erkenntnisse, welche Materialeigenschaften die Ladungsträgertrennung erleichtern und welche Mechanismen bei der Ladungsträgertrennung an der Donor-Akzeptor Grenzfläche ablaufen, können in Zukunft die gezielte Entwicklung neuer, leistungsstärkerer Solarzellenmaterialien erleichtern.

2.2 Aufbau und Funktionsweise organischer Solarzellen

Die charakteristischen Eigenschaften organischer Halbleiter beruhen auf der Alternation von Einfach- und Doppelbindungen zwischen Kohlenstoffatomen, der sogenannten Konjugation. Die Kohlenstoffatome sind sp^2 hybridisiert und bilden eine σ-Bindung aus.[28] Zusätzlich zur σ-Bindung kann das senkrecht dazu stehende p_z-Orbital eine π-Bindung eingehen, wodurch sich eine Doppelbindung ergibt. Die p_z-Orbitale überlappen gegenseitig und es bildet sich ein delokalisiertes π-Elektronensystem aus, wodurch die organischen Materialien ihre Leitfähigkeit erlangen.

In Analogie zu den Leitungs- und Valenzbändern in anorganischen Halbleitern spricht man in organischen Halbleitern von HOMO- und LUMO- Energieniveaus. Das HOMO (highest occupied molecular orbital) beschreibt das im Grundzustand höchste, vollständig besetzte Molekülorbital, das LUMO (lowest unoccupied molecular orbital) das niedrigste, unbesetzte Molekülorbital. HOMO und LUMO besitzen typischerweise einen Energieunterschied zwischen (1-3) eV, wodurch ein Übergang zwischen den zwei Energieniveaus durch Absorption von Licht im sichtbaren Spektralbereich möglich ist.[8]

Allerdings führt die Absorption von Licht in organischen Solarzellen nicht direkt zu aufgespalteten Ladungsträgern, wie man es von anorganischen Solarzellen her kennt. Die niedrige relative Dielektrizitätskonstante von 3-4 verursacht eine starke Coulombanziehung der positiven und negativen Ladungsträger, da das umgebende organische Material die elektrische Anziehung nur wenig abschirmt. Ein durch Lichtabsorption gebildetes Elektron-Loch-Paar, ein sogenanntes Exziton, besitzt darum eine Bindungsenergie in der Größenordnung von 0,5 eV und muss erst noch in freie Ladungsträger aufgespalten werden.[7] Die Exzitonenbindungsenergie E_B erhält man als Differenz der elektrischen Bandlücke E_{el} und der optischen Bandlücke E_{opt} zu $E_B = E_{el} - E_{opt}$. Hierbei entspricht die optische Bandlücke der Energie des optischen $S_1 \leftarrow S_0$ Übergangs. Die elektrische Bandlücke ergibt sich aus der Differenz des Ionisationspotentials I_p und der Elektronenaffinität E_a zu $E_{el} = I_p - E_a$. Die thermische Aktivierungsenergie reicht für die Überwindung der Exzitonenbindungsenergie alleine nicht aus und der komplette Mechanismus der Ladungstrennung in organischen Solarzellen ist ein mehrstufiger Prozess.

Effiziente organische Solarzellen bestehen deshalb im Gegensatz zu anorganischen Solarzellen aus zwei Materialien, einem Elektronendonator und einem Elektronenakzeptor, im Folgenden Donor und Akzeptor genannt. Der Akzeptor zeichnet sich dabei durch

ein tieferes HOMO- und LUMO-Niveau aus.* Ein auf dem Donor gebildetes Exziton kann innerhalb seiner Diffusionslänge beziehungsweise Lebenszeit an die D-A-Grenzfläche diffundieren und das Elektron seines angeregten Zustandes auf den elektronegativeren Akzeptor übertragen.[29] Dieser Übertrag funktioniert sehr schnell innerhalb einiger (10 - 100) fs.[30-31] Dabei verbleibt ein positives Loch auf dem Donor und der Akzeptor nimmt ein Elektron auf, wodurch ein Charge-Transfer-(CT)-Zustand, in englischsprachiger Literatur auch „geminate pair" genannt, entsteht. Falls das Exziton durch optische Anregung auf dem Akzeptor entsteht, wird im analogen Prozess ein Loch auf den Donor übertragen. Dieser Elektronen- bzw. Lochübertrag ist immer dann energetisch günstig, wenn die resultierende Energie des CT-Zustandes kleiner als die Energie des vorangegangenen Exzitons ist. Der CT-Zustand ist weiterhin Coulomb-gebunden und muss weiter aufgespalten werden. Die erfolgreiche Ladungstrennung steht dabei in Konkurrenz zu verschiedenen Rekombinationsmechanismen,[8, 32] wie der sogenannten „geminate" Rekombination zweier Ladungsträger selben Ursprungs[33], Triplettbildung mit anschließendem Zerfall in den Grundzustand[34-35] oder bimolekularem Zerfall („non-geminate Rekombination").[36] Die Exzitonentrennung wird später noch detaillierter anhand verschiedener theoretischer Modelle besprochen. Nach der Aufspaltung des CT-Zustandes müssen die freien Ladungen zu den Elektroden diffundieren, an denen sie aus der Solarzelle extrahiert werden. In modernen Blendsolarzellen liegt die technische Schwierigkeit darin, den morphologischen Kompromiss zu finden, einerseits die D-A-Grenzfläche für die Ladungstrennung zu maximieren und trotzdem ausreichende Perkolationspfade für den Abtransport der getrennten Ladungsträger aus der aktiven Schicht der Solarzelle zu generieren.

Die aufgezählten Funktionsschritte einer organischen Solarzelle sind in Abbildung 1 zusammengefasst.

* Die Begriffe HOMO und LUMO werden in dieser Arbeit, wie im Fachbereich organischer Halbleiter weit verbreitet, weitgehend synonym für das Ionisationspotential und die Elektronenaffinität verwendet, auch wenn sie sich, streng genommen, aufgrund der Elektron-Elektron-Wechselwirkungen in Molekülen unterscheiden.

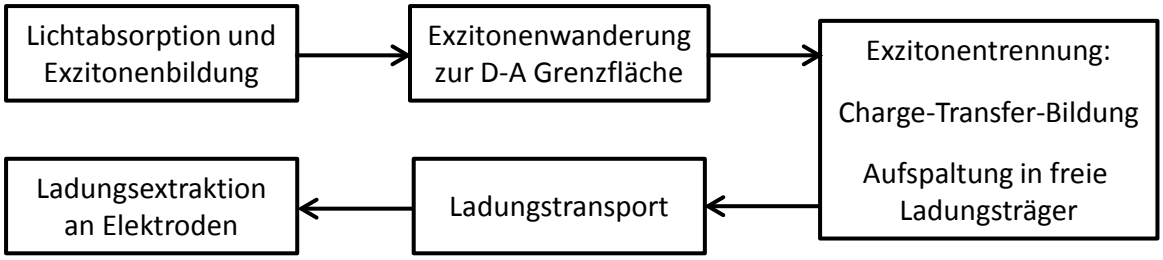

Abbildung 1: Schematische Funktionsabläufe in einer organischen Solarzelle, beginnend von der Lichtabsorption bis zur Extraktion der Ladungsträger.

Abbildung 2 zeigt den Aufbau einer D-A-Solarzelle in der einfachsten Form einer Zweischichtgeometrie. Durch eine lichtdurchlässige Elektrode, häufig ITO (Indiumzinnoxid), und eine PEDOT:PSS- (Poly(3,4-ethylendioxythiophene)/polystyrenesulfonate) Zwischenschicht kann das Licht in die darauf folgende aktive Schicht eindringen und vom Donor und Akzeptor absorbiert werden. PEDOT:PSS liefert eine definierte Austrittsarbeit, verhindert die Eindiffusion von Indium in die aktive Schicht und glättet die raue ITO-Oberfläche. [37-39] Als Gegenelektrode der Solarzelle wird häufig Aluminium aufgedampft.

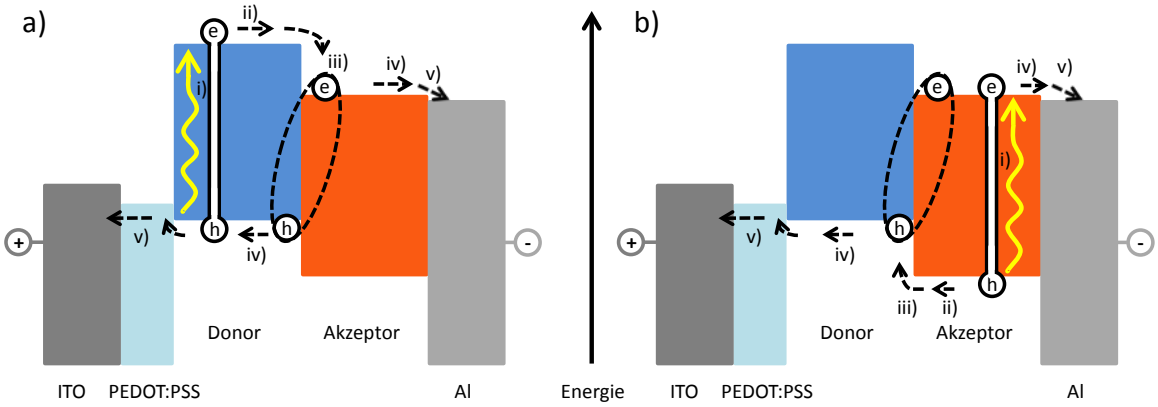

Abbildung 2: Schematischer Aufbau und vereinfachte Funktionsweise einer Zweischichtsolarzelle, inklusive der angedeuten Energieniveaus der verwendeten Materialien ohne Berücksichtigung von Wechselwirkungen. a) Durch Absorption eines Photons wird im Donor ein Exziton gebildet (i), das zur Grenzfläche diffundiert (ii). Das angeregte Elektron wechselt auf den Akzeptor und es bildet sich ein immer noch Coulomb-gebunder Charge-Transfer-(CT)-Zustand, der weiter aufgespalten werden muss (iii). Die getrennten freien Ladungsträger können zu den Elektroden wandern (iv), um extrahiert zu werden (v). b) Analoger Prozess zu a), aber mit der Bildung des Exzitons im Akzeptor (i). Bei der Bildung des CT-Zustandes wird ein Loch auf den Donor übertragen.

Ohne Beleuchtung fließt durch die Solarzelle ein Dunkelstrom, mit Beleuchtung wird zusätzlich ein Fotostrom I_{Foto} generiert. Beide überlagern sich im Betrieb der Solarzelle zu einem Gesamtstrom (Abbildung 3). Bei der Leerlaufspannung V_{OC} (open circuit) ist der netto fließende Gesamtstrom null. I_{SC} (short circuit) ist der ohne äußere Spannung fließende Kurzschlussstrom. Dieser sollte für effiziente Solarzellen betragsmäßig groß sein und einen flachen Kurvenverlauf besitzen. Ein flacher Kurvenverlauf des Gesamtstroms bei vernachlässigbar kleinem Dunkelstrom bedeutet, dass der generierte Fotostrom sättigt und sich Ladungsträger entsprechend den morphologischen Voraussetzungen der Solarzelle bestmöglich aufspalten und extrahiert werden. Der Betrag von I_{Foto} ist direkt proportional zur externen Quantenausbeute EQE (external quantum efficieny). Sie beschreibt das Verhältnis der im äußeren Stromkreis durch erfolgreiche Aufspaltung und Extraktion fließenden Elektronen zur Anzahl der in die Solarzelle eingestrahlten Photonen. Aus ihrem feldabhängigen Verlauf lassen sich Erkenntnisse über die Ladungsträgertrennung ableiten.

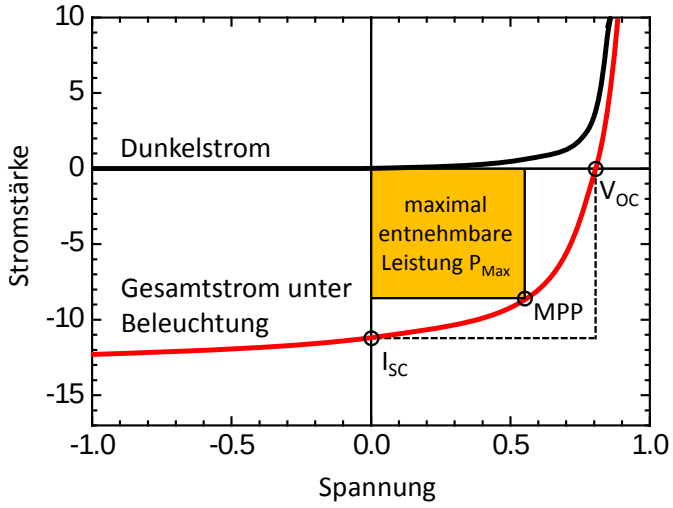

Füllfaktor:

$$FF = \frac{V_{MPP} \cdot I_{MPP}}{V_{OC} \cdot I_{SC}} = \frac{P_{Max}}{V_{OC} \cdot I_{SC}}$$

Wirkungsgrad:

$$\eta = \frac{P_{Max}}{P_L} = \frac{FF \cdot V_{OC} \cdot I_{SC}}{P_L}$$

Externe Quantenausbeute:

$$EQE = \frac{N_{Elektronen}}{N_{Photonen}} = \frac{I_{Foto}}{P_L} \cdot \frac{h \cdot c}{\lambda \cdot e}$$

Abbildung 3: Schematischer Verlauf einer I-U-Kennlinie unter Beleuchtung und der dazugehörigen Dunkelstromkennlinie. V_{OC} (open circuit) ist die Leerlaufspannung und I_{SC} (short circuit) der Kurzschlussstrom der Solarzelle. Der MPP (maximum power point) markiert den optimalen Arbeitspunkt der Solarzelle, bei der ihr die maximale Leistung P_{Max}, symbolisiert durch die Fläche des gelben Rechtecks, entnommen werden kann. Das Flächenverhältnis aus der gelben Rechteckfläche der maximal entnehmbaren Leistung und der Rechteckfläche gebildet aus dem Produkt von I_{SC} und V_{OC}, symbolisiert durch die gestrichelte schwarze Linie ergibt den Füllfaktor (FF). Dieser ist neben dem Wirkungsgrad η, der als Verhältnis von der maximal entnehmbaren zur eingestrahlten Lichtleistung definiert ist und der externen Quantenausbeute EQE (external quantum efficiency) ein wichtiges Charakterisierungsmerkmal. Zur Berechnung der EQE benötigt man den unter Beleuchtung generierten Fotostrom I_{Foto}, die Wellenlänge λ und Leistung P_L des eingestrahlten Lichts, sowie das Plancksche Wirkungsquantum h, die Lichtgeschwindigkeit c und die Elementarladung e.

Der optimal Arbeitspunkt der Solarzelle liegt am MPP (maximum power point), an dem der Solarzelle die größte Leistung entnommen werden kann. Ein weiteres Qualitätsmerkmal effizienter Solarzellen ist ein großer Füllfaktor (FF), der sich aus dem Verhältnis der maximal entnehmbaren Leistung und dem Produkt aus Leerlaufspannung V_{OC} und Kurzschlussstrom I_{SC} ergibt. Der Wirkungsgrad η der Solarzelle ist das Verhältnis aus der maximal entnehmbaren Leistung zur eingestrahlten Lichtleistung P_L. In den besten organischen Solarzellen wurden derzeit Füllfaktoren von annähernd 70 %[40] und Wirkungsgrade von 12 % gemessen.[3]

2.3 Modelle der Ladungsträgertrennung

Die Ladungsträgertrennung ist, wie in Abbildung 1 und Abbildung 3 beschrieben, der zentrale Schritt zur Ladungsgeneration in organischen Solarzellen, der im Detail noch nicht vollständig verstanden ist. Folgende Unterkapitel fassen häufig verwendete und aktuell diskutierte Modelle der Ladungsträgertrennung zusammen.

2.3.1 Braun-Onsager-Modell

Das 1984 von Braun entwickelte Modell der Ladungsträgertrennung in Donor-Akzeptor Systemen basiert auf den Onsager-Modellen zur Aufspaltung Coulomb-gebundener Ionenpaare, die durch die unterstützende Wirkung eines elektrischen Feldes, dargestellt in Abbildung 4, getrennt werden.[41-43] Im ersten feldunabhängigen Schritt wird bei Onsager durch eine optische Anregung mit ausreichend großer Energie ein Ionenpaar erzeugt. Das heiße, von seinem Molekül entfernte Elektron relaxiert durch Wechselwirkung mit seiner Umgebung und befindet sich nach dem Thermalisierungsprozess im Abstand r_0 vom Loch, hier dem ionisierten Molekül, entfernt. Die beim Relaxationsprozess abgegebene, überschüssige Energie steht im weiteren Verlauf nicht mehr zur Verfügung. Im zweiten Schritt, dem Dissoziationsprozess, durchlaufen die geladenen Teilchen eine temperaturaktivierte Brownsche Diffusionsbewegung im Gesamtpotential ihres Coulombfeldes und des äußeren elektrischen Feldes. Ist der Thermalisationsradius r_0 kleiner als der Coulombradius $r_C = \frac{e^2}{4\pi\varepsilon_r\varepsilon_0 kT}$, bei dem die Coulombenergie gleich der thermischen Energie kT ist, dann rekombinieren die Ladungen und stehen für weitere Dissoziationsschritte nicht mehr zur Verfügung. Hierbei ist e die Elementarladung, ε_r die relative und ε_0 die Permittivität, k die Boltzmann-Konstante und T die Temperatur.

Ein Anstoß zur Entwicklung des Braun Modells zur Ladungsträgertrennung waren Messungen von Melz, der die Ladungsträgertrennung an Polyvinyl-Carbazol-Systemen untersuchte, die mit 2,4,7-Trinitrofluorenon (TNF) dotiert waren.[44] Fits mit dem Onsager-Modell lieferten hier deutlich zu große Thermalisationsradien von (2,5 - 3,5) nm, obwohl man für einen Elektronentransfer zwischen einem benachbarten Donor und Akzeptor ein r_0 von 0,5 nm, in der Größenordnung eines nächste-Nachbarn-Abstandes, erwartet.[42, 45]

Dies veranlasste Braun für Donor-Akzeptor-Systeme den Charge-Transfer (CT)-Zustand als den niedrigsten angeregten Zustand als Ausgangspunkt des folgenden Dissoziationsprozesses zu wählen.[42] Dieser CT-Zustand kann direkt durch die Absorption eines

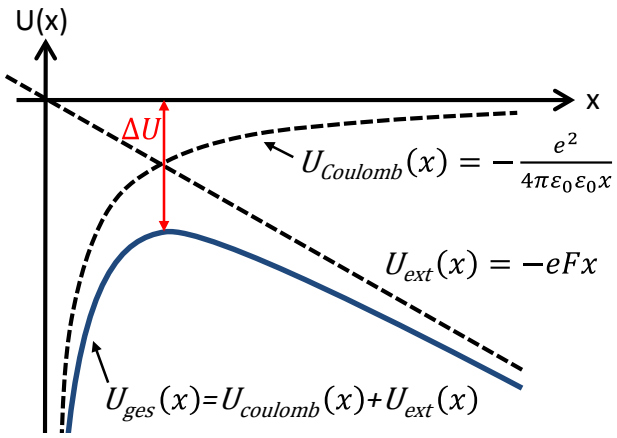

Abbildung 4: Einfluss eines äußeren elektrischen Feldes F auf Coulomb-gebundene Ladungsträger: Das Elektron-Loch-Paar muss einen durch das äußere elektrische Feld um ΔU verkleinerten Potentialwall überwinden, um in freie Ladungsträger aufzuspalten.

Photons oder indirekt entstehen, wenn ein angeregter neutraler Donor (Akzeptor) auf einen Akzeptor (Donor) trifft. Außerdem ist es dem CT-Zustand möglich, durch seine längere Lebenszeit τ von etwa 10^{-8} s mehrere unvollständige Dissoziationsversuche zu unternehmen, bevor er schließlich erfolgreich dissoziiert oder in den Grundzustand rekombiniert. Die Wahrscheinlichkeit zur erfolgreichen Dissoziation ergibt sich damit als Funktion der feldabhängigen Dissoziationsrate $k_d\,(F)$ und der feldunabhängigen Rekombinationsrate $k_r = \tau^{-1}$ in den Grundzustand zu:

$$\varphi(F) = \frac{k_d(F)}{k_d(F)+k_r} = \frac{1}{1+k_r k_d{}^{-1}(F)} \qquad (1)$$

Die Dissoziationsrate der Exzitonen ist temperatur- und stark feldabhängig:

$$k_d(F) = \frac{3\mu e}{4\pi\varepsilon_0\varepsilon_r {r_0}^3} \exp\left(\frac{-\Delta E}{kT}\right) \frac{J_1(2\sqrt{-2b})}{\sqrt{-2b}} \qquad \text{mit } b = \frac{e^3 F}{8\pi\varepsilon_0\varepsilon_r k^2 T^2} \qquad (2)$$

Dabei ist J_1 die Bessel-Funktion erster Ordnung, F das elektrische Feld, μ die gemittelte Summe der Elektron- und Lochmobilität, $\Delta E = e^2/4\pi\varepsilon_0\varepsilon_r r_0$ die Coulomb-Bindungsenergie des Elektron-Loch-Paars beim Thermalisationsradius r_0, ε_r die relative und ε_0 die Permittivität. In der Dissoziationsrate ist die bimolekulare Langevin Rekombinationsrate k_L freier Ladungsträger zurück in den CT-Zustand bereits im Vorfaktor von (2) mit berücksichtigt:[46]

$$k_L = \frac{\mu e}{\varepsilon_0\varepsilon_r} \qquad (3)$$

Das Braun-Onsager-Modell hat sich zur Beschreibung der feldabhängigen Dissoziation in D-A-Systemen, die aus kleinen Molekülen bestehen, bewährt.[45]

2.3.2 Effektive-Masse-Modelle

Ein wesentlicher Mangel des Braun-Modells ist die Betrachtung der Ladungsträger als Punktladungen. Dies ist bei kleinen Molekülen als Näherung möglich, doch es führt bei konjugierten Polymeren und der Verwendung realistischer Thermalisationsradien zu einer Unterschätzung der Dissoziationswahrscheinlichkeit.

Arkhipov beobachtete zudem kritisch die schwache Temperaturabhängigkeit des Fotostroms in Polyparaphenylen-Leiterpolymeren (MeLPPP), die Barth in Verbindung mit Fotoleitfähigkeitsmessungen gemessen hatte und die im Widerspruch zum Braun-Onsager Modell steht.[47] Arkhipov folgerte, dass ein bis dato noch vernachlässigter Parameter die Dissoziationsenergie in Polymeren minimiert und berücksichtigte deshalb erstmalig Delokalisationseffekte. Dabei betrachtet er zum einen die Ladungstrennung in dotierten Polymeren,[48] bei denen der Dotand als Fallenzustand wirkt, als auch die Ladungstrennung an einer D-A-Grenzfläche, bei der zusätzlich Grenzflächendipole berücksichtigt werden.[49]

In beiden Fällen wird nach der Fotoanregung des Polymers bzw. Donors ein Elektron auf den Fallenzustand bzw. Akzeptor übertragen, womit ein Loch auf der Polymerkette zurückbleibt und ein gebundener Elektron-Loch-Zustand entsteht. In Polymeren mit ausgedehnter Konjugation kann sich das Loch über mehrere Wiederholungseinheiten ausbreiten und delokalisieren, das Elektron wird als lokalisiert betrachtet. Arkhipov beschreibt die Delokalisation durch eine effektive Masse des Lochs, das quantenmechanische Nullpunktschwingungen im Coulombpotential seines gebundenen Elektrons ausführt. Dabei entspricht eine kleine effektive Masse einer besonders guten Delokalisation des Lochs auf der Polymerkette, was man mit einer größeren kinetischen Energie verbinden kann. Diese zusätzliche kinetische Energie der Nullpunktschwingung hilft dem Loch die Coulombanziehung des gebundenen Elektrons leichter zu überwinden.

i) Das Fehlstellenmodell

Arkhipov[48] betrachtete 2003 schwach dotierte Polymere mit einer Konzentration der Fallenzustände N_d im Polymermaterial. Als Ausgangsbasis dieses Modells, dargestellt in Abbildung 5, wird eine Polymerkette mit Konjugationslänge l angenommen, die sich zufällig orientiert in einem äußeren elektrischen Feld befindet. Nach der Fotoanregung tunnelt das Elektron mit der Rate $k_{Fehlstelle}$ zum Fallenzustand, der sich im Abstand r befindet und das zugehörige Loch muss entlang der Polymerkette entkommen. Die Wahrscheinlichkeit $w_{Fehlstelle}$ des Elektrons, diesen Fallenzustand innerhalb der Lebenszeit τ des Exzitons zu erreichen, ist gegeben durch:

$$w_{Fehlstelle} = \frac{k_{Fehlstelle}}{k_{Fehlstelle}+\tau^{-1}} = \frac{\nu_0 \exp(-2\gamma r)}{\nu_0 \exp(-2\gamma r)+\tau^{-1}} = [1 + (\nu_0 \tau)^{-1} \exp(2\gamma r)]^{-1} \qquad (4)$$

Dabei ist ν_0 die „attempt-to-jump-frequency“, also die Frequenz der versuchten Hüpfprozesse und γ der inverse Lokalisationsradius, der ein Maß für die Kopplung der Polymerketten in Tunnelrichtung ist.

Die Wahrscheinlichkeit $w_{Fehlstelle}$ muss mit der Poissonverteilung $P(r)$ gewichtet werden, die die Wahrscheinlichkeit angibt, innerhalb einer Weglänge r um die Polymerkette herum einen Fallenzustand zu finden:

$$P(r) = 2\pi r l N_d exp[-\pi l N_d (r^2 - r_{min}^2)] \qquad (5)$$

r_{min} ist der minimale Abstand, den ein Fallenzustand zur Polymerkette haben kann.

Wenn das Elektron erfolgreich in den Fallenzustand im Abstand r zur Polymerkette getunnelt ist, befindet es sich im Gesamtpotential des anziehenden Coulombpotentials und des äußeren elektrischen Feldes F, das im Winkel θ zur Polymerkette steht. Das Gesamtpotential kann man um ein Potentialminimum an der Stelle x_{min} auf der Polymerkette entwickeln, um die das Loch quantenmechanische Schwingungen ausführt. Hier ist die harmonische Näherung dargestellt:

$$U(x) = -eFcos\theta\ x - \frac{e^2}{4\pi\varepsilon_0\varepsilon_0 (x^2+r^2)^{\frac{1}{2}}} \qquad (6)$$

$$U(x) \approx -eF_x x_{min} - \frac{e^2}{4\pi\varepsilon_0\varepsilon_r (x_{min}^2+r^2)^{\frac{1}{2}}} + \frac{e^2(r^2-2x_{min}^2)}{8\pi\varepsilon_0\varepsilon_r (x_{min}^2+r^2)^{\frac{5}{2}}} (x - x_{min})^2 \qquad (7)$$

Dabei ist e die Elementarladung und ε_0 (ε_r) die (relative) Permittivität und $F \cdot cos\theta$ die Projektion F_x des elektrischen Feldes in x-Richtung.

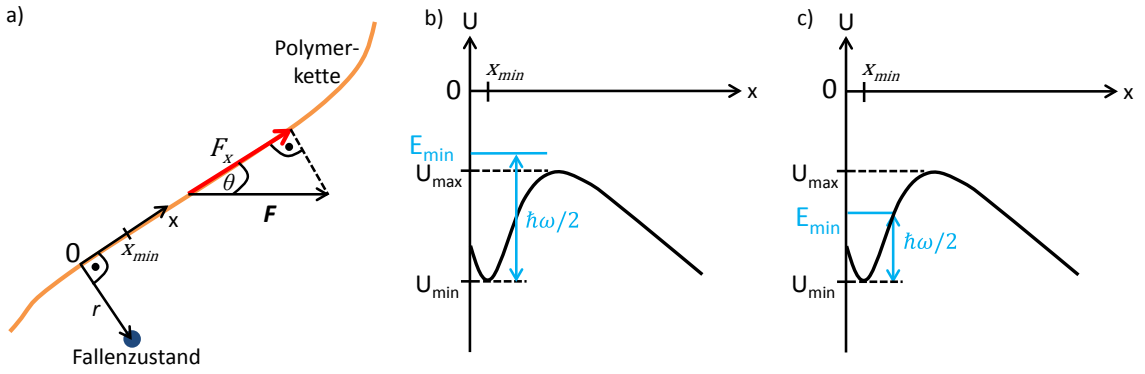

Abbildung 5: a) Schematische Darstellung des Fehlstellenmodells. Ein Polymerkettenabschnitt zeigt in Koordinatenrichtung x und unter dem Winkel θ dazu steht das äußere elektrische Feld *F*. In Richtung des betrachteten Polymerkettenabschnitts wirkt die Projektion des elektrischen Feldes F_x. Das Elektron eines auf der Polymerkette gebildeten Exzitons tunnelt zu einem Fallenzustand, der sich in einem Abstand r von der Polymerkette befindet. Sobald das Elektron im Fallenzustand angelangt ist, rutscht das Loch unter dem Einfluss der Überlagerung des Potentials des äußeren elektrischen Feldes und des Coulombpotentials in das Potentialminimum U_{min} an der Stelle x_{min} auf der Polymerkette. (b). Berücksichtigt man nun die Energie $\hbar\omega/2$ der Nullpunktsschwingung, die sich aufgrund der Delokalisationseffekte des Lochs auf der Polymerkette mit der potentiellen Energie U_{min} zur Gesamtenergie E_{min} addiert, so erhält das gebundene Elektron-Loch-Paar zusätzliche Energie bei der Dissoziation. Ist E_{min} größer als U_{max}, so trennen sich Elektron und Loch auf; ist E_{min} kleiner gleich U_{max} bleiben sie ohne weitere energetische Unterstützung vorerst gebunden (c).

Das Loch besitzt während der Schwingung auf der Polymerkette mindestens die Gesamtenergie E_{min}, die sich aus der minimalen Potentialenergie $U(x_{min})$ und der Energie der Nullpunktschwingung zusammensetzt:

$$E_{min} = U(x_{min}) + \frac{1}{2}\hbar\omega \qquad (8)$$

$$E_{min} = -eF_x x_{min} - \frac{e^2}{4\pi\varepsilon_0\varepsilon_r\left(x_{min}^2+r^2\right)^{\frac{1}{2}}} + \hbar\left[\frac{e^2\left(r^2-2x_{min}^2\right)}{16\pi\varepsilon_0\varepsilon_r\left(x_{min}^2+r^2\right)^{\frac{5}{2}}m_{eff}}\right]^{1/2} \qquad (9)$$

$\hbar$ ist das reduzierte Plancksche Wirkungsquantum, ω die Schwingungsfrequenz des Lochs im Potential und m_{eff} die dem Loch zugeordnete effektive Masse.

Damit das Loch sofort auf der Polymerkette entkommen kann, muss die Gesamtenergie E_{min} größer als die maximale Potentialbarriere U_{max} sein. Ist $E_{min} \leq U_{max}$, so kann die thermische Energie kT unterstützend zur Dissoziationsrate k_{Flucht} beitragen, die in Konkurrenz zur Rekombinationsrate k_r steht.

$$k_{Flucht}(r) = \nu_0 exp\left[-\frac{U_{max}(r)-E_{min}(r)}{kT}\right] \quad \textbf{(10)}$$

$$k_r(r) = \nu_0 \exp(-2\gamma r) \quad \textbf{(11)}$$

Damit ergibt sich analog Gleichung (1) eine Fluchtwahrscheinlichkeit des Lochs w_{Flucht}:

$$w_{Flucht} = \frac{k_{Flucht}}{k_{Flucht}+k_r} = \left\{1 + exp\left[-2\gamma r + \frac{U_{max}(r,z)-E_{min}(r,z)}{kT}\right]\right\}^{-1} \quad \textbf{(12)}$$

Die Gesamtwahrscheinlichkeit η einer erfolgreichen Ladungstrennung nach der optischen Anregung des Polymers mittels einer Fehlstelle ergibt sich aus dem Produkt der Wahrscheinlichkeit, dass das Elektron zu einer Fehlstelle tunnelt (4), in der Umgebung eine Fehlstelle auffindet (5) und das Loch schließlich auf der Polymerkette entkommt (12). Um alle möglichen Orientierungen der Polymerkette relativ zum äußeren elektrischen Feld und die zufällige Verteilung der Fehlstellen zu berücksichtigen, wir für die Gesamtwahrscheinlichkeit η der erfolgreichen Ladungstrennung noch über z und r gemittelt:

$$\eta = 2\pi l N_d \int_0^1 dz \left(\int_{max\{r_{min}, r_0(z)\}}^{\infty} dr\ r \cdot exp[-\pi l N_d (r^2 - r_{min}^2)] \right.$$

$$\cdot [1 + (\nu_0 \tau)^{-1} \exp(2\gamma r)]^{-1} + \int_{r_{min}}^{max\{r_{min}, r_0(z)\}} dr\ r \cdot exp[-\pi l N_d (r^2 - r_{min}^2)]$$

$$\left. \cdot [1 + (\nu_0 \tau)^{-1} \exp(2\gamma r)]^{-1} \cdot \left\{1 + exp\left[-2\gamma r + \frac{U_{max}(r,z)-E_{min}(r,z)}{kT}\right]\right\}^{-1} \right) \quad \textbf{(13)}$$

ii) Effektive-Masse-Modelle an der Donor-Akzeptor-Grenzfläche

Die im Folgenden betrachteten effektive-Masse-Modelle basieren auf der idealen Annahme einer Zweischichtsolarzelle, bei der parallel angeordnete Polymerketten als Donoreinheiten einem ebenfalls gitterähnlich angeordnetem Block aus Akzeptoreinheiten an einer gemeinsamen Grenzfläche gegenüberliegen. Das äußere elektrische Feld steht dabei senkrecht zu den Polymerketten und die Dissoziation des Coulomb-gebundenen Lochs erfolgt durch Hüpfprozesse ebenfalls senkrecht zur D-A-Grenzfläche. Die Dissoziation wird damit mathematisch quasi eindimensional, wobei die Delokalisation des Lochs auf der Polymerkette, beschrieben über die effektive Masse, indirekt die zweite Dimension berücksichtigt.

Nenashev gelang es 2011 erstmalig, aufbauend auf Arkhipovs Arbeiten unter obig genannten Voraussetzungen, die Dissoziation eines Exzitons an einer D-A-Grenzfläche anhand exakter analytischer Rechnungen zu beschreiben.[50] Das zugehörige Modell ist in Abbildung 6 dargestellt. Hierin wird für ein dissoziierendes Loch seine quantenmechanische Wellenfunktion über die eindimensionale Schrödingergleichung auf jeder besuchten Polymerkette *1* bis n im Gesamtpotential $U_n(y)$ des Coulombpotentials und des äußeren Feldes F berechnet und damit die Gesamtenergie E_n des Lochs bestimmt.

$$-\frac{\hbar^2}{2m_{eff}}\frac{d^2\psi(y)}{dy^2} + U_n(y)\psi(y) = E_n\psi(y) \qquad \textbf{(14)}$$

$$\text{mit } U_n(y) = -\frac{e^2}{4\pi\varepsilon_r\varepsilon_0\sqrt{y^2+x_n^2}} - eFx_n \qquad \textbf{(15)}$$

Dabei ist $\hbar$ das reduzierte Plancksche Wirkungsquantum, m_{eff} die dem Loch zugeordnete effektive Masse, $\psi(y)$ die Wellenfunktion des Lochs, e die Elementarladung, ε_0 (ε_r) die (relative) Permittivität und x_n der Abstand des Elektrons zur n-ten Kette.

Ein Loch auf der ersten Polymerkette (n = 1) an der D-A-Grenzfläche kann mit der Hüpfrate $a_{1\to2}$ auf die nächstentfernte Polymerkette springen, oder innerhalb seiner Exzitonenlebenszeit τ mit seinem zugehörigen Elektron rekombinieren. Zur Beschreibung der Hüpfraten $a_{n\to n\pm1}$ des gebunden Lochs von Kette zu Kette wird die von Rubel entwickelte exakte Lösung für die Dissoziation von Exzitonen verwendet, die auf Miller-Abrahams Hüpfraten basiert.[51-52] Hierbei sind explizit auch Hüpfraten zurück in Richtung der D-A-Grenzfläche erlaubt:

$$a_{n\to n\pm1} = \nu_0 exp(-2\gamma r)\begin{cases} exp\left(-\frac{E_{n\pm1}-E_n}{kT}\right) & E_{n\pm1} > E_n \\ 1 & E_{n\pm1} \leq E_n \end{cases} \qquad \textbf{(16)}$$

ν_0 ist die Frequenz der versuchten Hüpfprozesse des Lochs von einer Polymerkette zur nächsten im Abstand r; γ der inverse Lokalisationsradius in Sprungrichtung, k die Boltzmann-Konstante und T die Temperatur.

Das Exziton wird als getrennt betrachtet, wenn das Loch die N-te Polymerkette erreicht hat, wobei N in den Rechnungen so groß gewählt wird, dass die Dissoziationswahrscheinlichkeit p_{Diss} unabhängig davon wird:

$$p_{Diss} = \frac{\tau_0}{\tau_0 + \sum_{n=1}^{N-1} a_{n\to n+1}^{-1} exp\left(\frac{E_n - E_1}{kT}\right)} \qquad \textbf{(17)}$$

In diesen Gesamtausdruck für die Dissoziationswahrscheinlichkeit p_{Diss} müssen dann die berechneten quantenmechanischen Energien aus der Schrödingergleichung in Gleichung (14) und die damit berechneten Hüpfraten in Gleichung (16) eingesetzt werden. Häufig wird in der Praxis für die Lösung der Schrödingergleichung eine harmonische Näherung verwendet.

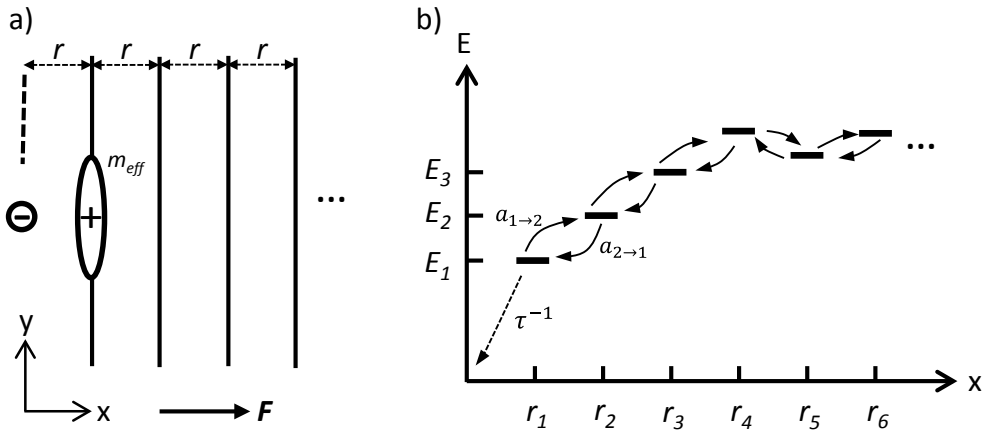

Abbildung 6: a) Schematische Darstellung des effektiven-Masse-Modells von Nenashev: Parallele Polymerketten liegen im Abstand r an der D-A-Grenzfläche. Ein optisch generiertes Exziton wird an der D-A-Grenzfläche aufgespalten und das Elektron auf den Akzeptor übertragen. Das Elektron wird als ortsfest betrachtet, wohingegen das zugehörige Loch auf der Polymerkette delokalisiert. Hier führt es quantenmechanische Nullpunktschwingungen aus, was durch eine effektive Masse m_{eff} berücksichtigt wird. Mit zusätzlicher Unterstützung des elektrischen Feldes *F* dissoziiert das Loch durch Miller-Abrahams-Hüpfraten $a_{n\to n\pm1}$ in b) von der Grenzfläche weg, bis es die Coulombanziehung überwunden hat, oder rekombiniert innerhalb seiner Exzitonlebenszeit mit der Rate τ^{-1}. Nach [50]

2011 erweiterte Wiemer[53] Nenashevs effektive-Masse-Modell von 2011 um Arkhipovs Grundidee[49], dass Dipole an der D-A-Grenzfläche die Coulombanziehung eines gebunden Elektron-Loch Paares abschirmen und somit die Dissoziationswahrscheinlichkeit zusätzlich erhöhen. Diese Annahme leitete Arkhipov zum einen von einer stark ansteigenden Dissoziationswahrscheinlichkeit in D-A-Systemen ab, wenn eine kritische Akzeptorkonzentration überschritten wurde[54], als auch von experimentell gemessenen Verschiebungen der Austrittsarbeit eines Polymers an einer D-A-Grenzfläche.[55]

Wiemer[53] geht in seinem effektive-Masse-Modell mit Grenzflächendipolen (Abbildung 7), im Folgenden nur noch Dipolmodell genannt, von M Dipolen aus, die im Abstand d auf der Polymerkette liegen. Der Abstand der parallelen Polymerketten, sowie der Abstand der ersten Polymerkette zu den Akzeptoreinheiten liegen hier in einem Gitter mit Abstand r. Die Dissoziation erfolgt senkrecht zur D-A-Grenzfläche in Richtung des elektrischen Feldes, analog zu Nenashevs effektivem Masse Modell.

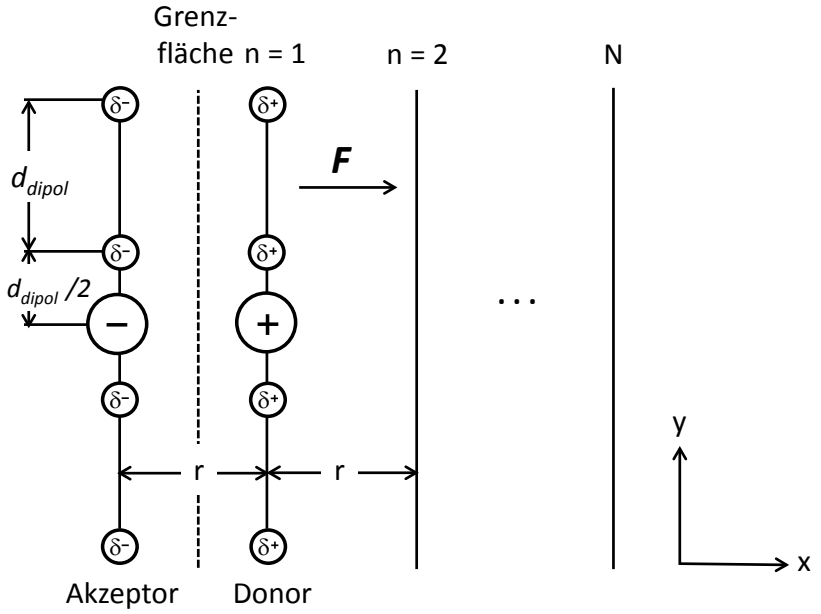

Abbildung 7: Schematische Darstellung des Dipolmodells nach Wiemer. Das Elektron des CT-Zustandes ist auf dem Akzeptor ortsfest, das Loch delokalisiert auf der Polymerkette. Zusätzlich zum effektive-Masse-Modell nach Nenashev werden Grenzflächendipole beim Dissoziationsprozess berücksichtigt, die das Coulompotential abschirmen und somit unterstützend zur Ladungsträgertrennung beitragen. Nach [56].

Ein an der D-A-Grenzfläche gebildeter CT-Zustand mit lokalisiertem Elektron auf dem Akzeptor und delokalisiertem Loch auf der Polymerkette n in Umgebung von M Dipolen der Dipolstärke α und des äußeren elektrischen Feldes F befindet sich im Gesamtpotential $U_n\,(x,y)$:

$$U_n(x_n, y) = -\frac{e^2}{4\pi\varepsilon_r\varepsilon_0}\frac{1}{\sqrt{x_n^2+y^2}}$$
$$+\frac{e^2}{4\pi\varepsilon_r\varepsilon_0}\left[\sum_{t=-M/2}^{M/2-1}\left(\frac{\alpha}{\sqrt{(x_n-r)^2+(y-[t+1/2]d)^2}}\right)+\left(\frac{-\alpha}{\sqrt{x_n^2+(y-[t+1/2]d)^2}}\right)\right]-eFx_n \quad \textbf{(18)}$$

e ist die Elementarladung, ε_0 (ε_r) die (relative) Permittivität und x_n der Abstand des Elektrons zur *n*-ten Kette. Berechnungen von Wiemer zeigen, dass eine Betrachtung von M = 20 Dipolen ausreichend ist; eine größere Anzahl verändert die Dissoziationswahrscheinlichkeit nicht mehr.[53]

Das Loch mit effektiver Masse m_{eff} führt Nullpunktschwingungen auf der Polymerkette durch. Die Lösung der Schrödingergleichung für diese Schwingung erfolgt mit der harmonischen Näherung. Damit ergibt sich für die Gesamtenergie E_n des Lochs, bestehend aus der kinetischen $E_{k,n}$ und potentiellen Energie $E_{p,n}$:

$$E_n = E_{p,n} + E_{k,n} \quad \textbf{(19)}$$

$$E_{p,n} = U_n(x_n, y)\big|_{y=0} \text{ und } \quad E_{k,n} = \frac{1}{2}\hbar\omega = \frac{\hbar}{2\sqrt{m_{eff}}}\sqrt{\frac{d^2}{dy^2}U_n(x_n, y)\big|_{y=0}} \quad \textbf{(20)}$$

Mit der Kenntnis von E_n können dann, analog zu Nenashevs effektiven-Masse-Modell anhand Gleichung (16) die Miller-Abrahams Hüpfraten und letztlich mit Gleichung (17) die Gesamtdissoziationswahrscheinlichkeit berechnet werden.

2.4 Aktueller Stand der Forschung

Zu Beginn der Arbeit war der komplexe Prozess der Ladungsträgertrennung noch nicht im Detail verstanden und es war unklar, welche Materialeigenschaften die Ladungsträgertrennung in organischen Solarzellen begünstigen. Hierzu fehlten speziell experimentelle Messungen der feldabhängigen Quantenausbeuten bis zur Sättigung bei hohen Feldstärken, um die bereits bestehenden Dissoziationsmodelle sicher zu überprüfen und die untersuchten Parameter gezielt zu unterscheiden.

In der Literatur wurden die oft zusammenhängenden Einflüsse der Lochmobilität, der Konjugationslänge und der energetischen Ordnung, sowohl in Ein- als auch Zweimaterialsystemen untersucht und dazu teils widersprüchliche Ergebnisse veröffentlicht. Weitere offene Fragen betreffen den Einfluss der Überschussenergie und der Grenzflächendipole auf die Ladungsträgertrennung.

Der Prozess der Ladungsträgertrennung wird in der Literatur oft als Zweischrittprozess betrachtet. Im ersten Schritt wird ein CT-Zustand gebildet, der im zweiten Schritt aufgespalten wird. Besonders kontrovers wird dabei der Einfluss der energetischen Ordnung auf die Ladungsträgertrennung diskutiert. Emelianova stellte an Einmaterialsystemen in ihrem theoretischen Modell eine Unterstützung der Ladungsträgertrennung im ersten Schritt durch energetische Unordnung fest.[57] Ähnliche Ergebnisse erzielten Monte-Carlo-Simulationen von Albrecht[58] an Einmaterialsystemen und Offerman[59] an D-A-Systemen, die eine Unterstützung der Dissoziation im zweiten Schritt durch energetische Unordnung beobachteten. Experimentell werden diese Resultate durch Barth unterstützt.[60] Differenziertere Ergebnisse erhielt Rubel bei seiner Beschreibung der Dissoziationsraten via Hüpfprozesse von der D-A-Grenzfläche weg: Die energetische Unordnung unterstützt die Dissoziation bei kleinen elektrischen Feldstärken, jedoch ist sie bei großen Feldstärken hinderlich.[51]

Diesen Ergebnissen über den Einfluss der energetischen Unordnung auf die Ladungsträgertrennung stehen Untersuchungen des Einflusses der Konjugationslänge gegenüber, da Polymere mit hoher effektiver Konjugationslänge in der Regel eine geringere energetische Unordnung zeigen.[61-62] In Einmaterialsystemen zeigte Barth an zwei PPV-Derivaten, dass das Material mit den planaren Ketten und damit der längeren Konjugationslänge größere Quanteneffizienzen aufweist, was auf einen unterstützenden Effekt der Konjugation schließen lässt.[63] Dies ist der Wegbereiter der bereits beschriebenen effektiven-Masse-Theorien, die allesamt von einem delokalisierten Loch auf einem konjugierten Kettensegment ausgehen, was die Ladungstrennung begünstigt.[48-50, 53] Der unterstützende Effekt einer guten Konjugation wurde auch von Deibel in D-A-Systemen anhand von Monte-Carlo-Simulationen gezeigt.[64] Diese hatten aber den Nachteil, dass auf den konjugierten linearen Ketten das Loch mit einer gleichmäßigen Dichteverteilung

angenommen wurde und somit eine modellbedingte zu hohe Dissoziationswahrscheinlichkeit an den Polymerenden aufweist.

Eng verbunden mit der effektiven Konjugationslänge und der energetischen Unordnung ist auch der Einfluss der Ladungsträgermobilität. In Brauns Modell der Ladungsträgertrennung in D-A-Systemen steigert eine höhere Ladungsträgermobilität die Dissoziationswahrscheinlichkeit.[42] Groves und Mihailetchi stellen mittels Monte-Carlo-Simulationen und Messungen an P3HT/PCBM Solarzellen tatsächlich eine Verbesserung der Solarzellenausbeute für größere Ladungsträgermobilitäten fest.[33, 65] Eine große Mobilität führt zwar zur Erhöhung des Kurzschlussstroms, allerdings auch zu einer Abnahme der Leerlaufspannung und damit zu schlechteren Wirkungsgraden, da die Grenzflächenrekombination der Minoritätsladungsträger an den Gegenelektroden zum dominierenden Verlustprozess aufsteigt.[66]

Ebenfalls ungeklärt ist der Einfluss der Überschussenergie.[67] Mit Überschussenergie bezeichnet man häufig die Differenz zwischen der Anregungsenergie des absorbierten Photons und des durch Elektronentransfer gebildeten CT-Zustandes. Bei der Überschussenergie wird angenommen, dass sie die Ladungstrennung begünstigen kann, indem sie zur Bildung heißer CT-Zustände führt, die delokalisierter sind und die Vorstufe zu freien Ladungsträgeren bilden.[7, 68] Unterstützt wird dieses Bild durch Versuche von Bakulin, der in sogenannten Pump-Push Messungen, bei denen kurz nach der optischen Anregung ein zusätzlicher niederenergetischer Infrarotstrahl auf die Probe eingestrahlt wird, einen betragsmäßig kleinen zusätzlichen Stromfluss im D-A-System beobachtet. Der Infrarotstrahl dient dabei zur Wiederanregung relaxierter CT-Zustände in heiße CT-Zustände.[69] Die Grundvoraussetzung für eine Begünstigung der Ladungsträgertrennung durch die Überschussenergie ist, dass die freien Ladungsträger schneller gebildet werden, als die interne vibronische Relaxation abläuft.[70] Vandewal und van der Hofstad finden dazu in umfangreichen Materialsystemen, dass die Überschussenergie nicht zur Unterstützung der Ladungsträgertrennung beiträgt und die interne Quantenausbeute der D-A-Systeme unabhängig von der eingestrahlten Wellenlänge und damit der Überschussenergie ist.[68, 70] Neueste Untersuchungen deuten darauf hin, dass es entscheidend ist, ob die Überschussenergie durch Anregung höherer vibronischer oder elektronischer Zustände entsteht. So kann eine Anregung höherer elektronischer Zustände tatsächlich die Ladungstrennung erleichtern, wie von Grancini in PDPCTBT/PCBM-Filmen gezeigt,[30] da höhere elektronische Zustände delokalisierter sind.[71]

Ein weiteres aktuelles Forschungsgebiet sind Grenzflächendipole und ihre Verbindung zur Ladungsträgertrennung in Solarzellen. Theoretische Modelle von Arkhipov und Wiemer zeigen, dass intermolekulare Dipole an D-A-Grenzflächen die Ladungsträgertrennung unterstützen, indem sie die Coulombanziehung der gebildeten Elektron-Loch-Paare abschirmen.[49, 53] Auch intramolekulare Dipole in D-A-Copolymeren beeinflussen die Ladungsträgertrennung. Bei D-A-Copolymeren werden Donor- und Akzeptorbausteine

bei der Polymersynthese miteinander verknüpft, um durch die intramolekulare D-A-Wechselwirkung Polymere mit niedriger Bandlücke zu generieren. Diese können dadurch einen größeren Spektralbereich des Sonnenlichts absorbieren, was D-A-Copolymere aktuell für effizientere Solarzellen als überarbeitete Donormaterialien unentbehrlich macht. Der Einfluss und das Zusammenspiel der Donor- und Akzeptorbausteine in den Copolymeren und ihre Auswirkungen auf die Ladungsträgertrennung sind dabei noch nicht systematisch untersucht. Aktuelle Untersuchungen von Carsten zeigen, dass eine möglichst große Dipoländerung zwischen dem Grundzustand und dem angeregten Zustand eines Copolymers zu effizienteren Solarzellen mit größerem Wirkungsgrad führt.[72] Ferner führen starke Dipole auf einer Copolymerkette zu einer Art Vortrennung des Elektrons und Lochs nach der Anregung, indem das Elektron auf dem Copolymer vorzugsweise auf den elektronegativeren Teilen des Copolymers lokalisiert ist, wodurch es leichter auf den Akzeptor wechseln kann.[73]

Grenzflächendipole und Grundzustandskomplexe sind eng miteinander verknüpft, da bei beiden ein gewisser Ladungstransfer stattfindet.[74-77] Grundzustandskomplexe sind bis dato durch zusätzliche, nichtadditive niederenergetische Absorption und Emission gekennzeichnet.[34, 78] Der genaue Einfluss der Grundzustandskomplexe auf die Ladungsträgertrennung bleibt dabei unklar. Die veröffentlichten Arbeiten schwanken zwischen den Aussagen, dass Grundzustandskomplexe an der Ladungstrennung beteiligt sind und diese unterstützen [34], dass sie nicht wesentlich zum Fotostrom beitragen[79-80], oder den Wirkungsgrad der Solarzelle sogar minimieren. [81]

Vor dem Hintergrund der hier dargestellten Forschungslandschaft konzentrieren sich die in dieser Arbeit dargestellten Untersuchungen besonders auf Effekte der Konjugationslänge, energetischer Ordnung und Grenzflächendipole im Bereich der D-A-Solarzellen.

3. Experimentelles

3.1 Messmethodik

Der Prozess der Ladungsträgertrennung in organischen Donor-Akzeptor Solarzellen wird in dieser Arbeit durch die Bestimmung der feldabhängigen Quantenausbeute untersucht. Diese Messmethode beruht auf der Grundidee, dass durch ein unterstützendes äußeres elektrisches Feld ab einer gewissen Feldstärke die Coulombanziehung der gebildeten Exzitonen überwunden wird, wodurch diese aufspalten und die getrennten Ladungsträger zu den Elektroden abwandern.

Für die Bestimmung der feldabhängigen Quantenausbeute misst man Strom-Spannungs-(I-U)-Kennlinien der Solarzellen ohne und mit Beleuchtung bis zu möglichst großen Spannungen in Sperrrichtung. Das aufgetragene elektrische Feld erhält man, indem man die angelegte äußere Spannung vom internen Potential der Zelle subtrahiert und das Ergebnis durch die aktive Schichtdicke der Solarzelle teilt. Das interne Potential wird gleich der Leerlaufspannung des Fotostroms gewählt. Für die Quantenausbeute ist der in der Solarzelle generierte Fotostrom von Bedeutung. Man erhält ihn, indem man vom Gesamtstrom unter Beleuchtung der Solarzelle den ohne Beleuchtung fließenden Dunkelstrom abzieht. Die Quantenausbeute erhält man aus dem Fotostrom unter Berücksichtigung der in der Solarzelle absorbierten Photonen, wie es in Abbildung 3 genauer beschrieben wird. Zur besseren Übersicht wird die Quantenausbeute häufig auf eins normiert dargestellt, falls sie bei großen Feldstärken sättigt und einen waagrechten Verlauf annimmt. Dabei nimmt man an, dass alle durch Absorption von Photonen angeregten Exzitonen an der Grenzfläche durch das äußere Feld erfolgreich aufgespalten werden und sich der maximale Fotostrom ausgebildet hat. Diese Annahme wurde überprüft und bestätigt, indem für mehrere Solarzellen die interne Quantenausbeute durch Berücksichtigung des gemessenen Absorptionskoeffizienten und einer Exzitonendiffusionslänge von circa 10 nm berechnet wurde.

Die Messungen der I-U-Kennlinien unter monochromatischer Beleuchtung und der Fotostromspektren erfolgten am modifizierten Solarmessplatz, dargestellt in Abbildung 8. Ausgehend vom Stand einer besonders schonenden, Lock-In-basierten Messmethode aus meiner Diplomarbeit, bei der ausschließlich der Fotostrom detektiert werden kann, wurde der Messplatz wieder auf die Keithley-Source-Measure-Unit (SMU) rückgebaut und erweitert. Dies ermöglicht, unter Einsatz eines angesteuerten Shutters, die Aufnahme des in der Solarzelle fließenden Dunkelstroms ohne Beleuchtung und des Gesamtstroms unter Beleuchtung bei jeder angelegten äußeren Spannung. Der Fotostrom wird sogleich für jeden Spannungswert über die Differenz des Gesamtstroms und des Dunkelstroms vom Labview Programm gebildet. Um auch bei diesen SMU-

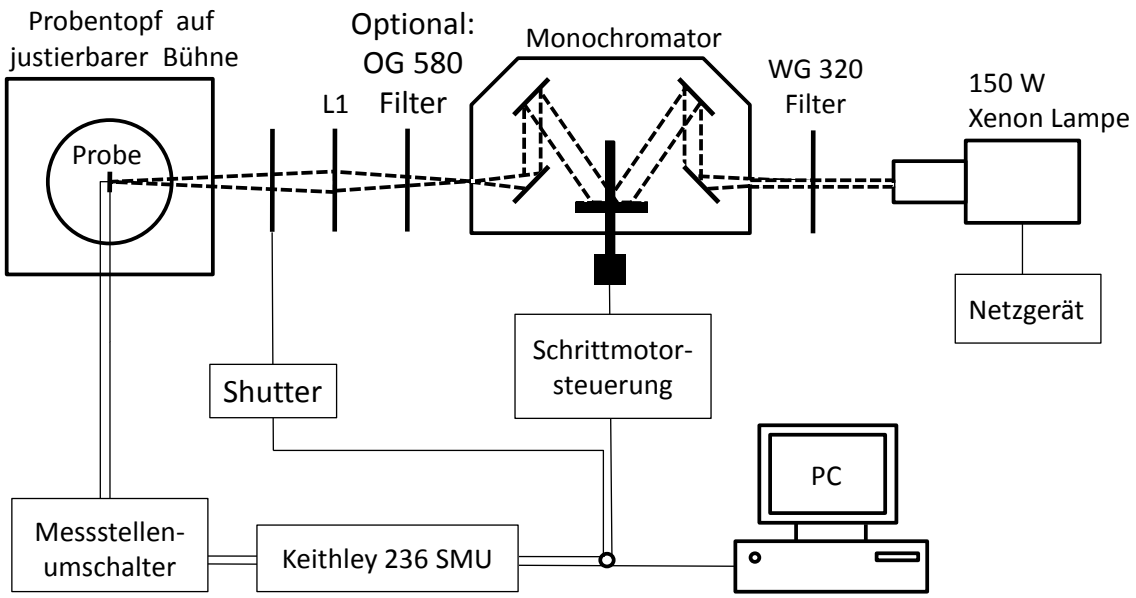

Abbildung 8: Solarzellenmessplatz für Fotostromspektren und I-U-Kennlinien unter monochromatischer Beleuchtung. Die Solarzellen befinden sich unter einem dynamischen Vakuum einer Drehschieberpumpe in einem Probentopf, der auf einer justierbaren Bühne sitzt. Die Ansteuerung der Messgeräte erfolgt über ein selbstgeschriebenes Labview-Programm.

basierten Messungen die Belastungen der Solarzelle während des Messvorgangs so gering wie möglich zu halten, wird an die Solarzellen die äußere Spannung nur für den kurzen Moment der eigentlichen Stromstärkemessung angelegt; die überwiegende Zeit verbringt die Solarzelle unter Kurzschlussbedingungen. Diese Messmethode hat den Vorteil, dass mögliche Ladungsansammlungen in der Solarzelle aufgrund eines dauerhaft starken elektrischen Feldes reduziert werden und angestaute Ladungsträger während den Kurzschlussbedingungen die Solarzelle verlassen können. Ferner schont die verkürzte Messzeit, besonders bei extrem großen Feldstärken in der Größenordnung von 10^6 V cm^{-1} die Solarzelle, indem die Gefahr eines elektrischen Durchbruchs an bauartbedingten Schwachstellen der aktiven Schicht reduziert wird.

Im weiteren Verlauf meiner Doktorarbeit war zudem ein Messplatz mit Sonnensimulator verfügbar, der ebenfalls mit einer Keithley-SMU und einem ähnlichem Labview-Messprogramm ausgestattet wurde. Der Sonnensimulator Newport Sol2A ermöglicht nun die Aufnahme der U-I-Kennlinie unter standardisierten AMG-1.5-Bedingungen.

Bei beiden Messplätzen befinden sich die Solarzellen in einem Probentopf unter einem dynamischen Vakuum. Der Ein- und Ausbau der Solarzellenproben erfolgt ausschließlich in der Glovebox, wodurch Oxidationsschäden der Solarzelle durch Luftsauerstoff weitgehend ausgeschlossen sind.

3.2 Probengeometrie

Der Schlüsselerfolg zum Erreichen der extrem hohen Feldstärken in der Größenordnung von 10^6 V cm^{-1} bei den feldabhängigen Quantenausbeutemessungen war die Verwendung einer angepassten Probengeometrie für homogene Felder die nach meiner Diplomarbeit am Lehrstuhl EP II etabliert wurde.[82] Allgemein ist im Fachgebiet eine Probengeometrie üblich, bei der die Kathode in Form eines Streifens orthogonal zur streifenförmigen Anode aufgedampft wird. Dadurch wird jedoch das elektrische Feld zwischen Anode und Kathode an der Anodenkante inhomogen. Da der organische Halbleiterfilm an dieser Kante in der Regel auch dünner als mittig auf der Elektrode ist, wird an der Kante das elektrische Feld zusätzlich verstärkt. Dieser sogenannte Kanteneffekt hat zur Folge, dass das elektrische Feld dort in seiner Größe nicht wohldefiniert ist, und dass zudem an der Kante vermehrt dielektrische Durchschläge auftreten. Dies macht eine Messung zu hohen Feldstärken unmöglich. Die Kanteneffekte werden durch den Einsatz einer isolierenden Fotolackschicht beseitigt,[83-85] wie graphisch in Abbildung 9 dargestellt.

Die Solarzellen werden nach einer in meiner Diplomarbeit erwähnten Vorschrift auf selbst strukturierte und auf 2 cm Kantenlänge zugeschnittene Glassubstrate gebaut, die vier symmetrische ITO- (Indiumzinnoxid) Elektroden mit 10 Ω/□ besitzen. Die Substrate werden zuerst mechanisch mit Tensid und Wasser und anschließend mit Aceton, Hexan, nochmals Aceton und Isopropanol gereinigt, bevor mit einem Spincoater die Fotolackschicht aus AZ 1518 von Microchemicals aufgetragen wird. Der Fotolack wird strukturiert, sodass sich vier kreisrunde Aussparungen für die späteren aktiven Flächen mit einer Größe von 7,07 mm^2 ergeben.

Ergänzend zum bereits erwähnten Bauprozess wurde für alle in dieser Arbeit gebauten Solarzellen ein weiterer neuer Reinigungsschritt nach der Fotolackstrukturierung eingebaut, bei dem die Substrate zwei Minuten lang mit einem Sauerstoffplasma geätzt werden. Dies führt zur Abtragung von circa (15-20) nm des Fotolacks, was auch in den Fotolackaussparungen eine besonders gründliche Reinigung der rauen ITO Oberfläche von Fotolackresten ermöglicht. Zudem wird durch den Ätzprozess die Oberflächenspannung des Substrats dem des PEDOT:PSS angeglichen, wodurch sich die PEDOT:PSS Schicht homogener aufbringen lässt. Das PEDOT:PSS wird ausschließlich mittels je eines kleinen Tröpfchens direkt in die Fotolackaussparungen getropft und dann gespincoatet. Dadurch bleiben die definierten aktiven Flächen trotz der PEDOT:PSS-Schicht weiterhin elektrisch voneinander isoliert. Das erhöht den Parallelwiderstand und ermöglicht in Verbindung mit einer flächengenauen Belichtung der aktiven Fläche eine unverfälschte Charakterisierung der Solarzelle.[86-87] Unter dem späteren Kontaktierungspunkt der aufgedampften

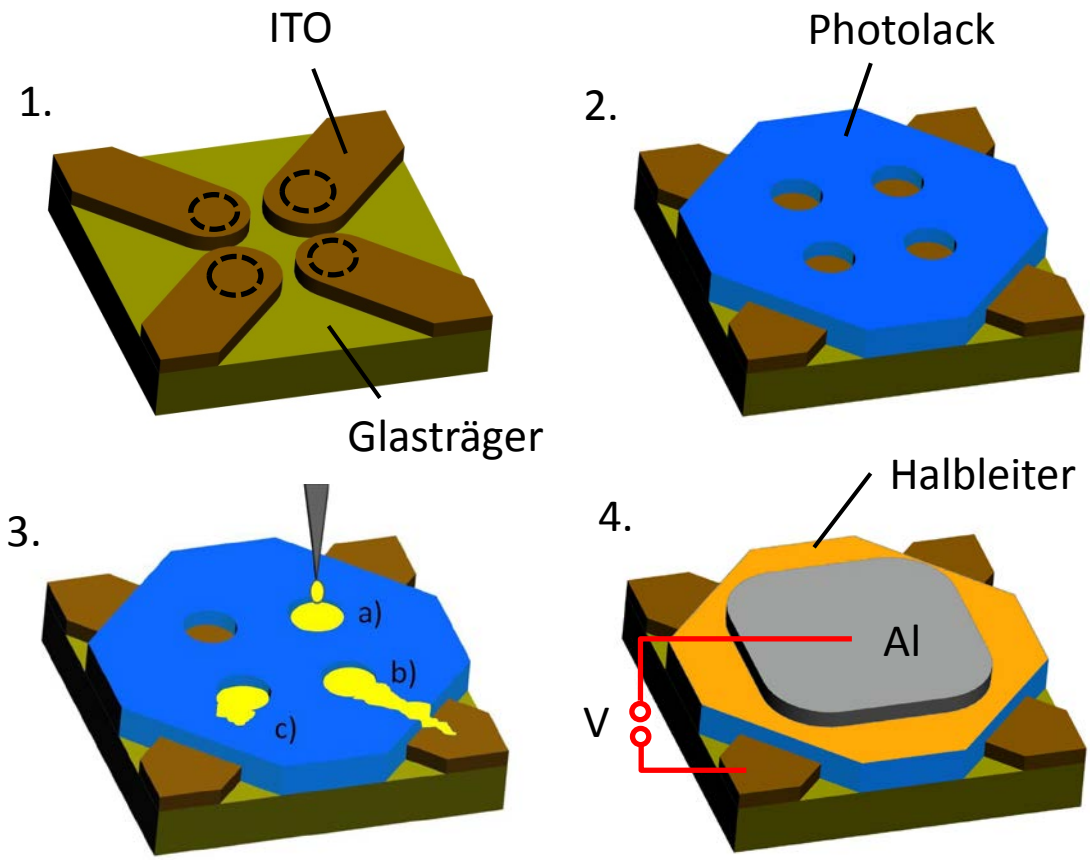

Abbildung 9: Schematische Darstellung des verwendeten Solarzellenaufbaus ohne Kanteneffekte: 1. Vier isolierte ITO-Elektroden sind symmetrisch auf einem Glassubstrat angeordnet. Die gestrichelten Kreise symbolisieren die zukünftigen aktiven Flächen. 2. Die ITO-Kanten werden durch Fotolack eliminiert und die Aussparungen der aktiven Flächen sind erkennbar. 3. In diese Fotolackaussparungen wird jeweils ein Tropfen PEDOT:PSS gefüllt (a)), dann gespincoated (b)) und schließlich die Ausflussspuren gereinigt (c)). 4. Die aktive Schicht wird ganzflächig aufgebracht und für eine Zweischichtstruktur werden ein Akzeptor und eine Gegenelektrode aufgedampft. Die Kontaktierung der Solarzelle erfolgt an den jeweiligen ITO-Ecken und zentriert auf der aufgedampften Gegenelektrode.

Gegenelektrode im Zentrum des Glassubstrats befindet sich kein leitfähiges PEDOT und kein ITO. Dadurch werden Kurzschlüsse vermieden, falls sich der Kontaktstift durch die aufgedampfte Elektrode drückt. Nach dem Ausheizen der PEDOT:PSS-Schicht in der Glovebox wird die aktive Schicht mit dem Spincoater aufgetragen und anschließend der Akzeptor und die Gegenelektrode aufgedampft.

Literaturverzeichnis

1. Brabec, C. J.; Durrant, J. R., Solution-Processed Organic Solar Cells. *MRS Bull.* **2008,** *33*, 670-675.
2. Peet, J.; Heeger, A. J.; Bazan, G. C., "Plastic" Solar Cells: Self-Assembly of Bulk Heterojunction Nanomaterials by Spontaneous Phase Separation. *Acc. Chem. Res.* **2009,** *42*, 1700-1708.
3. Heliatek http://www.heliatek.com/wp-content/uploads/2013/01/130116_pr_ heliatek_achieves_record_cell_effiency_for_opv.pdf.
4. Deibel, C.; Dyakonov, V.; Brabec, C. J., Organic Bulk-Heterojunction Solar Cells. *IEEE J.Sel. Top. Quant. Electron.* **2010,** *16*, 1517-1527.
5. Blankenburg, L.; Schultheis, K.; Schache, H.; Sensfuss, S.; Schrodner, M., Reel-to-Reel Wet Coating as an Efficient up-Scaling Technique for the Production of Bulk-Heterojunction Polymer Solar Cells. *Sol. Energy Mater. Sol. Cells* **2009,** *93*, 476-483.
6. Forrest, S. R., The Path to Ubiquitous and Low-Cost Organic Electronic Appliances on Plastic. *Nature* **2004,** *428*, 911-918.
7. Brédas, J. L.; Norton, J. E.; Cornil, J.; Coropceanu, V., Molecular Understanding of Organic Solar Cells: The Challenges. *Acc. Chem. Res.* **2009,** *42*, 1691-1699.
8. Deibel, C.; Dyakonov, V., Polymer-Fullerene Bulk Heterojunction Solar Cells. *Rep. Prog. Phys.* **2010,** *73*, 096401.
9. Pivrikas, A.; Sariciftci, N. S.; Juska, G.; Österbacka, R., A Review of Charge Transport and Recombination in Polymer/Fullerene Organic Solar Cells. *Prog.Photovoltaics* **2007,** *15*, 677-696.
10. Credgington, D.; Hamilton, R.; Atienzar, P.; Nelson, J.; Durrant, J. R., Non-Geminate Recombination as the Primary Determinant of Open-Circuit Voltage in Polythiophene:Fullerene Blend Solar Cells: An Analysis of the Influence of Device Processing Conditions. *Adv. Funct. Mater.* **2011,** *21*, 2744-2753.
11. Mauer, R.; Howard, I. A.; Laquai, F., Effect of Nongeminate Recombination on Fill Factor in Polythiophene/Methanofullerene Organic Solar Cells. *J. Phys. Chem. Lett.* **2010,** *1*, 3500-3505.
12. Friend, R. H.; Phillips, M.; Rao, A.; Wilson, M. W. B.; Li, Z.; McNeill, C. R., Excitons and Charges at Organic Semiconductor Heterojunctions. *Faraday Discuss.* **2012,** *155*, 339-348.
13. Brabec, C. J.; Shaheen, S. E.; Winder, C.; Sariciftci, N. S.; Denk, P., Effect of LiF/Metal Electrodes on the Performance of Plastic Solar Cells. *Appl. Phys. Lett.* **2002,** *80*, 1288-1290.
14. Mihailetchi, V. D.; Koster, L. J. A.; Blom, P. W. M., Effect of Metal Electrodes on the Performance of Polymer: Fullerene Bulk Heterojunction Solar Cells. *Appl. Phys. Lett.* **2004,** *85*, 970-972.
15. Lee, J. H.; Cho, S.; Roy, A.; Jung, H. T.; Heeger, A. J., Enhanced Diode Characteristics of Organic Solar Cells Using Titanium Suboxide Electron Transport Layer. *Appl. Phys. Lett.* **2010,** *96*, 163303.
16. Liang, Y. Y.; Xu, Z.; Xia, J. B.; Tsai, S. T.; Wu, Y.; Li, G.; Ray, C.; Yu, L. P., For the Bright Future-Bulk Heterojunction Polymer Solar Cells with Power Conversion Efficiency of 7.4%. *Adv. Mater.* **2010,** *22*, E135-E138.
17. Ahmed, E.; Ren, G. Q.; Kim, F. S.; Hollenbeck, E. C.; Jenekhe, S. A., Design of New Electron Acceptor Materials for Organic Photovoltaics: Synthesis, Electron Transport, Photophysics, and Photovoltaic Properties of Oligothiophene-Functionalized Naphthalene Diimides. *Chem. Mater.* **2011,** *23*, 4563-4577.
18. Li, Y. F., Molecular Design of Photovoltaic Materials for Polymer Solar Cells: Toward Suitable Electronic Energy Levels and Broad Absorption. *Acc. Chem. Res.* **2012,** *45*, 723-733.
19. Kim, J. Y.; Lee, K.; Coates, N. E.; Moses, D.; Nguyen, T. Q.; Dante, M.; Heeger, A. J., Efficient Tandem Polymer Solar Cells Fabricated by All-Solution Processing. *Science* **2007,** *317*, 222-225.

20. Dennler, G.; Scharber, M. C.; Ameri, T.; Denk, P.; Forberich, K.; Waldauf, C.; Brabec, C. J., Design Rules for Donors in Bulk-Heterojunction Tandem Solar Cells-Towards 15 % Energy-Conversion Efficiency. *Adv. Mater.* **2008,** *20*, 579-583.
21. Weickert, J.; Dunbar, R. B.; Hesse, H. C.; Wiedemann, W.; Schmidt-Mende, L., Nanostructured Organic and Hybrid Solar Cells. *Adv. Mater.* **2011,** *23*, 1810-1828.
22. Kumar, A.; Li, G.; Hong, Z. R.; Yang, Y., High Efficiency Polymer Solar Cells with Vertically Modulated Nanoscale Morphology. *Nanotechnology* **2009,** *20*, 165202.
23. Yang, X. N.; Loos, J.; Veenstra, S. C.; Verhees, W. J. H.; Wienk, M. M.; Kroon, J. M.; Michels, M. A. J.; Janssen, R. A. J., Nanoscale Morphology of High-Performance Polymer Solar Cells. *Nano Lett.* **2005,** *5*, 579-583.
24. Svanström, C. M. B.; Rysz, J.; Bernasik, A.; Budkowski, A.; Zhang, F.; Inganas, O.; Andersson, M. R.; Magnusson, K. O.; Benson-Smith, J. J.; Nelson, J.; Moons, E., Device Performance of APFO-3/PCBM Solar Cells with Controlled Morphology. *Adv. Mater.* **2009,** *21*, 4398-4403.
25. Campoy-Quiles, M.; Ferenczi, T.; Agostinelli, T.; Etchegoin, P. G.; Kim, Y.; Anthopoulos, T. D.; Stavrinou, P. N.; Bradley, D. D. C.; Nelson, J., Morphology Evolution Via Self-Organization and Lateral and Vertical Diffusion in Polymer: Fullerene Solar Cell Blends. *Nat. Mater.* **2008,** *7*, 158-164.
26. Peet, J.; Kim, J. Y.; Coates, N. E.; Ma, W. L.; Moses, D.; Heeger, A. J.; Bazan, G. C., Efficiency Enhancement in Low-Bandgap Polymer Solar Cells by Processing with Alkane Dithiols. *Nat. Mater.* **2007,** *6*, 497-500.
27. Opitz, A.; Wagner, J.; Brütting, W.; Salzmann, I.; Koch, N.; Manara, J.; Pflaum, J.; Hinderhofer, A.; Schreiber, F., Charge Separation at Molecular Donor-Acceptor Interfaces: Correlation between Morphology and Solar Cell Performance. *IEEE J. Sel. Top. Quant. Electron.* **2010,** *16*, 1707-1717.
28. Pope, M.; Swenberg, C. E., *Electronic Processes in Organic Crystals and Polymers, 2nd Edn*. New York: Oxford University Press: 1999.
29. Deibel, C.; Strobel, T.; Dyakonov, V., Role of the Charge Transfer State in Organic Donor-Acceptor Solar Cells. *Adv. Mater.* **2010,** *22*, 4097-4111.
30. Grancini, G.; Maiuri, M.; Fazzi, D.; Petrozza, A.; Egelhaaf, H. J.; Brida, D.; Cerullo, G.; Lanzani, G., Hot Exciton Dissociation in Polymer Solar Cells. *Nat. Mater.* **2013,** *12*, 29-33.
31. Herrmann, D.; Niesar, S.; Scharsich, C.; Köhler, A.; Stutzmann, M.; Riedle, E., Role of Structural Order and Excess Energy on Ultrafast Free Charge Generation in Hybrid Polythiophene/Si Photovoltaics Probed in Real Time by near-Infrared Broadband Transient Absorption. *J. Am. Chem. Soc.* **2011,** *133*, 18220-18233.
32. Janssen, R. A. J.; Nelson, J., Factors Limiting Device Efficiency in Organic Photovoltaics. *Adv. Mater.* **2013,** *25*, 1847-1858.
33. Groves, C.; Marsh, R. A.; Greenham, N. C., Monte Carlo Modeling of Geminate Recombination in Polymer-Polymer Photovoltaic Devices. *J. Chem. Phys.* **2008,** *129*, 114903.
34. Benson-Smith, J. J.; Goris, L.; Vandewal, K.; Haenen, K.; Manca, J. V.; Vanderzande, D.; Bradley, D. D. C.; Nelson, J., Formation of a Ground-State Charge-Transfer Complex in Polyfluorene/[6,6]-Phenyl-C-61 Butyric Acid Methyl Ester (PCBM) Blend Films and Its Role in the Function of Polymer/PCBM Solar Cells. *Adv. Funct. Mater.* **2007,** *17*, 451-457.
35. Veldman, D.; Meskers, S. C. J.; Janssen, R. A. J., The Energy of Charge-Transfer States in Electron Donor-Acceptor Blends: Insight into the Energy Losses in Organic Solar Cells. *Adv. Funct. Mater.* **2009,** *19*, 1939-1948.
36. Credgington, D.; Jamieson, F. C.; Walker, B.; Nguyen, T. Q.; Durrant, J. R., Quantification of Geminate and Non-Geminate Recombination Losses within a Solution-Processed Small-Molecule Bulk Heterojunction Solar Cell. *Adv. Mater.* **2012,** *24*, 2135-2141.

37. Friedel, B.; Keivanidis, P. E.; Brenner, T. J. K.; Abrusci, A.; McNeill, C. R.; Friend, R. H.; Greenham, N. C., Effects of Layer Thickness and Annealing of PEDOT:PSS Layers in Organic Photodetectors. *Macromolecules* **2009,** *42*, 6741-6747.
38. Greczynski, G.; Kugler, T.; Keil, M.; Osikowicz, W.; Fahlman, M.; Salaneck, W. R., Photoelectron Spectroscopy of Thin Films of PEDOT-PSS Conjugated Polymer Blend: A Mini-Review and Some New Results. *J. Electron. Spectrosc. Relat. Phenom.* **2001,** *121*, 1-17.
39. Huang, J. S.; Miller, P. F.; Wilson, J. S.; de Mello, A. J.; de Mello, J. C.; Bradley, D. D. C., Investigation of the Effects of Doping and Post-Deposition Treatments on the Conductivity, Morphology, and Work Function of Poly(3,4-ethylenedioxythiophene)/Poly(styrene sulfonate) Films. *Adv. Funct. Mater.* **2005,** *15*, 290-296.
40. Li, G.; Shrotriya, V.; Huang, J. S.; Yao, Y.; Moriarty, T.; Emery, K.; Yang, Y., High-Efficiency Solution Processable Polymer Photovoltaic Cells by Self-Organization of Polymer Blends. *Nat. Mater.* **2005,** *4*, 864-868.
41. Onsager, L., Deviations from Ohm's Law in Weak Electrolytes. *The Journal of Chemical Physics* **1934,** *2*, 599-615.
42. Braun, C. L., Electric-Field Assisted Dissociation of Charge-Transfer States as a Mechanism of Photocarrier Production. *J. Chem. Phys.* **1984,** *80*, 4157-4161.
43. Onsager, L., Initial Recombination of Ions. *Phys. Rev.* **1938,** *54*, 554-557.
44. Melz, P. J., Photogeneration in Trinitrofluorenone-Poly(N-Vinylcarbazole). *J. Chem. Phys.* **1972,** *57*, 1694-1699.
45. Goliber, T. E.; Perlstein, J. H., Analysis of Photogeneration in a Doped Polymer System in Terms of a Kinetic-Model for Electric-Field-Assisted Dissociation of Charge-Transfer States. *J. Chem. Phys.* **1984,** *80*, 4162-4167.
46. Langevin, P., Recombinaison Et Mobilités Des Ions Dans Les Gaz. *Annales de Chimie et de Physique* **1903,** *28*, 433-530.
47. Barth, S.; Bässler, H.; Scherf, U.; Müllen, K., Photoconduction in Thin Films of a Ladder-Type Poly-Para-Phenylene. *Chem. Phys. Lett.* **1998,** *288*, 147-154.
48. Arkhipov, V. I.; Emelianova, E. V.; Bässler, H., Dopant-Assisted Charge Carrier Photogeneration in Conjugated Polymers. *Chem. Phys. Lett.* **2003,** *372*, 886-892.
49. Arkhipov, V. I.; Heremans, P.; Bässler, H., Why Is Exciton Dissociation So Efficient at the Interface between a Conjugated Polymer and an Electron Acceptor? *Appl. Phys. Lett.* **2003,** *82*, 4605-4607.
50. Nenashev, A. V.; Baranovskii, S. D.; Wiemer, M.; Jansson, F.; Österbacka, R.; Dvurechenskii, A. V.; Gebhard, F., Theory of Exciton Dissociation at the Interface between a Conjugated Polymer and an Electron Acceptor. *Phys. Rev. B* **2011,** *84*, 035210.
51. Rubel, O.; Baranovskii, S. D.; Stolz, W.; Gebhard, F., Exact Solution for Hopping Dissociation of Geminate Electron-Hole Pairs in a Disordered Chain. *Phys. Rev. Lett.* **2008,** *100*, 196602.
52. Miller, A.; Abrahams, E., Impurity Conduction at Low Concentrations. *Physical Review* **1960,** *120*, 745-755.
53. Wiemer, M.; Nenashev, A. V.; Jansson, F.; Baranovskii, S. D., On the Efficiency of Exciton Dissociation at the Interface between a Conjugated Polymer and an Electron Acceptor. *Appl. Phys. Lett.* **2011,** *99*, 013302.
54. Im, C.; Tian, W.; Bässler, H.; Fechtenkotter, A.; Watson, M. D.; Müllen, K., Photoconduction in Organic Donor-Acceptor Systems. *J. Chem. Phys.* **2003,** *119*, 3952-3957.
55. Veenstra, S. C. Electronic Structure of Molecular Systems : From Gas Phase to Thin Films to Devices. Phd thesis, University of Groningen, 2002.
56. Schwarz, C.; Tscheuschner, S.; Frisch, J.; Winkler, S.; Koch, N.; Bässler, H.; Köhler, A., Role of the Effective Mass and Interfacial Dipoles on Exciton Dissociation in Organic Donor-Acceptor Solar Cells. *Phys. Rev. B* **2013,** *87*, 155205.

57. Emelianova, E. V.; van der Auweraer, M.; Bässler, H., Hopping Approach Towards Exciton Dissociation in Conjugated Polymers. *J. Chem. Phys.* **2008,** *128*, 224709
58. Albrecht, U.; Bässler, H., Yield of Geminate Pair Dissociation in an Energetically Random Hopping System. *Chem. Phys. Lett.* **1995,** *235*, 389-393.
59. Offermans, T.; Meskers, S. C. J.; Janssen, R. A. J., Monte-Carlo Simulations of Geminate Electron-Hole Pair Dissociation in a Molecular Heterojunction: A Two-Step Dissociation Mechanism. *Chem. Phys.* **2005,** *308*, 125-133.
60. Barth, S.; Hertel, D.; Tak, Y. H.; Bässler, H.; Horhold, H. H., Geminate Pair Dissociation in Random Organic Systems. *Chem. Phys. Lett.* **1997,** *274*, 165-170.
61. Hoffmann, S. T.; Bässler, H.; Köhler, A., What Determines Inhomogeneous Broadening of Electronic Transitions in Conjugated Polymers? *J. Phys. Chem. B* **2010,** *114*, 17037-17048.
62. Köhler, A.; Hoffmann, S. T.; Bässler, H., An Order-Disorder Transition in the Conjugated Polymer Meh-Ppv. *J. Am. Chem. Soc.* **2012,** *134*, 11594-11601.
63. Barth, S.; Bässler, H., Intrinsic Photoconduction in PPV-Type Conjugated Polymers. *Phys. Rev. Lett.* **1997,** *79*, 4445-4448.
64. Deibel, C.; Strobel, T.; Dyakonov, V., Origin of the Efficient Polaron-Pair Dissociation in Polymer-Fullerene Blends. *Phys. Rev. Lett.* **2009,** *103*, 036402.
65. Mihailetchi, V. D.; Xie, H. X.; de Boer, B.; Koster, L. J. A.; Blom, P. W. M., Charge Transport and Photocurrent Generation in Poly(3-Hexylthiophene): Methanofullerene Bulk-Heterojunction Solar Cells. *Adv. Funct. Mater.* **2006,** *16*, 699-708.
66. Kirchartz, T.; Pieters, B. E.; Taretto, K.; Rau, U., Mobility Dependent Efficiencies of Organic Bulk Heterojunction Solar Cells: Surface Recombination and Charge Transfer State Distribution. *Phys. Rev. B* **2009,** *80*, 035334.
67. Silva, C., Organic Photovoltaics Some Like It Hot. *Nat. Mater.* **2013,** *12*, 5-6.
68. van der Hofstad, T. G. J.; Di Nuzzo, D.; van den Berg, M.; Janssen, R. A. J.; Meskers, S. C. J., Influence of Photon Excess Energy on Charge Carrier Dynamics in a Polymer-Fullerene Solar Cell. *Adv. Energy Mat.* **2012,** *2*, 1095-1099.
69. Bakulin, A. A.; Rao, A.; Pavelyev, V. G.; van Loosdrecht, P. H. M.; Pshenichnikov, M. S.; Niedzialek, D.; Cornil, J.; Beljonne, D.; Friend, R. H., The Role of Driving Energy and Delocalized States for Charge Separation in Organic Semiconductors. *Science* **2012,** *335*, 1340-1344.
70. Vandewal, K.; Albrecht, S.; Hoke, E. T.; Graham, K. R.; Widmer, J.; Douglas, J. D.; Schubert, M.; Mateker, W. R.; Bloking, J. T.; Burkhard, G. F.; Sellinger, A.; Fréchet, J. M. J.; Amassian, A.; Riede, M. K.; McGehee, M. D.; Neher, D.; Salleo, A., Efficient Charge Generation by Relaxed Charge-Transfer States at Organic Interfaces. *Nat. Mater.* **2013,** *advance online publication*.
71. Köhler, A.; dos Santos, D. A.; Beljonne, D.; Shuai, Z.; Brédas, J. L.; Holmes, A. B.; Kraus, A.; Müllen, K.; Friend, R. H., Charge Separation in Localized and Delocalized Electronic States in Polymeric Semiconductors. *Nature* **1998,** *392*, 903-906.
72. Carsten, B.; Szarko, J. M.; Lu, L. Y.; Son, H. J.; He, F.; Botros, Y. Y.; Chen, L. X.; Yu, L. P., Mediating Solar Cell Performance by Controlling the Internal Dipole Change in Organic Photovoltaic Polymers. *Macromolecules* **2012,** *45*, 6390-6395.
73. Carsten, B.; Szarko, J. M.; Son, H. J.; Wang, W.; Lu, L. Y.; He, F.; Rolczynski, B. S.; Lou, S. J.; Chen, L. X.; Yu, L. P., Examining the Effect of the Dipole Moment on Charge Separation in Donor-Acceptor Polymers for Organic Photovoltaic Applications. *J. Am. Chem. Soc.* **2011,** *133*, 20468-20475.
74. Aarnio, H.; Sehati, P.; Braun, S.; Nyman, M.; de Jong, M. P.; Fahlman, M.; Österbacka, R., Spontaneous Charge Transfer and Dipole Formation at the Interface between P3HT and PCBM. *Adv. Energy Mat.* **2011,** *1*, 792-797.
75. Marchiori, C. F. N.; Koehler, M., Dipole Assisted Exciton Dissociation at Conjugated Polymer/Fullerene Photovoltaic Interfaces: A Molecular Study Using Density Functional Theory Calculations. *Synth. Met.* **2010,** *160*, 643-650.

76. Salzmann, I.; Heimel, G.; Duhm, S.; Oehzelt, M.; Pingel, P.; George, B. M.; Schnegg, A.; Lips, K.; Blum, R. P.; Vollmer, A.; Koch, N., Intermolecular Hybridization Governs Molecular Electrical Doping. *Phys. Rev. Lett.* **2012,** *108*, 035502.
77. Aryanpour, K.; Psiachos, D.; Mazumdar, S., Theory of Interfacial Charge-Transfer Complex Photophysics in π-Conjugated Polymer-Fullerene Blends. *Phys. Rev. B* **2010,** *81*, 085407.
78. Goris, L.; Haenen, K.; Nesladek, M.; Wagner, P.; Vanderzande, D.; De Schepper, L.; D'Haen, J.; Lutsen, L.; Manca, J. V., Absorption Phenomena in Organic Thin Films for Solar Cell Applications Investigated by Photothermal Deflection Spectroscopy. *J. Mater. Sci.* **2005,** *40*, 1413-1418.
79. Drori, T.; Holt, J.; Vardeny, Z. V., Optical Studies of the Charge Transfer Complex in Polythiophene/Fullerene Blends for Organic Photovoltaic Applications. *Phys. Rev. B* **2010,** *82*, 075207.
80. Drori, T.; Sheng, C. X.; Ndobe, A.; Singh, S.; Holt, J.; Vardeny, Z. V., Below-Gap Excitation of Pi-Conjugated Polymer-Fullerene Blends: Implications for Bulk Organic Heterojunction Solar Cells. *Phys. Rev. Lett.* **2008,** *101*.
81. Moghe, D.; Yu, P.; Kanimozhi, C.; Patil, S.; Guha, S., Charge Transfer Complex States in Diketopyrrolopyrrole Polymers and Fullerene Blends: Implications for Organic Solar Cell Efficiency. *Appl. Phys. Lett.* **2011,** *99*, 233307.
82. Schwarz, C. Entwicklung Eines Systems zur Messung der Feldabhängigen Ladungsträgertrennung in Organischen Halbleitern. Diplomarbeit, Uni Bayreuth, 2011.
83. Conchillo, B. A. Fabrication, Characterization and Modelling of Organic Electroluminescent Diodes with Blue Emission. Application to the Design and Manufacturing of Organic Displays. PhD Thesis, Universidad Rey Juan Carlos, 2008.
84. Cravino, A.; Schilinsky, P.; Brabec, C. J., Characterization of Organic Solar Cells: The Importance of Device Layout. *Adv. Funct. Mater.* **2007,** *17*, 3906-3910.
85. Haskal, E. I.; Vestweber, H.; Schmid, H.; Seidler, P. F., Substrate Designs and Contacts for Organic Light-Emitting Displays. In *SPIE Conference on Organic Light-Emitting Materials and Devices II*, San Diego, California, 1998.
86. Kim, M. S.; Kang, M. G.; Guo, L. J.; Kim, J., Choice of Electrode Geometry for Accurate Measurement of Organic Photovoltaic Cell Performance. *Appl. Phys. Lett.* **2008,** *92*, 133301.
87. Mallajosyula, A. T.; Srivastava, N.; Iyer, S. S. K.; Mazhari, B., Characterization of Matrix and Isolated Organic Solar Cells. *Sol. Energy Mater. Sol. Cells* **2010,** *94*, 1319-1323.

4. Überblick der Teilarbeiten

In dieser Arbeit wird der Prozess der Ladungsträgertrennung in organischen Donor-Akzeptor Solarzellen und dabei auftretende Wechselwirkungen zwischen den Donor- und Akzeptormaterialien an der gemeinsamen Grenzfläche untersucht. Das grundlegende Ziel dieser Arbeit ist den physikalischen Prozess der Ladungsträgertrennung besser zu verstehen. Mit den neu erlangten Erkenntnissen können langfristig hocheffiziente, neue Solarzellenmaterialien und Bauteilarchitekturen gezielt entwickelt werden.

In den durchgeführten Experimenten wurde dazu große Aufmerksamkeit auf ein möglichst breit angelegtes Materialsystem gelegt (siehe Abbildung 10), in dem sich Materialparameter systematisch unterscheiden, sodass ein größtmöglicher Wert an vergleichbaren, gemeinsamen Eigenschaften vorhanden bleibt. Nur so lässt sich sicherstellen, dass die experimentellen Ergebnisse eine große Allgemeingültigkeit besitzen, um damit theoretische Modelle zu testen und auch weiterzuentwickeln.

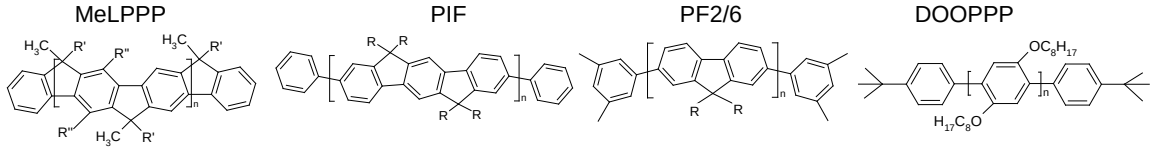

Abbildung 10: Strukturformeln und Abkürzungen verschiedener Poly(para-phenylene), wie sie in dieser Arbeit als Donor Materialsystem häufig verwendet werden. MeLPPP = methyl-ladder-type-poly(*p*-phenylene), PIF = poly(indeno-fluorene), PF2/6=ethyl-hexyl-poly(fluorene), DOOPPP = Dioctyloxy-poly(*p*-phenylene) (R = 2-ethylhexyl, R‘ = 1,4-C_6H_4-*n*-$C_{10}H_{21}$, R‘‘ = -*n*-C_6H_{13}). Die Konjugationslänge der Polymere nimmt von MeLPPP hin zu DOOPPP kontinuierlich ab, da die zunehmende Anzahl von nicht verbrückten Einzelbindungen zwischen den verbrückten Segmenten eine Verdrehung des Polymerrückgrads und damit eine Reduktion der Konjugation verursachen.

Die Solarzellenexperimente wurden bewusst an technisch einfachen Zweischichtsolarzellen durchgeführt, die sich im Idealfall durch eine definierte Donor-Akzeptor Grenzfläche beschreiben lassen. Dies ermöglicht, im Gegensatz zu den sonst häufig verwendeten Blendsolarzellen, eine einfachere Analyse der Ladungsträgertrennung. In der Zweischichtsolarzelle können störende Einflüsse der D-A-Morphologie und der „nongeminate“ Rekombination, also der Rekombination eines Lochs und Elektrons verschiedenen Ursprungs auf dem Weg zu den Elektroden vernachlässigt werden.

Zusätzlich wurden alle in dieser Arbeit beschriebenen elektrischen Messungen an speziell präparierten Solarzellen ohne Kanteneffekte durchgeführt, was eine exakte Messung der auftretenden Fotoströme auch bei sehr hohen elektrischen Feldstärken ermöglichte. Die Messungen bei großen Feldstärken waren in den Experimenten von großer Bedeutung, um bestehende theoretische Modelle zur Ladungsträgertrennung erstmalig konsequent über einen weiten Feldstärkebereich und bei verschiedensten Materialkombinationen systematisch zu überprüfen und sie anschließend anzupassen.

Aufbauend auf insgesamt vier Teilarbeiten untersucht diese Doktorarbeit experimentell und theoretisch den komplexen Prozess der Ladungsträgertrennung in organischen Solarzellen anhand elektrischer Messungen, optischer Charakterisierungen und Modellierung. In Kapitel 5 werden erstmalig feldabhängige Quantenausbeuten verschiedener Poly(*p*-phenylene) in Zweischichtsolarzellen mit den Akzeptoren C_{60} oder Trinitroflurenon (TNF) bis zu einer Sättigung des Fotostroms bei hohen elektrischen Feldstärken gemessen und der Zusammenhang zwischen dem Grad der Konjugation eines Polymers und der Neigung zur Ladungsträgertrennung hergestellt. Die Experimente in Kapitel 6 entwickeln die in Kapitel 5 aufgestellten Zusammenhänge weiter. Verschiedene theoretische Modelle werden an den Messdaten getestet und schließlich wird ein zusammenhängendes Modell präsentiert, das die Ladungsträgertrennung in allen betrachteten Materialkombinationen zufriedenstellend beschreibt. Zusätzlich werden in dem Modell die Beiträge der wesentlichen Materialparameter, wie der Konjugationslänge und der Stärke der Grenzflächendipole, quantifiziert. In Kapitel 7 wird der Einfluss der Akzeptorstärke und -position innerhalb des D-A-Copolymers auf die Ladungsträgertrennung in Zweischichtsolarzellen mit C_{60} untersucht. Kapitel 8 beschreibt abschließend elektronische Wechselwirkungen zwischen elektrisch leitfähigen Donor- und Akzeptormaterialien an einer gemeinsamen Grenzfläche und ihre Einflüsse auf die Ladungsträgertrennung in organischen Solarzellen.

In den folgenden Unterabschnitten werden die vier Teilarbeiten genauer vorgestellt.

“Does conjugation help exciton dissociation? A study on poly(*p*—phenylene)s in planar heterojunctions with C_{60} or TNF”

Diese Teilarbeit untersucht experimentell den Zusammenhang zwischen der Konjugation eines Polymers und deren Einfluss auf die Ladungsträgertrennung in D-A-Zweischichtsolarzellen. Dazu wird erstmalig an den auf Poly(*p*-phenylen)-basierenden Polymeren MeLPPP, PIF und DOOPPP in Verbindung mit jeweils C_{60} oder TNF als Akzeptor die feldabhängige Quantenausbeute systematisch bis hin zur Sättigung des Fotostroms bei hohen Feldstärken gemessen. Eine Besonderheit dieses Materialsystems ist, dass sich die Donor-Polymere neben der unterschiedlichen Konjugationslänge auch

hinsichtlich ihrer energetischen Unordnung unterscheiden. Mit abnehmender Konjugationslänge von MeLPPP über PIF zu DOOPPP lässt sich anhand von Frank-Condon-Analysen der Fluoreszenzspektren eine zunehmende Verbreiterung der energetischen Zustandsdichte σ von 28 meV, über 45 meV auf 106 meV bestimmen.

Von (ITO/PEDOT:PSS/Polymer (40 nm)/Akzeptor (40 nm)/Aluminium)-Zweischichtsolarzellen werden I-U-Kennlinien bis zu hohen negativen Spannungen aufgenommen und aus dem Fotostrom die feldabhängige Quantenausbeute berechnet. Um eine gezielte Analyse der Quantenausbeuten zu ermöglichen, erfolgt die Anregung der Solarzellen unter monochromatischer Beleuchtung selektiv in einem Spektralbereich, in dem entweder nur der Donor oder nur der Akzeptor absorbiert. Bei den Solarzellen mit C_{60} als Akzeptor wird entsprechend die niederenergetische C_{60}-Absorption bei 2,2 eV angeregt. Die Solarzellen mit TNF als Akzeptor werden im jeweiligen Absorptionspeak des Polymers angeregt. Unter der Annahme einer Exzitondiffusionslänge zur D-A-Grenzfläche von circa 10 nm und unter Berücksichtigung des jeweiligen Absorptionsspektrums errechnet sich aus dem maximal gemessenen Fotostrom in Sättigung eine interne Quanteneffizienz nahe 100% für alle untersuchten D-A-Kombinationen. Das bedeutet, dass ab der Sättigungsfeldstärke zu größeren Feldstärken hin tatsächlich alle gebildeten Elektron-Loch-Paare aufgespalten werden. Die Sättigungsfeldstärke ergibt sich in der doppellogarithmischen Auftragung der feldabhängigen Quantenausbeute aus dem Schnittpunkt der Tangente an die ansteigende Kurve bei kleinen Feldstärken und der Tangenten an die Kurve bei hohen Feldstärken im Sättigungsbereich. Für beide Akzeptoren zeigt MeLPPP die niedrigste Sättigungsfeldstärke, gefolgt von PIF. DOOPPP besitzt die höchste Sättigungsfeldstärke. Im Langevin-Bild klassischer Punktladungen, bei dem Ladungen erfolgreich getrennt werden, falls das Potential des äußeren elektrischen Feldes größer oder gleich des Coulombpotentials ist, kann man aus den gemessenen Sättigungsfeldstärken die erforderlichen Elektron-Loch-Abstände und Bindungsenergien berechnen. Hierbei ergeben für die D-A-Kombinationen bei MeLPPP große Elektron-Loch-Abstände von 9 nm aber nur 2 nm für DOOPPP. Entsprechend dazu sind Elektron und Loch bei den D-A-Kombinationen mit MeLPPP mit 50 meV nur sehr schwach gebunden und können dadurch leichter dissoziieren, wohingegen für die DOOPPP-Kombinationen 200 meV Bindungsenergie zu überwinden sind, was eine erfolgreiche Ladungsträgertrennung stark minimiert.

Bei der Anregung der Donor-Polymere ist die Energiedifferenz zwischen LUMO-Donor und LUMO-Akzeptor konsequent größer als der Energieunterschied zwischen HOMO-Akzeptor und HOMO-Donor bei der Anregung des Akzeptors. Bei Anregung der Polymere sind die jeweiligen Sättigungsfeldstärken durchgehend niedriger. Dies könnte als ein Indiz dafür gewertet werden, dass ein größerer Energieunterschied beim Ladungstransfer die Ladungsträgertrennung unterstützt.

Die Kernergebnisse zeigen, dass eine große Konjugationslänge bei Polymeren mit einem gleichzeitig hohen Grad an energetischer Ordnung die Ladungsträgertrennung entscheidend unterstützt. Das bei der Anregung gebildete, Coulombgebundene Loch des Exzitons kann innerhalb der effektiven Konjugationslänge des Polymers auf der Kette schnell delokalisieren, was den mittleren Elektron-Loch-Abstand vergrößert. Hierdurch wird die Bindungsenergie minimiert und die Ladungsträgertrennung erleichtert. Wäre dagegen ein hoher Grad der energetischen Unordnung zur Dissoziation förderlich, so hätte man in der Donorreihe von MeLPPP zu DOOPPP statt einer ansteigenden, eine abnehmende Sättigungsfeldstärke beobachten müssen.

“Role of the effective mass and interfacial dipoles on exciton dissociation in organic donor acceptor solar cells”

In dieser Teilarbeit werden fortführende Untersuchungen der Ladungsträgertrennung in D-A-Zweischichtsolarzellen durch Messungen der feldabhängigen Quantenausbeute an einem erweiterten System von Donormaterialien mit C_{60} als Akzeptor gemacht. Damit lassen sich zwischen Effekten der Konjugationslänge des Polymers und durch energetische Ordnung verursachte Auswirkungen auf die Ladungsträgertrennung weiter unterscheiden. Abschließend wird ein geschlossenes Modell der Ladungsträgertrennung vorgestellt, das Delokalisationseffekte in konjugierten Polymeren, sowie auch auftretende Grenzflächendipole an der D-A-Grenzfläche berücksichtigt und alle erhaltenen Messergebnisse beschreibt.

Das auf Poly(*p*-phenylen)-basierende Donor-Materialsystem bestehend aus MeLPPP, PIF und DOOPPP wird um PF2/6 ergänzt. Um den alleinigen Einfluss der Konjugationslänge auf die Ladungsträgertrennung zu untersuchen, wird zusätzlich ein MeLPP-Dimer mit dem zugehörigen MeLPP-Polymer verglichen. Zusätzlich wird das D-A-Copolymer PCDTBT (Poly[[9-(1-octylnonyl)-9H-carbazole-2,7-diyl]-2,5-thiopenediyl-2,1,3-benzothiadiazole-4,7-diyl-2,5-thiophenediyl] in die Versuchsreihe aufgenommen, da dafür in der Fachliteratur bereits sehr gute Wirkungsgrade berichtet wurden. Aus allen Donor-Materialien werden (ITO/PEDOT:PSS/Donor (40 nm)/C_{60} (40 nm)/Aluminium)-Zweischichtsolarzellen hergestellt, I-U-Kennlinien unter monochromatischer Beleuchtung bei 2,2 eV aufgenommen und die feldabhängigen Quantenausbeuten berechnet. Für die Polymere werden zusätzlich mit Ultraviolett-Photoelektronen-Spektroskopie-(UPS)-Messungen die Grenzflächendipole an der jeweiligen Polymer/C_{60}-Grenzfläche ermittelt.

Innerhalb der Poly(*p*-phenylen)-Donor-Materialserie nimmt die Sättigungsfeldstärke von MeLPPP, dem Polymer mit der längsten effektiven Konjugationslänge, über PIF und PF2/6 zu DOOPPP mit der kürzesten Konjugationslänge systematisch zu. Das MeLPP-Dimer hat eine größere Sättigungsfeldstärke als das zugehörige MeLPP-Polymer. PCDTBT besitzt von allen Donor-Materialien in Verbindung mit C_{60} als Akzeptor die kleinste Sätti-

gungsfeldstärke. Diese Messergebnisse an D-A-Solarzellen zeigen, dass besonders eine ausgedehnte Konjugation des Polymers und eine damit verbundene Delokalisation des Coulomb-gebundenen Lochs entlang der Polymerkette die Ladungsträgertrennung maßgeblich begünstigt und über Effekte der energetischen Unordnung dominiert. Die Sättigungsfeldstärke ist dabei innerhalb der Poly(*p*-phenylen)-Polymer-Materialserie exponentiell von der reziproken effektiven Konjugationslänge abhängig; große effektive Konjugationslängen führen zu kleinen Sättigungsfeldstärken.

Die experimentell gemessenen feldabhängigen Quantenausbeuten werden zum theoretischen Verständnis der Ladungsträgertrennung mit bestehenden Modellen simuliert und verglichen. Das in der bisherigen Fachliteratur häufig verwendete Onsager-Braun-Modell für D-A-Kombinationen beschreibt alle gemessenen Kurvenverläufe der feldabhängigen Quantenausbeuten nur unzureichend. Zudem liegen die verwendeten Fitparameter in untypischen physikalischen Größenordnungen. Der verlaufsmäßig beste Fit für DOOPPP mit C_{60} liefert Parameterwerte für das Produkt aus Ladungsträgermobilität und Lebensdauer des CT-Zustands, die eine deutlich zu hohe Charge-Transfer-Lebenszeiten von 30 ms ergeben, wenn man für dieses ungeordnete Material eine realistische Mobilität von 10^{-5} cm^2 $V^{-1}s^{-1}$ annimmt. Typischerweise misst man für die Lebensdauer eines CT-Zustandes nur einige zehn Nanosekunden. Da die Konjugationslänge eines Polymers die Ladungsträgertrennung, wie in den Experimenten gezeigt, deutlich beeinflusst, ist eine Berücksichtigung der Delokalisationseffekte des gebundenen Lochs auf der konjugierten Polymerkette auch in den Modellen nötig. Die dazugehörige Pionierarbeit lieferte Arkhipov, dessen Modell später von Nenashev und Wiemer nochmals aufgegriffen und verfeinert wurde. Alle Modelle basieren in der Grundidee auf der Delokalisation des gebundenen Lochs, das quantenmechanische Nullpunktschwingungen auf der Polymerkette im Coulombpotential seines zugehörigen Elektrons ausführt. Die Nullpunktschwingungen sind durch eine effektive Masse charakterisiert und stellen dem dissoziierenden Loch zusätzliche, kinetische Energie zur Überwindung der Coulombbarriere zur Verfügung. Die exakte Lösung der Dissoziationswahrscheinlichkeit im einfachen effektiven-Masse-Modell nach Nenashev, wie auch Wiemers Modell, das Grenzflächendipole berücksichtigt, jedoch eine harmonische Näherung des Potentials annimmt, beschreiben die feldabhängigen Quantenausbeuten der PCDTBT/C_{60} und MeLPPP/C_{60} Kombinationen erstmalig in guter Übereinstimmung mit dem Experiment. Hierbei werden bei den Fitparametern des Dipolmodells explizit die experimentell mit UPS gemessenen Grenzflächendipole berücksichtigt, welche die Coulombanziehung der gebildeten Elektron-Loch-Paare an der D-A-Grenzfläche abschirmen und dadurch die Dissoziationswahrscheinlichkeit erhöhen. Bei den anderen Materialkombinationen können die effektive-Masse-Modelle nur den Bereich großer elektrischer Feldstärken richtig beschreiben; bei kleineren elektrischen Feldstärken ist die experimentell gemessene Quantenausbeute größer als von den Modellen vorausgesagt. Diese in den Experimenten beobachtete erhöhte Quantenausbeute erfordert auch in den theoretischen Modellen eine zusätzli-

che Dissoziationswahrscheinlichkeit. In der Annahme, dass die erhöhte Quantenausbeute von der Aufspaltung lokalisierter CT-Zustände an Defekten herrührt, werden zwei Kombinationen in Betracht gezogen. Zum einen wird das Dipolmodell mit dem klassischen Braun-Onsager-Modell kombiniert. Der resultierende Fitverlauf hat aber besonders für die D-A-Kombinationen mit höherer Sättigungsfeldstärke wenig Übereinstimmung mit den experimentellen Daten. Als weiterer Modellansatz um die experimentell zusätzlich beobachte Quantenausbeute bei niedrigen elektrischen Feldstärken zu beschreiben, wird die Kombination des Dipolmodells mit Arkhipovs Fehlstellenmodell gewählt. Die Fehlstellen- oder Fallenzustände werden vor allem C_{60} zugeordnet, welches in das Donormaterial eindiffundiert ist.

Es zeigt sich, dass eine Kombination aus dem Dipolmodell in der Nenashev'schen Formulierung mit Arkhipovs Fehlstellenmodell die experimentell gemessenen feldabhängigen Quantenausbeuten am besten beschreibt. Die Kombination der beiden effektive-Masse-Modelle ermöglicht schließlich eine geschlossene und stimmige Beschreibung der Ladungsträgertrennung in D-A-Solarzellen. Der Anteil der über Fehlstellen aufgespalteten Ladungsträger an der Gesamtdissoziationswahrscheinlichkeit ist dabei umso kleiner, je kleiner die effektive Masse des Donors ist. Hierbei zeigt sich experimentell auch, dass die effektive Masse innerhalb der Poly(*p*-phenylen)-Polymerreihe von der reziproken effektiven Konjugationslänge abhängig ist; große effektive Konjugationslängen entsprechen in den effektive-Masse-Modellen kleinen effektiven Massen.

"Influence of the excited state charge-transfer character on the exciton dissociation in donor-acceptor copolymers"

In den ersten beiden Teilarbeiten wurden überwiegend Homopolymere als Donor in einer Zweischichtgeometrie mit einem Akzeptor untersucht. Für aktuelle Anwendungen werden jedoch vor allem Copolymere als Donor mit meistens einem Fullerenakzeptor verwendet. Die Copolymere sind ihrerseits wiederum aus je einer elektronenarmen und einer elektronenreichen Wiederholungseinheit zusammengesetzt, sodass sie auch als Donor-Akzeptor-(D-A)-Copolymere bezeichnet werden. Sie zeichnen sich in der Regel durch eine Absorptionskante im roten Spektralbereich aus, was zur optimalen Nutzung der einfallenden Sonnenstrahlung von Vorteil ist.

Diese Teilarbeit beschäftigt sich daher mit alternierenden D-A-Copolymeren. Hierbei ist die Fragestellung, wie der Donor und Akzeptor bezüglich ihrer Stärke und Position beschaffen sein müssen, dass nicht nur die Absorptionskante im Vergleich zu den entsprechenden Homopolymeren reduziert, sondern auch die Ladungsträgertrennung erleichtert wird. Als ersten Schritt dazu wird in dieser Teilarbeit an einem auf Triphenylamin-(TPA)-basierenden Materialsystem der Einfluss der Position und der Stärke des Copoly-

mer-Akzeptors auf die Charge-Transfer-Charakteristik und Ladungsträgertrennung anhand optischer und elektrischer Messungen untersucht.

Ein TPA-Homopolymer (P1), das als Vergleichsgrundlage dient und zwei neuartige D-A-Copolymere mit TPA-Bausteinen werden synthetisiert. Beim ersten D-A-Copolymer bilden ein TPA, verbunden mit einem weiteren TPA, das eine stark elektronegative Dicyanovinyl-Seitengruppe besitzt, die Wiederholungseinheit (P2). Beim anderen D-A-Copolymer ist ein Thieno[3,4-b]thiophencarboxylat und ein TPA zu einem Copolymerrückgrat miteinander verknüpft (P3), welches die Wiederholungseinheit bildet. Alle Polymere werden chemischen Standardanalysen unterzogen.

Die Copolymere P2 und P3 zeigen in dünnen Filmen, sowie in verdünnten Lösungen, im Vergleich zur typischen TPA-Absorption von P1, jeweils eine zusätzliche, niederenergetische Absorptionsbande. Aufgrund der niedrigeren Energie des Übergangs und der kleinen Oszillatorenstärke handelt es sich hierbei um intramolekulare CT-Übergänge, die besonders bei P2 auf einen geringen Wellenfunktionsüberlapp zwischen der Dicyanovinyl-Seitengruppe und dem Donorrückgrat zurückzuführen sind. Die niederenergetische Absorptionsbande von P3 besitzt eine größere Oszillatorenstärke als P2 und ist zu P2 rotverschoben. Diese höhere Oszillatorenstärke bei P3 ist auf einen zusätzlichen Anteil an π-π*-Übergängen zurückzuführen, was konsistent mit stärker delokalisierten π-Orbitalen in P3 ist. Weitere Einblicke in die CT-Eigenschaften erhält man durch das Fluoreszenzverhalten. P1 und P3 besitzen ein strukturiertes Emissionsspektrum, bei denen im Film für längere Zeiten eine strukturierte, niederenergetische Emission dominiert. Bei P2 löscht der sehr starke CT-Charakter durch die Dicyanovinyl-Seitengruppe fast die komplette Fluoreszenz. Das niederenergetische Fluoreszenzspektrum ist verbreitert, unstrukturiert und mit einer Verteilung von Lebenszeiten, wie man es für eine CT-Fluoreszenz erwartet.

Die elektrische Lochleitfähigkeit der Polymere wird in elektrischen Bauteilen mit (ITO/PEDOT:PSS/Polymer/Gold)-Aufbau anhand von raumladungsbegrenzten Strommessungen (space charge limited current, SCLC-measurements) ermittelt. Hierbei zeigt P2 die niedrigste Mobilität, P3 die Größte.

Aus dem Homopolymer und den zwei Copolymeren, die als Donormaterialien dienen, werden (ITO/PEDOT:PSS/Donor (40 nm)/C_{60} (40 nm)/Aluminium)-Zweischichtsolarzellen hergestellt und I-U-Kennlinien unter AM 1.5 Sonnensimulator-Beleuchtung gemessen. Hierbei zeigt P2 in Verbindung mit C_{60} den kleinsten Kurzschlussstrom und den geringsten Wirkungsgrad, was auf Probleme bei der Ladungsträgertrennung hinweist. Für die Copolymere werden aus dem Fotostrom deshalb zusätzlich die feldabhängigen Quantenausbeuten berechnet, um die Ladungsträgertrennung genauer zu untersuchen. Hierbei ergibt sich für P2 mit dem stark ausgeprägten CT-Charakter durch die elektronegative Dicyanovinyl-Seitengruppe eine deutlich höhere Sättigungsfeldstärke als bei P3, bei

dem der schwächere Akzeptor in das Polymerrückgrat eingebaut ist. Das bedeutet, dass die Elektron Loch-Paare in der P2/C_{60}-Kombination stärker als bei der P3/C_{60}-Kombination gebunden sind.

Die feldabhängigen Quantenausbeuten der D-A-Copolymere werden nach den bisherigen Erfahrungen der bereits beschriebenen anderen Teilarbeiten zur ersten, groben Untersuchung mit dem Dipol-Modell nach Wiemer analysiert. Die Fitparameter zeigen, dass das D-A-Copolymer P3 eine größere effektive Konjugationslänge als P2 besitzt, was sich in einer kleineren effektiven Masse widerspiegelt. Dieses Ergebnis ist in Übereinstimmung mit den Absorptionsmessungen und lässt auf eine bessere Delokalisation in P3 schließen. P2 besitzt dagegen die größeren Grenzflächendipole, was sich mit dem starken CT-Charakter der optischen Messungen deckt.

Die Untersuchung des Einflusses des CT-Charakters an TPA basierten D-A-Copolymeren zeigt, dass ein schwächerer, innerhalb des Copolymers gut mit dem Donor auf dem Polymerrückgrad konjugierter Akzeptor die Ladungsträgertrennung erleichtert. Eine stark elektronegative Dicyanovinyl-Seitengruppe führt dagegen zu stärker gebundenen Elektron-Loch-Paaren und kleineren Lochmobilitäten, die mit einem schlechteren Wirkungsgrad einhergehen.

“Ground state bleaching at Donor-Acceptor interfaces”

In dieser Teilarbeit werden systematische Absorptionsmessungen an D-A-Grenzflächen durchgeführt, die weitere Einblicke in die Ladungsträgertrennung ermöglichen. Aus den Experimenten wird deutlich, dass die Donor- und Akzeptormaterialien an einer gemeinsamen Grenzfläche im Grundzustand elektronisch miteinander wechselwirken und sich somit ein Grundzustandskomplex ausbildet, der die Ladungsträgertrennung unterstützt.

Quarzglassubstrate werden durch Spincoaten mit circa 40 nm dicken Polymerfilmen beschichtet. Eine Hälfte des Glassubstrates wird anschließend vollständig vom Polymer befreit und orthogonal dazu wird ein Akzeptorfilm aufgedampft. Man erhält auf dem Quarzglas einen Bereich mit einem reinen Polymerfilm, einen reinen Akzeptorfilm, einen Bereich, in dem die jeweiligen Filme übereinander liegen und eine D-A-Grenzfläche bilden und ein unbeschichtetes Quarzglas zur Referenz. Als erstes Kontrollexperiment wird der Akzeptorfilm in der gleichen Anordnung, aber auf der Rückseite des Quarzglases aufgedampft, sodass der Donor- und Akzeptorfilm durch das Quarzglas getrennt sind. Anschließend wird die Absorption der einzelnen Filmbereiche gemessen und die gemessene Absorption der D-A-Zweischicht mit der Summe der Absorption der beiden Einzelschichten verglichen.

Hierbei zeigt sich an einer Kombination aus substituiertem Poly-(*p*-phenylenevinylen) (MEH-PPV) und TNF, dass sich die optische Dichte beider Materialien bei direktem Kontakt an der gemeinsamen Grenzfläche nicht addiert, sondern dass ein signifikanter Anteil, besonders der Extinktion des Donors, fehlt. Im Kontrollexperiment der durch das Quarzglas getrennten Donor- und Akzeptorfilme ist die gemessene Absorption der zwei getrennten Schichten gleich der Summe der Absorption der Einzelschichten. Weitere Kontrollexperimente zeigen, dass die Schichtdicke der D-A-Zweischicht gleich der Summe der Einzelschichtdicken ist und dass die Absorptionsänderung nicht auf eine Veränderung der Polymerabsorption während des Aufdampfprozesses durch Wärmeeinwirkung zurückzuführen ist. Absorptionsmessungen in einer Ulbrichtkugel zeigen ferner, dass Streueffekte vernachlässigbar klein sind.

Weitere Versuche an einer MeLPPP-Perylendiimid-Derivat-(PDI)-Kombination, deren Einzelmaterialien ein sehr strukturiertes Absorptionsspektrum besitzen, zeigen deutlich, dass durch die D-A-Wechselwirkung sowohl ein gewisser Anteil der Absorption des Donor-, als auch des Akzeptormaterials fehlt. Versuche an unlöslichem PPV, das durch die Konvertierung eines Precursormaterials hergestellt wurde, in Kombination mit einem anschließend aufgedampftem C_{60} zeigen ebenfalls eine reduzierte Extinktion in der Zweischicht. Entfernt man von der harten PPV-Schicht allerdings die C_{60}-Schicht mit einem trockenen Wattestäbchen, so misst man wieder die ursprüngliche, unveränderte PPV-Absorption. Dieses Experiment zeigt, dass die D-A-Wechselwirkung ausschließlich an der Grenzfläche stattfindet und eine reversible Wechselwirkung ist. Zeitabhängige Dichtefunktionaltheorie-Rechnungen an einem MEH-PV-Trimer und einem darüber liegenden TNF Molekül belegen ebenfalls eine Abnahme der Extinktion bei der Bildung eines D-A-Komplexes.

Experimente an den Poly(*p*-phenylene)n MeLPPP, PIF und DOOPPP in Kombination mit TNF können so interpretiert werden, dass sich Grundzustandskomplexe bilden, indem das HOMO des Polymers und das LUMO des Akzeptors miteinander wechselwirken. Je kleiner der Energieunterschied des HOMO des Polymers und des LUMO des Akzeptors ist, desto größer ist der experimentell beobachtete Anteil der fehlenden Extinktion des Polymers. Ein großer Anteil fehlender Extinktion korreliert in den Experimenten außerdem direkt mit niedrigen Sättigungsfeldstärken der feldabhängigen Quantenausbeute der zugehörigen D-A-Zweischichtsolarzelle. Das bedeutet, dass in Materialkombinationen mit einem großen Anteil fehlender Absorption gebildete Elektron-Loch-Paare leichter getrennt werden. Dadurch lässt sich auf eine aktive Beteiligung des D-A-Komplexes bei der Ladungsträgertrennung schließen.

Die Dichtefunktionaltheorie-Rechnungen bescheinigen für das Modellsystem aus dem MEH-PV Trimer und dem TNF eine Absorption, die im Wesentlichen auf einem HOMO nach LUMO+4 Übergang beruht. Dieser HOMO nach LUMO+4 Übergang des D-A-Systems „ersetzt“ gewissermaßen die S_1 Absorption, die das MEH-PV in Abwesenheit

des Akzeptors hat. Da das LUMO+4 auch etwas Elektronendichte auf dem TNF hat, besitzt der HOMO->LUMO+4 Übergang auch etwas Charge-Transfer-Charakter. Entsprechend hat der HOMO->LUMO+4 Übergang eine Oszillatorenstärke, die im Vergleich zur S_1 Absorption des MEH-PVs reduziert ist. Die Rechnungen belegen weiterhin die Existenz eines Zustands mit verschwindender Oszillatorenstärke, der unterhalb der Absorption von Donor oder Akzeptor liegt, der als Charge-Transfer-Komplex betrachtet werden darf. Dieser führt zur Ausbildung eines treppenförmigen Energieniveausystems zwischen dem Donormaterial, dem D-A-Komplex und dem Akzeptormaterial. Bei einer Anregung des Donors kann beim Ladungstransfer das Elektron über den D-A-Komplex auf den Akzeptor übertragen werden, wodurch ein gebundener Elektron-Loch-Zustand („geminate pair“) gebildet wird. In analoger Weise wird bei der Anregung des Akzeptors ein Loch über den D-A-Komplex auf den Donor übertragen. Wird trotz der erniedrigten Oszillatorenstärke der D-A-Komplex direkt angeregt, wird das Elektron auf den Akzeptor und das Loch auf den Donor übertragen. Der D-A-Komplex wirkt bei der Bildung des gebundenen Elektron-Loch-Zustandes in allen Fällen als räumlicher Distanzhalter, der den anfänglichen Elektron-Loch-Abstand signifikant vergrößert. Damit wird die Rekombination unterdrückt und die Ladungsträgertrennung erleichtert, da sich mit zunehmendem Elektron-Loch-Abstand die energetisch zu überwindende Barriere des Coulombpotentials erniedrigt.

Zusammenfassend zeigt diese Teilarbeit, dass elektronische Wechselwirkungen zwischen Donor- und Akzeptormaterialien an einer gemeinsamen Grenzfläche zur Ausbildung von Grundzustandskomplexen mit reduzierter Absorption führen. Die Absorptionsexperimente zeigen deutlich, dass in Materialkombinationen mit einem großen Anteil reduzierter Extinktion die Elektron-Loch-Paare in den zugehörigen Solarzellen leichter getrennt werden. Einfache Absorptionsmessungen können damit in Zukunft schnelle und kostengünstige Abschätzungen über die Eignung verschiedener Materialkombinationen für die spätere Solarzellenanwendung liefern.

Eigene Beiträge

Diese Doktorarbeit beruht auf insgesamt vier Teilarbeiten. Davon sind drei veröffentlicht, die vierte Teilarbeit steht zur Einreichung an. Im Folgenden werden die eigenen Beiträge zu den Teilarbeiten aufgelistet.

Kapitel 5

Diese Teilarbeit ist in Advanced Materials (2012, *24*, 922-925) veröffentlicht unter dem Titel
"Does conjugation help exciton dissociation? A study on poly(*p*—phenylene)s in planar heterojunctions with C_{60} or TNF"
von Christian Schwarz, Heinz Bässler, Irene Bauer, Jan-Moritz Koenen, Eduard Preis, Ullrich Scherf, Anna Köhler

Ich habe den bestehenden Messaufbau und das Messprogramm zur Messung von I-U-Kennlinien bis zu hohen Feldstärken vom Stand meiner Diplomarbeit modifiziert und den Herstellungsprozess der Solarzellen nochmal verbessert. Dadurch konnte ich alle Solarzellen gezeigten Materialkombinationen bis zu hohen Feldstärken messen. Alle in der Teilarbeit verwendeten Proben wurden von mir gebaut und die gezeigten Daten, soweit nicht anders gekennzeichnet, wurden von mir gemessen und analysiert. Ich habe Teile des Skripts geschrieben.

Kapitel 6

Diese Teilarbeit ist in Physical Review B (2013, *87*, 155205) veröffentlicht unter dem Titel
"Role of the effective mass and interfacial dipoles on exciton dissociation in organic donor acceptor solar cells"
von Christian Schwarz, Steffen Tscheuschner, Johannes Frisch, Stefanie Winkler, Norbert Koch, Heinz Bässler, Anna Köhler

Ich habe die Solarzellen gebaut, die feldabhängigen Quantenausbeuten gemessen, analysiert und interpretiert. In den UPS-Experimenten habe ich die Probenpräparation in Berlin unterstützt. Außerdem habe ich bei der theoretischen Modellanalyse anfangs durch eigene Simulationen und später durch intensive Diskussion mitgewirkt. Ich habe Teile des Skripts geschrieben.

Kapitel 7

Diese Teilarbeit ist im Journal of Physical Chemistry C (2013, DOI: 10.1021/jp407014q) veröffentlicht unter dem Titel
"Influence of the excited state charge-transfer character on the exciton dissociation in donor-acceptor copolymers"
von Katharina Neumann, Christian Schwarz, Anna Köhler, Mukundan Thelakkat

Ich habe die optischen Messungen gemacht, die Solarzellen gebaut und gemessen. Meine Messdaten habe ich analysiert und interpretiert. Ich habe Teile des Skripts geschrieben.

Kapitel 8

Diese Teilarbeit ist zur Einreichung bereit unter dem Titel
"Ground state bleaching at donor-acceptor interfaces"
von Christian Schwarz, Felix Milan, Stephan Kümmel, Anna Köhler

Ich habe alle Proben hergestellt und gemessen. Außerdem habe ich die Messdaten analysiert und interpretiert. Ich habe den Großteil des Skripts geschrieben.

5. Does conjugation help exciton dissociation? A study on poly(*p*-phenylene)s in planar heterojunctions with C_{60} or TNF

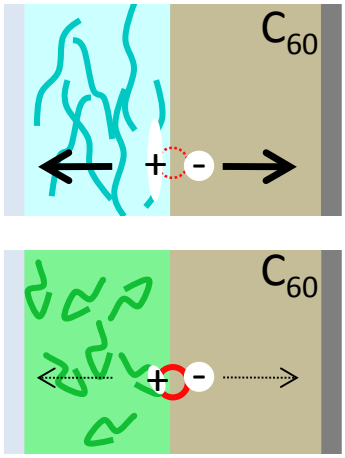

Christian Schwarz, Heinz Bässler, Irene Bauer, Jan-Moritz Koenen, Eduard Preis,

Ullrich Scherf, Anna Köhler

Veröffentlicht in

Advanced Materials 2012, *24*, 922-925

Does Conjugation Help Exciton Dissociation? A Study on Poly(*p*-phenylene)s in Planar Heterojunctions with C_{60} or TNF

*Christian Schwarz, Heinz Bässler, Irene Bauer, Jan-Moritz Koenen, Eduard Preis, Ullrich Scherf, and Anna Köhler**

The process of exciton dissociation in organic semiconductors is the key step that needs to be understood for the realization of efficient organic solar cells.[1] A systematic optimization of solar cells requires a well-founded and detailed understanding of the mechanism of exciton dissociation and its dependence on material parameters. Consequently, it is being investigated intensely.[2–11] There is widespread agreement on the elementary steps that accompany charge carrier generation at an organic molecular heterojunction.[1,12] Light absorption creates an excited state on one molecule. This is followed by electron transfer to a neighboring molecule, which results in the formation of a more or less strongly bound metastable intermolecular state. This excited state has a strong charge-transfer character and will eventually break up into free charge carriers or lead to recombination. The central question, therefore, is how to overcome the Coulombic binding energy that prevents the final separation of the opposite charges. There are studies implying that dissociation may be favored by a higher hole mobility,[13–15] which is typically associated with a larger conjugation length and a low degree of energetic disorder.[4] On the other hand, there are also reports that in certain circumstances an increased disorder or a lower hole mobility may be preferential.[16,17] Using a set of poly(*p*-phenylene)s (PPPs) as systematic model compounds, we have investigated how the conjugation length of the chromophore affects the process of charge carrier dissociation at a molecular heterojunction. In field-dependent photocurrent measurements we find the photocurrent yield to saturate at 100% at electric fields between 5×10^4 V cm^{-1} and 1×10^6 V cm^{-1}. Importantly, the saturation field that is required decreases with increasing conjugation length, implying that the excited state delocalization is of crucial importance for the yield. We conclude that the rate-limiting step of the photogeneration of charges is the formation of a loosely bound ("hot") electron–hole pair that can either be dissociated at moderate field or relax back to a tightly bound electron–hole pair.

C. Schwarz, Prof. H. Bässler, I. Bauer, Prof. A. Köhler
Experimental Physics II and Bayreuth Institute of Macromolecular Research (BIMF)
University of Bayreuth
95440 Bayreuth, Germany
E-mail: anna.koehler@uni-bayreuth.de
J.-M. Koenen, E. Preis, Prof. U. Scherf
Macromolecular Chemistry
Bergische Universität Wuppertal
42097 Wuppertal, Germany

DOI: 10.1002/adma.201104063

A systematic study requires changing as few parameters as possible. Therefore we chose the set of poly(*p*-phenylene)s (PPPs) shown in **Figure 1**a as a donor material system. Within this series, the polymer backbone is formed by the same chemical repeat unit, the phenylene, yet the rigidity of the backbone is varied by stiffening links. This results in an increased conjugation length and a narrower density of excited state energies from DOOPPP to MeLPPP, as evidenced by the reduced $S_1 \leftarrow S_0$ absorption energies and the concomitantly reduced linewidth (Figure 1b). This change in linewidth is particularly obvious when the fluorescence spectra are shifted in energy such that the 0-0 $S_1 \rightarrow S_0$ coincide (Figure 1c). A Franck–Condon analysis[18] of the thin-film fluorescence spectra yields variances of 106, 45, and 28 meV for DOOPPP, PIF, and MeLPPP, respectively. We have combined these donors with two different acceptor materials, C_{60} and trinitrofluorenone (TNF).[19] C_{60} is a well-known acceptor, yet it has excited states at lower energies than the PPPs. For an unambiguous data analysis, we want to excite only one of the two materials at the heterojunction. Using C_{60}, we can excite the acceptor only, however, it is not possible to excite the polymer donor without simultaneously exciting the acceptor. This can be achieved by using the strong electron acceptor TNF, as it has an onset of absorption around 3 eV, which is similar to DOOPPP and larger than PIF and MeLPPP.

For our study we employed the method of field-dependent photocurrent measurements.[8,20] We stress that this technique probes a different situation than the related field-dependent photoluminescence (PL) quenching experiment.[21,22] By PL quenching, one explores the field dependence of the recombination process. Recombination occurs from the intermolecular state when it is tightly bound. This situation is also referred to as a charge transfer state, exciplex, or tightly bound geminate pair.[11,21] In contrast, the photocurrent results from the break-up of the intermolecular state, which, immediately beforehand, will be only loosely bound. Sometimes this is termed a dark intermediate state, a polaron pair state, a hot charge transfer complex, or a weakly bound geminate pair.[5,21,23] Its weak binding energy and ultrafast split-up, on a time scale of 100 fs,[7,24] can lead researchers to disregard this intermediate state and to consider only the free carriers resulting from its dissociation.[6] The field-dependent photocurrent measurements probe the decisive process for the photogeneration of charge carriers, that is, the break-up of the weakly Coulomb bound geminate pair (GP). A priori, the experiment does not tell us whether the weakly bound intermolecular geminate pair was formed

ADVANCED MATERIALS
www.advmat.de

www.MaterialsViews.com

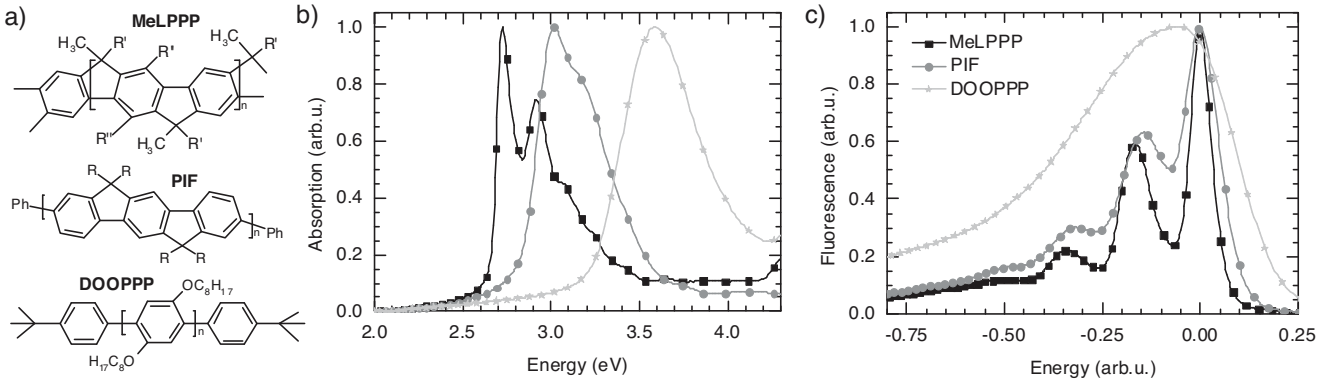

Figure 1. a) The chemical structures of the donor polymers (R = 2-ethylhexyl, R′ = 1,4-C_6H_4- *n* -$C_{10}H_{21}$, R″ = - *n* -C_6H_{13}), along with b) their absorption spectra and c) the fluorescence spectra for excitation at 3.5 eV. For comparison, the fluorescence spectra have been shifted along the energy axis so that the 0–0 transitions coincide at 0 eV.

directly by electron transfer from the intramolecular excited state or whether it results from evolution via an initially tightly bound geminate pair.

For the field-dependent photocurrent measurements, a planar heterojunction geometry was chosen as device structure to avoid non-geminate recombination as much as possible. The solar cells were prepared on glass substrates in the layer structure ITO/PEDOT:PSS (35 nm)/donor polymer (40 nm)/acceptor molecule (40 nm)/aluminum, where ITO is indium tin oxide and PEDOT:PSS is poly(3,4-ethylenedioxythiophene):poly(styrenesulfonate). The polymers were spun from chlorobenzene solution while the acceptor molecules were thermally evaporated. We note further that we employed a careful device design that ensures a homogeneous field distribution without edge effects in fully individually addressed photocells. This is an essential prerequisite for accurate measurements at high field strength.

Figure 2 shows the photocurrent quantum yield $J(F)/J(F_\infty)$ as a function of internal electric field F and normalized to unity at the field strength F_∞ at which the photocurrent yield saturates. To obtain the internal electric field, the open-circuit voltage was subtracted from the applied external voltage and the result was divided by the film thickness. In Figure 2a, the molecular acceptor C_{60} is excited, which results in electron transfer from the polymer highest occupied molecular orbital (HOMO) to the C_{60} HOMO. In contrast, in Figure 2b we excite the polymer donor, thus inducing electron transfer between the lowest unoccupied molecular orbitals (LUMOs) of the polymer and the TNF. In both cases, we observe the same trends. First, the photocurrent quantum yield saturates for high field strength. A quantitative analysis, taking into account the exciton diffusion length of about 10 nm inferred from a comparison of photocurrent and absorption spectra shows that the quantum yield at saturation is around 100%. This value is subject to inaccuracies regarding the exciton diffusion length. In other words, essentially all the excitations photogenerated on one compound that reach the interface split up at sufficiently high fields. Second, the electric field needed to induce this complete split-up decreases from DOOPPP to MeLPPP. In this order, the conjugation length increases and the energetic disorder decreases, as demonstrated in Figure 1. When using TNF as the acceptor, overall lower fields are required to dissociate all excitations than when C_{60} is used. The fact that we observe photocurrent saturation at high fields under illumination rather than device breakdown or uncontrolled photocurrent gain is remarkable. We consider this is mostly the result of using a device geometry with an insulating patterned photopaint layer that removes any edges at the transition between polymer film and ITO electrode. This structure eliminates any high inhomogeneous fields that promote multiple or uncontrolled carrier injection, in particular under high-energy illumination. Furthermore, when C_{60} is used the exciting photon energy is low, while with TNF the saturation field strength is moderate.

What do these data reveal about the process of charge carrier separation? In a naive classical picture, following Langevin, we

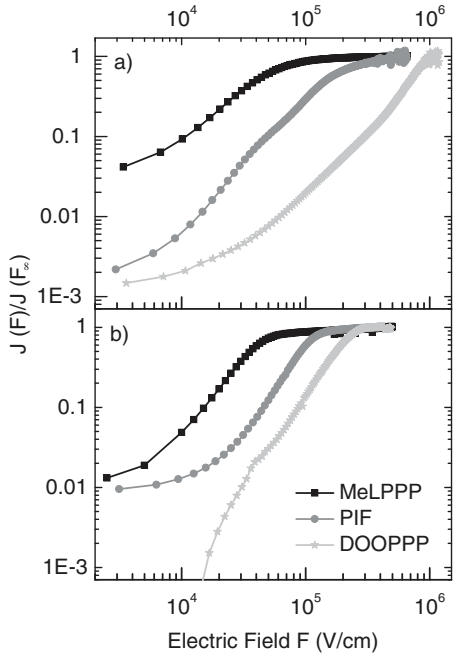

Figure 2. The external quantum yields of planar heterojunction devices made with MeLPPP, PIF, and DOOPPP, measured as a function of the internal field and normalized to unity at the saturation value. a) Using C_{60} as acceptor and exciting at 2.2 eV. b) Using TNF and exciting at the maximum of the polymer absorption.

Adv. Mater. **2012**,
DOI: 10.1002/adma.201104063

may associate the binding energy of the intermolecular excited state with the Coulomb energy of two opposite pointlike charges separated at a distance r_{GP}. When the intermolecular excited states dissociate into a free electron and hole at a high field this implies that the potential energy of the electric field compensates the binding energy of the geminate pair. This is the case from a certain saturation field value F_{sat} onwards. We can use this to calculate the binding energy of the intermolecular excited state and the associated distance r_{GP}. As a basic estimate we use $F_{sat} r_{GP} e = e^2/(4\pi\varepsilon_r\varepsilon_0 r_{GP})$, leading to $r_{GP} = \sqrt{e/(4\pi\varepsilon_r\varepsilon_0 F_{sat})}$, where e is the elementary Coulomb charge and ε_r and ε_0 are the dielectric constants at the interface (taken as 3.5) and of vacuum, respectively. This results in values from 9 nm to 2 nm for the electron–hole distance and from 0.05 eV to 0.2 eV for the binding energy of the geminate pair along the series from MeLPPP to DOOPPP, as detailed in the Supporting Information. The key message to take from this is that with increasing energetic order and conjugation length, the weakly bound geminate pair is more extended and it is more loosely bound. This general observation is independent of whether the donor or the acceptor is excited.

A comparison between devices made with C_{60} and with TNF shows a lower F_{sat}, implying larger electron–hole distances, when TNF is used. This can be associated with the different energy gain that accompanies the electron transfer from the photoexcited intramolecular state.[2,25] When C_{60} is excited and the electron transfers between the HOMOs, the excess energy between the HOMO levels ranges from 1.1 eV to 0.7 eV from MeLPPP to DOOPPP. In contrast, when the polymer is excited, the electron transferring between LUMOs gains an energy of about 1.3–1.5 eV (see Supporting Information). The data in Figure 2 suggest that this larger excess energy in particular for PIF and DOOPPP reduces the binding energy of the geminate pair. In the conceptual framework of two pointlike charges, this corresponds to a larger extent of the geminate pair created when TNF is used instead of C_{60}.

Figure 2 also allows us to draw conclusions about the nature of the intermolecular state. Consider the point that electron transfer from a photoexcited intramolecular state may, in principle, result in a tightly or loosely bound geminate pair. A tightly bound geminate pair with charges separated by less than 1 nm requires an electric field exceeding 4×10^6 V cm^{-1} in order to overcome its Coulomb binding energy of 0.4 eV. Our experiment tells us that much lower fields are sufficient to split up the geminate pairs. Thus the geminate pairs formed by electron transfer in the presence of a high electric field must be only weakly bound and well extended. Furthermore, our experiment results in a yield around 100% at high fields. This implies there are no efficient competing processes such as energy transfer to triplet excited states or radiative or non-radiative recombination.[2,26] It follows that such processes limit the efficiency of dissociation only if the geminate pair is tightly bound, as is the case for example at low fields or when the weakly bound geminate pair relaxes.[27]

How can we use the insight gained from Figure 2 to make more efficient solar cells? For applications, it is worth noting that the field required to separate all charges also affects the fill factor, which is a critical parameter for the efficiency of solar cells. This is illustrated in **Figure 3**, where the current densities obtained for the three different polymers are normalized to negative unity at the voltage at which the photocurrent saturates. For the performance of the solar cell, the operating range between zero applied volts and the open-circuit voltage is relevant. It is evident that the fill factor strongly decreases with increasing saturation field from MeLPPP (35%) to DOOPPP (20%). A low saturation field is also required as, ideally, one would like to obtain a quantum yield of 100% at the electrical field strength that prevails at the open-circuit voltage. The essence is that the saturation field strength needs to be close to the internal field strength. This is tantamount to saying that the extent of the intermolecular excited state needs to be large. In the picture of pointlike charges, they need to be separated by distances around 10 nm. From our data this seems to be enabled by the larger conjugation length of the more ordered polymers. It is known that right after generation the charge carrier on a conjugated segment is in a highly mobile state, characterized by a low effective mass and a large coherence length.[28,29] Scattering by conformational disorder quickly reduces the mobility of the charge carrier, and the coherent motion of the carrier becomes limited to the conjugation length.[30] A long conjugation length means the hole coherently oscillates over a large segment of the polymer chain, leading to a large mean separation from the electron on the acceptor site. We therefore conclude that the realization of efficient solar cells will benefit from the use of materials that are highly conjugated and allow for effective charge carrier delocalization.

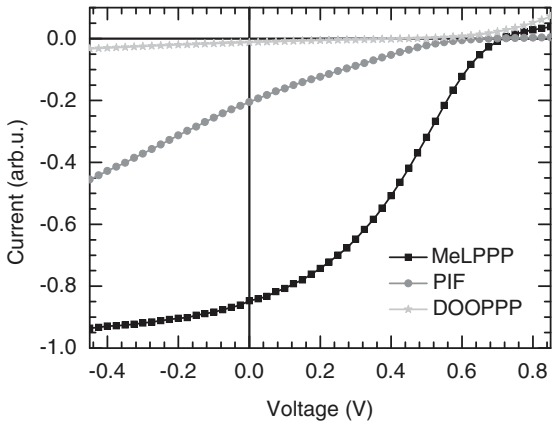

Figure 3. The current density of MeLPPP, PIF, and DOOPPP in a planar heterojunction with C_{60} for excitation at 2.2 eV, as a function of applied voltage. The curves are normalized to –1 at the saturation value of the photocurrent.

Experimental Section

MeLPPP, PIF and DOOPPP were synthesized by the group of U. Scherf as described elsewhere.[31–33] Trinitrofluorenone (TNF) was synthesized in Bayreuth following the method of Woolfolk and Orchin.[34] Cyclovoltammetry measurements were carried out in dichloromethane and the HOMO levels were calculated relative to ferrocene.

For spectroscopic measurements, about 40 nm thick polymer films were spun from filtered chlorobenzene solution (7.5 mg mL^{-1}). The films were heated at 80 °C for 10 min. Absorption was measured with a Cary 5000 (Varian) UV-vis spectrometer. The fluorescence spectra

were recorded using a charge-coupled device (CCD) camera at room temperature with the samples in vacuum under UV-multimode (351 nm/364 nm) excitation from an Ar^+ laser. Photoluminescence spectra of C_{60} and of TNF are included in the Supporting Information. For photocurrent measurements, heterojunction solar cell devices were fabricated on structured ITO-coated glass substrates. To ensure a homogeneous electric field without edge effects, a circular active area of the device was defined on top of the ITO anode using AZ 1518 photopaint from Microchemicals. The devices were then prepared by spin-coating 35 nm poly(3,4-ethylenedioxythiophene):poly(styrene-sulfonate) (PEDOT:PSS) into the active area, heating at 140 °C for 30 min, spin-coating 40 nm polymer on top of it, and heating again to 80 °C for 10 min to drive off any residual solvent. After this, we evaporated 40 nm C_{60} (99.9% purity, American Dye Source Inc.) or TNF, followed by 80 nm aluminum.

Current–voltage curves under monochromated illumination from a 150 W Xenon lamp were measured under active vacuum at room temperature with a Keithley source-measure unit. Light intensities were recorded with a Hamamatsu S1337-33BQ photodiode. The internal electric field was calculated as $F = (V - V_{oc})/d$, with applied external voltage V, open-circuit voltage V_{oc} (typically between 0.5 and 0.7 V, see the Supporting Information) and active film thickness d. The photocurrent quantum yield $J(F)$ was calculated taking into account photocurrent density of the solar cell, illumination light intensity, and the exciton diffusion length (typically around 10 nm)[35–38] derived by comparison between absorption and photocurrent spectra.

Supporting Information

Supporting Information is available from the Wiley Online Library or from the author.

Acknowledgements

We gratefully acknowledge the GRK 1640 of the Deutsche Forschungsgemeinschaft (DFG).

Received: October 24, 2011
Revised: December 6, 2011
Published 0nline:

[1] J. L. Brédas, J. E. Norton, J. Cornil, V. Coropceanu, *Acc. Chem. Res.* **2009**, *42*, 1691.
[2] J. J. Benson-Smith, L. Goris, K. Vandewal, K. Haenen, J. V. Manca, D. Vanderzande, D. D. C. Bradley, J. Nelson, *Adv. Funct. Mater.* **2007**, *17*, 451.
[3] T. M. Clarke, A. Ballantyne, S. Shoaee, Y. W. Soon, W. Duffy, M. Heeney, I. McCulloch, J. Nelson, J. R. Durrant, *Adv. Mater.* **2010**, *22*, 5287.
[4] C. Deibel, T. Strobel, V. Dyakonov, *Phys. Rev. Lett.* **2009**, *103*, 036402.
[5] C. Deibel, T. Strobel, V. Dyakonov, *Adv. Mater.* **2010**, *22*, 4097.
[6] F. Etzold, I. A. Howard, R. Mauer, M. Meister, T. D. Kim, K. S. Lee, N. S. Baek, F. Laquai, *J. Am. Chem. Soc.* **2011**, *133*, 9469.
[7] D. Herrmann, S. Niesar, C. Scharsich, A. Köhler, M. Stutzmann, E. Riedle, *J. Am. Chem. Soc.* **2011**, *133*, 18220.
[8] S. Inal, M. Schubert, A. Sellinger, D. Neher, *J. Phys. Chem. Lett.* **2010**, *1*, 982.
[9] R. A. Marsh, J. M. Hodgkiss, R. H. Friend, *Adv. Mater.* **2010**, *22*, 3672.
[10] M. Menšík, J. Pfleger, A. Rybak, J. Jung, J. Ulański, K. Halašová, J. Vohlídal, *Polym. Adv. Technol.* **2011**, *22*, 2075.
[11] D. Veldman, O. Ipek, S. C. J. Meskers, J. Sweelssen, M. M. Koetse, S. C. Veenstra, J. M. Kroon, S. S. van Bavel, J. Loos, R. A. J. Janssen, *J. Am. Chem. Soc.* **2008**, *130*, 7721.
[12] C. Deibel, V. Dyakonov, *Rep. Prog. Phys.* **2010**, *73*, 096401.
[13] V. I. Arkhipov, E. V. Emelianova, H. Bässler, *Chem. Phys. Lett.* **2003**, *372*, 886.
[14] V. D. Mihailetchi, H. X. Xie, B. de Boer, L. J. A. Koster, P. W. M. Blom, *Adv. Funct. Mater.* **2006**, *16*, 699.
[15] C. L. Braun, *J. Chem. Phys.* **1984**, *80*, 4157.
[16] E. V. Emelianova, M. van der Auweraer, H. Bässler, *J. Chem. Phys.* **2008**, *128*, 224709.
[17] T. Kirchartz, B. E. Pieters, K. Taretto, U. Rau, *Phys. Rev. B* **2009**, *80*, 035334.
[18] P. K. H. Ho, J. S. Kim, N. Tessler, R. H. Friend, *J. Chem. Phys.* **2001**, *115*, 2709.
[19] C. Im, J. M. Lupton, P. Schouwink, S. Heun, H. Becker, H. Bässler, *J. Chem. Phys.* **2002**, *117*, 1395.
[20] C. Im, W. Tian, H. Bässler, A. Fechtenkotter, M. D. Watson, K. Müllen, *J. Chem. Phys.* **2003**, *119*, 3952.
[21] A. C. Morteani, P. Sreearunothai, L. M. Herz, R. H. Friend, C. Silva, *Phys. Rev. Lett.* **2004**, *92*, 247402.
[22] H. Ohkita, S. Cook, Y. Astuti, W. Duffy, S. Tierney, W. Zhang, M. Heeney, I. McCulloch, J. Nelson, D. D. C. Bradley, J. R. Durrant, *J. Am. Chem. Soc.* **2008**, *130*, 3030.
[23] Y. S. Huang, S. Westenhoff, I. Avilov, P. Sreearunothai, J. M. Hodgkiss, C. Deleener, R. H. Friend, D. Beljonne, *Nat. Mater.* **2008**, *7*, 483.
[24] R. A. Marsh, J. M. Hodgkiss, S. Albert-Seifried, R. H. Friend, *Nano Lett.* **2010**, *10*, 923.
[25] K. Kato, C. L. Braun, *J. Chem. Phys.* **1980**, *72*, 172.
[26] J. J. Benson-Smith, H. Ohkita, S. Cook, J. R. Durrant, D. D. C. Bradley, J. Nelson, *Dalton Trans.* **2009**, 10000.
[27] D. Veldman, S. C. J. Meskers, R. A. J. Janssen, *Adv. Funct. Mater.* **2009**, *19*, 1939.
[28] P. Prins, F. C. Grozema, J. M. Schins, S. Patil, U. Scherf, L. D. A. Siebbeles, *Phys. Rev. Lett.* **2006**, *96*, 146601.
[29] J. W. van der Horst, P. A. Bobbert, M. A. J. Michels, H. Bässler, *J. Chem. Phys.* **2001**, *114*, 6950.
[30] S. Westenhoff, W. J. D. Beenken, R. H. Friend, N. C. Greenham, A. Yartsev, V. Sundström, *Phys. Rev. Lett.* **2006**, *97*, 166804.
[31] S. P. Huang, G. S. Huang, S. A. Chen, *Synth. Met.* **2007**, *157*, 863.
[32] U. Scherf, K. Müllen, *Makromol. Chem. – Rapid Commun.* **1991**, *12*, 489.
[33] S. Setayesh, D. Marsitzky, K. Müllen, *Macromolecules* **2000**, *33*, 2016.
[34] E. O. Woolfolk, M. Orchin, *Org. Synth.* **1948**, *28*, 91.
[35] S. Cook, A. Furube, R. Katoh, L. Han, *Chem. Phys. Lett.* **2009**, *478*, 33.
[36] S. R. Scully, M. D. McGehee, *J. Appl. Phys.* **2006**, *100*, 034907.
[37] O. V. Mikhnenko, F. Cordella, A. B. Sieval, J. C. Hummelen, P. W. M. Blom, M. A. Loi, *J. Phys. Chem. B* **2008**, *112*, 11601.
[38] T. J. Tang, A. Herrmann, K. Peneva, K. Müllen, S. E. Webber, *Langmuir* **2007**, *23*, 4623.

Supporting information to:

Does conjugation help exciton dissocation ? A study on poly(*p*-phenylene)s in planar heterojunctions with C_{60} or TNF

By *Christian Schwarz, Heinz Bässler, Irene Bauer, Jan-Moritz Koenen, Eduard Preis, Ullrich Scherf* and A*nna Köhler*[*]

[*]Prof. Dr. Anna Köhler, Christian Schwarz, Prof. Dr. Heinz Bässler, Irene Bauer
Experimental Physics II and Bayreuth Institut of Macromolecular Science,
University of Bayreuth, 95440 Bayreuth (Germany)
E-Mail: anna.koehler@uni-bayreuth.de

Jan-Moritz Koenen, Eduard Preis, Prof. Dr. Ullrich Scherf
Macromolecular Chemistry,
Bergische Universität Wuppertal, 42097 Wuppertal (Germany)

	HOMO (eV)	optical gap (eV)	LUMO (eV)	HOMO polymer - HOMO C_{60} (eV)	LUMO TNF – LUMO polymer (eV)
MeLPPP	-5.2	2.6	-2.6	1.1	1.3
PIF	-5.4	2.8	-2.6	0.9	1.3
DOOPPP	-5.6	3.2	-2.4	0.7	1.5
PCBM	-6.3	1.7	-4.6		
TNF	-7.9	-	-3.9		

Table 1: HOMO and LUMO energies

Cyclic voltammetry measurements of the polymers and of the C_{60}-derivative PCBM were done in dichloromethane and the HOMO levels were calculated against ferrocene. The LUMO levels were estimated by adding the optical gap (taken as the onset of absorption). The value we found for PCBM is consistent with the value reported for C_{60}. [a] For TNF, the HOMO and LUMO levels were taken from literature. [b]

	r_{GP} with C_{60}	r_{GP} with TNF	E_b with C_{60} (eV)	E_b with TNF (eV)
MeLPPP	8 nm	9 nm	0.05	0.05
PIF	4 nm	5 nm	0.10	0.08
DOOPPP	2 nm	4 nm	0.20	0.11

Table 2: Geminate pair radii and binding energies E_b

Photoluminescence of the acceptor materials

For reference, the photoluminescence of TNF is displayed in Figure S1. Excitation was with a HeCd laser at 325 nm at a few mW. The sample was placed in an evacuated cryo-stat at room temperature. The luminescence was recorded using CCD-camera coupled to a spectrograph.

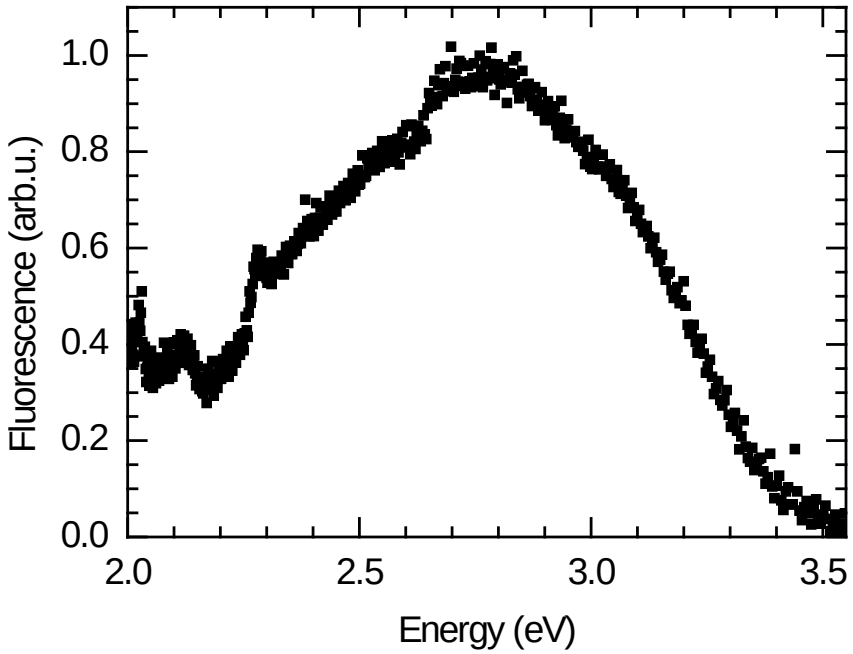

Figure S1: Photoluminescence of TNF

The photoluminescence of C_{60} is well known with a 0-0 peak at 1.7 eV and a vibrational side peak at 1.5 eV. A spectrum is displayed in Ref [c].

Photovoltaic parameters

	V_{oc} (V)	I_{sc} (A cm^{-2})	FF (%)	EQE (%)	Irradiance (W nm^{-1} cm^{-2})	λ (nm)
MeLPPP/C_{60}	0.7±0.1	$5.0x10^{-6}$	35	5.8	$3.4x10^{-4}$	570
PIF/C_{60}	0.7±0.1	$1.0x10^{-6}$	20	0.8	$3.4x10^{-4}$	570
DOOPPP/C_{60}	0.5±0.1	$6.8x10^{-8}$	21	0.1	$3.4x10^{-4}$	570
MeLPPP/TNF	0.5±0.1	$6.0x10^{-6}$	19	5.4	$3.4x10^{-4}$	450
PIF/TNF	0.7±0.1	$2.3x10^{-6}$	13	3.4	$2.4x10^{-4}$	412
DOOPPP/TNF	0.0±0.1	$9.0x10^{-10}$	0	10^{-3}	$8.6x10^{-5}$	350

Table 3: Photovoltaic parameters for the solar cells made with the acceptor C_{60} or TNF

The solar cells were illuminated at the irradiance and wavelength λ given in the table. V_{oc}, I_{sc} and FF denote the open circuit voltage, the short-circuit current density and the fill factor, respectively. EQE gives the external quantum yield at that irradiance derived by considering the short-circuit current at the wavelength listed. Note that this value is for zero applied field and does not take into account the fraction of excitons absorbed near the interface of the bilayer structure. The low EQE at zero volts is a manifestation of the significant recombination that takes place from the tightly bound geminate pair, in contrast to the efficient field-assisted dissociation from the loosely bound geminate pair.

References

[a] A. Opitz, J. Wagner, W. Brütting, I. Salzmann, N. Koch, J. Manara, J. Pflaum, A. Hinderhofer, F. Schreiber, IEEE Journal of selected topics in quantum electronics **2010**, 16, 1707

[b] D. P. West, M. D. Rahn, C. Im, H. Bässler, Chem Phys Lett **2000** 326, 407; C. Im, E. V. Emelianova, H. Bässler, H. Spreitzer, H. Becker, Journal of Chemical Physics **2002**, 117, 2961

[c] Y. Wang, J. M. Holden, A. M. Rao, P. C. Eklund, U. D. Venkateswaran, D. Eastwood, R. L. Lidberg, G. Dresselhaus, M. S. Dresselhaus, Phys Rev B **1995**, 51, 4547

6. Role of the effective mass and interfacial dipoles on exciton dissociation in organic donor acceptor solar cells

Christian Schwarz, Steffen Tscheuschner, Johannes Frisch, Stefanie Winkler,

Norbert Koch, Heinz Bässler, Anna Köhler

Veröffentlicht in

Physical Review B 2013, *87*, 155205

Role of the effective mass and interfacial dipoles on exciton dissociation in organic donor-acceptor solar cells

Christian Schwarz,[1] Steffen Tscheuschner,[1] Johannes Frisch,[2] Stefanie Winkler,[2,3] Norbert Koch,[2,3] Heinz Bässler,[1] and Anna Köhler[1,*]

[1]*Experimental Physics II and Bayreuth Institute of Macromolecular Research (BIMF), University of Bayreuth, 95440 Bayreuth, Germany*

[2]*Institut für Physik, Humboldt-Universität zu Berlin, 12489 Berlin, Germany*

[3]*Helmholz-Zentrum Berlin für Materialien und Energie GmbH, 12489 Berlin, Germany*

(Received 25 February 2013; published 15 April 2013)

Efficient exciton dissociation at a donor-acceptor interface is the crucial, yet not fully understood, step for obtaining high efficiency organic solar cells. Recent theoretical work suggested an influence of polymer conjugation length and of interfacial dipoles on the exciton dissociation yield. This necessitates experimental verification. To this end, we measured the dissociation yield of several polymer/C_{60} planar heterojunction solar cells up to high electric fields. The results indeed prove that the yield of exciton dissociation depends strongly on the conjugation length of the polymers. Complementary photoemission experiments were carried out to assess the importance of dipoles at the donor-acceptor interfaces. Comparison of exciton dissociation models with experimental data shows that the widely used Onsager-Braun approach is unsuitable to explain photodissociation in polymer/C_{60} cells. Better agreement can be obtained using "effective mass" models that incorporate conjugation length effects by considering a reduced effective mass of the hole on the polymer and that include dielectric screening effects by interfacial dipoles. However, successful modeling of the photocurrent field dependence over a broad field range, in particular for less efficient solar cell compounds, requires that the dissociation at localized acceptor sites is also taken into account.

DOI: 10.1103/PhysRevB.87.155205 PACS number(s): 72.20.Jv, 88.40.jr, 72.80.Le

I. INTRODUCTION

Organic solar cells have now reached power conversion efficiencies above 10%, which is often referred to as the lower limit for industrial mass production.[1] A significant contribution to this advance lies in the optimization of film-processing conditions and device architecture.[2–6] These steps serve to increase the fraction of photogenerated excitons that can dissociate, e.g., by reaching dissociation sites, and effectively reduce inadvertent recombination of electrons and holes.[7] For even more efficient solar cells, fill factor, short circuit current, and open circuit voltage need to be improved by increasing the exciton dissociation yield further.[8] A key step toward this lies in understanding the mechanisms and the material parameters that control how a photogenerated bound electron-hole (e-h) pair (exciton) dissociates into mobile charge carriers. Knowledge of the relevant processes allows for further optimization of film morphology and device architecture and, in particular, for guidelines in the design and choice of suitable high efficiency materials.

Today's organic solar cells involve at least two different types of molecular materials, i.e., a donor compound and an acceptor. In such a donor-acceptor (D-A) system, an exciton is created next to a molecular D-A interface or reaches it within its lifetime. There, it transfers its electron from the excited donor to the ground state acceptor molecule and forms a charge transfer state. This initial charge transfer step usually takes place on an ultrafast timescale.[9,10] Since the dielectric constant of organic semiconductors is typically only 3–4, dielectric screening is weak and the e-h pair is initially bound by its Coulomb potential. To become mobile, the charges need to escape from their mutual Coulombic potential without suffering geminate recombination. In a naïve picture of pointlike charges, they are unbound when they separate to a distance defined as the capture radius, which, in the absence of an electrostatic field, is $r_c = e^2/4\pi\varepsilon_0\varepsilon_r kT$. At that distance, the thermal energy exceeds the Coulomb energy, with typical room temperature values being $r_c \cong 16$ nm for $\varepsilon_r = 3.5$.

The central question is why the e-h pair can overcome the considerable Coulomb potential. One currently discussed possibility is that the excess energy, liberated when the excited donor electron transfers to the acceptor, facilitates complete dissociation. In this case, the yield should depend on the energy difference between the energy of the lowest unoccupied molecular orbital (LUMO) level of the donor and the acceptor. Although there are reports in the literature in favor of this possibility,[11–13] there is strong evidence that alternative dissociation channels must be operative as well. Experimental and theoretical investigations suggest that the degree of delocalization of both an exciton and a charge in a conjugated polymer may be of key importance,[9,12,14–16] the extreme view being the notion that conjugated polymers behave like a one-dimensional inorganic semiconductor with completely delocalized wavefunctions.[17] A more conservative view is that right after its creation, an e-h pair at a D-A interface is in a short-lived extended state with a high, yet finite chance for complete dissociation. Unsuccessful e-h pairs relax in energy and form more tightly bound meta-stable charge transfer states, from which subsequent dissociation attempts may occur.[12] In addition to exciton delocalization, it has emerged that interfacial dipoles may also be conducive to exciton dissociation. Theoretical,[18,19] as well as experimental,[20] evidence for such dipoles seems to correlate with increased photocurrent yields.

To discriminate between the different possibilities, one may compare the experimental photocurrent yields against

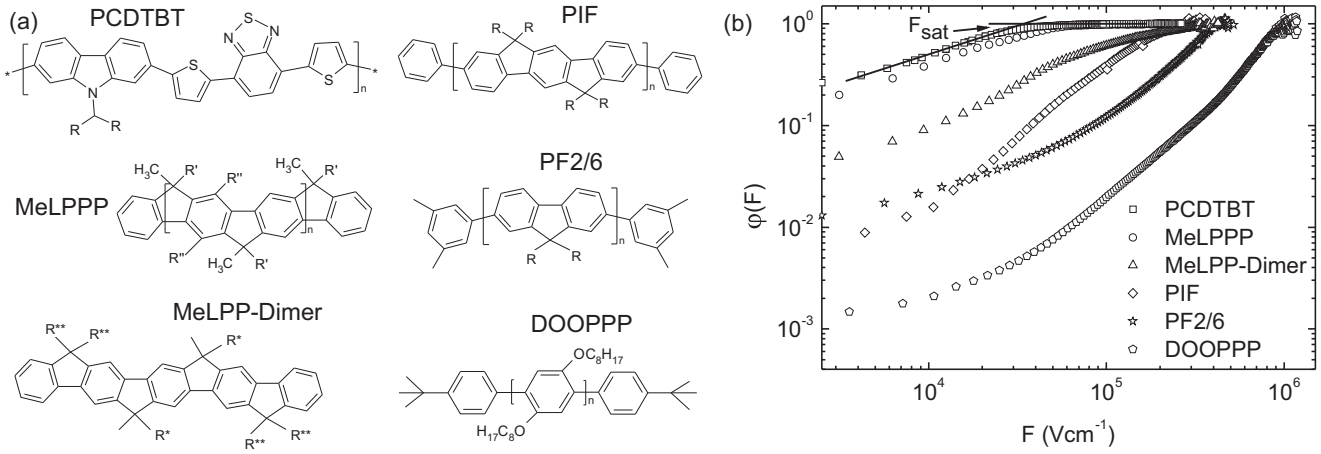

FIG. 1. (a) Chemical structures and abbreviations of the donor polymers (R = 2-ethylhexyl, R′ = 1,4-C_6H_4-*n*-$C_{10}H_{21}$, R″ = -*n*-C_6H_{13}, $R^* = C_6H_{13}$, $R^{**} = C_{10}H_{13}$). (b) External photocurrent quantum yields of bilayer C_{60} devices made with PCDTBT, MeLPPP, MeLPP-dimer, PIF, PF2/6, and DOOPPP, measured at 2.2 eV excitation as a function of the internal field and normalized to unity at the saturation value. For PCDTBT, the tangents whose intersection defines the saturation field F_{sat} are indicated as an example. PCDTBT = Poly[[9-(1-octylnonyl)-9H-carbazole-2,7-diyl]-2,5-thiophenediyl-2,1,3-benzothiadiazole-4,7-diyl-2,5-thiophenediyl], MeLPPP = methyl-ladder-type-poly(*p*-phenylene), MeLPP-dimer = methyl-ladder-type-*p*-phenylene-dimer, PIF = poly(indeno-fluorene), PF2/6=ethyl-hexyl-poly(fluorene), DOOPPP = Di-octyloxy-poly(*p*-phenylene).

predictive models. A classical approach, based on the seminal works by Onsager and Braun, consists in considering the dependence of exciton dissociation on an increasing electric field in the device.[21] A coulombically bound e-h pair requires a certain electric field for complete separation. Above a certain saturation field strength, the yield should become constant when the drop of the electrostatic potential exceeds the Coulomb-binding energy of the e-h pair. If geminate recombination was the dominant recombination process, then the saturation field strength F_{sat} is a measure of the Coulomb-binding energy of an e-h pair and also of the size, i.e., the mean e-h separation of the dissociating e-h pair. While the Onsager-Braun model is frequently employed to interpret organic solar cell performance, its premise of treating the e-h pair as point charges renders its application questionable for materials with extended, delocalized excited states such as polymers. Meanwhile, there are more sophisticated models available. For example, the delocalization of the photogenerated charges can be incorporated explicitly by considering their effective mass.[22–25] Similarly, the screening effect of interfacial dipoles on the Coulomb potential of the e-h pair has been implemented in the theoretical framework.[23,25] So far, however, these models have not yet been compared against experimental data.

Here, we aim to assess the impact of conjugation length and interfacial dipoles on exciton dissociation by comparing simulations of the aforementioned models with experimental data. We recently measured the field dependent photocurrent in a bilayer solar cell in which conjugated phenylene-type donor polymers were combined with a C_{60} acceptor layer. We found that the more ordered, and thus the more conjugated, a polymer chain is, the lower the saturation field strength.[16] To cover a wide range of donor materials in the same series of experiments and under exactly the same experimental conditions, we confirmed the previous experiments on DOOPPP, PIF, and MeLPPP and expanded them to further include PF2/6, a dimer of MeLPPP and the widely used low band-gap material PCDTBT (see Fig. 1 for chemical structure and abbreviations). To obtain information on possible interfacial dipoles, ultraviolet photoelectron spectroscopy (UPS) experiments were carried out for the interfaces of these compounds with C_{60}. The experimental results were analyzed by parameterizing and simulating the existing models. We are able to quantify the effect of charge delocalization, expressed in terms of the effective mass, and of ground state dipoles on the field dependent exciton dissociation. Further, we show that a single mechanism cannot explain the field dependence of the photocurrent, yet it can be modeled adequately by considering a superposition of two processes.

II. EXPERIMENTAL RESULTS

Figure 1 shows the chemical structures of the investigated polymers and the dimer, as well as the relative photocurrent quantum yields $\varphi(F)$ of bilayer devices (with C_{60} as acceptor) as a function of the internal electric field. The key parameter derived from these data is the saturation field strength F_{sat}, defined by the intersection of the tangents to the photocurrent in the regimes of low electric field and high electric field (i.e., at photocurrent saturation) in a double logarithmic plot (see Fig. 1). The existence of the saturation field implies that there is a field-dependent recombination mechanism that can be overcome at high fields. This can be seen by considering that photoexcitation with rate G results in bound or unbound charge carriers. This leads to a photocurrent that is controlled by the competition between a field-dependent escape rate $\mu F/d$ from the recombination zone, with μF being the transport velocity and d the layer thickness, and a recombination rate k_r. The recombination mechanism may, in principle, be geminate or nongeminate. The photocurrent then depends on the field as $j \propto G \cdot \mu F d^{-1}/(\mu F d^{-1} + k_r) = G \cdot 1/(1 + \frac{dk_r}{\mu F})$. Thus, at low fields, the photocurrent will be reduced due to recombination, while at high field, it eventually saturates. We

now argue that, in our case, this recombination is predominantly geminate. As detailed in the Supplemental Material,[26] one can estimate that monomolecular and bimolecular decay become comparable at a critical light intensity of about $2 \cdot 10^{18}$ photons/cm^{2}s. Our photocells were measured at a photon flux of about $4 \cdot 10^{15}$ photons/cm^{2}s, i.e., at an intensity that is 1/500ths of the intensity where bimolecular recombination becomes important. This is consistent with the observation that for all materials the photocurrents depend linearly on the pump intensity I_{ex}. If the carrier would recombine bimolecularly, as were the case for trap-free nongeminate recombination, a dependence such as $j \propto \sqrt{I_{ex}}$ should result. The existence of a saturation field at the light intensities used in our experiment therefore shows that there is a field-dependent geminate-pair recombination mechanism. Such a dominant role of geminate recombination is in agreement with reports by other research groups, even when using higher light intensities.[27] When comparing the polymer MeLPPP and the associated dimer MeLPP, one observes a significant drop of F_{sat} from $4 \cdot 10^4$ V cm^{-1} to $2 \cdot 10^5$ V cm^{-1}. This is the first clear indication that wave-function delocalization in the donor is important. It turns out that the saturation field strength, and thus the binding energy of the interfacial e-h pair, decreases in the order DOOPPP, PF2/6, PIF, MeLPP-dimer, MeLPPP, and PCDTBT (Fig. 1, and Table II further below). For the poly-*p*-phenylene based systems, yet not for the donor-acceptor copolymer PCDTBT, this also correlates with a red-shift of the absorption [Fig. 2(a)].

The red-shift of the optical spectra within a series of structurally related compounds is a well-established signature of increased delocalization of the π-electron system in conjugated oligomers and polymers. A heuristic way to correlate the transition energy of an oligomer or polymer with a certain number of conjugated monomers is provided in the coupled oscillator model of W. Kuhn.[28,29] In the case of poly-*p*-phenylene-type polymers, the coupling elements are identified with phenylene rings. By using fluorescence spectra of ladder-type phenylene oligomers, one can parameterize the chain-length dependence of the transition energy of a chain of perfectly aligned phenylenes.[30] Deviations from chain planarity raise the transition energy and can be translated into an effective conjugation length. This parameterization allows extracting the effective conjugation length of the polymers in both absorption and emission. The two values differ as the excited state geometry is usually more planar than the ground state geometry. In addition, in a film of disordered polymers, there is energy transfer from (shorter) absorbing to (longer) emitting chromophores. In Fig. 2(b), we show the saturation field strengths as a function of the effective conjugation length in absorption and fluorescence for the poly-*p*-phenylene-type systems. The dramatic decrease of F_{sat} with the increasing conjugation length of the polymers proves that the spatial extent of the conjugation length in a π-conjugated polymer has an important bearing of exciton dissociation in our solar cells. We also note that the MeLPP-dimer, which contains five phenylene units so that $1/n = 0.2$, behaves differently. Although F_{sat} for the dimer is four times higher than that for the polymer, one expected a much higher value based upon the parameterization data of the conjugation length. This is evident in Fig. 2(b), where F_{sat} for the dimer is compared to the saturation field strength for the polymers.

Having established that there is a clear dependence of the saturation field strength on the effective conjugation length, we now consider whether there is an influence of interfacial dipoles that exist at the heterojunction in the ground state. To this end, the energy-level line-up at the polymer/C_{60} interfaces was investigated by UPS. C_{60} was sequentially deposited by thermal sublimation in ultrahigh vacuum conditions. After each deposition step, valence band and secondary electron cutoff (SECO) spectra were recorded. The typical SECO evolution upon deposition of C_{60} on the polymer film is shown for the example of PCDTBT in Fig. 3(a). We observe that the initial work function of the pristine PCDTBT film (4.60 eV) is increased to 4.72 eV upon 8 Å C_{60} deposition, and it remains constant for higher C_{60} coverage. The valence spectra show the evolution of C_{60}-derived molecular levels. The valence band onset of pristine PCDTBT is at a binding energy of 0.63 eV below the Fermi level (E_F), as indicated in Fig. 3(a) this yields an ionization energy of 5.23 eV. The position of the PCDTBT valence band onset was found to be independent of the C_{60}

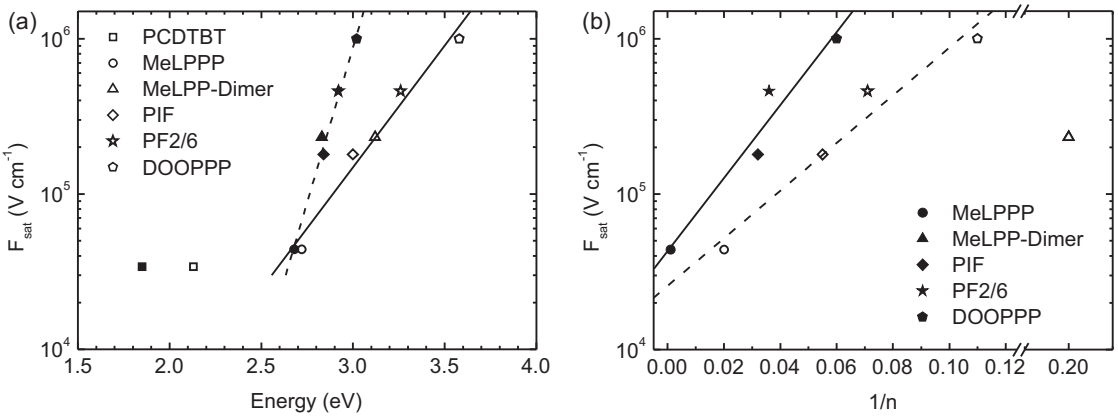

FIG. 2. Saturation field strengths of the bilayer field-dependent photocurrent yields; (a) as a function of the donor absorption energy (empty symbols) and emission energy (filled symbols), (b) as a function of the inverse effective conjugation length of the donors in the ground state geometry (data taken from absorption, empty symbols) and in the excited state geometry (data taken from emission, filled symbols). The lines serve as a guide to the eye.

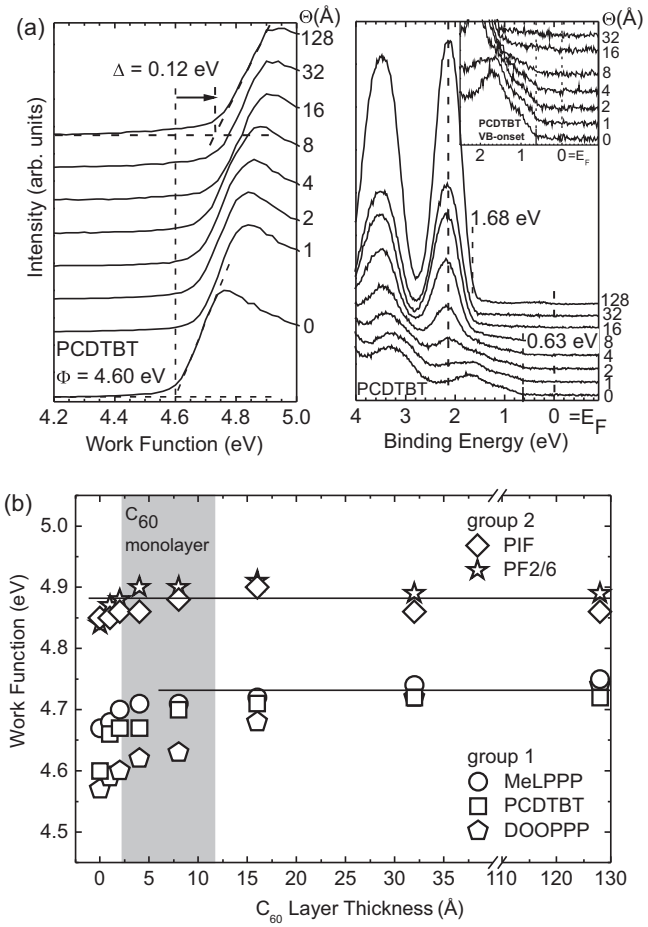

FIG. 3. (a) SECO (left) and low-binding energy region (right) of a 20-nm PCDTBT film spin coated on a PEDOT/PSS-ITO substrate and subsequently deposited C_{60} on top. (b) Work function evolution as a function of subsequent deposited C_{60} coverage. Two groups can be distinguished: group 1 (MeLPPP, PCPTBT, and DOOPPP) Fermi-level pinning of C_{60}-LUMO is found; group 2 (PF2/6 and PIF) vacuum-level alignment is established.

coverage, as it can be observed in the valence band region spectra up to a C_{60} coverage of 8 Å [see close-up spectra in Fig. 3(b)]. The low binding energy onset of emission from the C_{60} highest occupied molecular orbital (HOMO) levels is constant at 1.68-eV binding energy for all coverages. Adding the final work function of 4.72 eV to the energy difference between the C_{60} HOMO onset and the Fermi level yields an ionization energy of 6.40 eV for C_{60}, which is in line with previously reported values.[31,32]

The situation of a constant HOMO position and an increase of the sample work function for the very early stage of interface formation is typical for an interface dipole due to Fermi-level pinning at unoccupied states of C_{60}, i.e., the LUMO level or gap states at slightly lower energy.[33,34] In this scenario, the work function changes until a full monolayer is reached and remains constant for higher film thickness, which we indeed observe beyond 8 Å C_{60} coverage. This coverage corresponds approximately to a monolayer of C_{60} since the diameter of a C_{60} molecule is ∼10 Å.[35] Similar results are obtained for DOOPPP and MeLPPP. In both cases, the initial work function

TABLE I. The ionization energy (IE), the work function Φ of the pristine film, and the change in work function ΔΦ due to the deposition of C_{60}, along with the derived value for the fractional dipole strengths α.

Material	PCDTBT	MeLPPP	PIF	PF2/6	DOOPPP
IE (eV)	5.23	5.28	5.82	5.85	5.22
Φ (eV)	4.60	4.67	4.85	4.84	4.57
ΔΦ (eV)	0.12	0.08	0.02	0.05	0.17
α (10^{-3})	21.4	14.2	3.6	8.9	30.3

of the pristine polymer films increases due to C_{60} deposition. Note that in all three cases, including PCDTBT, the final work function of a multilayer C_{60} deposited film onto the polymer film reaches the same value. Thus, ground state interface dipoles of varying magnitude, dependent on the initial polymer work function, are found (Table I). In contrast, vacuum-level alignment was found at the C_{60}/PIF and C_{60}/PF2/6 interfaces [Fig. 3(b)]. Within accuracy of our measurement (±0.05 eV), the work function of the PIF and PF2/6 polymers film did not change due to C_{60} deposition. The evolution of the sample work function as a function of C_{60} coverage is summarized in Fig. 3(b) for all five different polymers. As indicated in Fig. 3, a transition from vacuum-level alignment to Fermi-level pinning at the polymer/C_{60} interface occurs for a work function of a pristine polymer film below ∼4.75 eV. Nevertheless, Fermi-level pinning at unoccupied states of C_{60} was unexpected because of the C_{60} threshold electron affinity of 4.50 eV in the solid phase[31] (obtained by inverse photoelectron spectroscopy). This is 0.25 eV lower as the obtained transition work function of ∼4.75 eV. This difference can be explained by unoccupied gap states that are created within the C_{60} film due to impurities coming from the spin-coated polymer films or structural defects. The resulting work function values, ionization energies, and work function changes ΔΦ for the five interfaces are summarized in Table I.

From these studies, two key experimental observations emerge.

(i) The electric field strength F_{sat}, at which $\varphi(F)$ saturates decreases by about a factor of 20–30 in the series DOOPPP, PF2/6, PIF, MeLPP-dimer, MeLPPP, and PCDTBT. This correlates with the bathochromic shift of the S_1-S_0 0-0 transition, except for PCDTBT. This is a strong indication that electronic delocalization of the hole residing on the donor is of key importance.

(ii) The photoemission experiments show that there is, indeed, some ground state charge transfer between donor and acceptor, but this effect is relatively weak. In the case of PF2/6, PIF, and MeLPPP, it is barely noticeable. For DOOPPP and PCDTBT, the interfacial potential drop is 170 meV and 120 meV, respectively.

III. ANALYSIS AND DISCUSSION

A. Individual models

One of the most widely applied models to account for exciton dissociation is the Onsager-Braun model, even though it does not account for the effects of effective conjugation length or for interface dipoles.[36,37] The high popularity of

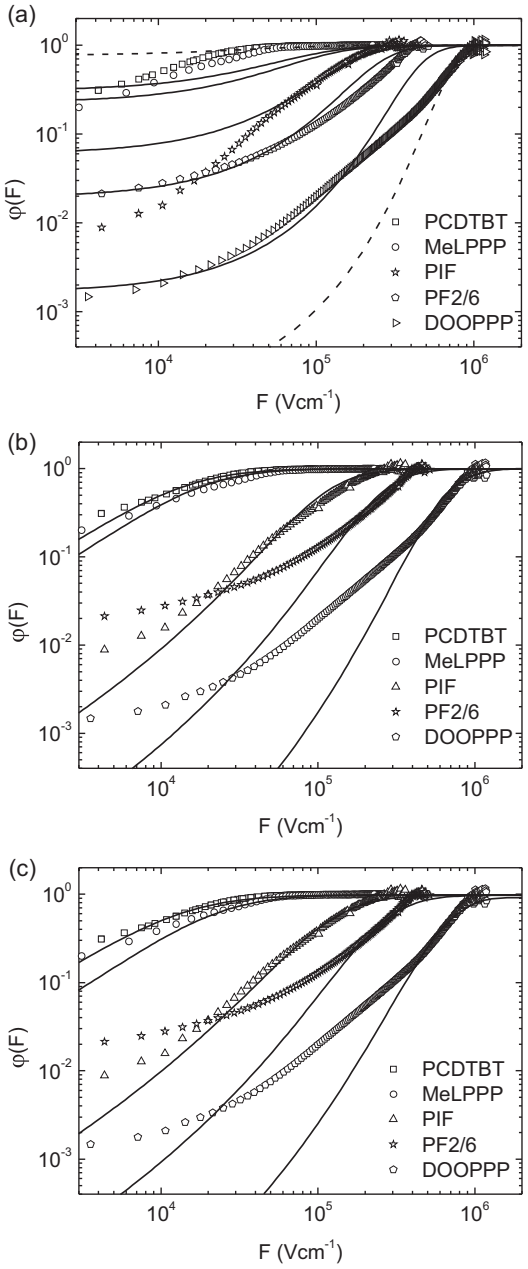

FIG. 4. Comparison of the field-dependent photocurrent yields (symbols) of donor /C_{60} bilayer solar cells with simulations (lines) based on (a) the Braun model [Eqs. (1), (2)], (b) the effective mass model [Eqs. (3)–(5)], and (c) the dipole model [Eqs. (3), (6), and (7)]. The parameters are presented in Table II.

this model warrants a detailed consideration. Onsager's theory for photogeneration in a single component molecular solid rests upon the notion that optical excitation with sufficient energy can autoionize and form a Coulombically bound e-h pair.[38] This pair of pointlike charges can rather fully dissociate in the course of temperature and field-assisted random walk of one carrier in the field of the other, or it may recombine geminately to the ground state. Braun extended this concept to D-A systems in which the lowest excited state is a charge transfer state that can live long enough to make several attempts toward complete dissociation before decaying geminately to the ground state.[39] This dissociation yield is determined by the trade-off between the field-dependent dissociation rate $k_d(F)$ and the field-independent e-h pair decay rate to the ground state k_f, i.e.,

$$\varphi(F) = \frac{k_d(F)}{k_d(F) + k_f} = \frac{1}{1 + k_f k_d(F)^{-1}}. \tag{1}$$

The theory predicts a strong field dependence of the dissociation rate $k_d(F)$, that is,

$$k_d(F) = \frac{3\mu e}{4\pi\varepsilon_0\varepsilon_r r_0^3} \exp\left(\frac{-\Delta E}{kT}\right) \frac{J_1(2\sqrt{-2b})}{\sqrt{-2b}} \quad \text{with}$$
$$b = \frac{e^3 F}{8\pi\varepsilon_0\varepsilon_r k^2 T^2}. \tag{2}$$

Here, J_1 is the Bessel function of order one, F is the electric field, μ is the sum of the mean electron and hole mobility, $\Delta E = e^2/4\pi\varepsilon_0\varepsilon_r r_0$ is the Coulombic-binding energy of the e-h pair, which is controlled by the initial intrapair separation r_0. Inserting (2) into (1) allows simulating the field dependence of the dissociation yields and comparing it with the experimental data; this is shown in Fig. 4(a). For the simulation, we employed $\varepsilon_r = 3.5$ and we used the Bessel function J_1 and not the frequently employed approximation $(1 + b + b^2/3 + b^3/18 + ...)$, as the deviations become significant in the regime of high field strengths that is of interest here. The free parameters in the simulation are the intrapair separation r_0 and the ratio μ/k_f; they are listed in Table II.

We find that the Onsager-Braun model yields unsatisfactory results in two respects. First, and most importantly, the field dependence for the compounds with low F_{sat}, MeLPPP, and PCDTBT, cannot be reproduced at all, and for the remaining compounds, agreement between the experimental data and the Onsager-Braun fits is poor. The main reason for this is that the field dependence predicted by the Braun model is steeper than the experimentally found one. For illustration, if the simulation parameters are adjusted so that there is not an overall agreement with the experimental curve but rather the value of the saturation field is matched [dashed in Fig. 4(a)], one finds that for the regime of low-field strengths, the Onsager-Braun model underestimates the photocurrent yield for DOOPPP while it overestimates it for PCDTBT. Second, the simulation parameters required are unphysical. While the values obtained for r_0 in the nm range are plausible, the values inferred for μ/k_f imply either charge mobility or a lifetime that are too high to be consistent with existing knowledge. Consider, for example, PCDTBT, where $\mu/k_f = 2 \cdot 10^{-8}$ cm^2 V^{-1}. The lifetime at zero electric field is $\tau_0 = [k_f + k_d(0)]^{-1}$. $k_d(0)$ can be evaluated as $k_d(0) = \frac{\mu e}{\varepsilon_0\varepsilon_r}\frac{3}{4\pi r_0^3}\exp(\frac{-\Delta E}{kT})$. Taking μ to be dominated by the hole mobility, and using a value of $1 \cdot 10^{-4}$ cm^2/Vs,[40] one obtains $k_d(0) = 1.3 \cdot 10^3$ s^{-1}, $k_f = 5 \cdot 10^3$ s^{-1}, and $\tau_0 = 158\mu$s. Similar calculations can be carried out for the other polymers in Table II. From this estimate, one can see first that $k_d(0) < k_f$, so that $\tau_0 \approx 1/k_f$, and, more importantly, the values for τ_0 range from 6 μs (for MeLPPP, based upon $\mu = 2 \cdot 10^{-3}$ cm^2/Vs) to more than 30 ms (for DOOPPP, assuming $\mu < 10^{-5}$ cm^2/Vs, which is an upper limit for the hole mobility in highly disordered polymers). Typical lifetimes for charge transfer states between

TABLE II. Fit parameter for different individual models, along with the experimentally measured saturation field strength F_{sat}.

Material	PCDTBT	MeLPPP	PIF	PF2/6	DOOPPP	MeLPP-dimer
F_{sat} [Vcm^{-1}]	$3.4 \cdot 10^4$	$4.4 \cdot 10^4$	$1.8 \cdot 10^5$	$4.6 \cdot 10^5$	$1.0 \cdot 10^6$	$2.3 \cdot 10^5$
Onsager-Braun model[a]						
r_0 [nm]	1.03	1.02	0.92	0.86	0.80	1.02
μ/k_f [10^{-12} m^2 V^{-1}]	2.0	1.5	1.3	1.1	0.3	0.50
Effective mass model (numerical)						
m_{eff}/m_e	0.060	0.067	0.110	0.170	0.300	0.115
$\tau_0 \nu_0 \exp(-2\gamma r)$	3910	3830	3500	100	40	3830
Effective mass model (parabolic approximation)						
m_{eff}/m_e	0.060	0.067	0.110	0.170	0.300	0.115
$\tau_0 \nu_0 \exp(-2\gamma r)$	60	65	40	37	12	65
Dipole model						
m_{eff}/m_e	0.117	0.109	0.130	0.250	1.000	0.20
$\tau_0 \nu_0 \exp(-2\gamma r)$	60	65	40	37	12	65

[a]For the solid lines in Fig. 4(a). See Supplemental Material[26] for the dashed lines.

conjugated polymers and C_{60} derivatives tend to be up to few tens of nanoseconds.[37,41–43] Thus, the Braun model is clearly inadequate to describe the field dependence of exciton dissociation in conjugated polymers. In the same way, we found the mathematically more rigorous treatment of the Onsager-Braun model presented recently by Wojcik and Tachiya[44] to be inappropriate for these conjugated polymers.

Why should the Onsager-Braun treatment be an unsuitable model for conjugated polymer systems when it has been shown to be highly successful for molecular donor-acceptor crystals? One difference between aromatic molecules such as the polyacenes and the conjugated polymers used in today's solar cells is the degree of charge and exciton delocalization. The experimental results clearly show that the photodissociation yield increases with the effective conjugation length of the polymers. A way to explicitly include the effects due to conjugation has been presented by Arkhipov *et al.* by considering the effective mass of a hole on a polymer chain.[22,23] The original motivation for this effective mass model was the observation of a very weak temperature dependence of the photocurrent in MeLPPP that was incompatible with the predictions of the Onsager-Braun model.[45] Such weak temperature dependence has more recently been confirmed for bilayers[46] as well as blends.[47] In order to account for the lack of temperature activation for a well-conjugated polymer like MeLPPP, Arkhipov suggested there should be an additional term that reduces the energy needed to separation of electron and hole.

The central idea of Arkhipov's model is simple. After photoexcitation of the polymer donor, the electron is transferred to the acceptor, and the hole remains on the polymer chain. The two carriers are bound by their mutual Coulomb potential. The hole on the polymer is delocalized within the effective conjugation length, i.e., it can be viewed to carry out zero-point quantum oscillations in the Coulomb potential due to the electron [Fig. 5(a)]. This quantum oscillation is associated with an energy that depends on the effective mass m_{eff} of the hole. This kinetic energy assists the hole in overcoming the Coulomb potential. The effective mass is introduced here in a heuristic way as a measure for the electronic coupling within the polymer chain that depends on intrachain disorder. A low relative effective mass implies a highly delocalized hole. Arkhipov applied this effective mass model to two different situations. One case comprises the situation of a donor doped with only few acceptors;[22] the other considers an extended interface between donor and acceptor, where dark interfacial dipoles prevail.[23] This idea of the effective mass model has been taken up and developed further by the Baranovskii group. A particularly elegant formulation of the effective mass model has been presented by Nenashev and coworkers, and we have therefore applied the Nenashev formulation to our data.[24] Nenashev considers the polymer as a set of one-dimensional chains that are placed parallel to the polymer fullerene interface. The electric field is acting orthogonal to the interface. The geometry of this model is illustrated in Fig. 5(b). The chains are numbered from 1 to n, starting at the interface, with spacing r. The electron on the fullerene is taken as immobile while the hole on the polymer is taken to hop. The dissociation yield $\varphi(F)$ is controlled by the rates for the recombination of the e-h pair, $k_r = 1/\tau_0$, where τ_0 is the lifetime of the e-h pair, and by the rate for dissociation k_d

$$\varphi(F) = \frac{k_d}{k_d + k_r} = \frac{\tau_0}{\tau_0 + k_d^{-1}} = \frac{\tau_0}{\tau_0 + \sum_{n=1}^{N-1} a_{n\to n+1}^{-1} \exp\left(\frac{E_n - E_1}{kT}\right)}. \quad (3)$$

Here, $a_{n\to n+1}$ is the Miller-Abrahams hopping rate of the hole,

$$a_{n\to n+1} = \nu_0 \exp(-2\gamma r) \begin{cases} \exp\left(-\frac{E_{n+1}-E_n}{kT}\right) & E_{n+1} > E_n \\ 1 & E_{n+1} \leqslant E_n \end{cases} \quad (4)$$

ν_0 and γ take their usual meaning as frequency factor and as a measure for the electronic coupling, respectively. The hopping and dissociation process is controlled by energy of the hole on each chain, E_n, which results from the Coulomb potential due to the electron, from the potential of the applied field and from the zero-point oscillation along the conjugated segment within

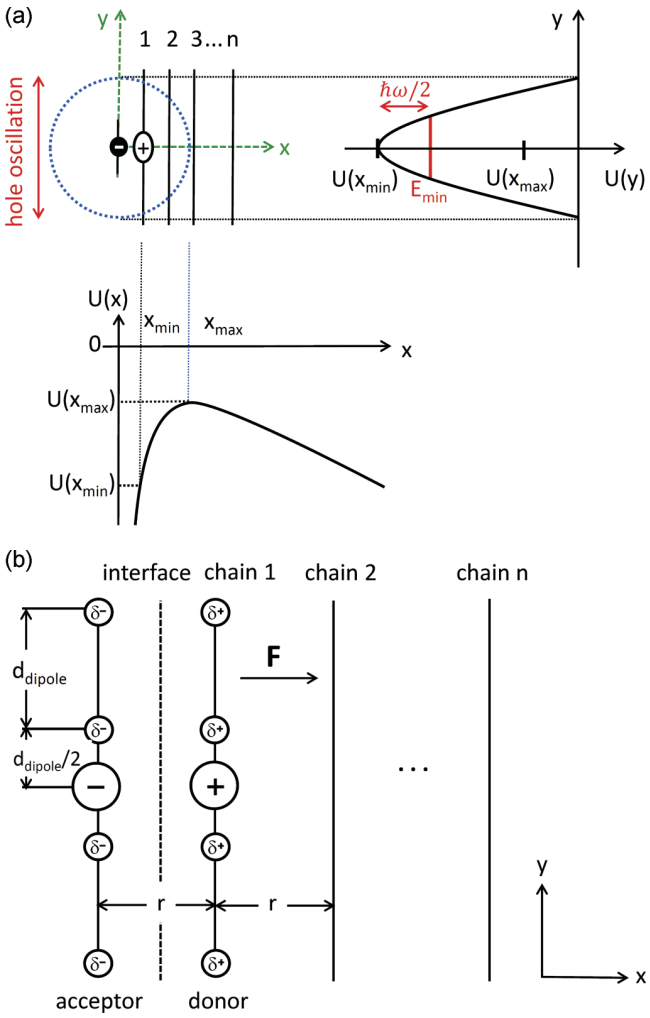

FIG. 5. (Color online) Schematic illustrating electron-hole dissociation at the bilayer interface with an electron on C_{60} at $x = 0$ and a hole on a polymer chain. The chains are assumed parallel to the interface and are labeled 1 to n. (a) The hole on the polymer chain executes a zero-point oscillation along the y direction inside the Coulomb well set up by the electron. The potential along x direction is due to the Coulomb field from an electron at $x = 0$ and a constant applied electric field in x direction. The energy of the hole located at $x_{\min}$ is raised by a zero-point oscillation energy $\hbar\omega/2$, $E_{\min} = U(x_{\min}) + \hbar\omega/2$. To escape, the energy barrier between $E_{\min}$ and $U(x_{\max})$ needs to be overcome. The potential along the y direction is approximated by a parabola. (b) Detailed geometry at the donor-acceptor interface. In the effective mass model, $\delta^+ = \delta^- = 0$. In the dipole model, interfacial ground state dipoles δ^+ and δ^- modify the potential and assist the hole's escape. For simplicity, we used $d_{\text{dipole}} = r$ in our modeling.

the Coulomb potential. As detailed in the original paper by Nenashev, it can be calculated solving the Schrödinger equation

$$-\frac{\hbar^2}{2m_{\text{eff}}}\frac{d^2\psi}{dy^2} + U_n\psi = E_n\psi_n, \tag{5}$$

with

$$U_n = -\frac{e^2}{4\pi\varepsilon_0\varepsilon_r}\frac{1}{\sqrt{y^2 + x_n^2}} - eFx_n, \quad x_n = nr.$$

The dependence of the dissociation rate on the electric field and on the effective mass is thus included implicitly via the hole energy E_n. To implement the Nenashev formalism, we solved (5) numerically and inserted the resulting E_n in (4) and (3), so that $\varphi(F)$ could be calculated parametric in the relative effective mass m_{eff}/m_e and in the product of the e-h pair lifetime with the isoenergetic hopping parameter $\tau_0\nu_0\exp(-2\gamma r)$. The resulting curves with optimized parameters listed in Table II [as "effective mass model (numerical)"] are compared to the experimental data in Fig. 4(b).

In contrast to the Onsager-Braun model, the agreement of the simulated and experimental field dependence is quite satisfactory over the entire field range for the more delocalized compounds PCDTBT, MeLPPP, and PIF. For the compounds with shorter conjugation length, simulation and experiment match only at high fields, and one finds that experimentally there is an additional photocurrent quantum-yield contribution at low field strength. Before we address this additional contribution, let us discuss the values obtained for the parameters. If we know the isoenergetic jump rate $\nu_0\exp(-2\gamma r)$, we can derive the lifetime τ_0 of the geminate e-h pair from the $\tau_0\nu_0\exp(-2\gamma r)$ value.

As an estimate, we consider first the jump rate of an electron from an optically excited donor to a silicon nanoparticle as an acceptor in a P3HT/Si solar cell, which was recently reported.[9] Using ultrafast pump-probe spectroscopy, Herrmann and coworkers showed that the exciton state, created instantaneously during the rise of the laser pulse, decays to yield a polaron signal. The time constant of the exciton decay and the concomitant polaron rise was found to be 120 fs, corresponding to a jump rate of $8 \cdot 10^{12}$ s^{-1}. This jump rate associated with the initial charge transfer step can be taken as the rate for an isoenergetic jump. Second, one may argue that the rate for an isoenergetic jump should be of the same range of that of a charge carrier in an ordered organic solid. There, the charge carrier mobility is around 1 cm^2/Vs.[48] By using the Einstein ratio between mobility μ and the carrier diffusion constant D, $\mu/D = e/kT$, and assuming isotropic diffusion in a cubic system, where $D = \frac{1}{6}a^2[\nu_0\exp(-2\gamma r)]$, with a typical lattice constant for a crystal of 0.6 nm, one ends up with an estimate of the jump rate of $4 \cdot 10^{13}$ s^{-1}. Adopting a representative value for $\tau_0\nu_0\exp(-2\gamma r) \cong 3800$ and a jump rate of about $4 \cdot 10^{13}$ s^{-1} thus yields a lifetime of about 95 ps for the geminate e-h pair, which is a realistic lifetime.

The relative effective masses obtained from the simulation decrease in line with the increase in conjugation length of the compounds. This confirms the notion that improved electronic coupling along the polymer chain is crucial for improving the dissociation efficiency. However, the values for the relative effective masses m_{eff}/m_e range from 0.3 for DOOPPP to 0.060 for PCDTBT, which is rather low. For comparison, for polydiacetylene, which is the most ordered conjugated polymer that is known, electroreflectance measurements by Weiser and Möller yielded an effective mass of 0.05 m_e,[49] and theoretical calculations by Van der Horst placed its effective mass at 0.1 m_e.[50] In the more disordered compounds studied here, the effective mass can be expected to be somewhat higher. Thus, in summary, while the incorporation of the conjugation lengths' effects through the effective mass leads to an improved description of the charge dissociation process, in particular for

the well-delocalized compounds, the values required for the effective mass to account for the dissociation are too low.

The fact that there must be an additional factor that contributes to efficient exciton dissociation at the D-A interface had already been noticed by Arkhipov a decade ago.[23] This was prompted by the observation that in a D-A system, the dissociation yield increases abruptly above a critical acceptor concentration.[51] Dissociation yields exceeding 50% at moderate electric field strengths, as well as the usually weak temperature and field dependence, were taken as an indication that the Coulomb attraction between carriers within a short geminate pair must be effectively screened or counterbalanced. To allow for such a screening, Arkhipov *et al.* invoke the existence of a layer of dipoles that exist in the dark (i.e., in the ground state) at the interface between donors and acceptors with different electron affinities. There are experimental and theoretical results in favor of this notion.[18–20] Arkhipov thus extended the effective mass model to account for the effect of dipoles.[23] We refer to the resulting model as the dipole model.

Arkhipov considered a bilayer system where photoexcitation results in a hole on the first chain adjacent to the interface and an electron on the acceptor on the other side of the interface [Fig. 5(b)]. Suppose there is an additional partial positive charge on the donor chain 1 and a partial negative one on the acceptors, caused by interfacial dipoles. The hole executes zero-point oscillations, as described previously, for the effective mass model, but now these oscillations occur within the Coulomb potential modified by the fractional positive charges, thus raising the energy of the hole on chain 1. A jump of the hole to chain 2 is favorable for two reasons. First, the attractive Coulomb force to the negative sibling charge is partially shielded due to the positive fractional charges on chain 1. Second, on chain 2, the energy of the zero-point oscillations is diminished since the Coulomb potential there is wider and shallower (as there are no fractional charges on chain 2). Both effects will reduce the energy needed to overcome the attractive Coulomb potential. Note that this mechanism requires internal interfaces that can exist in a bilayer system or in a blend system where phase separation occurs. In the model by Arkhipov, the interfacial dipoles are, however, not formed in a donor phase doped by a low concentration of acceptors.

Meanwhile, Wiemer *et al.*[25] improved the theoretical treatment and showed that the existence of a dipole layer has a profound effect. For the practical implementation, we follow the formulation by Wiemer, though for simplicity, we used a square grid with the distance between the chains equal to the distance between the dipoles equal to r. As before, the dissociation yield $\varphi(F)$ is given by (3) and (4). The hole energy E_n is given by the sum of its kinetic energy and potential energy,

$$E_n = E_{p,n} + E_{k,n}, \quad \text{where} \quad E_{p,n} = U(x_n,y)|_{y=0} \quad \text{and}$$
$$E_{k,n} = \frac{1}{2}\hbar\omega = \frac{\hbar}{2\sqrt{m_{\text{eff}}}}\sqrt{\frac{d^2}{dy^2}U(x_n,y)|_{y=0}}, \tag{6}$$

which uses a parabolic approximation for the energy of the zero-point oscillations. The potential energy is modified compared to (5) by considering the effect of dipoles with fractional strength α.

$$U(y,x_n) = \frac{e^2}{4\pi\varepsilon_0\varepsilon_r}\frac{-1}{\sqrt{x_n^2+y^2}} + \frac{e^2}{4\pi\varepsilon_0\varepsilon_r}\left(\sum_{j=-N/2}^{N/2}\frac{\alpha}{\sqrt{(x_n-r)^2+\left(y-\left(j+\frac{1}{2}\right)r\right)^2}} + \sum_{i=-N/2}^{N/2}\frac{-\alpha}{\sqrt{x_n^2+\left(y-\left(i+\frac{1}{2}\right)r\right)^2}}\right) - eFx_n. \tag{7}$$

The number N of dipoles we used is 200. For r we took 0.92 nm as before, and values for the dipole fraction α were derived from the work function difference $\Delta\Phi$ obtained from the photoemission experiments (Table I). The change in work function $\Delta\Phi$ can be related to the fractional dipole strength α at the interface using the Helmholtz equation for interfacial dipoles. When $\Delta\Phi$ is measured in eV, the strength of an interfacial dipole can be expressed as $\varepsilon_0\varepsilon_r\frac{\Delta\Phi}{e} = ep\sigma$, where $p = \alpha er$ is the dipole moment and σ is the area density of dipoles, $\sigma = 1/r^2$, with σ being the fractional dipole. This yields $\alpha = \varepsilon_0\varepsilon_r r\Delta\Phi/e$. Using the measured values for $\Delta\Phi$ and taking $\varepsilon_r = 3.5$ and $r = 0.92$ nm, we arrive at the rather low values for α up to 0.03 listed in Table I. Inserting (7) into (6) allows us to simulate the dissociation yield $\varphi(F)$ using (3) and (4) as before. The resulting curves shown in Fig. 4(c) are very similar to those of the pure effective mass model in two respects, noting, however, that the values for the effective masses are larger (vide infra). First, we can reproduce the field dependence and, in particular, the decrease of F_{sat} in the polymer series, from DOOPPP to PCDTBT. Second, the comparison of experimental and theoretical efficiencies still indicates that at lower electric fields the model predicts lower yields than experimentally measured.

To compare the simulation parameters of the dipole model with the effective mass model, we need to take a little detour. In the effective mass model, we could use accurate values for E_n by solving the Schrödinger Equation (5) numerically. This is valuable and needed when evaluating the resulting simulation parameters quantitatively. In the dipole model (6), a numerical solution to E_n was not possible, and the quantization energy needs to be approximated by a harmonic oscillator [$U(y)$ in Fig. 5(a)]. Since we want to directly compare how the incorporation of dipoles affects the simulation and its associated parameters, we have first repeated the simulations to the effective mass model using also the harmonic oscillator approximation (Eq. 12 in Ref. 24), while keeping the effective masses equal to those obtained with the numerical solution [Table II, "effective mass model (parabolic approximation)"]. The resulting field dependence of the photocurrent yield is identical to Fig. 4(b) and is therefore not shown. Changes caused by the parabolic approximation are manifested in the different values obtained for the factor $\tau_0\nu_0\exp(-2\gamma r)$, which reduces by one to two orders of magnitude and shall not be considered any further. Having used the same level of approximation and very similar values for $\tau_0\nu_0\exp(-2\gamma r)$, we can now consider the impact of including the dipoles on the effective masses (Table II, dipole model). We find m_{eff}/m_e still decreases from DOOPPP to MeLPPP, yet the values are

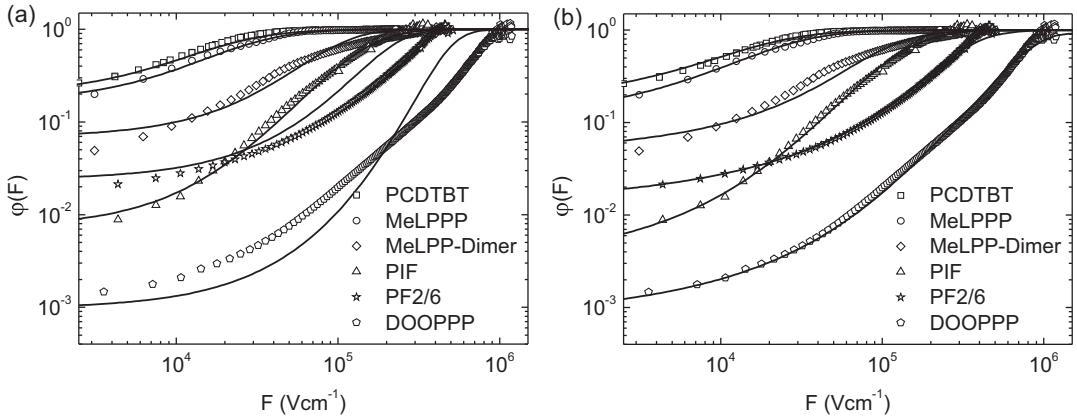

FIG. 6. Comparison of the field-dependent photocurrent yields (symbols) of donor /C_{60} bilayer solar cells with simulations (lines) based on (a) the combination of dipole model with Braun model, and (b) the combination of dipole model with dopant assisted dissociation model. The parameters are presented in Table III.

higher and more realistic than those needed when the dipoles are ignored. Thus, we have seen that charge dissociation in the more efficient, well-delocalized polymers PCDTBT, MeLPPP, and PIF can be described well by taking into account the effects from both, zero-point oscillations and interfacial dipoles. For the efficient polymers with shorter conjugation length, PF2/6 and DOOPPP, there is an additional photocurrent at lower fields that is not yet included in the modeling.

B. Combined models

We now attend to the additional contribution to the dissociation yield observed experimentally at lower electric fields. It is tempting to consider localized charge transfer states as candidates for the additional contribution. To test this hypothesis we tried to fit that extra contribution employing the Onsager-Braun model, i.e., we combined the dipole model and the Onsager-Braun model as $\varphi(F) = \varphi_{\text{dipole}}(F) + (1 - \varphi_{\text{dipole}}(F))\varphi_{\text{Onsager-Braun}}(F)$. As is evident in Fig. 6(a) and Table III, this was unsuccessful. To reproduce the yield at low electric fields, one had to invoke parameters that lead to a lower saturation field than experimentally observed, and, vice versa, if the saturation field is reproduced, the yields at low field cannot be matched. We therefore abandoned the Braun model (and its modification by Tachiya) to describe our results.

As a second option, we explored the idea of *dopant-assisted carrier photogeneration* at C_{60} molecules that may have diffused into the polymer donor layer.[52] The field dependence of the photocurrent resulting from such a process has been worked out by Arkhipov in 2003 as a variation of the effective mass model.[22] Arkhipov *et al.* consider a polymer film containing a low dopant concentration. The idea is again that the electron is transferred to the dopant, leaving behind a hole that oscillates coherently in the conjugated polymer segment. Due to the isolated, localized nature of the dopant, no interfacial dipoles are considered, which is in contrast to the situation of an extended dopant layer forming an interface. Note that while the dopant concentration is low and dopants are isolated within the polymer matrix, the concentration needs to be sufficient to allow for trap-to-trap motion of the electrons to the electrode in order for this process to result in a photocurrent.

If an exciton initially happens to be on a conjugated polymer segment adjacent to an individual C_{60} molecule at a distance r, then the probability w for it to dissociate into free carriers is given by the product of the probability for the electron to transfer to the C_{60}, w_t, multiplied by the probability for the hole to escape from the mutual Coulomb potential, w_{esc}. For an exciton with lifetime τ_0 and a tunneling rate to C_{60} given by $k_t = \nu_0 \exp(-2\gamma r)$, this yields

$$w_t = \frac{k_t}{k_t + \tau_0^{-1}} = \frac{1}{1 + (\nu_0\tau_0)^{-1}\exp(2\gamma r)}. \tag{8}$$

Similarly, w_{esc} is given by considering the escape rate $k_{\text{esc}} = \nu_0 \exp\left(-(U_{\max} - E_{\min})/kT\right)$ and the recombination rate, which is equal to the tunneling rate k_t. Thus,

$$w_{\text{esc}} = \frac{k_{\text{esc}}}{k_{\text{esc}} + k_t} = \frac{1}{1 + \exp(-2\gamma r)\exp\left(\frac{U_{\max} - E_{\min}}{kT}\right)}. \tag{9}$$

The potential U considered here is the sum of Coulomb potential and electric field, as expressed in (5). As indicated in Fig. 5(a), $U_{\max}$ is the maximum value of the potential. $E_{\min}$ is the energy of the hole. Analogous to (6), it can be expressed as the sum of the potential energy at the hole position $x_{\min}$ and the zero-point oscillation energy, so that $E_{\min} = U(x_{\min}) + 0.5\hbar\omega$. To facilitate the calculations, the parabolic approximation is used for ω analogous to (6). The difference between $U_{\max}$ and $E_{\min}$ is the height of the barrier that the hole needs to overcome in order to escape. The probability for dissociation at a site at distance r is then

$$w(r) = \frac{1}{1 + (\nu_0\tau_0)^{-1}\exp(2\gamma r)} \cdot \frac{1}{1 + \exp(-2\gamma r)\exp\left(\frac{U_{\max} - E_{\min}}{kT}\right)}. \tag{10}$$

Arkhipov considers that the dopants are distributed randomly so that the probability of finding the nearest dopant over the distance r from a conjugated segment is determined by the Poisson distribution $P(r) = 2\pi r l N_d \exp\left(-\pi l N_d (r^2 - r_{\min}^2)\right)$.

TABLE III. Fit parameter for different combined models

Material	PCDTBT	MeLPPP	PIF	PF2/6	DOOPPP	MeLPP-dimer
			Dipole model + Onsager-Braun model			
m_{eff}/m_e (dipole)	0.125	0.110	0.135	0.310	1.180	0.180
$\tau_0\nu_0\exp(-2\gamma r)$	39	40	39	38	12	40
r_0 [nm]	0.92	0.92	0.92	0.92	0.92	0.92
$\mu\tau$[10^{-12} m^2 V^{-1}]	5.00	4.00	0.15	0.40	0.02	1.50
			Dipole model + dopant model			
m_{eff}/m_e (dipole)	0.125	0.110	0.135	0.310	1.180	0.180
$\tau_0\nu_0\exp(-2\gamma r)$	39	40	39	38	12	40
m_{eff}/m_e (dopant)	0.125	0.133	0.250	0.490	1.300	0.340
$\tau_0\nu_0$ [10^3]	55	36	22	15	8	36
γ [nm^{-1}]	2.8	3.0	4.0	4.0	7.0	6.3
$\tau_0\nu_0\exp(-2\gamma r)$[a]	318	120	14	9	0.02	0.3
r_{min} [nm]	0.60	0.60	0.60	0.63	0.70	0.60
lN_d [10^{18} m^{-2}]	1.32	1.98	4.86	1.32	3.6	1.8

[a]Calculated from the parameters $\tau_0\nu_0$ and γ, using $r = 0.92$ nm.

r_{min} is the smallest possible distance between dopant and chain, l is the conjugation length, and N_d is the dopant concentration. The overall dissociation yield $\varphi(F)$ is then obtained by integrating $P(r)w(r)$ over space [Eq. (8) in Ref. 22]. By combining the dipole model with the dopant-assisted model, the experimental data can be fitted in a perfect manner, giving the parameters in Table III. The high quality of fit for all polymers considered over the entire field range is very satisfying [Fig. 6(b)].

We shall consider the values obtained for the parameters. The two physical processes that are combined here in the fashion $\varphi(F) = \varphi_{\text{dipole}}(F) + (1 - \varphi_{\text{dipole}}(F))\varphi_{\text{dopant}}(F)$ are (i) the dissociation at an interface between an extended polymer phase and an extended C_{60} phase, where interfacial dipoles can form, and (ii) the dissociation at localized polymer/C_{60} sites that arise from the diffusion of individual C_{60} molecules into the polymer phase. It is gratifying that the values for the effective mass inferred from the data for both processes are close (Table III). Those values should, indeed, be similar because both processes are based upon the concept of a hole oscillating within the conjugated segment of the polymer. They differ insofar that, at the extended interface, the oscillation happens in the Coulomb well modified by the interfacial dipoles, yet at always the same distance from the C_{60}. In contrast, for the dopant-assisted dissociation process, the Coulomb potential is only due to the geminate charges, yet the polymer–C_{60} distance varies, and thus the position of the hole within the potential well. At this point, it is appropriate to consider the numerical error that might arise if the built-in potential, used to calculate the internal field, was 100 meV or 200 meV lower than the open-circuit voltage $V_{\text{oc}}^{\text{photo}}$ determined for the photocurrent. Repeating the fits for such a case (see Supplemental Material[26]) shows that the effective masses change by up to 30%, yet they remain within the error margin indicated in Fig. 7. In view of the large variation of effective mass between the compounds, this variation obtained when using a different built-in potential is not significant.

We now turn to the remaining parameters. To evaluate whether the values obtained for lN_d are reasonable, consider a conjugation length l of about 10 nm and take the result of $lN_d = 2 \cdot 10^{18}$ m^{-2} obtained for MeLPPP as representative example. This translates into a dopant concentration of $N_d = 2 \cdot 10^{20}$ cm^{-3}. A typical concentration of molecules in a molecular crystal is about $4 \cdot 10^{21}$ cm^{-3} (using, for anthracene, a density of 1.2 g/cm^3, a molar mass of 178g, and Avogadro's number). Assuming a similar concentration of conjugated segments (chromophores) here, this would suggest a doping concentration of about 5%. This is a realistic value. Similarly, the value obtained for r_{min} is plausible. Considering the values for the product of the lifetime and probability in detail is not meaningful. As discussed previously, they are underestimated due to the technical need of using the parabolic approximation for the potential. Nevertheless, it is encouraging that their trend and magnitude is consistent with that obtained for the effective mass model when also using the parabolic approximation.

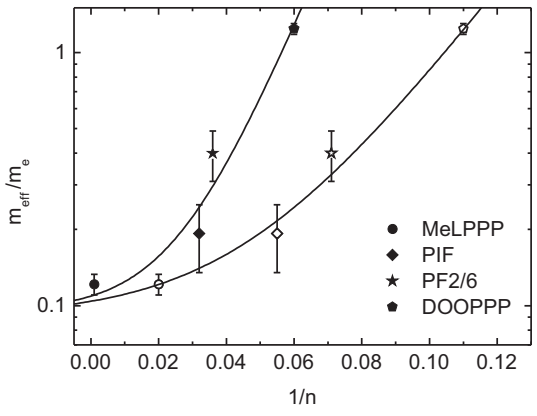

FIG. 7. The dependence of the relative effective masses on the inverse effective conjugation length of the donors for the ground state geometry (data taken from absorption, empty symbols) and for the excited state geometry (data taken from emission, filled symbols). The effective masses are taken from the dipole model (Table II) and the dipole model + dopant model (Table III), with the error bar indicating the spread of values between these models. The solid lines are fits to an exponential curve with a baseline, as described in the text.

Overall, the combination of experiment and modeling demonstrates that taking into account the effect of conjugation length by an effective mass approach is essential for an appropriate description of the dissociation process. In this context, it is useful to recall that the degree of delocalization can be quantified through the effective conjugation length. It is the number of repeat units over which an excitation, be it an exciton or a charge carrier, is coherently coupled considering, though, that there is, on average, no sharp boundary between different conjugated segments but rather a gradual local decrease of the coupling strength. In this sense, the effective mass should be viewed as an average effective mass that depends on the size of coherently coupled repeat units. The concept of a conjugation length-dependent effective mass is confirmed by Fig. 7. It shows the variation of the values for the effective mass inferred from the data fits on the reciprocal effective conjugation lengths taken from either the absorption or fluorescence spectra. The effective mass decreases roughly exponentially toward a value of about $0.1\,m_e$ at infinite conjugation length. This value is in good agreement with both experiment[49] and theory[50] on perfect π-conjugated chains. Empirically, the dependence of the relative effective mass on the effective conjugation lengths in either the ground state geometry (i.e., for the energy taken from the $S_1 \leftarrow S_0$ 0-0 transitions seen in absorption) or the excited state geometry (i.e., for the energy taken from the $S_1 \rightarrow S_0$ 0-0 transitions seen in fluorescence) can be expressed as

$$\frac{m_{\text{eff}}}{m_e} = 0.090 + 0.014 \cdot e^{\frac{40}{n}} \tag{11a}$$

for the excited state geometry, and

$$\frac{m_{\text{eff}}}{m_e} = 0.095 + 0.014 \cdot e^{\frac{74}{n}} \tag{11b}$$

for the ground state geometry.

This is an entirely empirical relationship, obtained for the poly(*p*-phenylene) type polymers, since for these materials the parameterization of transition energy versus conjugation lengths is known.[30]

IV. CONCLUSIONS

The present experiments on polymeric donor/C_{60} bilayer systems demonstrate that measuring the photocurrent over a broad range of electric field provides a unique source of information on the elementary step of photodissociation.

(i) The existence of a saturation field confirms the notion that mobile charge carriers originate from the dissociation of geminately bound e-h pairs. These are generated by a preceding ultrafast charge transfer step. [9,10]

(ii) The experiments show that the Coulomb-binding energy, evidenced by F_{sat}, scales inversely with the conjugation length of the donor polymer. If that conjugation length is large, the Coulomb-binding energy is small, and the built-in potential of the solar cell can be sufficient to break up all initially generated geminate e-h pairs. This is the case desired for solar cell applications, and it is associated with a high fill factor. Here, this is realized for MeLPPP and PCDTBT, with the latter having a far more suitable optical gap for actual solar cell applications. In contrast, if the conjugation length is short, the hole cannot overcome the Coulomb barrier and will recombine eventually with its sibling electron. The recombination can be prevented, and escape from the Coulomb well can be assisted by supplying additional activation energy, for example, in the form of an infrared light pulse as demonstrated by Bakulin *et al.*[12]

(iii) Photoemission measurements and modeling show that in a bilayer device, the dissociation process can be facilitated by a weak ground state dipole layer that exists at the donor-acceptor interface and that screens the Coulomb potential.

(iv) Except for electric field strengths that are much lower than the saturation field strengths, the experimental results can be quantitatively explained in terms of a model that was set up by Arkhipov *et al.* and subsequently refined and extended by Nenashev *et al.*[22–25] The key idea is that the hole on the e-h pair is delocalized within a segment of the π-conjugated polymer and executes zero-point oscillations within the Coulomb potential well of the localized electron at the C_{60}. The energy of those zero-point oscillations is controlled by the effective mass of the hole.

(v) When modeling the experimental results, we find that the effective mass correlates inversely with the effective conjugation length, i.e., the larger the conjugation lengths, the smaller the effective mass and, concomitantly, the Coulomb-binding energy of the dissociating e-h pair.

(vi) The present results show there is also an additional photogeneration channel. It originates from the dissociation of e-h pairs at individual C_{60} molecules that diffused into the donor layer. The description of this process is also based on an effective mass model except for the absence of the interfacial dipole layer. This channel is relevant at low fields for polymers with short conjugation lengths. In systems with large effective conjugation lengths of the polymeric donor, this contribution of dopant-assisted dissociation becomes virtually negligible.

V. EXPERIMENTAL METHODS

MeLPPP, MeLPP-dimer, PIF, PF2/6, and DOOPPP were synthesized by the group of U. Scherf, as described elsewhere.[53–56] PCDTBT was bought from "1-material." The structure formulae for the materials are given in Fig. 1. For photocurrent measurements, bilayer solar cell devices were fabricated using structured ITO-coated glass substrates in a special device architecture that eliminates edge effects.[16] This allows applying electric fields up to 1.3 MV/cm without risking spurious breakdown effects. For the series of solar cells reported here, 50–60-nm-high conductive PEDOT:PSS (Sigma Aldrich, neutral pH) was spin coated on top of the ITO and heated up to 180 °C for 30 min. Onto this, 40-nm-thick polymer films were spin coated from filtered chlorobenzene solutions (5.0–7.5 mg/ml) and annealed at 80 °C for 10 min to remove any residual solvent. This was followed by vapor deposition of a 40-nm layer of C_{60} (99.9% purity, AmericainDyeSourceInc). A 100-nm vapor-deposited layer of aluminum as a top electrode completed the diode structure.

Current-voltage curves were measured under monochromatic illumination at 2.2 eV (570 nm) from a 150 W Xenon lamp at 1.5 mW/cm^2. At this wavelength, the light is absorbed by the C_{60} acceptor while the polymer donors are not excited, except for the low-bandgap polymer PCDTBT. The photocurrent was determined by measuring the dark current

and the total current under illumination and then subtracting the dark current from the total current under illumination. This is done after each data point before stepping to the next voltage step. The solar cells were evaporated under a vacuum of $5 \cdot 10^{-7}$ mbar at room temperature. A Keithley 236 source-measure unit was used to record current and applied voltage. The internal electric field was calculated as $|F| = (V - V_{\mathrm{bi}})/d$, where V is the applied external voltage, V_{bi} is the built-in field, taken as $V_{\mathrm{bi}} = V_{\mathrm{oc}}^{\mathrm{photo}}$ unless stated otherwise. $V_{\mathrm{oc}}^{\mathrm{photo}}$ is the open-circuit voltage determined for the photocurrent (i.e., after subtracting the dark current from the total current).

Its value is slightly higher than that of the usual open-circuit voltage, V_{oc}, where the total current (dark current + photocurrent) is zero. d is the active film thickness determined using a Dektak surface profilometer. The relative photocurrent quantum yield $\varphi(F)$ corresponds to the photocurrent per illuminated light intensity, both normalized to unit area. $\varphi(F)$ is normalized to unity at the high field saturation value. In our earlier work,[16] we have confirmed that $\varphi(F)$ indeed is on the order of unity at the high field saturation value by considering the absorption coefficient and modeling the exciton diffusion to the interface. The incident light intensities were recorded with a calibrated Hamamatsu S1337-33BQ photodiode, and the absorption of the films was measured using a Cary 5000 absorption spectrometer.

For UPS studies, the polymer samples were spincoated on PEDOT:PSS coated ITO glass substrates from chlorobenzene solutions (2 mg/ml, 25 rps), similar as previously described.

C_{60} was vacuum sublimed (base pressure $p = 3 \cdot 10^{-9}$ mbar) from resistively heated glass crucibles. The mass thickness of the layers was monitored using a quartz crystal microbalance [$\rho(C_{60}) = 1.6$ g/cm^3]. The UPS measurements were performed using a multitechnique ultra high vacuum (UHV) apparatus (base pressure: $1 \cdot 10^{-10}$ mbar) and a Helium discharge lamp ($h\nu = 21.22$ eV). The initial photon flux was attenuated by a factor of ~100 using a silicon filter to avoid irradiation damage of the sample. All spectra were recorded at room temperature and normal emission using a hemispherical Specs Phoibos 100 energy analyzer with 90 meV energy resolution. To determine the work function, the SECO was recorded with the sample biased at -10 V to clear the analyzer work function. Binding energies are reported relative to the Fermi-level spectra, and the error of energy values is estimated to be ± 0.05 eV.

ACKNOWLEDGMENTS

We thank the group of Prof. Ullrich Scherf for supplying the ladder type polymers and dimer and Prof. J. P. Rabe for providing access to a photoelectron spectroscopy setup. This work was supported by the GRK 1640 and the SPP1355 of the Deutsche Forschungsgemeinschaft (DFG), the Helmholtz-Energie-Allianz "Hybrid-Photovoltaik," and the network "SolTechGoHybrid" of the Bayerische Staatsministerium für Wissenschaft, Forschung und Kunst.

*Corresponding author: anna.koehler@uni-bayreuth.de

[1] Heliatek, http://www.heliatek.com/wp-content/uploads/2013/01/130116_PR_Heliatek_achieves_record_cell_effiency_for_OPV.pdf, 2013.
[2] L. Müller-Meskamp, Y. H. Kim, T. Roch, S. Hofmann, R. Scholz, S. Eckardt, K. Leo, and A. F. Lasagni, Adv. Mater. **24**, 906 (2012).
[3] C. Müller, T. A. M. Ferenczi, M. Campoy-Quiles, J. M. Frost, D. D. C. Bradley, P. Smith, N. Stingelin-Stutzmann, and J. Nelson, Adv. Mater. **20**, 3510 (2008).
[4] J. Y. Kim, K. Lee, N. E. Coates, D. Moses, T. Q. Nguyen, M. Dante, and A. J. Heeger, Science **317**, 222 (2007).
[5] C. Deibel and V. Dyakonov, Rep. Prog. Phys. **73**, 096401 (2010).
[6] R. H. Friend, M. Phillips, A. Rao, M. W. B. Wilson, Z. Li, and C. R. McNeill, Faraday Discuss. **155**, 339 (2012).
[7] J. L. Brédas, J. E. Norton, J. Cornil, and V. Coropceanu, Acc. Chem. Res. **42**, 1691 (2009).
[8] J. Nelson, Mater Today **14**, 462 (2011).
[9] D. Herrmann, S. Niesar, C. Scharsich, A. Köhler, M. Stutzmann, and E. Riedle, J. Am. Chem. Soc. **133**, 18220 (2011).
[10] F. Etzold, I. A. Howard, R. Mauer, M. Meister, T. D. Kim, K. S. Lee, N. S. Baek, and F. Laquai, J. Am. Chem. Soc. **133**, 9469 (2011).
[11] T. M. Clarke and J. R. Durrant, Chem. Rev. **110**, 6736 (2010).
[12] A. A. Bakulin, A. Rao, V. G. Pavelyev, P. H. M. van Loosdrecht, M. S. Pshenichnikov, D. Niedzialek, J. Cornil, D. Beljonne, and R. H. Friend, Science **335**, 1340 (2012).
[13] T. G. J. van der Hofstad, D. Di Nuzzo, M. van den Berg, R. A. J. Janssen, and S. C. J. Meskers, Adv. Energy Mater **2**, 1095 (2012).
[14] C. Deibel, T. Strobel, and V. Dyakonov, Phys. Rev. Lett. **103**, 036402 (2009).
[15] A. Köhler, D. A. dos Santos, D. Beljonne, Z. Shuai, J. L. Brédas, A. B. Holmes, A. Kraus, K. Müllen, and R. H. Friend, Nature **392**, 903 (1998).
[16] C. Schwarz, H. Bässler, I. Bauer, J. M. Koenen, E. Preis, U. Scherf, and A. Köhler, Adv. Mater. **24**, 922 (2012).
[17] A. J. Heeger, Chem. Soc. Rev. **39**, 2354 (2010).
[18] S. Verlaak, D. Beljonne, D. Cheyns, C. Rolin, M. Linares, F. Castet, J. Cornil, and P. Heremans, Adv. Funct. Mater. **19**, 3809 (2009).
[19] A. Ojala, A. Petersen, A. Fuchs, R. Lovrincic, C. Pölking, J. Trollmann, J. Hwang, C. Lennartz, H. Reichelt, H. W. Höffken, A. Pucci, P. Erk, T. Kirchartz, and F. Würthner, Adv. Funct. Mater. **22**, 86 (2012).
[20] H. Aarnio, P. Sehati, S. Braun, M. Nyman, M. P. de Jong, M. Fahlman, and R. Österbacka, Adv. Energy Mater **1**, 792 (2011).
[21] R. R. Chance and C. L. Braun, J. Chem. Phys. **59**, 2269 (1973).
[22] V. I. Arkhipov, E. V. Emelianova, and H. Bässler, Chem. Phys. Lett. **372**, 886 (2003).
[23] V. I. Arkhipov, P. Heremans, and H. Bässler, Appl. Phys. Lett. **82**, 4605 (2003).
[24] A. V. Nenashev, S. D. Baranovskii, M. Wiemer, F. Jansson, R. Österbacka, A. V. Dvurechenskii, and F. Gebhard, Phys. Rev. B **84**, 035210 (2011).

[25]M. Wiemer, A. V. Nenashev, F. Jansson, and S. D. Baranovskii, Appl. Phys. Lett. **99**, 013302 (2011).
[26]See Supplemental Material at http://link.aps.org/supplemental/10.1103/PhysRevB.87.155205 for (i) an estimate of the critical photon density at which geminate and non-geminate recombination become comparable, (ii) more parameters for the Braun model, (iii) the photocurrent yield and fits to the MeLPP-Dimer, (iv) parameters and fits to the combined Dipole model + Dopant model using different values for the built-in field.
[27]B. P. Rand, D. Cheyns, K. Vasseur, N. C. Giebink, S. Mothy, Y. P. Yi, V. Coropceanu, D. Beljonne, J. Cornil, J. L. Brédas, and J. Genoe, Adv. Funct. Mater. **22**, 2987 (2012).
[28]W. Kuhn, Helv. Chim. Acta **31**, 1780 (1948).
[29]J. Gierschner, J. Cornil, and H. J. Egelhaaf, Adv. Mater. **19**, 173 (2007).
[30]S. T. Hoffmann, H. Bässler, and A. Köhler, J. Phys. Chem. B **114**, 17037 (2010).
[31]K. Akaike, K. Kanai, H. Yoshida, J. Tsutsumi, T. Nishi, N. Sato, Y. Ouchi, and K. Seki, J. Appl. Phys. **104**, 023710 (2008).
[32]J. Niederhausen, P. Amsalem, A. Wilke, R. Schlesinger, S. Winkler, A. Vollmer, J. P. Rabe, and N. Koch, Phys. Rev. B **86**, 081411 (2012).
[33]S. Braun, W. R. Salaneck, and M. Fahlman, Adv. Mater. **21**, 1450 (2009).
[34]H. Ishii, K. Sugiyama, E. Ito, and K. Seki, Adv. Mater. **11**, 605 (1999).
[35]M. Körner, F. Loske, M. Einax, A. Kühnle, M. Reichling, and P. Maass, Phys. Rev. Lett. **107**, 016101 (2011).
[36]A. C. Morteani, P. Sreearunothai, L. M. Herz, R. H. Friend, and C. Silva, Phys. Rev. Lett. **92**, 247402 (2004).
[37]D. Veldman, Ö. Ipek, S. C. J. Meskers, J. Sweelssen, M. M. Koetse, S. C. Veenstra, J. M. Kroon, S. S. van Bavel, J. Loos, and R. A. J. Janssen, J. Am. Chem. Soc. **130**, 7721 (2008).
[38]L. Onsager, Phys. Rev. **54**, 554 (1938).
[39]C. L. Braun, J. Chem. Phys. **80**, 4157 (1984).
[40]K. K. H. Chan, S. W. Tsang, H. K. H. Lee, F. So, and S. K. So, Org. Electron. **13**, 850 (2012).
[41]R. A. Marsh, J. M. Hodgkiss, and R. H. Friend, Adv. Mater. **22**, 3672 (2010).
[42]C. S. Ponseca, A. Yartsev, E. Wang, M. R. Andersson, D. Vithanage, and V. Sundström, J. Am. Chem. Soc. **134**, 11836 (2012).
[43]J. Kirkpatrick, P. E. Keivanidis, A. Bruno, F. Ma, S. A. Haque, A. Yarstev, V. Sundström, and J. Nelson, J. Phys. Chem. B **115**, 15174 (2011).
[44]M. Wojcik and M. Tachiya, J. Chem. Phys. **130**, 104107 (2009).
[45]S. Barth, H. Bässler, U. Scherf, and K. Müllen, Chem. Phys. Lett. **288**, 147 (1998).
[46]A. Petersen, A. Ojala, T. Kirchartz, T. A. Wagner, F. Würthner, and U. Rau, Phys. Rev. B **85**, 245208 (2012).
[47]N. Christ, S. W. Kettlitz, S. Valouch, J. Mescher, M. Nintz, and U. Lemmer, Org. Electron. **14**, 973 (2013).
[48]M. Pope and C. E. Swenberg, *Electronic Processes in Organic Crystals and Polymers* (Oxford University Press, New York, 1999).
[49]G. Weiser and S. Möller, Phys. Rev. B **65**, 045203 (2002).
[50]J. W. van der Horst, P. A. Bobbert, M. A. J. Michels, and H. Bässler, J. Chem. Phys. **114**, 6950 (2001).
[51]C. Im, W. Tian, H. Bässler, A. Fechtenkötter, M. D. Watson, and K. Müllen, J. Chem. Phys. **119**, 3952 (2003).
[52]D. E. Markov, E. Amsterdam, P. W. M. Blom, A. B. Sieval, and J. C. Hummelen, J. Phys. Chem. A **109**, 5266 (2005).
[53]M. Grell, W. Knoll, D. Lupo, A. Meisel, T. Miteva, D. Neher, H. G. Nothofer, U. Scherf, and A. Yasuda, Adv. Mater. **11**, 671 (1999).
[54]S. P. Huang, G. S. Huang, and S. A. Chen, Synth. Met. **157**, 863 (2007).
[55]U. Scherf and K. Müllen, Makromol Chem-Rapid **12**, 489 (1991).
[56]S. Setayesh, D. Marsitzky, and K. Müllen, Macromolecules **33**, 2016 (2000).

Supporting Information to

On the Role of the Effective Mass and Interfacial Dipoles on Exciton Dissociation in Organic Donor-Acceptor Solar Cells

Christian Schwarz, Steffen Tscheuschner, Johannes Frisch, Stefanie Winkler, Norbert Koch, Heinz Bässler, and *Anna Köhler**

C. Schwarz, S. Tscheuschner, H. Bässler, A. Köhler,
Experimental Physics II and Bayreuth Institute of Macromolecular Research (BIMF)
University of Bayreuth
95440 Bayreuth, Germany
E-mail: Anna.Koehler@uni-bayreuth.de

J. Frisch, S. Winkler, N. Koch
Institut für Physik
Humboldt-Universität zu Berlin

The critical photon density at which geminate and non-geminate recombination become comparable can be estimated roughly as follows.

The rate equation for the density of photogenerated charges *n* is given by

$$\frac{dn}{dt} = 0 = G - \frac{n}{\tau_{tr}} - \gamma n^2 \tag{1}$$

where γ is the bimolecular recombination coefficient, τ_{tr} is the transit time i.e. the inverse of the rate constant for getting the charges through the film to the electrodes. G is the generation rate per cm^3, i.e. the photon flux (photons/cm^2) divided by the penetration depths.
The quadratic equation in (1) can be solved as

$$n = -\frac{1}{2\gamma\tau_{tr}} + \sqrt{\frac{G}{\gamma} + \left(\frac{1}{2\gamma\tau_{tr}}\right)^2} \tag{2}$$

which may be written as

$$n = \frac{1}{2\gamma\tau_{tr}}\left[-1+\sqrt{1+(2\tau_{tr})^2 G\gamma}\right]. \tag{3}$$

γ is a material constant that is the same, independent of illumination intensity. Two cases can be distinguished. First, consider the case of a very low photon flux, i.e. low generation rate, so that $(2\tau_{tr})^2 G\gamma << 1$. Developing the root leads to

$$\frac{n}{\tau_{tr}} = G \qquad \text{for} \qquad (2\tau_{tr})^2 G\gamma << 1. \tag{4}$$

This is identical to the result one obtains from (1) if bimolecular recombination is negligible. The other case is that of a very high generation rate, so that $(2\tau_{tr})^2 G\gamma >> 1$. The number of 1 under the root and in front of the root can then be neglected, leading to

$$n = \sqrt{\frac{G}{\gamma}} \qquad \text{for} \qquad (2\tau_{tr})^2 G\gamma >> 1. \tag{5}$$

This is the same than would be obtained from (1) if bimolecular decay dominates. We now consider the number of charges getting out of the device, n/τ_{tr}. For high generation rate, this is

$$\frac{n}{\tau_{tr}} = \frac{1}{\tau_{tr}}\sqrt{\frac{G}{\gamma}} \quad \text{for} \qquad (2\tau_{tr})^2 G\gamma >> 1. \tag{6}$$

From (4) and (6), the effects of monomolecular decay and bimolecular decay are equal if,

$$G = \frac{1}{\gamma\tau_{tr}^2}. \tag{7}$$

The transit time is given by $\tau_{tr} = d/\mu F$, with d being the film thickness and F the electrical field across the film. The rate constant for bimolecular recombination can be taken from the Langevin condition

$$\frac{\gamma}{\mu} = \frac{e}{\varepsilon_0\varepsilon_r}. \tag{8}$$

Inserting this into equation (7) gives

$$G = \frac{\varepsilon_0\varepsilon_r\mu F^2}{ed^2}. \tag{9}$$

Typical parameters of F = 10^5 V/cm, μ = 10^{-3} cm^2/Vs, d = 100 nm imply that $G = 2\cdot10^{23}$ cm^{-3}s^{-1} is the volume generation rate at which bimolecular and monomolecular decay become comparable. If we presume that every photon absorbed generates an electron (and a hole), and that absorption is linear, then for a film thickness of 100 nm, the critical photon flux G_A is

$$G_A = 2\cdot10^{18}\ \text{cm}^{-3}\text{s}^{-1} \tag{10}$$

In our experiments, we used monochromatic illumination at 570 nm from a Xenon lamp. The intensity at the position of the solar cell was 1.5 mW/cm^2. This corresponds to a photon flux of about $4 \cdot 10^{15}$ photons/cm^{2}s, i.e. the intensity used in our experiment is 1/500 of the intensity at which bimolecular recombination becomes important.

	PCDTBT dashed	PCDTBT solid	DOOPPP dashed	DOOPPP solid
r_0 [nm]	1.03	1.03	0.80	0.80
$\nu\tau$ [10^{-12}m^{2}V^{-1}]	2.0	15.0	0.30	0.02

Table S1: Parameters for the Braun model, comparison of dashed and solid lines in Fig. 4a

Photocurrent yield and fits to the MeLPP-Dimer

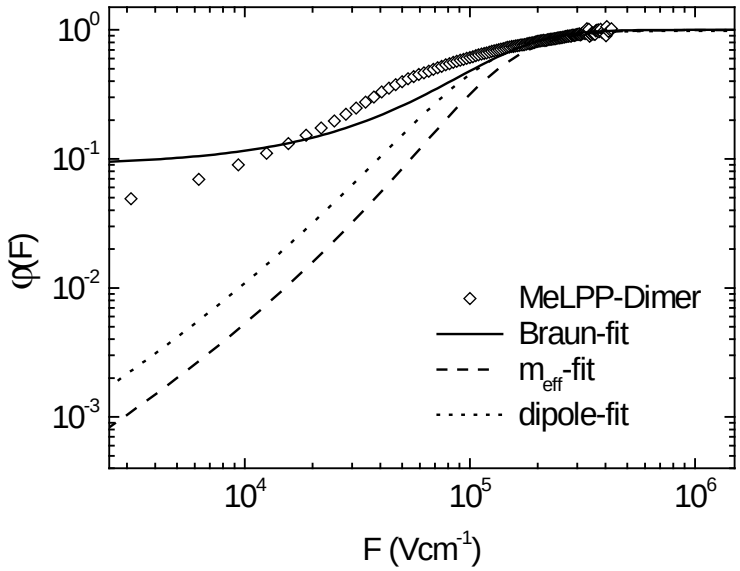

Figure S1 : Fits of the experimental external quantum yields of bilayer MeLPP-Dimer/C_{60} devices with different models. The fit parameters are shown in the paper.

In order to assess the impact of the uncertainty in determining the built-in field, we have repeated the combined fit (Dipole model + Dopant model), using the same parameters in Table 3 except for the effective mass, for the case $V_{bi} = V_{oc}^{photo}$ - 100 meV, $V_{bi} = V_{oc}^{photo}$ - 200 meV. The resulting parameters are compared in Table S2.

	DOOPPP		PIF		MeLPPP	
	m_{eff}/m_e (dipol)	m_{eff}/m_e (dopant)	m_{eff}/m_e (dipol)	m_{eff}/m_e (dopant)	m_{eff}/m_e (dipol)	m_{eff}/m_e (dopant)
$V_{bi} = V_{oc}^{photo}$	1.180	1.300	0.135	0.250	0.110	0.133
$V_{bi} = V_{oc}^{photo}$ - 100 meV	1.200	1.000	0.160	0.190	0.115	0.110
$V_{bi} = V_{oc}^{photo}$ - 200 meV	1.300	0.900	0.160	0.175	0.110	0.100

Table S2: Adapted m_{eff}/m_e to assess the impact of uncertainty in determining the built-in field in the combined fit (Dipole model + Dopant model).

The corresponding fits (lines) to the data (symbols) are shown here for different V_{bi}:

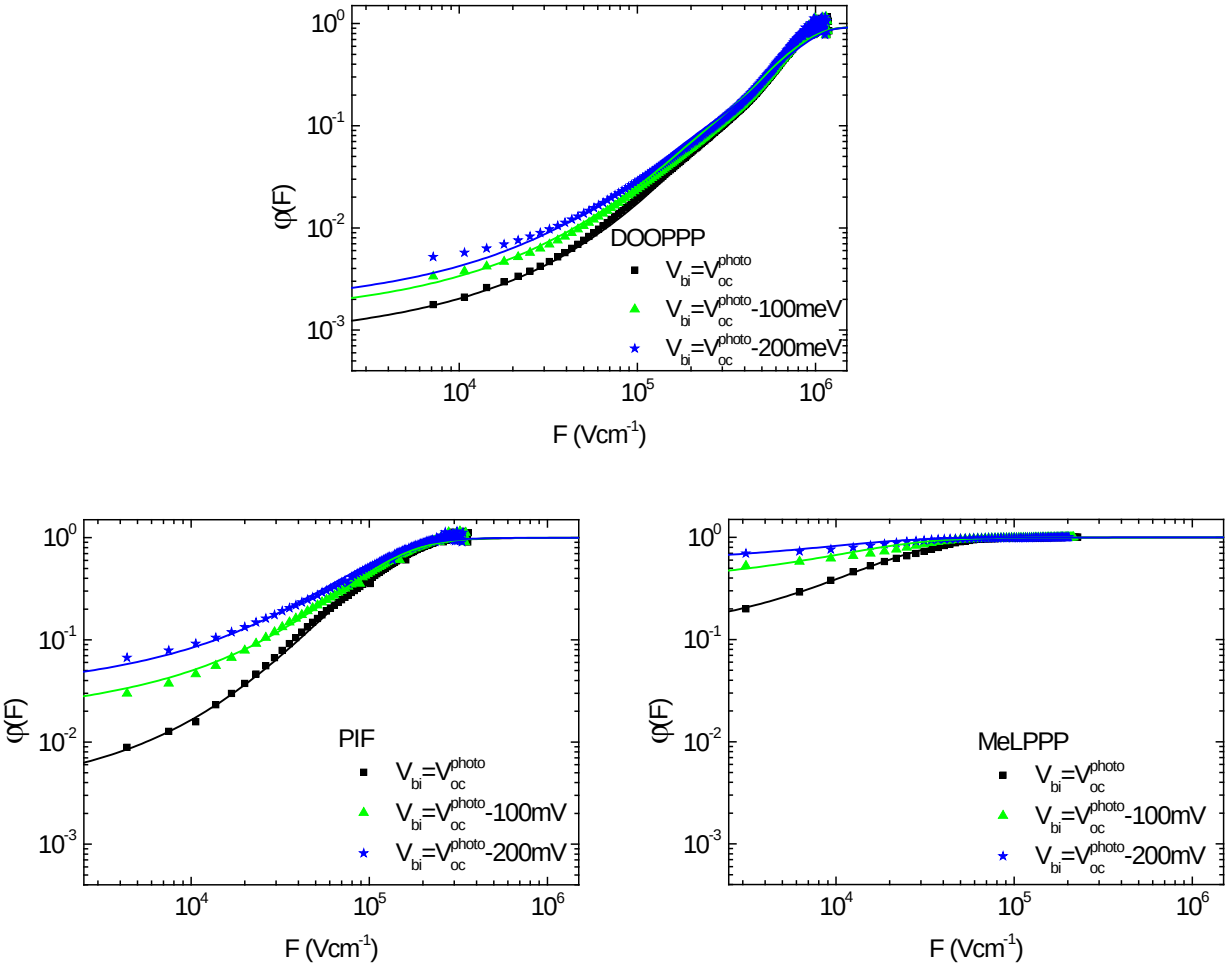

7. Influence of the excited state charge-transfer character on the exciton dissociation in donor-acceptor copolymers

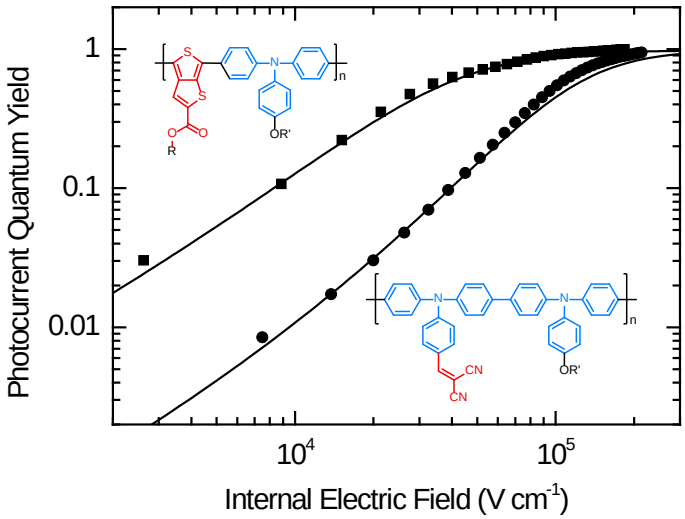

Katharina Neumann, Christian Schwarz, Anna Köhler, Mukundan Thelakkat

Veröffentlicht in

Journal of Physical Chemistry C, 2013, DOI: 10.1021/jp407014q

THE JOURNAL OF PHYSICAL CHEMISTRY C

Article

pubs.acs.org/JPCC

Influence of the Excited-State Charge-Transfer Character on the Exciton Dissociation in Donor−Acceptor Copolymers

Katharina Neumann,[†] Christian Schwarz,[‡] Anna Köhler,[‡] and Mukundan Thelakkat*,[†]

[†]Applied Functional Polymers, Macromolecular Chemistry I, University of Bayreuth, 95440 Bayreuth, Germany

[‡]Experimental Physics II and Bayreuth Institute of Macromolecular Research (BIMF), University of Bayreuth, 95440 Bayreuth, Germany

Supporting Information

ABSTRACT: We synthesize a polytriphenylamine homopolymer and two donor−acceptor copolymers (D−A-copolymers) based on triphenylamine (TPA) as donor in combination with two different acceptor moieties to study the effect of the acceptor unit on the excited-state charge-transfer characteristics (CT-characteristics) and charge separation. The two acceptor moieties are a dicyanovinyl group in the side chain and a thieno[3,4-*b*]thiophene carboxylate in the main chain. Absorption and photoluminescence studies show new CT-bands for both of the D−A-copolymers. Field-dependent charge extraction studies in bilayer solar cells indicate a stronger CT-character for the copolymer in which the acceptor group is less conjugated with the copolymer backbone. The D−A-copolymer carrying the acceptor unit in the main chain exhibits smaller excitonic CT-character and good conjugation leading to less-bound electron−hole pairs and a better charge separation. This fundamental study gives insight into the interdependence of conjugation, charge carrier mobility, and solar cell performance for two different D−A-copolymers.

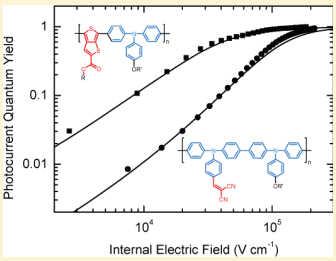

1. INTRODUCTION

There is intensive research in the field of bulk heterojunction solar cells comprising alternating donor−acceptor copolymers (D−A-copolymers) and fullerene derivatives with the aim to design novel D−A-copolymers and thus to increase the power conversion efficiency.[1−3] In general, two strategies are widely used as the design principle for these D−A-copolymers: (a) introduction of the A unit as a side chain on the donor backbone and (b) incorporation of D and A in the main chain to get alternating D−A-copolymers.[4−10] The diverse elementary processes and dynamics of charge transfer (CT) and charge separation in such a bulk heterojunction solar cell have been intensively studied.[11,12] After light absorption a bound metastable intermolecular CT-state is formed by electron transfer to a neighboring molecule. This state can separate into free charge carriers or recombine. Since the charge separation is a key step, it is very important to understand the influence of conjugation and excited-state CT-character on this process. Commonly, the CT-character of the excited state between D−A-copolymer and fullerene acceptor has been investigated.[13] It is equally important to understand and correlate the degree of excited-state CT-character of the D−A-copolymer itself with its charge carrier mobility as well as the charge separation with fullerenes. It was shown by Tautz et al. that the polaron pair yield in D−A-copolymers is dependent on the electron affinity of the acceptor moiety.[14] A correlation of this observation with charge separation and device characteristics was not reported there. Furthermore, Carsten et al. showed that not only the energetics but also the internal dipole moment along the polymer chain may be critical for the CT-state, and these results were compared with charge separation in bulk heterojunction devices.[15] Here, we first correlate the observed CT-character with the conjugation/delocalization as well as with the charge carrier mobility in the D−A-polymer itself. The observed CT-character is then compared with the charge separation in fullerene bilayer devices. We selected a well-defined bilayer device to avoid possible morphological differences in blend devices on using different polymers. Our material system consists of two novel D−A-copolymers based on triphenylamine (TPA). We chose a system containing TPA which is a widely examined and well-known donor material with excellent thermal and electrochemical stability.[16] The CT-character of the excited state of D−A-copolymers depends on the nature of attachment of the acceptor unit to the donor moiety. Here, we compare two different D−A-copolymers: (a) with a dicyanovinyl acceptor in the side chain (**P2**) and (b) with a thieno[3,4-*b*]thiophene acceptor in the main chain (**P3**) with the homopolymer (**P1**) without any acceptor unit. Since the resulting interaction between electron donating and the electron withdrawing molecules usually leads to the formation of an intramolecular CT-state,[17] the two different strategies adopted here can result in different degrees of CT-character and conjugation or delocalization between the D and A moieties.

2. EXPERIMENTAL SECTION

2.1. Synthesis and Polymerization. **P1**: 4-Bromo-*N*-(4-bromophenyl)-*N*-(4-(2-ethylhexyloxy)phenyl)aniline (**1**; 516

Received: July 16, 2013
Revised: December 5, 2013

   dx.doi.org/10.1021/jp407014q | *J. Phys. Chem. C* XXXX, XXX, XXX−XXX

mg, 0.97 mmol) and 4-(2-ethylhexyloxy)-*N*,*N*-bis(4-(4,4,5,5-tetramethyl-1,3,2-dioxaborolan-2-yl)phenyl)aniline (**2**; 607 mg, 0.972 mmol) were dissolved in 8 mL of tetrahydrofuran (THF). A 5.3 mL aliquot of 2 M K_2CO_3 in water and dimethylformamide (DMF; 1:1) were added, and the mixture was purged with argon for 30 min. $Pd(PPh_3)_4$ (45 mg, 0.04 mmol) and $Pd(OAc)_2$ (4 mg, 0.02 mmol) were added, and the reaction mixture was heated to 70 °C. After 72 h the polymerization was end-capped by the addition of phenylboronic acid pinacol ester and bromobenzene for 3 h. After cooling, the reaction mixture was extracted with dichloromethane (DCM) and water. The crude product poly[*N*,*N*′-bis(4-(2-ethylhexyloxy)phenyl)-*N*,*N*′-di-*p*-tolylbiphenyl-4,4′-diamine] (**P1**) was precipitated in MeOH and purified by sequential Soxhlet extraction in MeOH and EtOH. Yield: 66%. ^{1}H NMR (300 MHz, $CDCl_3$, 298 K; ppm): δ 7.51−7.36 (d, 2H, H_{ar}), 7.18−6.99 (d, 2H, H_{ar}), 6.93−6.81 (m, 6H, H_{ar}), 3.83 (d, 2H, O−CH_2), 1.80−1.66 (m, 1H, CH), 1.60−1.39 (m, 8H, CH_2), 1.34 (s, 12 H, CH_3), 0.97−0.84 (m, 6H, CH_3).

P2: First, an aldehyde functionalized copolymer was synthesized as precursor. For that, 4-(bis(4-bromophenyl)-amino)benzaldehyde (0.79 g, 1.83 mmol) and **2** (1.15 g, 1.83 mmol) were dissolved in 15 mL of THF. After addition of 2.33 mL of 2 M K_2CO_3 in water and DMF (1:1), the mixture was degassed. A 20 mg (0.017 mmol) amount of $Pd(PPh_3)_4$ and 2 mg (0.009 mmol) of $Pd(OAc)_2$ were added, and the reaction mixture was heated to 70 °C. After 5 days, phenylboronic acid pinacol ester and bromobenzene were added for end-capping and the mixture was stirred for 3 h. The reaction mixture was cooled to room temperature and extracted with dichloromethane (DCM) and brine. The organic phase was dried over Na_2SO_4, and the solvent was evaporated under reduced pressure. The dark brown residue was dissolved in THF, and a small amount of the scavenger *N*,*N*-diethylphenylazothioformamide was added. After 3 h at room temperature the polymer was precipitated in MeOH followed by a Soxhlet extraction in EtOH for 12 h. Poly[4-((4′-((4-(2-ethylhexyloxy)phenyl)(*p*-tolyl)amino)biphenyl-4-yl)(*p*-tolyl)-amino)benzaldehyde] was obtained as beige powder. Yield: 70%. ^{1}H NMR (300 MHz, $CDCl_3$, 298 K; ppm): δ 9.83 (s, 1H, CHO), 7.84−7.64 (s, 2H, H_{ar}), 7.64−7.34 (m, 4H, H_{ar}), 7.23−6.95 (m, H_{ar}), 6.95−6.64 (s, H_{ar}), 3.93−3.67 (d, 2H, O−CH_2), 1.85−1.62 (m, 1H, CH), 1.59−1.37 (m, 8H, CH_2), 1.34 (s, 12H, CH_3), 0.91 (s, 6H, CH_3). IR (cm^{-1}): ν 2915 (s), 2842 (s), 1692 (m), 1588 (m), 1488 (m), 1469 (s), 1263 (m), 1161 (m), 1109 (m), 816 (m), 718 (s).

Second, the precursor copolymer poly[4-((4′-((4-(2-ethylhexyloxy)phenyl)(*p*-tolyl)amino)biphenyl-4-yl)(*p*-tolyl)-amino)benzaldehyde] (736 mg, 1.14 mmol) was dissolved in 9 mL of pyridine and 2 mL of acetic acid. After purging with argon for 30 min, malonodinitrile (2 mg, 0.24 mmol) and one crystal of NH_4OAc were added and the solution was stirred for 70 h at room temperature. The reaction mixture was extracted with DCM and water. The organic phase was washed with water and dried over Na_2SO_4. After evaporation of the solvent under reduced pressure, the polymer was precipitated from THF in MeOH. 2-(4-((4′-((4-(2-Ethylhexyloxy)phenyl)(*p*-tolyl)amino)biphenyl-4-yl)(*p*-tolyl)amino)benzylidene)-malonodinitrile (**P2**) was obtained as dark red powder. Yield: 98%. ^{1}H NMR (300 MHz, $CDCl_3$, 298 K; ppm): δ 7.87−7.67 (m, 2H, H_{ar}), 7.56 (s, 1H, H_{vinyl}), 7.52−7.33 (m, 4H, H_{ar}), 7.20−6.92 (m, 10H, H_{ar}), 6.92−6.56 (m, 2H, H_{ar}), 3.93−3.67 (d, 2H, OCH_2), 1.81−1.58 (m, 1H, CH), 1.58−1.37 (m, 8H, CH_2), 0.95−0.73 (m, 6H, CH_3). IR [cm^{-1}]: ν 2927 (m), 2222 (m), 1567 (m), 1487 (s), 1237 (m), 1181 (m), 1112 (m), 817 (s), 696 (m).

P3: Compound **2** (590 mg, 0.94 mmol) and 4-bromothiophene-3-carbaldehyde (**4**; 429 mg, 0.94 mmol) were dissolved in 8 mL of THF. A 5 mL aliquot of 2 M K_2CO_3 in water and DMF (1:1) were added, and the mixture was purged with argon for 30 min. Then $Pd(PPh_3)_4$ (22 mg, 0.02 mmol) and $Pd(OAc)_2$ (2 mg, 0.01 mmol) were added, and the reaction mixture was heated to 70 °C in a microwave. After 5 h the reaction mixture was extracted with DCM and water. The crude product poly[octyl-6-(4-((4-(2-ethylhexyloxy)-phenyl)(*p*-tolyl)amino)phenyl)-*alt*-4-octylthieno[3,4-*b*]-thiophene-2-carboxylate] (**P3**) was precipitated in MeOH and purified by Soxhlet extraction in EtOH and acetone. Yield: 40%. ^{1}H NMR (300 MHz, $CDCl_3$, 298 K; ppm): δ 8.06−7.87 (s, 1H, H_{ar}), 7.68−7.40 (m, 4H, H_{ar}), 7.25−7.02 (m, 6H, H_{ar}), 7.02−6.72 (m, 2H, H_{ar}), 4.47−4.19 (d, 2H, OCH_2), 4.02−3.72 (d, 2H, OCH_2), 1.88−1.68 (m, 1H, CH), 1.68−1.12 (m, 26H, CH_2), 1.10−0.72 (m, 9H, CH_3).

2.2. Physical Measurements. Number-average (M_n) and weight-average (M_w) molecular weights were determined by size exclusion chromatography (SEC) using a Waters 515-HPLC pump with stabilized THF as the eluent. The flow rate was 0.5 mL min^{-1}. The column setup consisted of a guard column (Varian; 50 × 0.75 cm; ResiPore; particle size, 3 μm) and two separation columns (Varian; 300 × 0.75 cm; ResiPore; particle size, 3 μm). The compounds were monitored with a Waters UV detector at 254 nm. SEC in chlorobenzene was carried out at 60 °C on an Agilent 1100 series SEC using two Polymer Laboratories mixed B columns. Both SEC systems were calibrated against polystyrene. Thermogravimetric analysis (TGA) measurements were carried out using a Mettler Toledo TGA/SDTA 851^e with a heating rate of 40 °C min^{-1} under nitrogen flow, and the temperature of degradation (T_d) corresponds to a 5% weight loss. Differential scanning calorimetry (DSC) analysis was performed on a Perkin-Elmer Diamond differential scanning calorimeter, calibrated with indium. Glass transition temperature (T_g) was determined using a scanning rate of 20 °C min^{-1} under a nitrogen flow.

Cyclic voltammograms (CVs) were recorded under moisture- and oxygen-free conditions using a standard three-electrode assembly connected to a potentiostat (model 263A, EG&G Princeton Applied Research) and at a scanning rate of 50 mV s^{-1}. The working electrode was a glassy carbon disk electrode (area, $^1/_4 \times 0.0314$ cm^2), a platinum wire was used as auxiliary electrode, and the quasi-reference electrode was Ag/Ag^+ composed of a Ag wire and $AgNO_3$ in acetonitrile. Tetrabutylammonium hexafluorophosphate (Bu_4NPF_6, 0.1 M) was used as the conducting salt. Each measurement was calibrated with an internal standard (ferrocene/ferrocenium). The HOMO values were determined from the value of −5.16 eV for ferrocene with respect to vacuum level and correcting for the solvent effects.

For spectroscopic measurements polymer films were spin-coated from filtered chlorobenzene solutions (10 mg mL^{-1}). Solution measurements were also performed in chlorobenzene with a concentration of the repetition units of 10^{-5}−10^{-3} mol L^{-1}. Absorption was measured with a Cary 5000 (Varian) UV−vis spectrometer. The fluorescence quantum yields were measured in an integration sphere filled with nitrogen under illumination with an Ar^+ laser (**P1**, UV-multiline 351 nm/364 nm; **P2** and **P3**, 488 nm) with a charge-coupled-device (CCD)

dx.doi.org/10.1021/jp407014q | J. Phys. Chem. C XXXX, XXX, XXX−XXX

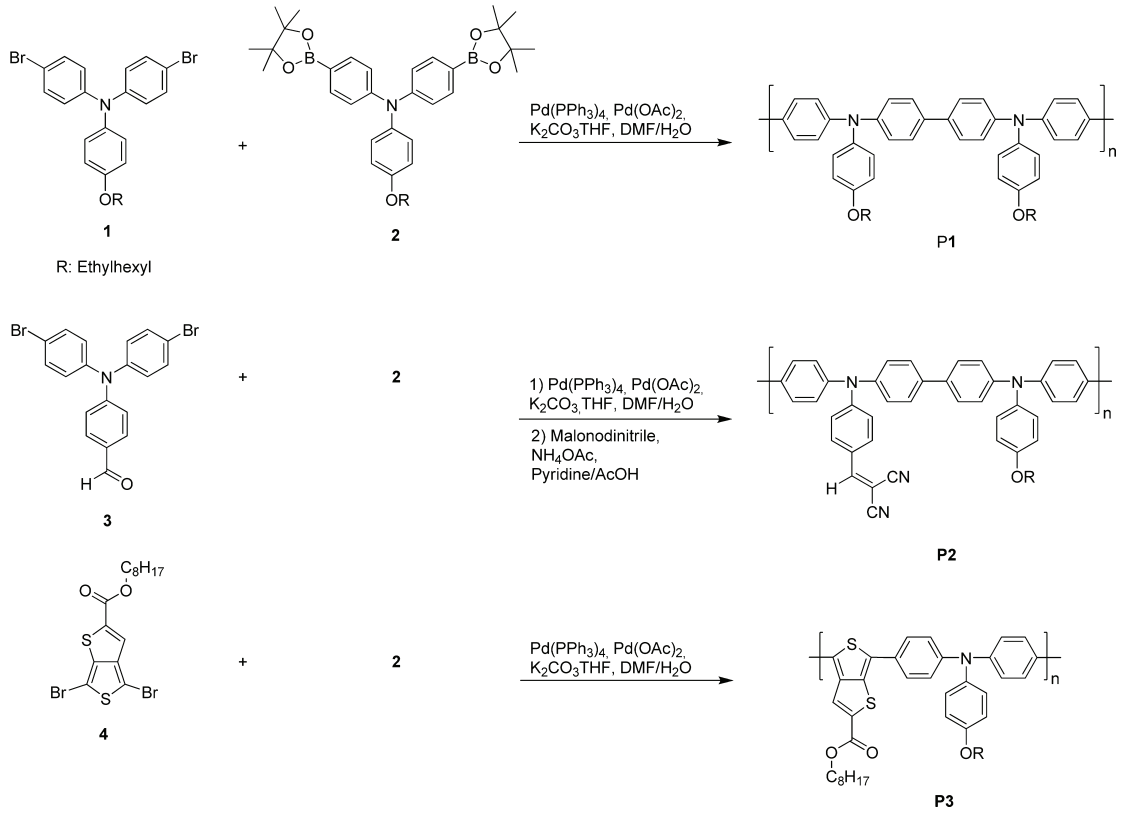

Figure 1. Scheme of the syntheses of polymers **P1**, **P2**, and **P3** via Suzuki polycondensation. The bis-boronic ester monomer **2** was reacted with the three different dibrominated monomers **1**, **3**, and **4**. The polycondensation of **P3** was carried out under microwave irradiation.

camera as described elsewhere.[18] The fluorescence spectra were recorded on a time-correlated single photon counting (TCSPC) setup at room temperature with the samples in vacuum under excitation from a laser diode (**P1**, 375 nm; **P2** and **P3**, 485 nm).

Electric devices were fabricated on structured ITO-coated glass substrates using AZ 1518 photopaint from Microchemicals to define the active area and to prevent edge effects. The devices were then plasma-edged, and a 50 nm layer of poly(3,4-ethylenedioxythiophene):poly(styrene-sulfonate) (PEDOT:PSS; Clevios) was spin-coated into the active area. The PEDOT:PSS layer was heated to 180 °C for 30 min, followed by spin-coating a 40 nm polymer layer on top of it for the bilayer solar cells. Then a 40 nm C_{60} layer (99.9% purity, American Dye Source Inc.) and a 100 nm aluminum layer were evaporated at 5 × 10^{-7} mbar. For the space−charge-limited current (SCLC) devices, the polymers were blade-coated from chlorobenzene solutions and a 40 nm gold electrode was evaporated.

All device measurements were performed under active vacuum at room temperature with a Keithley source measure unit. For performance and field-dependent measurements a Newport 1.5 AM solar simulator was used, and the solar spectrum measurements were recorded under monochromatic illumination of a 150 W xenon lamp. Light intensities were recorded with a Hamamatsu S1337-33BQ photodiode. The internal field F was calculated as $F = (V_{oc} - V)/d$ with applied external voltage V, the open-circuit voltage V_{oc}, and the active film thickness d.

3. RESULTS

3.1. Synthesis. Here, we present the synthesis and characterization of a main chain homopolymer (**P1**, poly-[*N*,*N*′-bis(4-(2-ethylhexyloxy)phenyl)-*N*,*N*′-di-*p*-tolylbiphenyl-4,4′-diamine]), an alternating D−A-copolymer with dicyanovinyl in the side chain (**P2**, poly[2-(4-((4′-((4-(2-ethylhexyloxy)phenyl)(*p*-tolyl)amino)biphenyl-4-yl)-*alt*-(*p*-tolyl)amino)benzylidene)malononitrile]) and the D−A-copolymer carrying thieno[3,4-*b*]thiophene-2-carboxylate in the main chain (**P3**, poly[octyl-6-(4-((4-(2-ethylhexyloxy)phenyl)(*p*-tolyl)amino)phenyl)-*alt*-4-octylthieno[3,4-*b*]thiophene-2-carboxylate]. The dicyanovinyl group is strongly electron withdrawing. It has been shown that the introduction of this group as a side chain lowers the optical gap, by mainly lowering the LUMO value.[10] On the other hand, the electron withdrawing comonomer thieno[3,4-*b*]thiophene carboxylate stabilizes the quinoidal form and therefore lowers the optical gap when coupled with a suitable donor comonomer.[19,20] We used Suzuki AA/BB type polycondensation as a synthetic method to obtain the conjugated polymers[21] because it enables the synthesis of well-defined alternating copolymers. The symmetrically difunctionalized monomers were synthesized according to the literature with good yields (see the Supporting Information).[22,23]

Homopolymer **P1** was obtained by polycondensation between a dibromo-TPA and a TPA bis-boronic acid ester (Figure 1). The synthesis of **P2** was realized by a precursor method. We used monomer **3**, a dibromo-TPA with an aldehyde group which is stable under Suzuki polycondensation conditions, and polymerized it with the common bis-boronic acid ester monomer **2**. After purifying the precursor copolymer

dx.doi.org/10.1021/jp407014q | J. Phys. Chem. C XXXX, XXX, XXX−XXX

by Soxhlet extraction, the dicyanovinyl group was introduced via a polymer analogous Knoevenagel condensation with malonodinitrile. ^{1}H NMR spectroscopy and FT-IR spectroscopy clearly proved the complete conversion of the aldehyde functionality to the dicyanovinyl group (see the Supporting Information).

The alternating main chain D−A-copolymer **P3** was synthesized by reacting directly the dibromo-monomer thieno-[3,4-*b*]thiophene carboxylate **4** with monomer **2** under microwave irradiation. All polymers were soluble in THF, $CHCl_3$, and chlorobenzene, whereas **P3** was soluble only in $CHCl_3$ and chlorobenzene.

3.2. Polymer Properties. M_w and M_n of polymers **P1**, **P2**, and **P3** were determined by SEC with THF as eluent. For calibration a polystyrene standard was used. Copolymer **P3** was analyzed in a chlorobenzene SEC at 60 °C due to the low solubility in THF. Homopolymer **P1** has a M_n of 10330 g mol^{-1} and a M_w of 15770 g mol^{-1}. Both D−A-copolymers show a comparable M_n with 7400 and 7770 g mol^{-1} for **P2** and **P3**, respectively. The corresponding M_w are 18760 g mol^{-1} and 11610 g mol^{-1}, and all of the relevant SEC data are given in Table 1. The homopolymer and all copolymers showed high thermal stability in TGA with temperatures for 5% weight loss ranging from 402 to 410 °C. All of the polymers form optically clear and smooth films, which is advantageous for device preparation. DSC analysis showed that all compounds were amorphous and had glass transition temperatures of 203, 212 and 118 °C for **P1**, **P2**, and **P3**, respectively.

Table 1. Molecular Weights and Thermal Properties of Homopolymer P1 and D−A-Copolymers P2 and P3[a]

polymer	M_n (g mol^{-1})	M_w (g mol^{-1})	PDI	T_d (°C)	T_g (°C)
P1	10330	15770	1.52	402	203
P2	7400	18760	2.54	410	212
P3	7770	11610	4.91	370	118

[a]SEC analysis was carried out in THF as eluent and polystyrene standards at room temperature. **P3** was measured in chlorobenzene at 60 °C.

Cyclic voltammetry measurements were employed to investigate the redox behavior and the influence of the different electron withdrawing groups on the HOMO/LUMO levels. The HOMO values were calculated by calibrating with ferrocene and correcting for solvent effects.[24,25] The polymers were measured in DCM vs $AgNO_3$. **P1** and **P3** have similar oxidation potential values (0.15 V vs Fc), whereas the oxidation potential of **P2** is slightly higher (0.3 V vs Fc). Thus, the calculated HOMO levels are −5.31, −5.45, and −5.30 eV for **P1**, **P2**, and **P3**, respectively. The values are summarized in Table 2. The LUMO levels were estimated from the optical gap (determined from the onset of absorption bands, vide infra) and the HOMO energy values. Due to the slightly lower optical gap of **P3** the LUMO levels of both D−A-copolymers are similar. Thus, the introduction of the strong electron withdrawing dicyanovinyl acceptor unit as substituent reduces the electron richness and delocalization of the TPA main chain, resulting in an increased oxidation potential by about 0.14 V. Additionally, the redox potential is drastically lowered, resulting in low LUMO values. However, the incorporation of the thieno[3,4-b]thiophene acceptor unit in the main chain does not affect the oxidation potential, indicating a similar oxidizability or delocalization of the main chain as in the homopolymer **P1**. This means that the thieno[3,4-*b*]thiophene carboxylate does not withdraw electrons from the TPA moiety but maintains the conjugation between two TPA units resulting in the same oxidation potential for both **P3** and **P1**. This conclusion can be derived from the fact that an individual TPA unit exhibits an oxidation potential of about 0.2 eV higher than that for a dimer in which the TPA units are in conjugation.[16]

A further relevant parameter for semiconductor materials is the charge carrier mobility. We investigated the hole transport mobilities (μ_h) of the three polymers in hole-only diodes using the SCLC method. This method allows the determination of the bulk charge carrier mobility. A PEDOT:PSS-coated ITO electrode and a gold electrode were used to fabricate the devices. In this case, PEDOT:PSS serves as a hole-injecting electrode. Furthermore, the high work function of the gold electrode hinders the injection of electrons but allows for hole collection. Therefore, the transport of the holes is only limited by the charge carrier mobility of the polymer and can be described by the Mott−Gurney eq 1.[26]

$$J = \frac{9}{8}\varepsilon\varepsilon_0\mu_h\frac{V^2}{L^3} \quad (1)$$

According to this equation the current density J is dependent on the permittivity of free space ε_0, the dielectric constant of the polymer ε (assumed to be 3), the charge carrier mobility μ_h, the thickness of the polymer layer L, and the voltage drop across the device V. Assuming ohmic contacts to the injecting electrode, the current is space−charge-limited at high voltages. The measured I−V curves were fitted according to eq 1 to obtain the hole transport mobility μ_h. By recording different active layer thicknesses, the thickness scaling of the space−charge-limited currents was verified. The log−log plots of J vs L and the fits according to the relation $J \sim V^2/L^3$ are illustrated in the Supporting Information. This clearly indicates that the measured current is space−charge-limited. The contact resistance and series resistance were measured in a reference device without a polymer layer, and the corresponding voltage drop V_r was subtracted from the applied voltage. The built-in

Table 2. (a) HOMO Values of P1, P2, and P3 Obtained from Oxidation Potential (E_{ox}) vs Ferrocene in Cyclic Voltammetry Measurements at 50 mV s^{-1} in DCM with 0.1 M Tetrabutylammonium Hexafluorophosphate[a] **and (b) Hole Transport Mobilities (μ_h) Determined by SCLC Measurements in Hole-Only Devices with PEDOT:PSS and Au as Electrodes**[b]

polymer	E_{ox} vs Fc (eV)	HOMO (eV)	E_g (eV)	LUMO (eV)	μ_h (cm^2 V^{-1} s^{-1})
P1	0.15	−5.31	2.97	−2.34	1.4×10^{-4}
P2	0.29	−5.45	2.24	−3.21	7.6×10^{-5}
P3	0.14	−5.30	2.10	−3.20	3.1×10^{-4}

[a]The HOMO value for ferrocene/ferrocenium oxidation in DCM was taken as −5.16 eV.[25] LUMO values were estimated using the onset of absorption (E_g) from UV−vis measurements and corresponding HOMO values. [b]Given values are the average values of three different measured thicknesses.

dx.doi.org/10.1021/jp407014q | J. Phys. Chem. C XXXX, XXX, XXX−XXX

potential V_{bi} for PEDOT:PSS and gold is estimated to be 0 V. Figure 2 gives the half-log plots of J vs V of the three polymers at similar layer thicknesses and the device geometry.

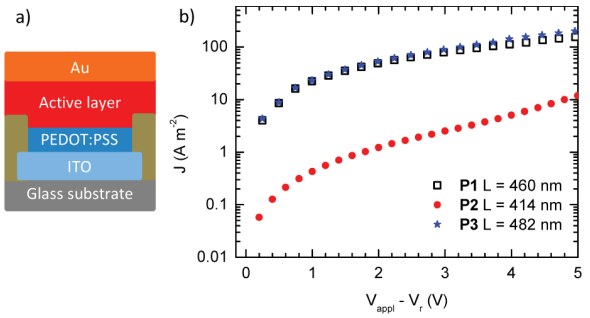

Figure 2. (a) Schematic structure of a hole-only device with PEDOT:PSS and gold as electrodes. (b) Half-log plot of current density J vs voltage V of **P1**, **P2**, and **P3** for comparable layer thicknesses. Additional measurements for different layer thicknesses are given in the Supporting Information.

We found that the homopolymer **P1** shows a hole transport mobility of 1.4×10^{-4} cm^2 V^{-1} s^{-1}. The introduction of the dicyanovinyl groups leads to a decrease of 1 order of magnitude, 7.6×10^{-5} cm^2 V^{-1} s^{-1}, for **P2**. The low mobility of **P2** indicates that the side chain acceptor unit does affect the delocalization or conjugation of the TPA main chain. However, the incorporation of the thieno[3,4-*b*]thiophenecarboxylate does not change the hole transport mobility considerably for **P3** (μ_h = 3.1×10^{-4} cm^2 V^{-1} s^{-1}). These hole transport mobility values are in full agreement with the influence of the acceptor units on the delocalization or the easiness of the oxidation as observed in cyclic voltammetry.

3.3. Absorption and Photoluminescence Spectroscopy. The absorption spectra of **P1**, **P2**, and **P3** in solution and film are shown in Figure 3. We first consider the solution spectra which were recorded at a concentration of the repetition units of 10^{-4} mol L^{-1}. Identical spectra were found at a concentration of 10^{-5} mol L^{-1} with a reduced signal-to-noise ratio. For the homopolymer **P1** we observe an absorption band in the high-energy region centered at 3.22 eV that is characteristic for TPAs and that is assigned to a $\pi-\pi^*$-transition. For copolymer **P2** containing the pendant dicyanovinyl group, we find a lower energy absorption peak centered at 2.66 eV with lower oscillator strength that appears in addition to the original TPA absorption band. The latter is blue-shifted by 100 meV to 3.32 eV and has a slightly decreased oscillator strength compared to the homopolymer **P1**. On the basis of the low oscillator strength and low energy, we attribute the 2.66 eV absorption peak present in dilute solution to an intramolecular CT-transition with low wave function overlap from the donor backbone to the dicyanovinyl in the side chain. A similar absorption behavior was also shown for other D−A-copolymers.[10] Overall, the copolymer **P2** is able to cover the whole low- and middle-wavelength region of the visible spectrum.

In **P3**, the thieno[3,4-*b*]thiophene carboxylate, acting as an electron pulling unit, is placed directly in the main chain of the copolymer, allowing for a good electronic interaction with the TPA unit. As for **P2**, we observe a low-energy absorption band centered at 2.49 eV in addition to the original TPA absorption at 3.26 eV. Compared to **P2**, this low-energy band is shifted further to the red by 0.17 eV and carries a higher oscillator strength. Concomitantly, the oscillator strength of the high-energy 3.26 eV band is strongly reduced. We consider the high oscillator strength of the additional, red-shifted absorption peak of **P3** and the reduction of the 3.26 eV intensity to indicate a significant contribution of $\pi-\pi^*$-transitions to the intramolecular CT-band that arises from the D−A-type interaction of the electron withdrawing thieno[3,4-*b*]thiophene carboxylate with the TPA unit. Similarly, we interpret the red shift of the low-energy band compared to that of **P2** to indicate a higher degree of conjugation, consistent with a stronger contribution of the delocalized π-orbitals. We obtain the same results for the absorption spectra taken in thin films, except for a small solvent shift. The positions of the absorption peaks are summarized in Table 3.

Table 3. Absorption Peaks (Position of the Center) In a Chlorobenzene Solution at a Concentration of the Repetition Units of 10^{-4} mol L^{-1} and in the Film, Made from Solutions of 10 mg mL^{-1} in Chlorobenzene

polymer	$E_{solution}$ (eV)	E_{film} (eV)
P1	3.22	3.26
P2	2.66, 3.32	2.68, 3.36
P3	2.49, 3.36, 4.11	2.46, 3.34, 4.11

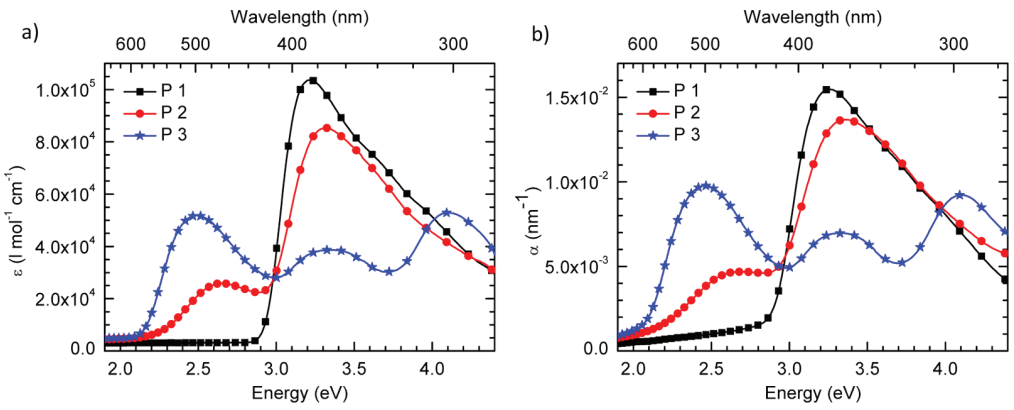

Figure 3. UV−vis absorption spectra of **P1**, **P2**, and **P3**: (a) in chlorobenzene, concentration of the repetition units of 10^{-4} mol L^{-1}; (b) in film from 10 mg mL^{-1} solutions in chlorobenzene.

dx.doi.org/10.1021/jp407014q | J. Phys. Chem. C XXXX, XXX, XXX−XXX

Further information on the nature of excited states in the polymers can be obtained from photoluminescence measurements. First, we find that the three polymers differ strongly in their thin film photoluminescence efficiencies. While integrating sphere measurements taken on thin films give a moderate photoluminescence quantum yield (PL QY) of 3.4% for homopolymer **P1**, the emission is below the detection threshold of this setup for **P2**, and it is as low as 0.7% for **P3**. The uncertainty on the PL QY is about 1%. This trend is consistent with the observed absorption strengths of the lowest energy bands in all three polymers and confirms the indication of a stronger CT-character in **P2** compared to **P3**, and, naturally, of no CT-characteristics in **P1**. Due to the low-emission efficiencies, we used the sensitive technique of TCSPC to measure the photoluminescence spectra and lifetimes. The spectra are shown in Figure 4. No reliable data can be obtained for the spectral window from 2.35 to 2.50 eV due to a technical limitation. Photoluminescence decay curves are included as Supporting Information. We shall discuss the data for the compounds in increasing order of intramolecular CT-character.

For homopolymer **P1**, the same emission band with a 0−0 peak at 2.89 eV and vibronic replica at 2.72 and 2.55 eV is seen in solution and, shifted by 40 meV to the red, in film. This emission dominates for a few nanoseconds after excitation with a lifetime of 0.9 ns in solution and 0.3 ns in the film. At longer times, this emission disappears and a weak, structured emission can be observed. It is shifted to the red by about 0.3 eV and has a lifetime of about 6 ns in solution and 5 ns in film. Since this signal is rather weak with poor spectral to noise ratio, we can spectrally resolve it only for the film, where the higher energy emission decays away fast, yet not for solution. Due to the moderate Stokes's shift of about 0.33 eV between absorption and emission and the concomitant mirror symmetry, we attribute the higher energy emission with 0−0 peak at 2.89 eV to the $\pi-\pi^*$-transition in the TPA-homopolymer, possibly with some mixing of the nonbonding orbital of the nitrogen lone pair. The electronic origin of the lower energy emission at about 2.55 eV is not clear. This emission is present in both phases, solution and film, with the same lifetime, yet in solution it is masked by the stronger higher energy emission. The reduction of the fast component in photoluminescence lifetime in film compared to solution suggests that the weakly red emitting sites can only be populated effectively by energy transfer in the condensed phase of the film.

We next consider the copolymer **P3** where electron-rich and electron-deficient groups alternate in the chain backbone. The spectra in solution and in film immediately after excitation have a spectral shape similar to that in **P1** with similar full width at half-maximum (fwhm) of about 0.2 eV and a comparable Stokes's shift of 0.40 eV. The spectra show a 0−0 peak at 2.10 eV in solution and slightly below, at 2.03 eV, in film. Whereas no spectral change with time is noticeable in solution, in film the higher energy emission decays and exposes a weak emission centered at 1.79 eV that was initially hidden in the red tail of the higher energy peak. The energy difference between the comparatively intense higher energy emission and the weak lower energy emission bands is similar for **P1** and **P3**. In **P1**, it is about 0.30 eV, and in **P3**, it is 0.24 eV. Overall, the dominant decay lifetimes in copolymer **P3** are longer than those of homopolymer **P1**. For **P3** in solution, the decay is not entirely exponential and can best be approximated by a biexponential decay with lifetimes of 2.0 ns (amplitude 20.000) and 3.2 ns

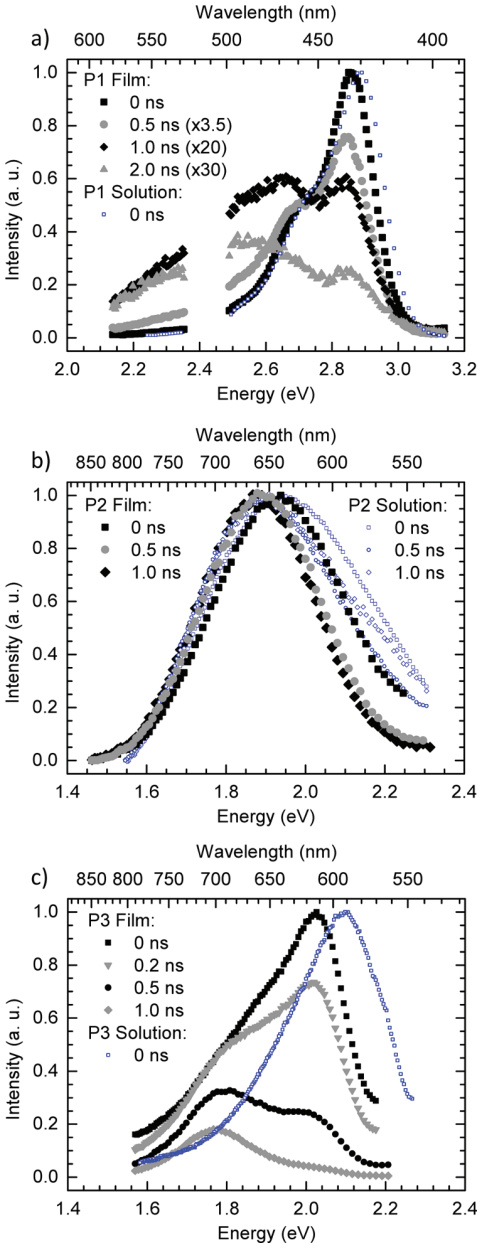

Figure 4. Fluorescence spectra of the polymers in chlorobenzene solutions at a concentration of the repetition units of (**P1** and **P3**, 10^{-5} mol L^{-1}; **P2**, 10^{-3} mol L^{-1}) and in the film under UV-irradiation (**P1**, 375 nm; **P2** and **P3**, 485 nm) measured in a TCSPC setup. In the spectral window from 2.35 to 2.50 eV, no reliable data could be obtained due to a technical limitation.

(amplitude 7.000); i.e., the dominant contribution is twice as long as that for **P1**. This is consistent with the reduced oscillator strength of **P3** compared to **P1** that is also manifested in the intensity of the low-energy absorption peak and the photoluminescence quantum yield. For **P3** in film, the luminescence decay proceeds faster and it is characterized by a distribution of lifetimes.

In contrast to **P1** and **P3**, for **P2** with the dicyanovinyl in the side group we observe a very weak, broad, unstructured emission centered at about 1.9 eV. To enable detection of this inefficiently emitting compound in solution, we used a concentration of the repetition units of 10^{-3} mol L^{-1} instead

dx.doi.org/10.1021/jp407014q | J. Phys. Chem. C XXXX, XXX, XXX−XXX

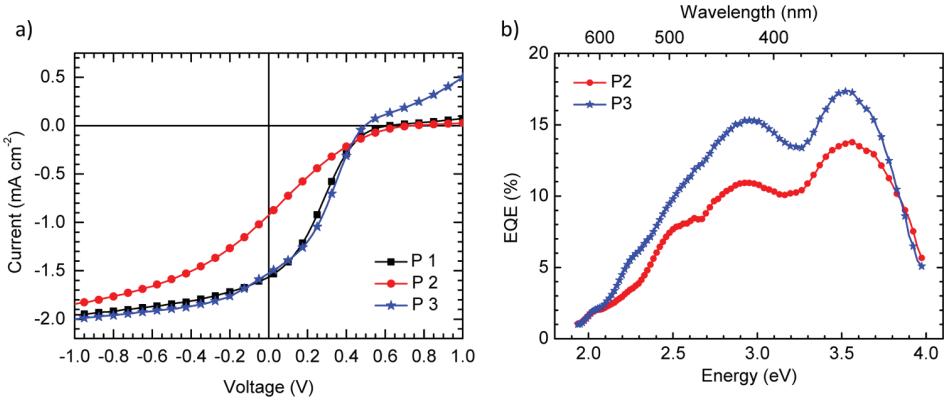

Figure 5. a) Current–voltage characteristics of bilayer solar cells built with the presented polymers **P1**, **P2**, **P3**, and C_{60} under AM 1.5 illumination. (b) Corresponding external quantum efficiency (EQE) spectra of copolymers **P2** and **P3**.

of the 100 times lower value used for **P1** and **P3**. For both, solution and film, the emission does not change with time except for an initial slight red shift that is common for condensed media where spectral diffusion in the density of states prevails.[27] We stress that, in particular, in contrast to **P1** and **P3**, there is no significant change of the spectral shape over time. The emission is characterized by a distribution of lifetimes in the nanosecond range, with more longer lived contributions for the film. Such a broad, unstructured weak emission with a distribution of lifetimes is a general signature for a CT-type transition.

The overall picture that emerges from the absorption and photoluminescence spectroscopy is that, in **P2**, the excited state is dominated by CT-character, manifested in weak absorption and weak, unstructured emission. The homopolymer **P1** shows the moderately intense emission and good absorption associated with $\pi-\pi^*$-transitions as well as a weak, lower energy emission of unclear origin. The nature of the first excited state in the copolymer **P3** lies between the two limiting cases defined by **P1** and **P2**.

3.4. Photocurrent Measurements. We next consider how the different nature of the excited states impacts on their performance as solar cell materials. Therefore, we built bilayer solar cells where C_{60} is evaporated on top of a spin-coated polymer film. Indium–tin-oxide covered by a layer of PEDOT:PSS was used as anode and aluminum as a cathode. The simple device geometry of a bilayer allows for spatially distinct electron and hole pathways to the electrodes, thus preventing the nongeminate recombination of accidentally meeting charge carriers that is inherently problematic in the intermingled morphology of blends. The observed photocurrent characteristics in a bilayer structure can therefore be interpreted as arising mainly from the charge generation at the D–A-interface itself. The current–voltage curves of the bilayer solar cells for the different materials under AM 1.5 illumination are shown in Figure 5, along with the external quantum efficiency (EQE) spectra. The resulting solar cell parameters are given in the Supporting Information.

Homopolymer **P1** and copolymer **P3** show nearly identical current–voltage ($I-V$) curves up to the open-circuit voltage V_{oc}, with similarly moderate performance. The moderate performance is expected for bilayer cells with such material combination.[10] Copolymer **P2** that has the stronger CT-character, however, is distinct and displays a reduced short-circuit current I_{sc} and a concomitantly reduced fill factor FF. The lower efficiency of **P2** compared to **P3** over the whole spectral range is also evident in the EQE spectra that largely follow the absorption data of the blend. All three cells have a pronounced "S-shape", i.e., a zero or low photocurrent for forward bias, at voltages exceeding the open-circuit voltage. The appearance of low current upon further voltage increase is occasionally reported, and it is tentatively attributed to imbalanced mobilities of the donor and the acceptor in planar heterojunction cells.[28]

4. DISCUSSION

The aim of our study is to understand what controls charge separation in D–A-copolymers **P2** and **P3**. The impacts both of dipolar or electrostatic effects and of excited-state delocalization have been demonstrated to be of importance.[29−32] Here, we try to differentiate between both influences by comparing a homopolymer to two D–A-copolymers that represent two different chemical architectures. D–A-copolymer **P2** with a dicyanovinyl group in the side chain (with reduced delocalization with the main chain) shows a stronger CT-character than **P3** where the acceptor moiety is incorporated in the main chain. This is evident from the reduced oscillator strengths of the first absorption band in **P2** compared to **P1** and a barely detectable, broad, unstructured fluorescence that decays nonexponentially. D–A-copolymer **P3** possesses a weaker CT-character as demonstrated by the absorption and photoluminescence properties (vide supra); this results in a lower prominence of the intrachain CT-character due to significant contributions of delocalized π- and π^*-orbitals. The question in now whether the more dipolar character of **P2** favors charge separation, e.g., by preseparation of the hole and electron on the copolymer and concomitant dielectric screening,[29] or whether the higher degree of excited-state delocalization in **P3** is a more beneficial approach. From the $I-V$ curve in Figure 5, a reduced performance of **P2** compared to **P3** is already evident. The data of Figure 5 can be analyzed by comparison with exciton dissociation models. For this, the photocurrent quantum yield for **P2** and **P3** is plotted as a function of internal electric field in Figure 6. The photocurrent quantum yield has been normalized to unity at the saturation value obtained for high field strengths since, for sufficiently high field, complete exciton dissociation and extraction are obtained.[30] The internal field F is calculated by subtracting the applied voltage from the open-circuit voltage and dividing the result by the active layer thickness of the device. The effect

dx.doi.org/10.1021/jp407014q | J. Phys. Chem. C XXXX, XXX, XXX–XXX

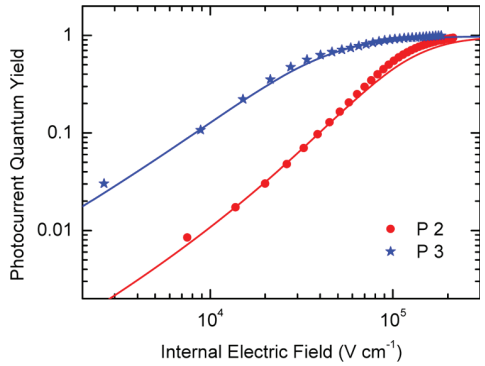

Figure 6. Normalized field-dependent photocurrent quantum yields of copolymer/C_{60} bilayer devices calculated from the photocurrent under AM 1.5 conditions. The lines indicate fits based on an effective mass model that includes interfacial dipole effects.

of possible deviations in the internal field from the value obtained by this method is discussed in detail in ref 31. Figure 6 shows that a higher electrical field is needed to dissociate all excitons in **P2** ($F_{saturation}$ = 1.5 × 10^5 V cm^{-1}) than in **P3** ($F_{saturation}$ = 6 × 10^4 V cm^{-1}), implying that excitons in **P2** are more tightly bound than those in **P3**.

Exciton dissociation at the interface between a polymer donor material and a fullerene acceptor is understood to be assisted by both electrostatic interface effects ("interfacial dipole", parametrized through a fractional dipole strength α) and charge delocalization. The latter can be parametrized in terms of a heuristic "effective mass" of the hole on the polymer.[31] Whereas electrostatic effects screen the mutual coulomb attraction of electron and hole, the kinetic energy associated with a delocalized hole helps its escape from the coulomb potential of its geminate electron.[33−35] In order to obtain insight into the observed photodissociation behavior, we have fitted the field-dependent photocurrent quantum yields with a model containing the effects of both interfacial dipoles and hole delocalization (eqs 3, 6, and 7 in[31]). Good agreement with the experimental data can be obtained when the fractional dipole strength α at the interface to C_{60} is set at 0.050 in **P2** and at 0.045 in **P3**, leading to effective relative hole masses m_{eff}/m_e of 0.44 for **P2** and 0.25 for **P3**, where m_e is the mass of a free electron. These parameter values obtained are consistent with earlier work on homopolymers in bilayers with C_{60}.[31] The fractional dipole strengths are about twice as high as those measured for homopolymer/C_{60} interfaces, and the effective masses are in a similar range, depending on the degree of conjugation of the polymers. As detailed in the Supporting Information, it is possible to increase the fractional dipole strength for **P2** while maintaining a good agreement with the data when simultaneously increasing the hole effective mass further.

What is the insight obtained from these values? This analysis tells us that the improved performance of **P3** compared to **P2**, i.e. the higher photodissociation at low internal field strength, and concomitantly the higher short-circuit current and fill factor, are a result of the lower effective mass in **P3**. A more delocalized character of the hole on **P3** is fully consistent with the overall more delocalized character of the excited state in **P3** that is manifested in the optical measurements, and the higher hole mobility in **P3**. Furthermore, the photocurrent analysis shows a more localized hole on **P2** to be associated with a poor photodissociation, while the CT-character of **P2** does not turn out to be of benefit to the charge separation process. A more localized hole with a higher effective mass derived in the photocurrent fit corresponds well with the reduced hole mobility measured for **P2** in SCLC measurements. The fact that this correlates with a low HOMO level points at trapping effects or localization effects.[36,37] Comparing these results of field-dependent photocurrent quantum yields with previous work on charge separation emphasizes the importance of a good conjugation to facilitate charge separation.

5. CONCLUSION

On comparison of the homopolymer **P1** with the two D−A-copolymers **P2** and **P3**, we could get conclusive information regarding the effective design of D−A-copolymers for an efficient delocalization/conjugation and good charge generation. The introduction of the strong electron withdrawing dicyanovinyl acceptor unit as side chain in **P2** reduces the electron richness and delocalization of the TPA main chain. As a consequence the HOMO level is lowered in **P2** and the hole mobility is decreased. **P2** has a pronounced excited-state CT-character compared to **P3** in which the acceptor enters into delocalization with the backbone. Field-dependent photocurrent measurements in bilayer devices clearly indicate the advantage of the alternating D−A-copolymer strategy in which the donor and acceptor moieties exhibit a better conjugation. Thus, for this material system, charge separation is obtained more readily when the acceptor group is located within the copolymer backbone guaranteeing delocalization along the main chain. The concept of adding a strong acceptor to the side group which lowers the delocalization in the main chain, in contrast, results in a lower hole mobility and stronger bound electron hole pairs and thus lower solar cell power conversion efficiency.

■ ASSOCIATED CONTENT

Supporting Information

Syntheses of the monomers, ^{1}H NMR and FT-IR spectra, cyclic voltammetry data, SCLC curves for different layer thicknesses and corresponding fit parameters, lifetime measurements, and fits with the dipole model and solar cell parameters. This material is available free of charge via the Internet at http://pubs.acs.org.

■ AUTHOR INFORMATION

Corresponding Author

*Phone: +49-921-553108. E-mail: mukundan.thelakkat@uni-bayreuth.de.

Notes

The authors declare no competing financial interest.

■ ACKNOWLEDGMENTS

We acknowledge the Graduate School GRK 1640 of the Deutsche Forschungsgemeinschaft (DFG) and the Bavarian State Ministry of Science, Research, and the Arts for the Collaborative Research Network "Solar Technologies go Hybrid" for financial support and K.N. thanks the Universität Bayern e.V. for financial support in the form of a scholarship of the Bayerische Graduiertenförderung and the Elitenetzwerk Bayern (ENB). We also thank Sabrina Willer for support in the synthesis work and Sebastian Hoffmann and Stephan Kümmel for fruitful discussions.

REFERENCES

(1) Deibel, C.; Dyakonov, V., Polymer-Fullerene Bulk Heterojunction Solar Cells. *Rep. Prog. Phys.* **2010**, *73*.

(2) Green, M. A.; Emery, K.; Hishikawa, Y.; Warta, W.; Dunlop, E. D. Solar Cell Efficiency Tables (Version 40). *Prog. Photovoltaics* **2012**, *20*, 606−614.

(3) Li, Y. Molecular Design of Photovoltaic Materials for Polymer Solar Cells: Toward Suitable Electronic Energy Levels and Broad Absorption. *Acc. Chem. Res.* **2012**, *45*, 723−733.

(4) Boudreault, P. L. T.; Najari, A.; Leclerc, M. Processable Low-Bandgap Polymers for Photovoltaic Applications. *Chem. Mater.* **2011**, *23*, 456−469.

(5) Duan, C. H.; Cai, W. Z.; Huang, F.; Zhang, J.; Wang, M.; Yang, T. B.; Zhong, C. M.; Gong, X.; Cao, Y. Novel Silafluorene-Based Conjugated Polymers with Pendant Acceptor Groups for High Performance Solar Cells. *Macromolecules* **2010**, *43*, 5262−5268.

(6) Hellström, S.; Lindgren, L. J.; Zhou, Y.; Zhang, F. L.; Inganäs, O.; Andersson, M. R. Synthesis and Characterization of Three Small Band Gap Conjugated Polymers for Solar Cell Applications. *Polym. Chem.* **2010**, *1*, 1272−1280.

(7) Hou, J. H.; Tan, Z. A.; Yan, Y.; He, Y. J.; Yang, C. H.; Li, Y. F. Synthesis and Photovoltaic Properties of Two-Dimensional Conjugated Polythiophenes with Bi(thienylenevinylene) Side Chains. *J. Am. Chem. Soc.* **2006**, *128*, 4911−4916.

(8) Zhang, Z. G.; Liu, Y. L.; Yang, Y.; Hou, K. Y.; Peng, B.; Zhao, G. J.; Zhang, M. J.; Guo, X.; Kang, E. T.; Li, Y. F. Alternating Copolymers of Carbazole and Triphenylamine with Conjugated Side Chain Attaching Acceptor Groups Synthesis and Photovoltaic Application. *Macromolecules* **2010**, *43*, 9376−9383.

(9) Zhang, Z.-G.; Wang, J. Structures and Properties of Conjugated Donor-Acceptor Copolymers for Solar Cell Applications. *J. Mater. Chem.* **2012**, *22*, 4178−4187.

(10) Zhang, Z. G.; Zhang, K. L.; Liu, G.; Zhu, C. X.; Neoh, K. G.; Kang, E. T. Triphenylamine-Fluorene Alternating Conjugated Copolymers with Pendant Acceptor Groups: Synthesis, Structure-Property Relationship, and Photovoltaic Application. *Macromolecules* **2009**, *42*, 3104−3111.

(11) Clarke, T. M.; Ballantyne, A.; Shoaee, S.; Soon, Y. W.; Duffy, W.; Heeney, M.; McCulloch, I.; Nelson, J.; Durrant, J. R. Analysis of Charge Photogeneration as a Key Determinant of Photocurrent Density in Polymer: Fullerene Solar Cells. *Adv. Mater.* **2010**, *22*, 5287−5291.

(12) Clarke, T. M.; Durrant, J. R. Charge Photogeneration in Organic Solar Cells. *Chem. Rev.* **2010**, *110*, 6736−6767.

(13) Veldman, D.; Ipek, O.; Meskers, S. C. J.; Sweelssen, J.; Koetse, M. M.; Veenstra, S. C.; Kroon, J. M.; van Bavel, S. S.; Loos, J.; Janssen, R. A. J. Compositional and Electric Field Dependence of the Dissociation of Charge Transfer Excitons in Alternating Polyfluorene Copolymer/Fullerene Blends. *J. Am. Chem. Soc.* **2008**, *130*, 7721−7735.

(14) Tautz, R.; Da Como, E.; Limmer, T.; Feldmann, J.; Egelhaaf, H. J.; von Hauff, E.; Lemaur, V.; Beljonne, D.; Yilmaz, S.; Dumsch, I.; Allard, S.; Scherf, U. Structural Correlations in the Generation of Polaron Pairs in Low-Bandgap Polymers for Photovoltaics. *Nat. Commun.* **2012**, *3*, No. 970.

(15) Carsten, B.; Szarko, J. M.; Son, H. J.; Wang, W.; Lu, L. Y.; He, F.; Rolczynski, B. S.; Lou, S. J.; Chen, L. X.; Yu, L. P. Examining the Effect of the Dipole Moment on Charge Separation in Donor-Acceptor Polymers for Organic Photovoltaic Applications. *J. Am. Chem. Soc.* **2011**, *133*, 20468−20475.

(16) Thelakkat, M. Star-Shaped, Dendrimeric and Polymeric Triarylamines as Photoconductors and Hole Transport Materials for Electro-Optical Applications. *Macromol. Mater. Eng.* **2002**, *287*, 442−461.

(17) Roncali, J. Synthetic Principles for Bandgap Control in Linear Pi-Conjugated Systems. *Chem. Rev.* **1997**, *97*, 173−205.

(18) deMello, J. C.; Wittmann, H. F.; Friend, R. H. An Improved Experimental Determination of External Photoluminescence Quantum Efficiency. *Adv. Mater.* **1997**, *9*, 230−232.

(19) Hong, S. Y.; Marynick, D. S. Understanding the Conformational Stability and Electronic-Structures of Modified Polymers Based on Polythiophene. *Macromolecules* **1992**, *25*, 4652−4657.

(20) Liang, Y. Y.; Feng, D. Q.; Guo, J. C.; Szarko, J. M.; Ray, C.; Chen, L. X.; Yu, L. P. Regioregular Oligomer and Polymer Containing Thieno[3,4-B]thiophene Moiety for Efficient Organic Solar Cells. *Macromolecules* **2009**, *42*, 1091−1098.

(21) Schlüter, A. D. The Tenth Anniversary of Suzuki Polycondensation (Spc). *J. Polym. Sci., Part A: Polym. Chem.* **2001**, *39*, 1533−1556.

(22) Park, J. H.; Seo, Y. G.; Yoon, D. H.; Lee, Y. S.; Lee, S. H.; Pyo, M.; Zong, K. A Concise Synthesis and Electrochemical Behavior of Functionalized Poly(Thieno[3,4-B]Thiophenes): New Conjugated Polymers with Low Bandgap. *Eur. Polym. J.* **2010**, *46*, 1790−1795.

(23) Kun, H.; Yi, H.; Johnson, R. G.; Iraqi, A. Fluoro-Protected Carbazole Main-Chain Polymers as a New Class of Stable Blue Emitting Polymers. *Polym. Adv. Technol.* **2008**, *19*, 299−307.

(24) Noviandri, I.; Brown, K. N.; Fleming, D. S.; Gulyas, P. T.; Lay, P. A.; Masters, A. F.; Phillips, L. The Decamethylferrocenium/Decamethylferrocene Redox Couple: A Superior Redox Standard to the Ferrocenium/Ferrocene Redox Couple for Studying Solvent Effects on the Thermodynamics of Electron Transfer. *J. Phys. Chem. B* **1999**, *103*, 6713−6722.

(25) Gräf, K.; Rahim, M. A.; Das, S.; Thelakkat, M. Complementary Co-Sensitization of an Aggregating Squaraine Dye in Solid-State Dye-Sensitized Solar Cells. *Dyes Pigm.* **2013**, *99*, 1101−1106.

(26) Goh, C.; Kline, R. J.; McGehee, M. D.; Kadnikova, E. N.; Fréchet, J. M. J. Molecular-Weight-Dependent Mobilities in Regioregular Poly(3-Hexyl-thiophene) Diodes. *Appl. Phys. Lett.* **2005**, *86*, No. 122110.

(27) Meskers, S. C. J.; Hübner, J.; Oestreich, M.; Bässler, H. Dispersive Relaxation Dynamics of Photoexcitations in a Polyfluorene Film Involving Energy Transfer: Experiment and Monte Carlo Simulations. *J. Phys. Chem. B* **2001**, *105*, 9139−9149.

(28) Tress, W.; Petrich, A.; Hummert, M.; Hein, M.; Leo, K.; Riede, M. Imbalanced Mobilities Causing S-Shaped IV Curves in Planar Heterojunction Organic Solar Cells. *Appl. Phys. Lett.* **2011**, *98*, No. 063301.

(29) Carsten, B.; Szarko, J. M.; Lu, L. Y.; Son, H. J.; He, F.; Botros, Y. Y.; Chen, L. X.; Yu, L. P. Mediating Solar Cell Performance by Controlling the Internal Dipole Change in Organic Photovoltaic Polymers. *Macromolecules* **2012**, *45*, 6390−6395.

(30) Schwarz, C.; Bässler, H.; Bauer, I.; Koenen, J. M.; Preis, E.; Scherf, U.; Köhler, A. Does Conjugation Help Exciton Dissociation? A Study on Poly(*p*-Phenylene)s in Planar Heterojunctions with C_{60} or TNF. *Adv. Mater.* **2012**, *24*, 922−925.

(31) Schwarz, C.; Tscheuschner, S.; Frisch, J.; Winkler, S.; Koch, N.; Bässler, H.; Köhler, A. Role of the Effective Mass and Interfacial Dipoles on Exciton Dissociation in Organic Donor-Acceptor Solar Cells. *Phys. Rev. B* **2013**, *87*, No. 155205.

(32) Verlaak, S.; Beljonne, D.; Cheyns, D.; Rolin, C.; Linares, M.; Castet, F.; Cornil, J.; Heremans, P. Electronic Structure and Geminate Pair Energetics at Organic-Organic Interfaces: The Case of Pentacene/C-60 Heterojunctions. *Adv. Funct. Mater.* **2009**, *19*, 3809−3814.

(33) Arkhipov, V. I.; Heremans, P.; Bässler, H. Why Is Exciton Dissociation So Efficient at the Interface between a Conjugated Polymer and an Electron Acceptor? *Appl. Phys. Lett.* **2003**, *82*, 4605−4607.

(34) Nenashev, A. V.; Baranovskii, S. D.; Wiemer, M.; Jansson, F.; Österbacka, R.; Dvurechenskii, A. V.; Gebhard, F. Theory of Exciton Dissociation at the Interface between a Conjugated Polymer and an Electron Acceptor. *Phys. Rev. B* **2011**, *84*, No. 035210.

(35) Wiemer, M.; Nenashev, A. V.; Jansson, F.; Baranovskii, S. D. On the Efficiency of Exciton Dissociation at the Interface between a Conjugated Polymer and an Electron Acceptor. *Appl. Phys. Lett.* **2011**, *99*, No. 013302.

(36) Nicolai, H. T.; Kuik, M.; Wetzelaer, G. A. H.; de Boer, B.; Campbell, C.; Risko, C.; Brédas, J. L.; Blom, P. W. M. Unification of

Trap-Limited Electron Transport in Semiconducting Polymers. *Nat. Mater.* **2012**, *11*, 882−887.
(37) Hoffmann, S. T.; Jaiser, F.; Hayer, A.; Bässler, H.; Unger, T.; Athanasopoulos, S.; Neher, D.; Köhler, A. How Do Disorder, Reorganization, and Localization Influence the Hole Mobility in Conjugated Copolymers. *J. Am. Chem. Soc.* **2013**, *135*, 1772−1782.

Supporting Information to

Influence of the Excited State Charge-Transfer Character on the Exciton Dissociation in Donor-Acceptor Copolymers

*Katharina Neumann, Christian Schwarz, Anna Köhler[#] and Mukundan Thelakkat**

K. Neumann, M. Thelakkat
Applied Functional Polymers, Macromolecular Chemistry I
University of Bayreuth
95440 Bayreuth, Germany
*E-mail: mukundan.thelakkat@uni-bayreuth.de

C. Schwarz, A. Köhler
Experimental Physics II and Bayreuth Institute of Macromolecular Research (BIMF)
University of Bayreuth
95440 Bayreuth, Germany
[#]E-mail: anna.koehler@uni-bayreuth.de

1. Materials

Commercially available starting materials were purchased from Aldrich or abcr and used without further purification. Solvents for chromatography, extraction and reactions were distilled prior to use.

1.1 Monomer 1 and 2

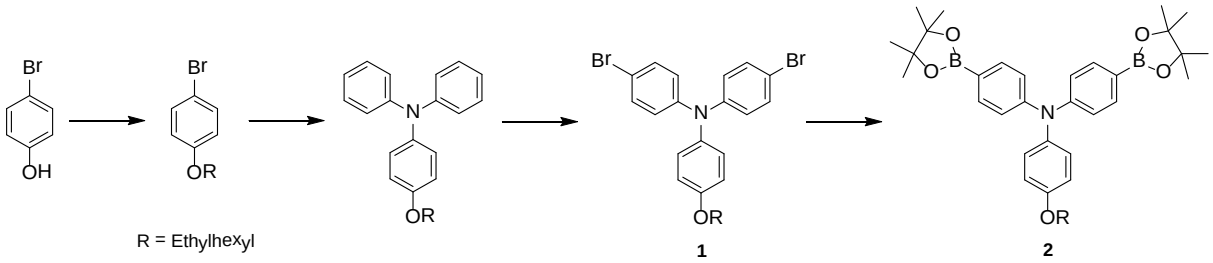

1-Bromo-4-[(2-ethylhexyl)oxy]-benzene

4-Bromophenole (18.08 g, 0.1 mol) and K_2CO_3 (33.83 g, 0.24 mol) were dissolved in dry DMF. 2-Ethylhexylbromide (15.45 g, 0.08 mol) was added slowly and the reaction mixture was stirred for 24 h at 60 °C. After cooling, the reaction mixture was extracted with hexane and 1 M HCl. The crude product was used without further purification. Yield: 75 %.

^{1}H NMR (300 MHz, CDCl3, 298 K): δ (ppm) = 7.42 - 7.34 (d, 2H, H_{ar}), 6.84 - 6.75 (d, 2H, H_{ar}), 3.84 - 3.79 (d, 2H, OCH_2), 1.80 - 1.66 (m, 1H, CH), 1.60 - 1.25 (m, 8H, CH_2), 1.00 - 0.83 (m, 6H, CH_3).

MS-EI *m/z* calcd for $C_{14}H_{21}BrO$ 285.22, found [M^+] 284.

4-(2-Ethylhexyloxy)-N,N-diphenylaniline

Diphenylamine (4.91 g, 0.029 mol), 1-bromo-4-[(2-ethylhexyl)oxy]-benzene (10 g, 0.035 mol), sodium-*tert*-butoxide (3.62 g, 0.038 mol) and 0.07 g (0.30 mmol) $Pd(OAc_2)$ were dissolved in dry toluene. Tri-*tert*-butylphosphine (1 M in toluene, 1ml) was added and the reaction mixture was heated to 60 °C for 24 h. After cooling to room temperature the solution was filtered over Alox N. The solvent was removed by reduced pressure and the crude product was precipitated in MeOH from THF and filtered. The white powder was dried in vacuum. Yield: 87 %.

1H NMR (300 MHz, CDCl3, 298 K): δ (ppm) = 7.26 - 7.16 (m, 4H, Ha), 7.90 - 7.00 (m, 6H, H_{ar}), 6.97 - 6.90 (m, 2H, H_{ar}), 6.87 - 6.80 (m, 2H, H_{ar}), 3.85 - 3.79 (d, 2H, OCH_2), 1.76 - 1.65 (m, 1H, CH), 1.57 - 1.26 (m, 8H, CH_2), 0.97 - 0.86 (m, 6H, CH_3).

MS-EI *m/z* calcd for $C_{26}H_{31}NO$ 373.53, found [M^+] 373.

4-Bromo-N-(4-bromophenyl)-N-(4-(2-ethylhexyloxy)phenyl)aniline (1)

4-[(2-Ethylhexyl)oxy]-N,N-diphenylaniline (8.36 g, 22.4 mmol) was dissolved in 190 ml of a 5:1 $CHCl_3$/AcOH mixture and degassed for 30 min with an argon stream. After cooling the solution to -10 °C NBS (7.97 g, 44.8 mmol) was added in small portions under exclusion of light. After stirring for 3.5 h at -10 °C the reaction was quenched with 1 M NaOH. The reaction mixture was extracted with DCM and water. The organic phase was washed with 1 M NaOH and two times with water. After drying over Na_2SO_4 the solvent

was evaporated under reduced pressure. 4-Bromo-N-(4-bromophenyl)-N-(4-(2-ethylhexyloxy)phenyl)aniline was achieved as a viscous oil. Yield: 99 %.
^{1}H NMR (300 MHz, DMSO, 298 K): δ (ppm) = 7.33 - 7.25 (m, 4H, H_a), 7.06 - 6.98 (m, 2H, H_b), 6.92 - 6.81 (m, 6H, H_c), 3.85 - 3.80 (d, 2H, O-CH_2), 1.77 - 1.66 (m, 1H, CH), 1.58 - 1.26 (m, 8H, CH_2), 0.97 - 0.88 (s, 6H, CH_3).
MS-EI m/z calcd for $C_{26}H_{29}Br_2NO$ 531.32, found [M^+] 531.

4-(2-Ethylhexyloxy)-N,N-bis(4-(4,4,5,5-tetramethyl-1,3,2-dioxaborolan-2-yl)phenyl) aniline (2)

4-Bromo-N-(4-bromophenyl)-N-(4-(2-ethylhexyloxy)phenyl)aniline **1** (3.30 g, 6.12 mmol) were dissolved in THF under an argon atmosphere. The solution was cooled to -78 °C and a solution of n-BuLi in hexane (8.15 mL, 1.6 M, 13.04 mmol) were added dropwise. After 2 h at -78 °C 2-isopropoxy-4,4,5,5-tetramethyl-1,2,3-dioxaborolane (8.6 ml, 7.80 g, 41.92 mmol) was added quickly. The reaction mixture was warmed to room temperature and stirred for 50 h. The reaction was quenched carefully with water. The following extraction was carried out with DCM and water. After drying over Na_2SO_4 the solvent was evaporated under reduced pressure. The residue was recrystallized in THF hexane (1:8). The non-crystallized part was purified chromatographically (CH:EE; 10:1). Yield: 27 %.
^{1}H NMR (300 MHz, $CHCl_3$, 298 K): δ (ppm) = 7.68 - 7.58 (d, 4H, H_a), 7.07 - 6.99 (m, 6H, H_b), 6.86 - 6.79 (m, 2H, H_c), 3.84 - 3.79 (d, 2H, O-CH_2), 1.76 - 1.66 (m, 1H, CH), 1.53 - 1.16 (m, 32H, CH_2, CH_3), 0.97 - 0.85 (m, 6H, CH_3).
MS-EI m/z calcd for $C_{38}H_{53}B_2NO_5$ 625.45, found [M^+] 625.

1.2 Monomer 3

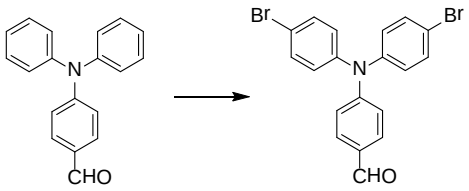

3

4-(Bis(4-bromophenyl)amino)benzaldehyde (3)

4-Diphenylaminobenzaldehyde (5.0 g, 19.9 mmol) was dissolved in 195 ml $CHCl_3$/AcOH (5:1) and degassed with an argon stream. The solution was cooled to -5 °C and N-bromosuccinimide (8 g, 45.77 mmol) were added in small portions. After stirring for 10 h the solution was warmed to room temperature and stirred for 30 h. The reaction was quenched with 1 M NaOH, extracted with DCM and washed with brine. The organic phase was dried over Na_2SO_4 and the solvent was evaporated under reduced pressure. The crude product was purified chromatografically (n-hexane:DCM, gradually from 5:1

to 1:1). 4-(Bis(4-bromophenyl)amino)benzaldehyde **3** was obtained as yellow powder. Yield: 81 %

^{1}H NMR (300 MHz, $CDCl_3$, 298 K): δ (ppm) = 9.85 - 9.83 (s, 1H, CHO), 7.74 - 7.66 (m, 2 H, H_a), 7.48 - 7.40 (m, 4H, H_b), 7.07 - 6.98 (m, 6H, H_c, H_d).

MS-EI m/z calcd 431.12, found [M^+] 431.

1.3 Monomer 4

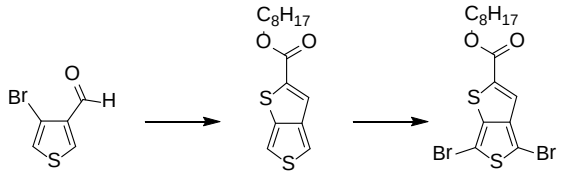

4

4-Bromothiophene-3-carbaldehyde

3,4-Dibromothiophene (14.44 g, 0.06 mol) were dissolved in dry diethylether and cooled to -78 °C. Afterwards 37 ml of n-BuLi (1.6 M in hexane) were added slowly. After 30 min DMF (5.97 ml, 0.08 mol) was added, the reaction mixture was warmed to room temperature and stirred overnight. The reaction was quenched with saturated NH_4Cl solution in water and extracted with diethylether. The organic phase was dried over Na_2SO_4 and the solvent was evaporated under reduced pressure. The crude product was purified by column chromatography (hexane : diethylether 5:1).

Yield: 56 %.

^{1}H NMR (300 MHz, $CHCl_3$, 298 K): δ (ppm) = 9.97 (s, 1H, H_{al}), 8.18 (d, 1H, H_{ar}), 7.39 (d, 1H, H_{ar}).

MS-EI m/z calcd for C_5H_3BrOS 191.05, found [M^+] 191.

Octyl-thieno[3,4-b]thiophene-2-carboxylate

4-Bromothiophene-3-carbaldehyde (5.82 g, 0.03 mol) and thioglycolicacid-octyl ester (6.85 g, 0.03 mol) were dissolved in 50 ml DMF. K_2CO_3 (6.22 g, 0.04 mol) and CuO nanopowder (0.07 g, 0.9 mmol) were added. The reaction mixture was heated to 80 °C for 16 h. The reaction mixture was extracted with DCM and water. The organic phase was dried over Na_2SO_4 and the solvent was evaporated under reduced pressure. The crude product was purified by column chromatography (Hexane : Ethylacetate, 90:1).

Yield: 31 %

^{1}H NMR (300 MHz, $CHCl_3$, 298 K): δ (ppm) = 7.71 (s, 1H, H_{ar}), 7.61 (d, 1H, H_{ar}), 7.30 (dd, 1H, H_{ar}), 4.33 (t, 2H, OCH_2), 1.78 (q, 2H, CH_2), 1.35 (m, 10H, CH_2), 0.91 (t, 3H, CH_3).

MS-EI m/z calcd for $C_{15}H_{20}O_2S_2$ 296.45, found [M^+] 296.

Octyl-4,6-dibromo-thieno[3,4-b]thiophene-2-carboxylate (4)

Octyl-thieno[3,4-b]thiophene-2-carboxylate (2.77 g, 9.34 mmol) were dissolved in 30 ml dry DMF and degassed with an argon stream for 30 minutes. After cooling the solution in an ice bath 4.16 g (23.36 mmol) NBS were added in small portions. The reaction mixture was warmed up to room temperature. After stirring for 12 h the solution was poured into a 10% aqueous solution of $Na_2S_2O_3$ and extracted with diethylether twice. The organic phase was dried over Na_2SO_4 and the solvent was evaporated under reduced pressure. The crude product was purified by column chromatography (DCM).

Yield: 53 %

^{1}H NMR (300 MHz, $CHCl_3$, 298 K): δ (ppm) = 7.53 (s, 1H, H_{ar}), 4.32 (t, 2H, OCH_2), 1.76 (q, 2H, CH_2), 1.35 (m, 10H, CH_2), 0.89 (t, 3H, CH_3).

MS-EI m/z calcd for $C_{15}H_{20}O_2S_2$ 453.91, found [M^+] 454.

2. ^{1}H-NMR

^{1}H NMR spectra were recorded using a Bruker Avance 300 spectrometer at 300 MHz at 298 K in deuterated chloroform.

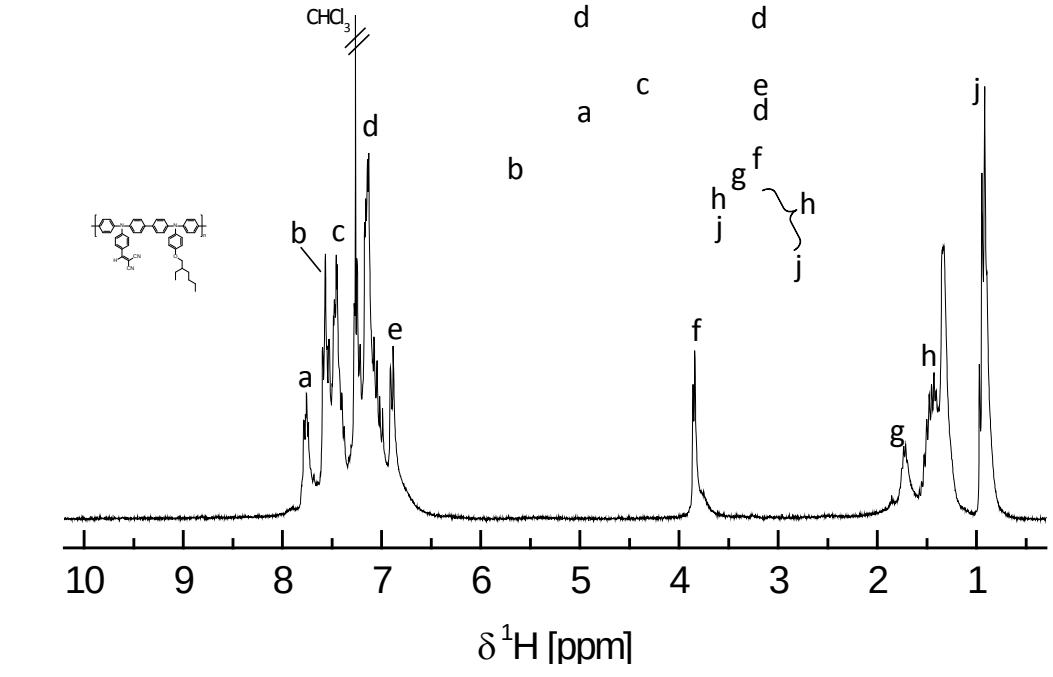

Figure 1. ^{1}H-NMR spectrum of **P3**. No signal for the aldehyde group was observed.

3. FT-IR spectra

FT-IR spectra were recorded on a *Perkin Elmer Spectrum 100* spectrometer in solid using a ATR unit.

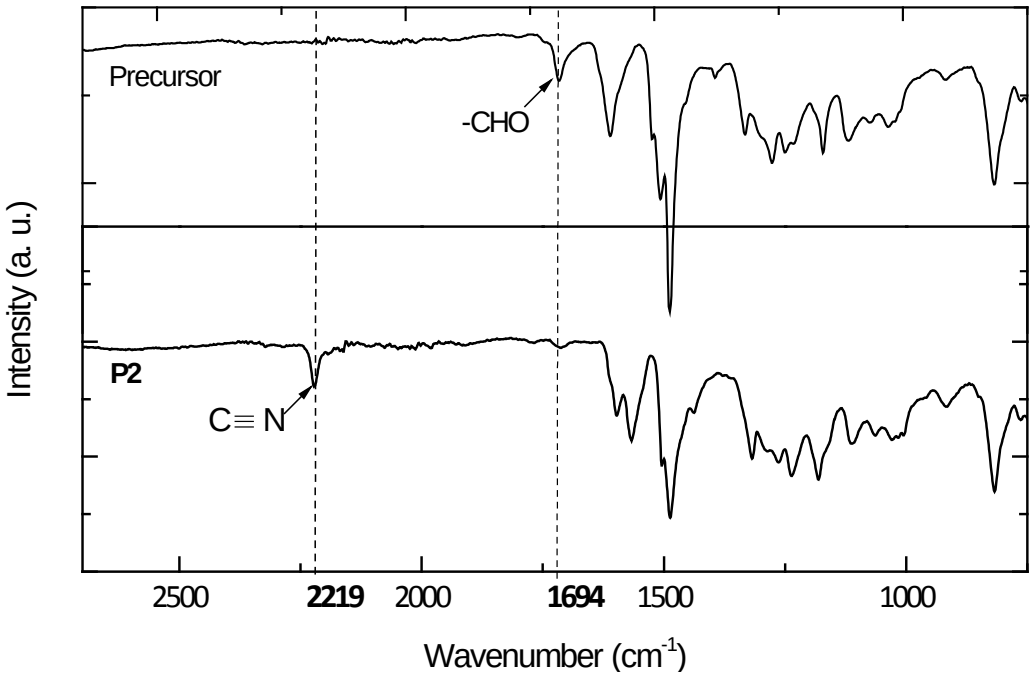

Figure 2. FT-IR-spectra of the precursor alternating copolymer with aldehyde-group showing a typical absorption band of the -CHO group at 1694 cm^{-1} and the D-A-copolymer **P2** showing the CN-stretching vibration of the dicyanovinyl group at 2219 cm^{-1}.

4. Cyclic voltammetry

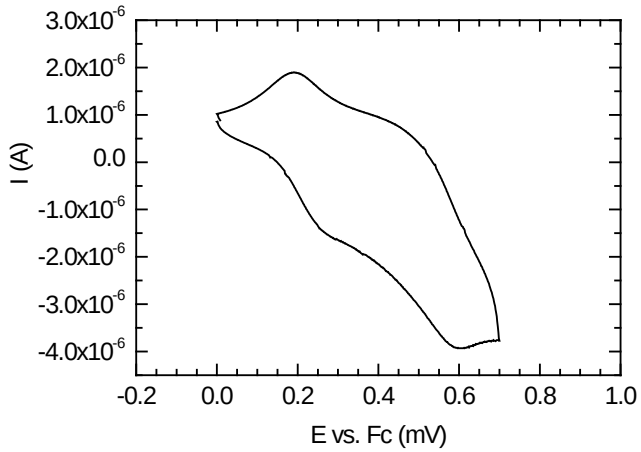

Figure 3. Cyclic voltammogram of **P1**.

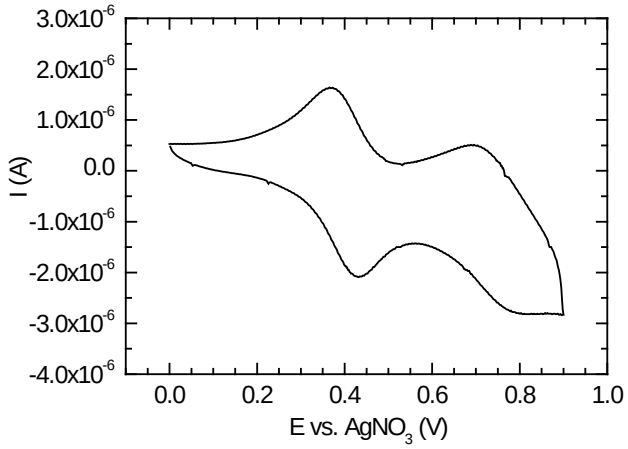

Figure 4. Cyclic voltammogram of **P2**.

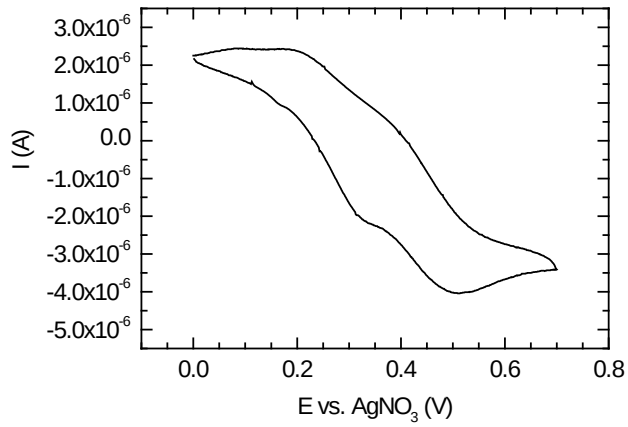

Figure 5. Cyclic voltammogram of **P3**.

5. Space charge limited current measurements

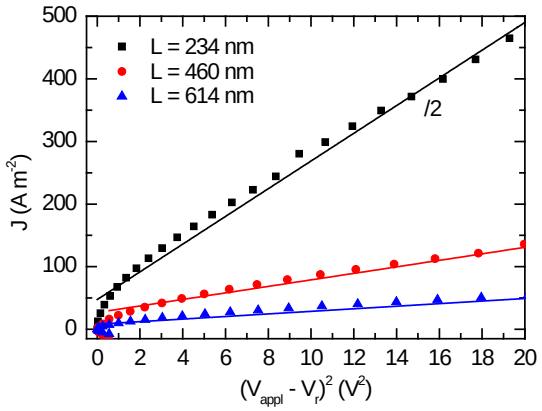

Figure 6. Hole-only devices of **P1** with varied layer thicknesses. The current density values for the layer thickness of 234 nm are divided by a factor of 2 to provide a better view on the other values.

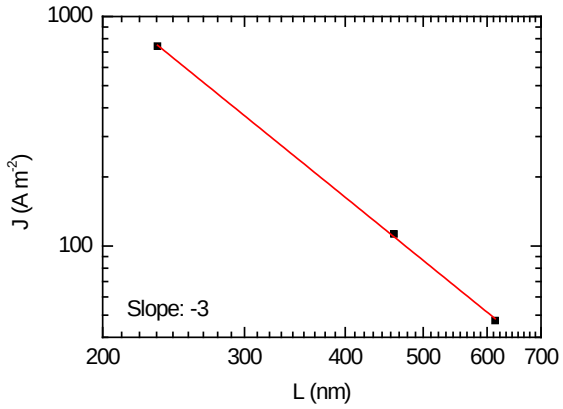

Figure 7. Log-log plot of the thickness dependence of the current density at a fixed bias of 4 V for **P1**. The squares are experimental data and the solid line is the fit according to relation $J \sim V^2/L^3$, where L is the thickness of the sample.

Device	L [nm]	μ_h [$cm^2V^{-1}s^{-1}$]
1	234	$1.8 \cdot 10^{-4}$
2	460	$1.4 \cdot 10^{-4}$
3	614	$1.0 \cdot 10^{-4}$
Average		***$1.4 \cdot 10^{-4}$***

Table 1. Calculated hole transport mobilities μ_h for three layer thicknesses as well as their average value.

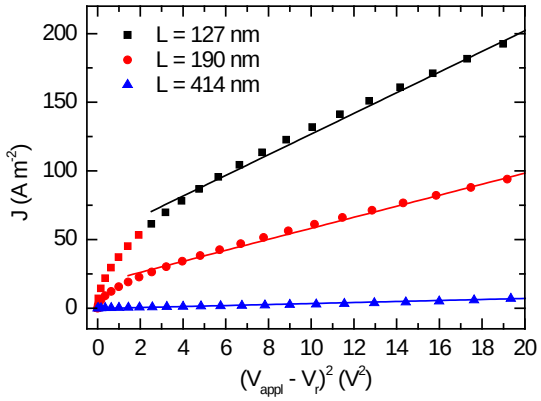

Figure 8. Hole-only devices of **P2** with varied layer thicknesses.

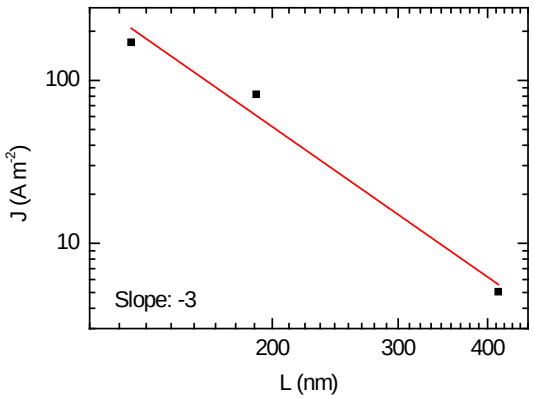

Figure 9. Log-log plot of the thickness dependence of the current density at a fixed bias of 4 V for **P2**. The squares are experimental data and the solid line is the fit according to relation $J \sim V^2/L^3$, where L is the thickness of the sample.

Device	L [nm]	μ_h [$cm^2V^{-1}s^{-1}$]
1	127	$5.0 \cdot 10^{-6}$
2	190	$8.5 \cdot 10^{-6}$
3	414	$9.2 \cdot 10^{-6}$
Average		***7.6 · 10^{-6}***

Table 2. Calculated hole transport mobilities μ_h for three layer thicknesses as well as their average value.

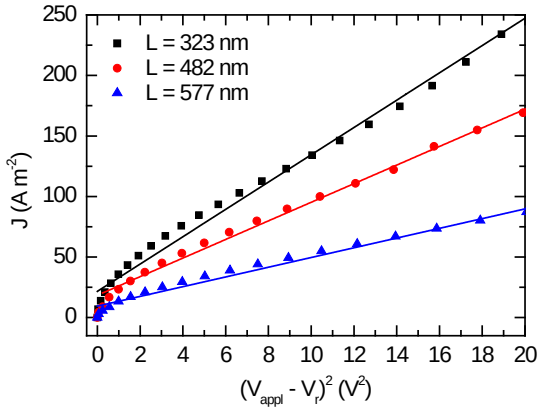

Figure 10. Hole-only devices of **P3** with varied layer thicknesses.

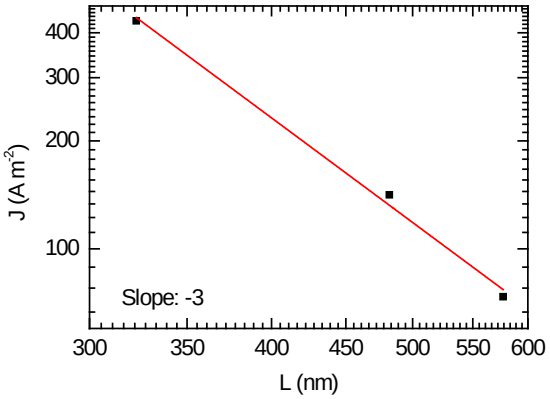

Figure 11. Log-log plot of the thickness dependence of the current density at a fixed bias of 4 V for **P3**. The squares are experimental data and the solid line is the fit according to relation $J \sim V^2/L^3$, where L is the thickness of the sample.

Device	L [nm]	μ_h [$cm^2V^{-1}s^{-1}$]
1	323	$4.1 \cdot 10^{-4}$
2	482	$2.9 \cdot 10^{-4}$
3	577	$2.4 \cdot 10^{-4}$
Average		***3.1 · 10^{-4}***

Table 3. Calculated hole transport mobilities μ_h for three layer thicknesses as well as their average value.

6. Lifetime measurements

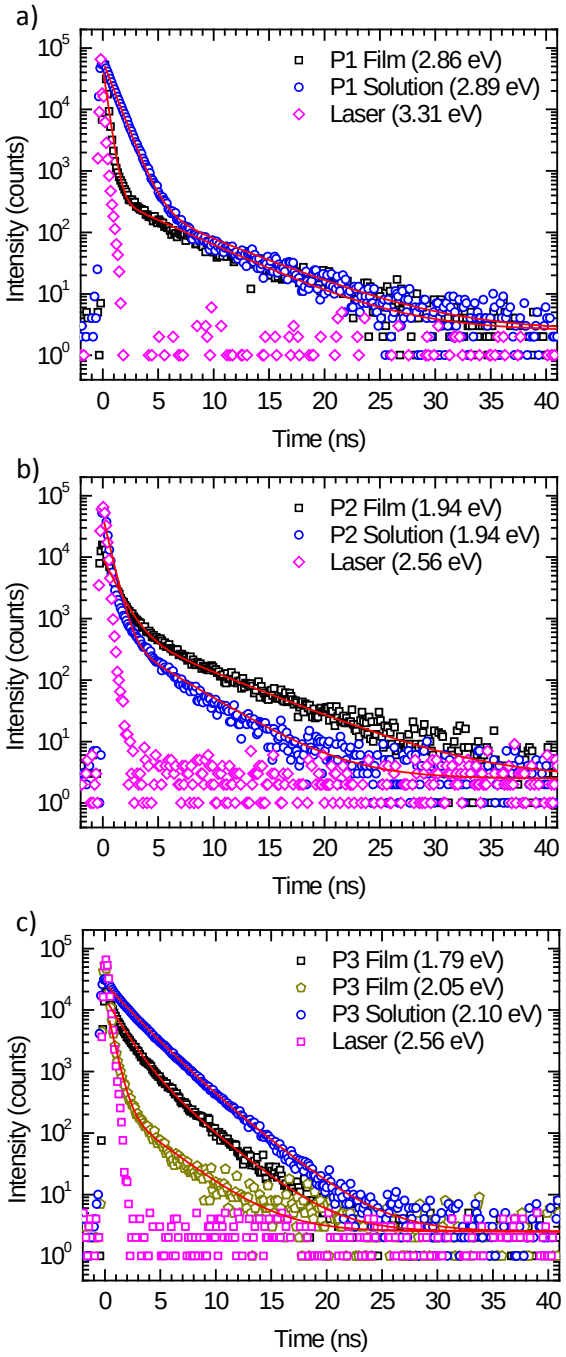

Figure 12. Lifetime measurements of the (co)polymers in a time correlated single photon counting (TCSPC) setup. The fit parameters are shown in table 4.

Polymer	A1	t1 (ns)	A2	t2 (ns)	y_0
P1 Film	45600	0.3	400	5.3	2.5
P1 Solution	60800	0.9	400	6.0	2.5
P2 Film	9000	1.1	700	6.0	2.5
P2 Solution	45000	0.6	600	4.0	2.5
P3 Film (2.05 eV)	14000	0.5	320	3.2	2.5
P3 Film (1.79 eV)	13000	1.3	2600	3.0	2.5
P3 Solution	20000	2.0	7000	3.2	2.5

Table 4. Fit parameters of the lifetime fits in Figure 12, fitted with the biexponential equation y = 1*exp(-x/t1) + A2*exp(-x/t2) + y0

7. Photocurrent voltage curve for monochromatic illumination

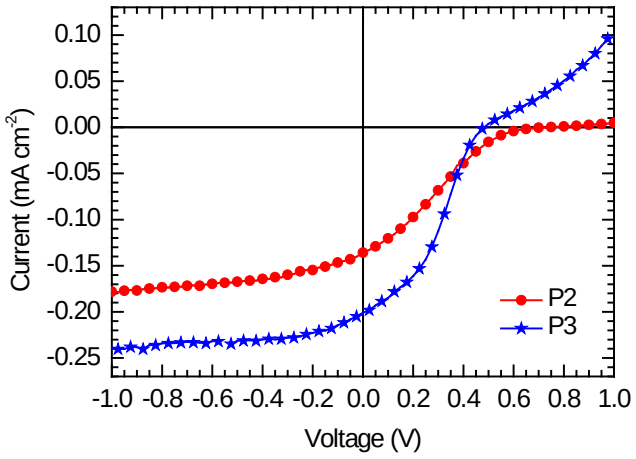

Figure 13. Photocurrent voltage curve of the copolymers under monochromatic illumination at 570 nm.

8. P2: fits with the dipole model

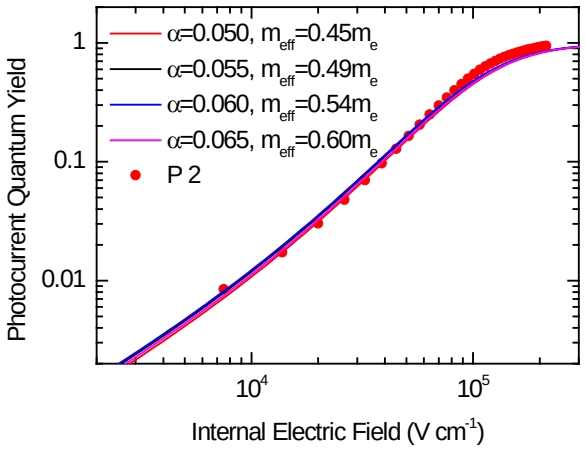

Figure 14. Fits with the dipole model and different fit parameters.[1] It is shown that the data of **P2** can be fitted with increased dipole strength α by increasing the effective mass m_{eff}. All other fit parameters stayed the same. Other fit parameters used (also in the main article): $\tau_0 \nu_0 \exp(-2\gamma r) = 40$.

9. Solar cell parameters

Polymer	I_{SC} (mA cm^{-2})	V_{OC} (V)	FF (%)	PCE (%)
P1	1.56	0.62	24.6	0.23
P2	0.92	0.74	16.4	0.11
P3	1.52	0.50	36.0	0.26

Table 5. Characteristic parameters for the bilayer (co)polymer/C_{60} solar cells measured under AM 1.5 illumination.

10. References

1. Wiemer, M.; Nenashev, A. V.; Jansson, F.; Baranovskii, S. D., On the Efficiency of Exciton Dissociation at the Interface between a Conjugated Polymer and an Electron Acceptor. Appl Phys Lett **2011**, 99, 013302.

8. Ground state bleaching at donor-acceptor interfaces

Christian Schwarz, Felix Milan, Stephan Kümmel, Anna Köhler

Zur baldigen Einreichung

Ground state bleaching at donor-acceptor interfaces

Christian Schwarz, Felix Milan, Stephan Kümmel, Anna Köhler[#]

Intended for Advanced Functional Materials

C. Schwarz, A. Köhler
Experimental Physics II and Bayreuth Institute of Macromolecular Research (BIMF)
University of Bayreuth
95440 Bayreuth, Germany
[#] E-mail: anna.koehler@uni-bayreuth.de

F. Milan, S. Kümmel
Theoretical Physics IV
University of Bayreuth
95440 Bayreuth, Germany

Abstract

Charge transfer (CT) at the donor-acceptor interface is the rate limiting step in organic solar cells. If interfacial hybrid states exist already in the dark it is plausible that they can have a major impact on the dissociation of optically generated excitations. In this work we monitor such interfacial states via high precision steady state absorption spectroscopy. We find that depositing an electron accepting layer of either trinitrofluorenone (TNF), C_{60}, or a perylene-diimide derivative on top of a layer of electron donating conjugated polymers, such as MEH-PPV or various poly-phenylenes, causes a substantial bleaching of the absorption spectrum near the absorption edge. This is attributed to the formation of ground state complexes that have reduced oscillator strength. The experiments bear out a correlation between the reduction of the absorbance with the energy gap between the donor-HOMO and acceptor-LUMO, the effective conjugation length of the donor, and the efficiency of exciton dissociation in the solar cell. The effect originates from mixing of the donor-HOMO and the acceptor LUMO. Calculations using density functional theory support this reasoning. Implications for efficiency of organic solar cells will be discussed.

1. Introduction

The efficiency of promising low cost organic bulk heterojunction donor-acceptor (D-A) solar cells is successively increasing over the past decade reaching now power conversion efficiencies greater than 10%.[1] These efforts are mainly based on progresses in morphology control and in the development of low bandgap materials to harvest a larger part of the suns solar spectrum. In these solar cells ideally composited blend films with large D-A interfaces and interpenetrating networks are responsible for efficient charge separation and charge transport. A deeper understanding of the electronic processes at these donor-acceptor interfaces is needed to develop further improved strategies towards organic solar cells with even enhanced efficiencies.

For organic solar cells, the key role of photoinduced charge-transfer states in the process of dissociating an excited state at the donor-acceptor interface is well known and well documented.[2-6] Similarly, the intermediate formation of excited state complexes (exciplexes) in the course of electron-hole recombination has long been recognized as a central step in the operation of organic light-emitting diodes.[7-8]

More recently it was noted that interfacial donor-acceptor complexes with some charge-transfer character may also prevail in the *ground state*,[9-10] and that their presence and nature may impact on the photogeneration of charges. [11-13]. Evidence for such ground state (GS) complexes is frequently brought forward by detecting the weak absorption associated with the GS complexes, for example through photothermal deflection spectroscopy.[14] A limiting case of a "donor-acceptor-system" is obtained when the electron affinity of the acceptor is so strong that the acceptor may even be employed to obtain p-type doping.[15] An example for this is the acceptor molecule F4-TCNQ (2,3,5,6-tetrafluoro-7,7,8,8-tetracyanoquinodimethane). Using ultraviolet photoemission spectroscopy in combination with quantum chemical calculations, Méndez, Salzmann and coworkers have recently shown that for the D-A-system comprising pentacene as donor and F4-TCNQ as acceptor, electronic interaction leads to the formation of a ground state charge-transfer complex.[16-17] Their work explicitly spells out and demonstrates that the frontier orbitals of the GS complex result from mixing of the highest molecular orbital (HOMO) of the donor with the lowest unoccupied molecular orbital (LUMO) of the acceptor. Both electrons in the HOMO of the GS complex then result from the former donor molecule. Salzmann and coworkers were also able to detect the weak absorption due to the GS complex.

When a GS complex is formed due to electronic interaction between a donor and an acceptor, it is not surprising that there should be an associated weak new absorption feature, with the low oscillator strength of the GS complex resulting from its charge transfer character. Concomitantly, one may expect that the original absorption from the donor polymer and the acceptor molecule that now comprise the complex should have

vanished. Assessing the existence of such a ground state bleach in a quantitative manner is difficult for intermixed donor-acceptor blends. Here, we have used a bilayer geometry to compare the absorption of the donor-acceptor bilayer with the sum of the two individual layers. We observe a strong ground state bleach that we attribute to the formation of ground-state charge-transfer complexes. The ground state bleach is more intense for better conjugated chromophores. It correlates with the energy gap between the donor HOMO and the acceptor LUMO as well as with the dissociation efficiency of photo excitations. The systems investigated comprise the polymers MEH-PPV, PPV (poly-(*p*-phenylenevinylene)), MeLPPP (a ladder-type poly(*p*-phenylene)), PIF (poly-(indenofluorene)), DOOPPP (Dioctyloxy-poly(*p*-phenylene)), and the acceptor molecules TNF (2,4,7-trinitro-9-fluorenone), C_{60} and a PDI derivative (N,N'-bis-(1-ethylpropyl)-perylene-3,4:9,10-tetracarboxi-diimide). Given the ease of measuring the absorption of bilayers, we suggest this may provide a convenient means for initial material screening with a view to their suitability for solar cell applications.

2. Results

(i) The observation of a ground state bleach in MEH-PPV/TNF

In order to assess whether there might be any interaction between a donor and an acceptor molecule in the ground state, we compare the absorption of a bilayer film consisting of an acceptor layer on top of a donor film with the algebraic sum of the absorption of a film of donor and a film of acceptor. For this experiment, we cover a quadratic fused silica substrate with a 40 nm layer of donor polymer by spin-coating from solution. We then clean half of the substrate from the polymer layer using a cotton bud with solvent. This results in a strip of donor film. Orthogonal to the donor strip, we then evaporate a strip of an acceptor layer of 50 nm thickness using a shadow mask. As illustrated in figure 1, this results in four areas of the sample prepared by the same fabrication process, that is the donor layer on its own, the acceptor layer on its own, a bilayer with acceptor on top of the donor and an uncoated area for reference. We refer to this arrangement where donor and acceptor are in contact at the bilayer as configuration **I**. For comparison, we also employ a configuration **II**, where we turn over the fused silica substrate prior to the acceptor evaporation, so that the donor and acceptor are physically separated by the quartz substrate, while still obtaining the three areas of donor, acceptor, and their superposition. If there was no interaction between donor and acceptor, one might expect that both configurations should yield the same absorption spectra.

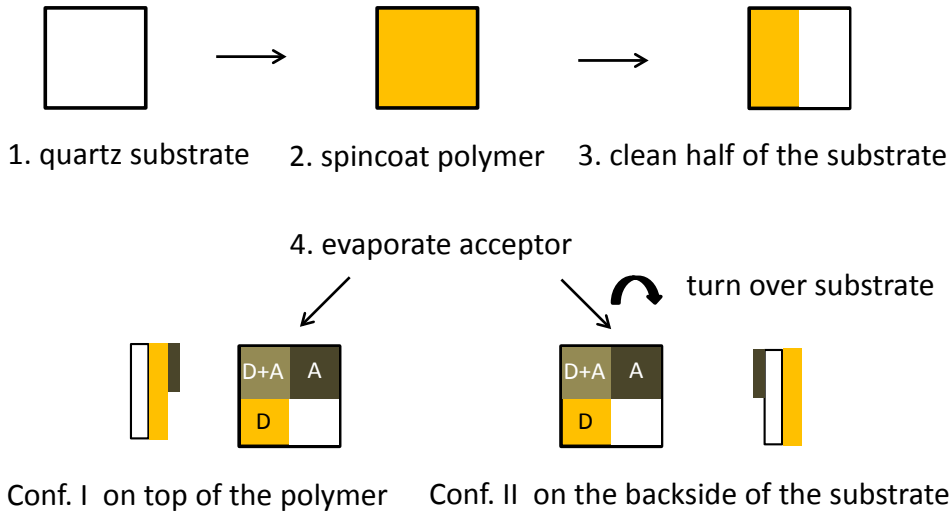

Figure 1: Scheme of the D-A-interaction experiment: In configuration I the acceptor is evaporated on top of the polymer donor, in configuration II on the backside of the fused silica substrate.

As is demonstrated in figure 2 for the donor-acceptor pair of MEH-PPV and TNF, the absorption spectra of MEH-PPV and of TNF are identical in both configurations. For the area where donor and acceptor overlap, there is, however, a striking difference. In configuration **II**, where donor and acceptor are separated by the fused silica substrate, the resulting measured absorption (dark blue line with star symbols) perfectly matches the algebraic sum of the absorption spectra of the individual donor and acceptor layers (light blue line with triangle symbols). When subtracting the measured spectrum from the sum of the individual spectra, a flat line of zero intensity results (pink line with pentagons). In contrast in configuration **I**, where the acceptor is directly deposited onto the donor, the spectrum obtained by measuring the bilayer (dark blue line with star symbols) differs from the sum of the donor and acceptor spectra (light blue line with triangle symbols). This difference is displayed by the pink line with pentagons. Compared to the direct superposition of the individual spectra, the bilayer shows a lack of absorption in the spectral range characteristic for the $S_1 \leftarrow S_0$ absorption of MEH-PPV, centered around 2.5 eV. At this energy, the bilayer in configuration **I** absorbs only about 60% of the light compared to the superposition in configuration **II**. Furthermore, the peak of the bilayer absorption is shifted to the red by about 30 meV compared to the peak of the superposition spectrum. While the intensity of the first absorption band in MEH-PPV is reduced in the bilayer, we find an additional absorption signal below the absorption edge of MEH-PPV, i.e. below 2.2 eV, as well as in the ultraviolet spectral range (3.2-4.0) eV.

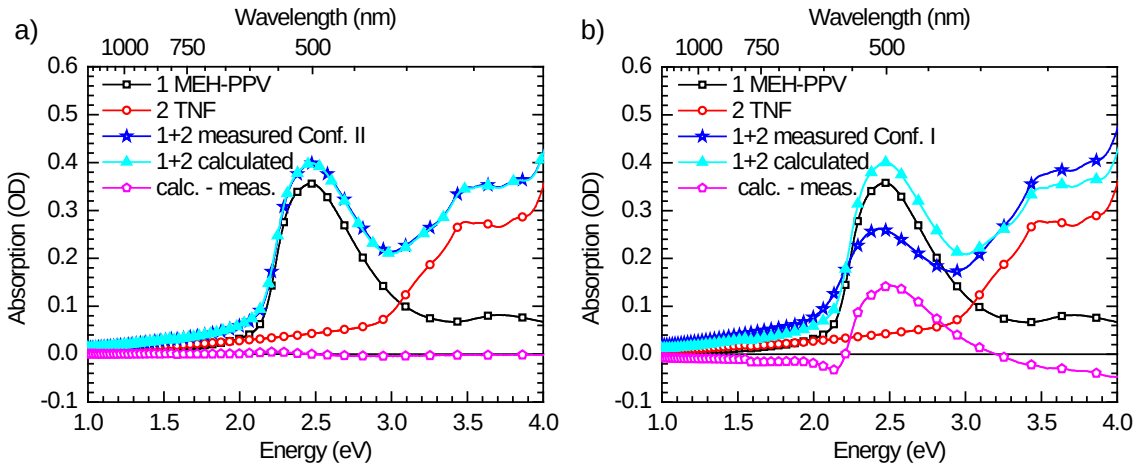

Figure 2: Absorption spectra of the different film areas in the samples prepared a) in Configuration II and b) in Configuration I. The black line with squares and the red line with circles show the absorption spectra measured for the areas containing only a film of MEH-PPV or TNF, respectively. The dark blue line with stars shows the absorption measured for the area where MEH-PPV and TNF films overlap. The algebraic sum of the MEH-PPV film spectrum and the TNF film spectrum is shown as light blue line with triangles. The difference between the calculated and measured superposition spectra is shown as pink line with pentagons.

(ii) The role of the acceptor molecule

The observation of an altered bilayer absorption spectrum is not limited to the MEH-PPV/TNF system but also occurs for other acceptors such as C_{60} and a perylene-diimide derivative (PDI). Figure 3 shows the absorption spectra obtained for the combination of the insoluble polymer poly(*p*-phenylene vinylene) (PPV) with C_{60}. To prepare the sample, a soluble precursor-polymer is deposited from solution and converted into an insoluble layer of PPV by heating. In this way, we prepared a sample consisting of 41 nm of PPV with about 30 nm of C_{60} on top of it in the geometry of configuration **I**, i.e. two stripes orthogonal to each other, with direct contact between donor and acceptor in the bilayer formed by the stripes' overlapping area. Analogous to the case of MEH-PPV with TNF, we find that the absorption of the bilayer (dark blue line with triangles) differs from the sum of the absorption of the individual layers (light blue line with stars). The absorption that is missing matches the absorption of PPV from about 2.5 to 3.5 eV, and it also follows the absorption of the C_{60} in the range from about 1.8-2.8 eV. At the peak of the polymer absorption band, at 3.1 eV, the absorption in the bilayer is reduced by 25% compared to the sum of the individual layers. Above 3.5 eV, absorption is not missing, and centered around 1.6 eV, there seems to be a very small additional absorption signal. The reduction of the $S_1 \leftarrow S_0$ absorption band in PPV is analogous to that in MEH-PPV, while the reduction in acceptor absorption is a new feature. Before considering the reduction in acceptor absorption in more detail, we draw the reader's attention to an

extension of this absorption experiment. Compared to MEH-PPV, PPV is characterized by a high packing density of the polymer backbone due to the lack of side chains, a high glass transition temperature, and concomitantly a hard surface.[18-19] We can therefore remove the evaporated layer of C_{60} simply by swiping over the film with a dry cotton bud. If we then measure the sample again (orange line with tilted triangles), we find a spectrum that is identical to that of the individual PPV layer measured previously. From the fact that the PPV absorption is recovered by wiping with a dry cotton bud we infer that C_{60} does not significantly diffuse into the PPV layer within the timeframe of the experiment. This implies that the lack of absorption originates from a reversible donor-acceptor interaction at the bilayer interface.

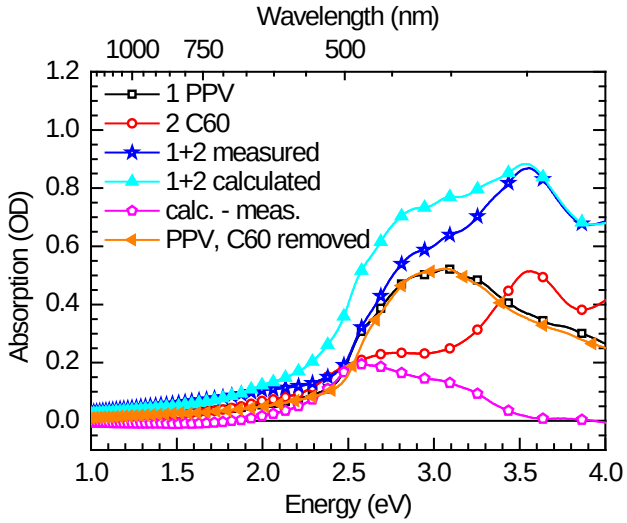

Figure 3: Absorption spectra of the different film areas in the samples prepared in Configuration I, for the combination of a 41 nm film of PPV with about 30 nm of C_{60}. Lines and symbols are used analogously to figure 2. In addition, the orange line with tilted triangles shows the absorption of the former bilayer area after the C_{60} had been mechanically removed.

We now attend to the issue of reduced acceptor absorption indicated in the measurement of the PPV/C_{60} bilayer. The contributions of donor and acceptor absorption can be identified more clearly when compounds are used that display well-structured absorption spectra. In figure 4a, we therefore consider the pair of MeLPPP as donor with a PDI derivative as acceptor. The absorption spectra of the individual compounds show well-resolved peaks. As for the previous samples, the absorption of the bilayer (dark blue line with stars) is reduced compared to the sum of the individual layers (light blue line with triangles). The difference spectrum (pink line with circles) can be matched by combining the spectra of the individual layers in the form $I_{Difference} = 0.17 * I_{MeLPPP} + 0.34 * I_{PDI}$. In other words, 17% of the polymer absorption are lacking as well as 34 % of the PDI derivative absorption. This experiment shows that not only the polymer $S_1 \leftarrow S_0$ ab-

sorption is reduced but also the acceptor $S_1 \leftarrow S_0$ absorption. To probe whether this is indeed due to an electronic interaction between donor and acceptor, we conducted a control experiment where the MeLPPP was replaced by a 40 nm layer of the electronically inert polymer polystyrene. When polystyrene is used, the bilayer absorption spectrum is nearly identical to the spectrum obtained by the addition of the two individual layers (fig. 4b).

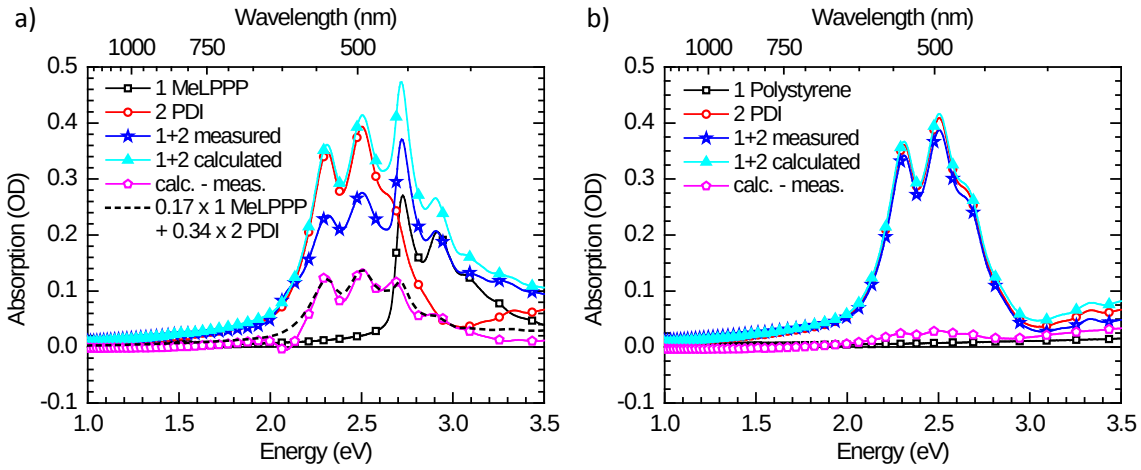

Figure 4: (a) Absorption spectra of a of the different film areas in the samples prepared in Configuration I for MeLPPP and a PDI derivative, with lines and symbols used analogous to figure 2. In addition, the dashed line shows the calculated linear combination of the spectra measured for the MeLPPP-only and PDI derivative-only areas. (b) The same for polystyrene and the PDI derivative.

With the aim to probe whether the observed bilayer absorption spectrum and its intensity is free from measurement artefacts, we performed a number of auxiliary experiments. The associated spectra are displayed in the supporting information.

(i) For a MeLPPP and PDI derivative system, we measured the absorption spectra with and without an integrating sphere. We found no significant changes between the two, suggesting that the influence of light scattering and reflection is negligible.

(ii) The spectra obtained are independent on the direction of the light path, i.e. whether the light is incident first onto the donor layer or first onto the acceptor layer makes no difference, thus excluding optical and scattering effects. This is most evident for the MeLPPP/PDI derivative bilayer which has a well-resolved spectrum

(iii) We wondered whether the changes to the polymer absorption may be related to annealing effects caused by thermal radiation of the evaporation source when the acceptor is evaporated. To test this hypothesis for the polymers MEH-PPV, MeLPPP and PPV, we heated the evaporation source without acceptor material in it yet at the same source temperature and for the same length of time used as for an acceptor evaporation

while having the polymer film in its usual place. We found the polymer absorption to be unaltered by this process.

We take these auxiliary experiments to confirm that the difference between the observed bilayer absorption and the superposition of the individual spectra is a genuine signature of the material system.

(iii) The relation of the missing absorption to solar cell performance

From the above mentioned experiments it appears that absorption is missing in the bilayer as a result of some interaction at the interface between a π-conjugated donor polymer and a π-conjugated acceptor molecule. We were wondering whether this bleaching of the ground state absorption correlates in some way with the performance of the donor-acceptor system in solar cells. We had previously considered exciton dissociation in a series of poly(*p*-phenylene)-(PPP)-based polymers in combination with TNF or C_{60} as acceptors in a bilayer solar cell.[20-21] When measuring the photocurrent as a function of the internal field in the device, we found the photocurrent to increase with the applied field until it saturates for a critical field strength F_{sat} , roughly at about 100% internal quantum yield. The value of the saturation field, where exciton dissociation into charges is at its maximum, reduces with increasing effective conjugation length of the PPP-type polymer. We shall now compare this to the bleaching of the ground state absorption that we find in the associated donor-acceptor bilayers. The polymers considered are MeLPPP, which is a ladder-type PPP with a stiff backbone, a polyindenofluorene (PIF) where three phenyl rings are bridged to form a stiff unit, and a PPP with sidechains (DOOPPP) where each phenyl ring can rotate. The chemical structures are given in the supporting information. As acceptor we use TNF since it has less overlap with the donor absorption spectra than C_{60}, which is beneficial for the analysis. For all three donor-acceptor combinations, the measured absorption in the bilayer is lower than the mathematical superposition of the individual donor and acceptor absorption (Fig. 5).

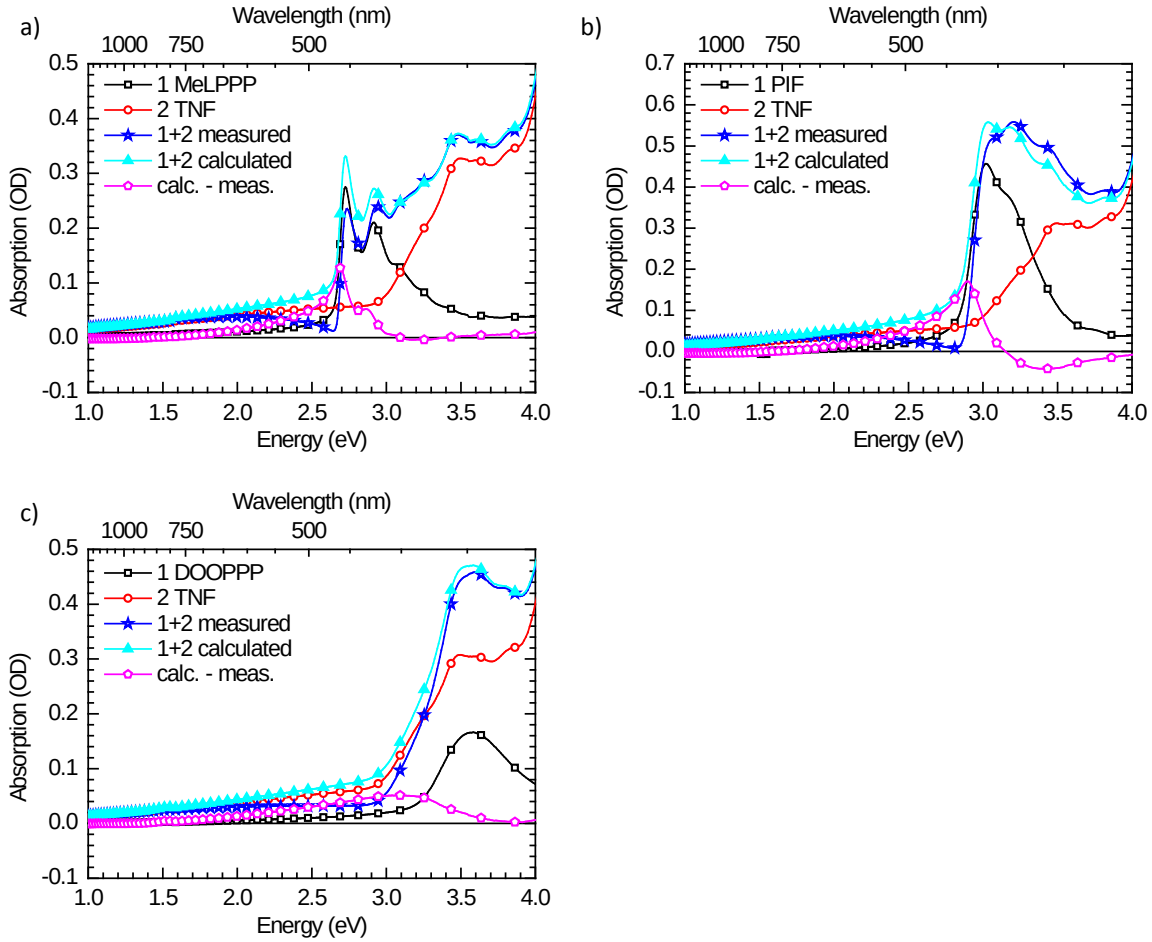

Figure 5: Absorption spectra of a of the different film areas in the samples prepared in Configuration I for (a) MeLPPP with TNF, (b) PIF with TNF and (c) DOOPPP with TNF. Lines and symbols are used analogously to figure 2. The thickness of the polymer film is about 40 nm that of the TNF layer is about 57 nm.

Absorption is bleached in particular in the lower energy range of the polymer absorption band, such that the bleach signal appears like a red-shifted absorption spectrum of the polymer, even matching the vibrational structure. The amount of the polymer ground state bleach, compared to the superposition of the individual donor and acceptor signal, is summarized in Table 1 for the PPP-type polymers and MEH-PPV in combination with TNF. Also listed are the saturation field F_{sat} required for maximum exciton dissociation, the HOMO level of the polymer and the energy difference ΔE between the polymer HOMO and the acceptor LUMO. For MEH-PPV and MeLPPP, about 34-40 % of the absorption is missing. In contrast, for PIF and DOOPPP, the absorption is reduced by only 8-13 %. This amount of ground state bleaching correlates with the energy gap between donor HOMO and acceptor LUMO which is lower for MEH-PPV and MeLPPP than for PIF and DOOPPP. Importantly, it also parallels the critical field strength F_{sat} needed for complete exciton dissociation, which is an order of magnitude lower for MeLPPP than

for PIF and DOOPPP, and concomitantly, the amount ground state bleach increases with the effective conjugation length in the PPP-type system.

Polymer	Reduction of the ground state absorption	Polymer HOMO (eV)	ΔE_{gap} (eV)	F_{Sat} (10^4 V cm^{-1})
MEH-PPV	40 %	-5.1	1.2	-
MeLPPP	34 %	-5.2	1.3	5
PIF	13 %	-5.4	1.5	15
DOOPPP	8 %	-5.6	1.6	30

Table 1: The reduction of the ground state absorption observed for the polymers MEH-PPV, MeLPPP, PIF and DOOPPP in a bilayer with TNF, along with the values of the polymer HOMO energy, the energy difference ΔE_{gap} between the polymer HOMO and the TNF LUMO energy (taken to be -3.9 eV) and the saturation field strength F_{Sat} required for maximum exciton dissociation in a bilayer solar cell structure. F_{Sat} is taken from [20], the MEHPPV and TNF energy levels from [40-41].

(iv) quantum chemical calculation of the absorption spectra

To assist the interpretation of the experimental data, we have calculated the absorption spectra of an model MEH-PV trimer, of TNF and of a sandwich type model dimer where TNF is placed above the MEH-PV trimer using time-dependent density functional theory (TD-DFT). For this, the geometry of the trimer and of TNF were optimized first individually and then the ground state geometry of both molecules together was optimized. Different initial orientations of the two molecules resulted in a very similar, sandwich type final geometry, as detailed in the experimental section. The lowest vertical transition energies with their respective intensities were calculated, and these delta-functions were broadened by multiplying with a Gaussian function to allow comparison with experiment. Figure 6 shows the absorption spectra obtained for the model MEH-PV trimer, the TNF and the sandwich-type model dimer (middle blue line with stars) with TNF on top of the MEH-PV-trimer. For comparison, the sum of the calculated absorption spectra of the TNF and the MEH-PV-Trimer is also shown (light blue line with triangles), as well as the difference between the calculated dimer absorption and the sum of the individual absorptions (pink line with circles). The calculations indicate a reduced absorption of the sandwich-type dimer compared to the MEH-PV-trimer as well as a slight additional absorption at the onset of the MEH-PV trimer absorption. In a qualitative manner, this agrees very well with the experimental results displayed in figure 2. An analysis of the transitions contributing to this absorption band of the donor-acceptor sandwich dimer,

centered around 2.5 eV, indicates that it results mainly from a transition from the dimer's HOMO to the dimer's LUMO+4 orbital. Importantly, the dimer's LUMO+4 has some charge density on the TNF molecule, thus suggesting some resonance interaction between the TNF and the PV-trimer to take place. The excited state analysis also indicates a number of transitions with vanishing oscillator strength roughly around 2 eV.[42]

In figure 6, we have summarized the HOMO and LUMO energies of the non-interacting MEH-PV-trimer and TNF as well as the HOMO, LUMO and LUMO+4 of the sandwich-type dimer. For reference, the values are also listed in the supporting information. In the sandwich-type dimer, the HOMO is stabilized compared to that of the donor MEH-PV, and the LUMO is destabilized compared to the TNF acceptor. The LUMO+4 of the dimer, that contributes significantly to the first optically active excited state, is between the LUMOs of the MEH-PPV and the TNF.

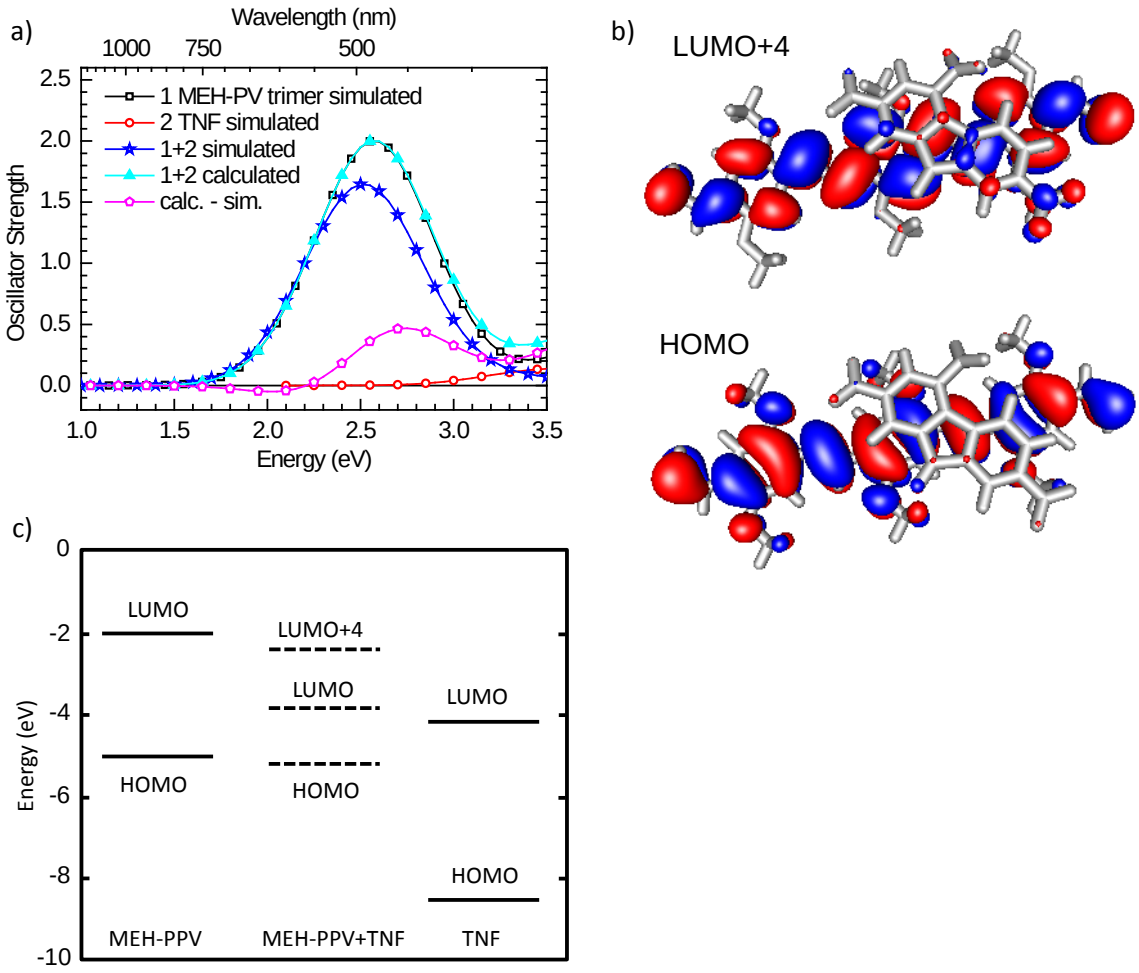

Figure 6: TDDFT calculations of MEH-PPV and TNF.(a) Calculated absorption spectra of a single MEH-PV trimer, a single TNF and a sandwich-type dimer of MEH-PV trimer with TNF on top of it (dark blue line with stars). For comparison, the sum of the individual spectra of MEH-PV timer and TNF is also shown (light blue line with triangles). The difference between the sum spectrum and the calculated spectrum of the sandwich-type dimer is shown by the pink line with pentagons. (b) Orbital plots of the sandwich-type dimer for the HOMO and the LUMO+4.(c) Energy level diagram showing the HOMOs and LUMOs of the MEH-PV trimer, the TNF and the sandwich-type dimer formed between them. For the latter, the energy of the LUMO+4 is also indicated.

4. Discussion

To summarize the results obtained on different donor-acceptor systems, we observe a lack in the ground state absorption of donor and acceptor when the two are brought into immediate contact such as to form a bilayer. Through various control measurements, we ascertained that this is a genuine experimental feature associated with electronic interaction and not an artefact. This is further confirmed by quantum chemical calculation on the absorption of an adjacent pair of donor and acceptor, i.e. a MEH-PV trimer and TNF that also yield a reduced intensity of the absorption. As evident from table 1, the lack of ground state absorption correlates with the energy difference between the donor HOMO and the acceptor LUMO, and with the electrical field strength needed for maximum exciton dissociation. The latter is a measure for the ease of exciton dissociation. Concurrently, lack of ground state absorption also increases with the effective conjugation length in the system of PPP-type polymers.

The energy levels obtained for the donor-acceptor system (Fig. 6) are reminiscent of those suggested by Salzmann and coworkers for a ground state (GS) complex. They propose such a species may form when a strong acceptor is brought in contact with a donor with the purpose to p-dope the donor. [16-17] The GS complex would have a HOMO and LUMO resulting from mixing of the polymer HOMO with the acceptor LUMO, with both electrons for the HOMO of the GS complex being supplied from the former polymer's HOMO. In their picture, the splitting between the frontier orbitals of the GS complex as well as the doping efficiency depend on the intermolecular resonance integral, (β in a Hückel treatment, or referred to as transfer integral t in a tight-binding treatment), and thus on the energy difference between the donor HOMO and the acceptor LUMO. The evidence they provide for this picture is based on photoemission spectroscopy supported by quantum chemical calculations.

We interpret our data in similar fashion. This is, we suggest that upon depositing the acceptor molecule onto the donor polymer, a ground state complex is formed with the frontier orbitals having some hybrid character. The two electrons in the complex HOMO being will result from the donor polymer, i.e. the MEH-PPV. Since the polymer chromophore and the acceptor molecule no longer exist as individual entities after the formation of such a complex, their lowest optical transitions no longer prevail in the same manner. Concurrently, an absorption from the GS complex is expected. In fact, the spectra of Salzmann, Méndez and coworkers shown in ref [16] and in the associated supporting information reveal both, a reduction of the S_1 absorption band of the donor as well as the appearance of low energy absorption features. The latter are attributed to transitions of the GS complex. The intensity of the spectral features are not analysed further in their work. Obviously, for the purpose of making solar cells, molecules with weaker acceptor strength are typically chosen than for the purpose of obtaining p-type doping. For doping, an ideal acceptor will have a LUMO with the same or even with lower energy

than the donor's HOMO. For isoenergetic levels, resonance splitting and hybridization of orbitals is at maximum. The finite energy difference ΔE_{gap} between donor HOMO and acceptor LUMO that prevails in a typical donor-acceptor system employed for solar cells, however, implies a weaker mixing. Let us, in a gedankenexperiment, tune ΔE_{gap} from zero offset to a very large limit, in a simple Hückel-type picture. With increasing value of ΔE_{gap} , the splitting reduces, and the hybrid orbitals of the complex acquire a weighted character, with the donor HOMO contributing dominantly to the complex HOMO and the acceptor LUMO prevailing in the complex LUMO. Eventually, for very large ΔE_{gap}, the individual donor HOMO and acceptor LUMO would be retained.(Fig. 7) Let us now consider the expected oscillator strengths. For zero ΔE_{gap} (Fig. 7a), the transitions from the complex HOMO to the complex LUMO should have reasonable oscillator strength, since the well mixed character of these orbitals should ensure good overlap of initial and final state wavefunctions, while the absorption from the parent donor and acceptor molecule will be strongly quenched. This is indeed what is observed in refs [16-17]. With increasing ΔE_{gap} (Fig. 7b), the low-energy transitions in the complex however acquire a stronger charge-transfer character and a concomitantly weaker oscillator strength, so that their detection requires sensitive techniques such as photothermal deflection spectroscopy. Concomitantly, the bleaching of the parent donor or acceptor absorption should become less pronounced, until for very large ΔE_{gap}, the independent absorption features are retained.

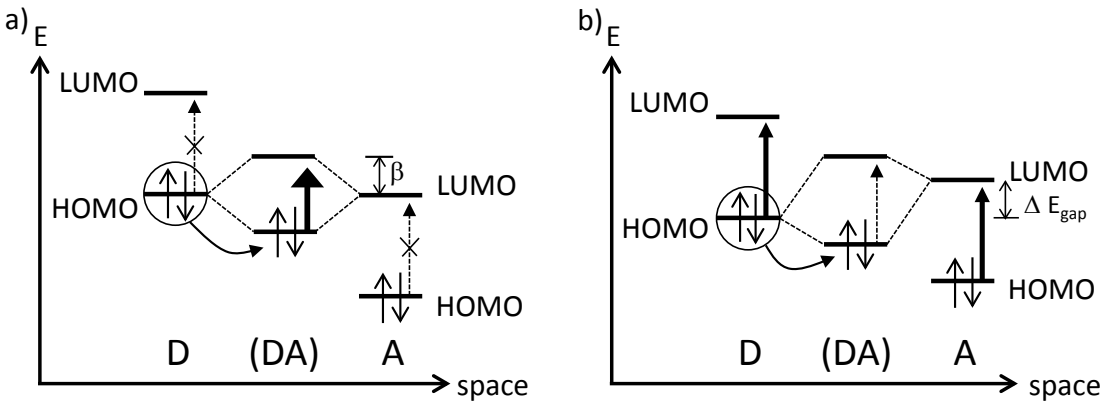

Figure 7: Schematic illustration of the effect of increasing the energy gap ΔE_{gap} between the donor HOMO and acceptor LUMO on the hybridization and thus on the intensity of the transitions.

This picture is supported by the experimental data. From table 1, the correlation between ΔE_{gap} and the bleaching of the absorption is evident. Within the PPP series, ΔE_{gap} reduces with the S_1 energy of the polymer due to the concomitant destabilization of the polymer HOMO, so that the amount of ground state bleach also concurs with the of S_1 energy and, implicitly, the effective conjugation length. The reduced extinction of

the donor interacting with the acceptor was also observed in the TDDFT calculations, reproducing the experimental data qualitatively. Quantitatively, the amount for ground state bleach found in the calculation for the MEH-PV trimer/TNF system, i.e. 18 %, is low compared to the value of 34 % measured experimentally for the bilayer formed with MEH-PPV and TNF. We consider that a number of factors contribute to this difference. Most importantly, the calculations have been carried out for a MEH-PV trimer. In the MEH-PPV polymer, however, the effective conjugation length for the ground state geometry has been found in the range of 6 repeat units for the disordered phase, and about twice as long for the planar phase. This larger effective conjugation length with concomitant lower ΔE_{gap} implies a stronger ground state bleach. Multiple interactions, such as clustering of GS complexes proposed by Parashchuk and coworkers, [22] subsequent planarization of the donor after complex formation, the complex formation of one TNF molecule with two or more MEH-PPV chromophores as proposed by Bruevich et al,[23-24] or alternatively, of one donor chromophore with several acceptor molecules[25], are not taken into account. While more extensive computations would be required for a detailed quantitative analysis, the simple initial model calculations employed here are sufficient to qualitatively account for the key features observed experimentally, i.e. the appearance of missing ground state absorption.

The interpretation of the data in the picture of an interfacial ground state complex can also elucidate why the amount of missing ground state absorption concurs with the ease of exciton dissociation, as evident in table 1. Consider an initial arrangement of chromophores in the order donor, donor, acceptor, acceptor, that results in a three-component system of donor, complex, acceptor. As illustrated in figure 8, light absorption by either donor, acceptor or complex, followed by exothermic electron transfer will eventually result in a configuration with an electron missing from the donor and being added to the acceptor, with the two opposite, coulomb-bound charges being separated by the complex. The energy levels of the complex form a barrier to geminate recombination in a way, similar to a small insulating tunnelling barrier[26-27] or a cascading energy level trilayer system[28], thus enhancing the probability for the charges to escape from their mutual coulomb potential. The height of the barrier to recombination scales with reducing ΔE_{gap}, and thus with the amount of missing absorption. In earlier work,[20-21] we have observed that the saturation field strength for complete exciton dissociation, F_{sat}, decreases with increasing conjugation within the PPP series. On the basis of numerical modelling, this was attributed to an increase in kinetic energy of the hole, parameterized through an effective mass, and to the formation of an interfacial electrostatic potential that assists the dissociation process. It is gratifying that the formation of a GS complex proposed here is consistent with the notion of a repulsive interfacial electrostatic potential preventing geminate recombination.

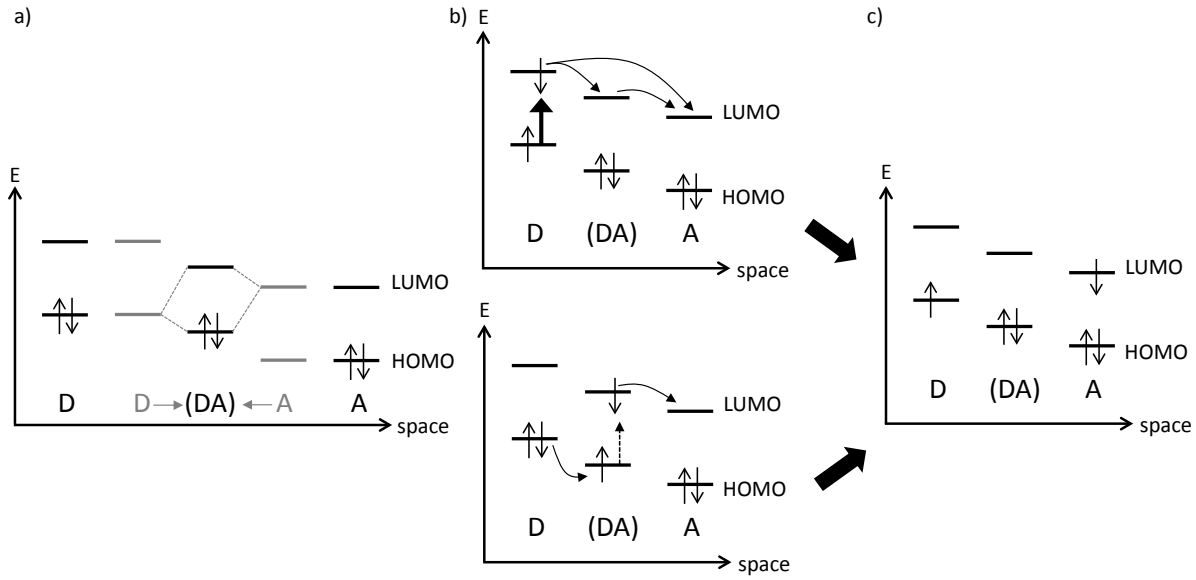

Figure 8: Schematic illustration of the effect of interfacial hybridization on the interfacial energies. (a) formation of a ground state complex at the interface (b) excitation of the donor or the complex (DA) and subsequent electron transfer (c) the resulting interfacial geminate pair, spatially separated by the complex (DA).

The observation that a ground state complex may form in donor-acceptor system is well established in the field. The pioneering work of the researchers around Dimitry Paraschuk and Olga Paraschuk on the MEH-PPV/TNF system ascertained the formation of a GS complex by Raman spectroscoy. [24, 29] Using crystallography and modelling, they showed that upon complex formation the MEH-PPV chromophore planarizes and becomes more ordered. GS complexes have further been demonstrated by the observation of weak sub-gap absorption using photothermal deflection spectroscopy (PDS), for example for the PPV-derivative MDMO-PPV, the thiophene-derivative P3HT or the copolymer TFMO (poly[9,9-dioctylfluorene-*co*-N-(4-methoxyphenyl)diphenylamine] with the fullerene PCBM. [11, 14, 30] While it is well possible to detect the weak low-energy absorption of the GS complexes, PDS is a sophisticated technique that is not routinely available for material screening. Our approach of investigating the existence of a GS complex by focussing on the reduction of the donor and acceptor absorption in a bilayer, in contrast, requires merely a commercial ultraviolet-visible spectrometer, which is a common resource in many laboratories. Due to the observed connection between the amount of ground state bleach and ease of exciton dissociation, this approach may lend itself to screen material combinations for their potential in solar cell applications.

Experimental and theoretical methods

MEH-PPV and C_{60} (99.9% purity) were bought from American Dye Source Inc, polystyrene from Sigma Aldrich. MeLPPP, PIF and DOOPPP were synthesized by the group of U. Scherf as described elsewhere.[31-33] The precursor PPV was synthesized in Bayreuth using the method described in [34]. The PPV-precursor was converted to PPV by heating for one hour at 165°C. TNF was also synthesized in Bayreuth following the method of Woofolk and Orchin.[35] The PDI derivative was synthesized by the group of K. Müllen as described as compound PDI-2 in Ref. [36].

The samples have been prepared by covering a quadratic fused silica substrate with an about 40 nm polymer donor layer by spin coating from solutions in chlorobenzene at concentrations of 4-10 $mgml^{-1}$ and at an angular speed of 1000-4000 rpm. The polymer layer is then conscientiously removed from half of the substrate with a cotton bud previously dipped into the solvent. In configuration I, a stripe of acceptor layer is then thermally evaporated through a shadow mask orthogonal onto the polymer layer. In configuration II, the acceptor layer is evaporated in the same geometry yet the substrate is turned over prior to the evaporation, so that polymer and acceptor are separated by the fused silica layer. This results in three different areas: a polymer-only layer, an acceptor-only layer and an area with a superposition of the donor and the acceptor layer. The absorption was recorded using a Cary 5000 (Varian) ultraviolet-visibile (UV-vis)spectrometer. The film thicknesses were measured by a Dektak profilometer.

For the DFT and TDDFT calculations, a MEH-PV-trimer was used as model system for the MEH-PPV polymer. The geometry of the MEH-PV trimer and the TNF were first optimized separately using the PBE0 hybrid exchange-correlation functional[37] and the turbomole program suite.[38] Then the geometry of both molecules together was optimized with PBE0 starting from different initial spatial separations and relative orientations of the two molecules. Different relaxations lead to very similar end geometries. As expected for molecules with conjugated π-systems, the configuration in which the two molecular planes are parallel to each other is consistently found as the ground state, lowest energy configuration. The thus obtained gas-phase configuration cannot be expected to be identical to the molecular situation in layered films, but it serves as a reasonable starting point for the exploratory calculations that we aim at in this work.

The ground state configurations of each individual molecule and the combined D-A system served as input to linear-response TDDFT calculations with the exchange-correlation functional PBE0. The spectra are produced within the range of 0 to approximately 4 eV ranging from the lowest to the highest excitation. The lowest 20 excitations were calculated for the donor MEHPPV and the lowest 10 for the acceptor TNF, as these numbers of excited states are sufficient to cover the spectral range of interest. The 30 lowest excitations were determined for the D-A-system. These 30 excitations cover the

spectral range of interest, i.e. up to approximately 3.5 eV. In order to ensure that the optically active excitation in the DA system is not underestimated due to TDDFT's well know charge transfer problem [39] we repeated the TDDFT calculation for the donor-acceptor system with a hybrid functional with an increased amount of exact exchange. This influenced several of the optically dark, low lying excitations noticeably, but changed the energy of the optically active excitation only very little. This finding is in line with the observation that this excitation has only a weak charge-transfer character. Both ground- and excited state calculations used the TZVP basis set. For ease of comparison calculated excitation peaks in the TDDFT spectra were broadened via a Gaussian function with width chosen such that it roughly matches the experimental width.

Acknowledgements

We acknowledge the Graduate School GRK 1640 of the Deutsche Forschungsgemeinschaft (DFG) for financial support. We thank I. Bauer for the synthesis of TNF and J. Gmeiner for the PPV. Furthermore, we thank the group of U. Scherf for synthesizing ladder type polymers and the group of K. Müllen for the PDI derivative. We are grateful to C. Grill and E. Riedle for fruitful discussions. Supporting Information is available online from Wiley InterScience or from the author.

References

1. Heliatek http://www.heliatek.com/wp-content/uploads/2013/01/130116_pr_heliatek_achieves_record_cell_effiency_for_opv.pdf.
2. Brédas, J. L.; Norton, J. E.; Cornil, J.; Coropceanu, V., Molecular Understanding of Organic Solar Cells: The Challenges. *Acc. Chem. Res.* **2009,** *42*, 1691-1699.
3. Deibel, C.; Dyakonov, V., Polymer-Fullerene Bulk Heterojunction Solar Cells. *Rep. Prog. Phys.* **2010,** *73*, 096401.
4. Deibel, C.; Strobel, T.; Dyakonov, V., Role of the Charge Transfer State in Organic Donor-Acceptor Solar Cells. *Adv. Mater.* **2010,** *22*, 4097-4111.
5. Vandewal, K.; Albrecht, S.; Hoke, E. T.; Graham, K. R.; Widmer, J.; Douglas, J. D.; Schubert, M.; Mateker, W. R.; Bloking, J. T.; Burkhard, G. F.; Sellinger, A.; Fréchet, J. M. J.; Amassian, A.; Riede, M. K.; McGehee, M. D.; Neher, D.; Salleo, A., Efficient Charge Generation by Relaxed Charge-Transfer States at Organic Interfaces. *Nat. Mater.* **2013,** *advance online publication*.
6. Veldman, D.; Ipek, O.; Meskers, S. C. J.; Sweelssen, J.; Koetse, M. M.; Veenstra, S. C.; Kroon, J. M.; van Bavel, S. S.; Loos, J.; Janssen, R. A. J., Compositional and Electric Field Dependence of the Dissociation of Charge Transfer Excitons in Alternating Polyfluorene Copolymer/Fullerene Blends. *J. Am. Chem. Soc.* **2008,** *130*, 7721-7735.
7. Huang, Y. S.; Westenhoff, S.; Avilov, I.; Sreearunothai, P.; Hodgkiss, J. M.; Deleener, C.; Friend, R. H.; Beljonne, D., Electronic Structures of Interfacial States Formed at Polymeric Semiconductor Heterojunctions. *Nat. Mater.* **2008,** *7*, 483-489.
8. Morteani, A. C.; Sreearunothai, P.; Herz, L. M.; Friend, R. H.; Silva, C., Exciton Regeneration at Polymeric Semiconductor Heterojunctions. *Phys. Rev. Lett.* **2004,** *92*.
9. Aryanpour, K.; Psiachos, D.; Mazumdar, S., Theory of Interfacial Charge-Transfer Complex Photophysics in π-Conjugated Polymer-Fullerene Blends. *Phys. Rev. B* **2010,** *81*.
10. Marchiori, C. F. N.; Koehler, M., Dipole Assisted Exciton Dissociation at Conjugated Polymer/Fullerene Photovoltaic Interfaces: A Molecular Study Using Density Functional Theory Calculations. *Synth. Met.* **2010,** *160*, 643-650.
11. Benson-Smith, J. J.; Goris, L.; Vandewal, K.; Haenen, K.; Manca, J. V.; Vanderzande, D.; Bradley, D. D. C.; Nelson, J., Formation of a Ground-State Charge-Transfer Complex in Polyfluorene/[6,6]-Phenyl-C-61 Butyric Acid Methyl Ester (PCBM) Blend Films and Its Role in the Function of Polymer/PCBM Solar Cells. *Adv. Funct. Mater.* **2007,** *17*, 451-457.
12. Drori, T.; Holt, J.; Vardeny, Z. V., Optical Studies of the Charge Transfer Complex in Polythiophene/Fullerene Blends for Organic Photovoltaic Applications. *Phys. Rev. B* **2010,** *82*.
13. Drori, T.; Sheng, C. X.; Ndobe, A.; Singh, S.; Holt, J.; Vardeny, Z. V., Below-Gap Excitation of Pi-Conjugated Polymer-Fullerene Blends: Implications for Bulk Organic Heterojunction Solar Cells. *Phys. Rev. Lett.* **2008,** *101*.
14. Goris, L.; Haenen, K.; Nesladek, M.; Wagner, P.; Vanderzande, D.; De Schepper, L.; D'Haen, J.; Lutsen, L.; Manca, J. V., Absorption Phenomena in Organic Thin Films for Solar Cell Applications Investigated by Photothermal Deflection Spectroscopy. *J. Mater. Sci.* **2005,** *40*, 1413-1418.
15. Pingel, P.; Neher, D., Comprehensive Picture of P-Type Doping of P3ht with the Molecular Acceptor F(4)TCNQ. *Phys. Rev. B* **2013,** *87*.

16. Méndez, H.; Heimel, G.; Opitz, A.; Sauer, K.; Barkowski, P.; Oehzelt, M.; Soeda, J.; Okamoto, T.; Takeya, J.; Arlin, J. B.; Balandier, J. Y.; Geerts, Y.; Koch, N.; Salzmann, I., Doping of Organic Semiconductors: Impact of Dopant Strength and Electronic Coupling. *Angew. Chem. Int. Ed.* **2013,** *52*, 7751-7755.
17. Salzmann, I.; Heimel, G.; Duhm, S.; Oehzelt, M.; Pingel, P.; George, B. M.; Schnegg, A.; Lips, K.; Blum, R. P.; Vollmer, A.; Koch, N., Intermolecular Hybridization Governs Molecular Electrical Doping. *Phys. Rev. Lett.* **2012,** *108*.
18. Halls, J. J. M.; Pichler, K.; Friend, R. H.; Moratti, S. C.; Holmes, A. B., Exciton Diffusion and Dissociation in a Poly(*p*-Phenylenevinylene)/C_{60} Heterojunction Photovoltaic Cell. *Appl. Phys. Lett.* **1996,** *68*, 3120-3122.
19. Markov, D. E.; Amsterdam, E.; Blom, P. W. M.; Sieval, A. B.; Hummelen, J. C., Accurate Measurement of the Exciton Diffusion Length in a Conjugated Polymer Using a Heterostructure with a Side-Chain Cross-Linked Fullerene Layer. *J. Phys. Chem. A* **2005,** *109*, 5266-5274.
20. Schwarz, C.; Bässler, H.; Bauer, I.; Koenen, J. M.; Preis, E.; Scherf, U.; Köhler, A., Does Conjugation Help Exciton Dissociation? A Study on Poly(*p*-Phenylene)s in Planar Heterojunctions with C_{60} or TNF. *Adv. Mater.* **2012,** *24*, 922-925.
21. Schwarz, C.; Tscheuschner, S.; Frisch, J.; Winkler, S.; Koch, N.; Bässler, H.; Köhler, A., Role of the Effective Mass and Interfacial Dipoles on Exciton Dissociation in Organic Donor-Acceptor Solar Cells. *Phys. Rev. B* **2013,** *87*.
22. Parashchuk, O. D.; Bruevich, V. V.; Paraschuk, D. Y., Association Function of Conjugated Polymer Charge-Transfer Complex. *Phys. Chem. Chem. Phys.* **2010,** *12*, 6021-6026.
23. Bruevich, V. V.; Makhmutov, T. S.; Elizarov, S. G.; Nechvolodova, E. M.; Paraschuk, D. Y., Raman Spectroscopy of Intermolecular Charge Transfer Complex between a Conjugated Polymer and an Organic Acceptor Molecule. *J. Chem. Phys.* **2007,** *127*.
24. Parashchuk, O. D.; Grigorian, S.; Levin, E. E.; Bruevich, V. V.; Bukunov, K.; Golovnin, I. V.; Dittrich, T.; Dembo, K. A.; Volkov, V. V.; Paraschuk, D. Y., Acceptor-Enhanced Local Order in Conjugated Polymer Films. *J. Phys. Chem. Lett.* **2013,** *4*, 1298-1303.
25. Parashchuk, O. D.; Sosorev, A. Y.; Bruevich, V. V.; Paraschuk, D. Y., Threshold Formation of an Intermolecular Charge Transfer Complex of a Semiconducting Polymer. *JETP Lett.* **2010,** *91*, 351-356.
26. Campbell, I. H.; Crone, B. K., Improving an Organic Photodiode by Incorporating a Tunnel Barrier between the Donor and Acceptor Layers. *Appl. Phys. Lett.* **2012,** *101*.
27. Liu, F. L.; Crone, B. K.; Ruden, P. P.; Smith, D. L., Control of Interface Microscopic Processes in Organic Bilayer Structures and Their Effect on Photovoltaic Device Performance. *J. Appl. Phys.* **2013,** *113*.
28. Tan, Z. K.; Johnson, K.; Vaynzof, Y.; Bakulin, A. A.; Chua, L. L.; Ho, P. K. H.; Friend, R. H., Suppressing Recombination in Polymer Photovoltaic Devices Via Energy-Level Cascades. *Adv. Mater.* **2013,** *25*, 4131-4138.
29. Paraschuk, D. Y.; Elizarov, S. G.; Khodarev, A. N.; Shchegolikhin, A. N.; Arnautov, S. A.; Nechvolodova, E. M., Weak Intermolecular Charge Transfer in the Ground State of a Pi-Conjugated Polymer Chain. *JETP Lett.* **2005,** *81*, 467-470.

30. Goris, L.; Poruba, A.; Hod'akova, L.; Vanecek, M.; Haenen, K.; Nesladek, M.; Wagner, P.; Vanderzande, D.; De Schepper, L.; Manca, J. V., Observation of the Subgap Optical Absorption in Polymer-Fullerene Blend Solar Cells. *Appl. Phys. Lett.* **2006,** *88*.
31. Huang, S. P.; Huang, G. S.; Chen, S. A., Deep Blue Electroluminescent Phenylene-Based Polymers. *Synth. Met.* **2007,** *157*, 863-871.
32. Scherf, U.; Müllen, K., Polyarylenes and Poly(Arylenevinylenes), 7. A Soluble Ladder Polymer Via Bridging of Functionalized Poly(Para-Phenylene)-Precursors. *Makromol. Chem.-Rapid Commun.* **1991,** *12*, 489-497.
33. Setayesh, S.; Marsitzky, D.; Müllen, K., Bridging the Gap between Polyfluorene and Ladder-Poly-*p*-Phenylene: Synthesis and Characterization of Poly-2,8-Indenofluorene. *Macromolecules* **2000,** *33*, 2016-2020.
34. Herold, M.; Gmeiner, J.; Schwoerer, M., Preparation of Light-Emitting-Diodes on Flexible Substrates - Elimination-Reaction of Poly(*p*-phenylene vinylene) at Moderate Temperatures. *Acta Polym.* **1994,** *45*, 392-395.
35. Woolfolk, E. O.; Orchin, M., 2,4,7-Trinitrofluorenone - Fluorenone, 2,4,7-Trinitro. *Org. Synt.* **1948,** *28*, 91-93.
36. Kamm, V.; Battagliarin, G.; Howard, I. A.; Pisula, W.; Mavrinskiy, A.; Li, C.; Müllen, K.; Laquai, F., Polythiophene:Perylene Diimide Solar Cells - the Impact of Alkyl-Substitution on the Photovoltaic Performance. *Adv. Energy. Mater.* **2011,** *1*, 297-302.
37. Adamo, C.; Barone, V., Toward Reliable Density Functional Methods without Adjustable Parameters: The PBE0 Model. *J. Chem. Phys.* **1999,** *110*, 6158-6170.
38. Ahlrichs, R.; Bär, M.; Häser, M.; Horn, H.; Kölmel, C., Electronic-Structure Calculations on Workstation Computers - The Program System Turbomole. *Chem. Phys. Lett.* **1989,** *162*, 165-169.
39. Kümmel, S.; Kronik, L., Orbital-Dependent Density Functionals: Theory and Applications. *Rev. Mod. Phys.* **2008,** *80*, 3-60.
40. Holt, A. L.; Leger, J. M.; Carter, S. A., Electrochemical and Optical Characterization of p- and n-Doped Poly[2-methoxy-5-(2-ethylhexyloxy)-1,4-phenylenevinylene]. *J. Chem. Phys.* **2005,** *123*.
41. West, D. P.; Rahn, M. D.; Im, C.; Bässler, H., Hole Transport through Chromophores in a Photorefractive Polymer Composite Based on Poly(N-Vinylcarbazole). *Chem. Phys. Lett.* **2000,** *326*, 407-412.
42. Milan, F., Theoretical Investigation of a MolecularDonor-Acceptor System, Bachelor thesis, **2013**, University of Bayreuth

Supporting Information to:

Ground state bleaching at donor-acceptor interfaces

Christian Schwarz, Felix Milan, Stephan Kümmel, Anna Köhler[#]

C. Schwarz, A. Köhler
Experimental Physics II and Bayreuth Institute of Macromolecular Research (BIMF)
University of Bayreuth
95440 Bayreuth, Germany
[#] E-mail: anna.koehler@uni-bayreuth.de

F. Milan, S. Kümmel
Theoretical Physics IV
University of Bayreuth
95440 Bayreuth, Germany

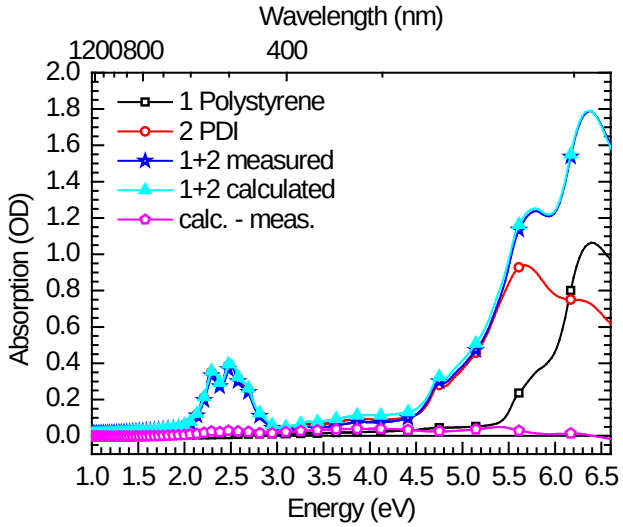

Figure S1: Absorption spectra of a single polystyrene layer (40 nm) and an evaporated PDI derivative (56 nm), as well as the bilayer of both, measured in the geometry of Figure 1 Configuration I, as presented in the main article. The mathematical superposition of the single layers is within vanishing small deviations of maximum 1.7% similar to the absorption of the bilayer.

	HOMO	LUMO	LUMO+4
MEH-PV	-5.0	-2.0	
TNF	-8.5	-4.2	
MEH-PV + TNF	-5.2	-3.8	-2.3

Table S1: The HOMO and LUMO energies calculated for the MEH-PV trimer, the TNF and the sandwich dimer comprising both. For the latter, the LUMO+4 energy is also given.

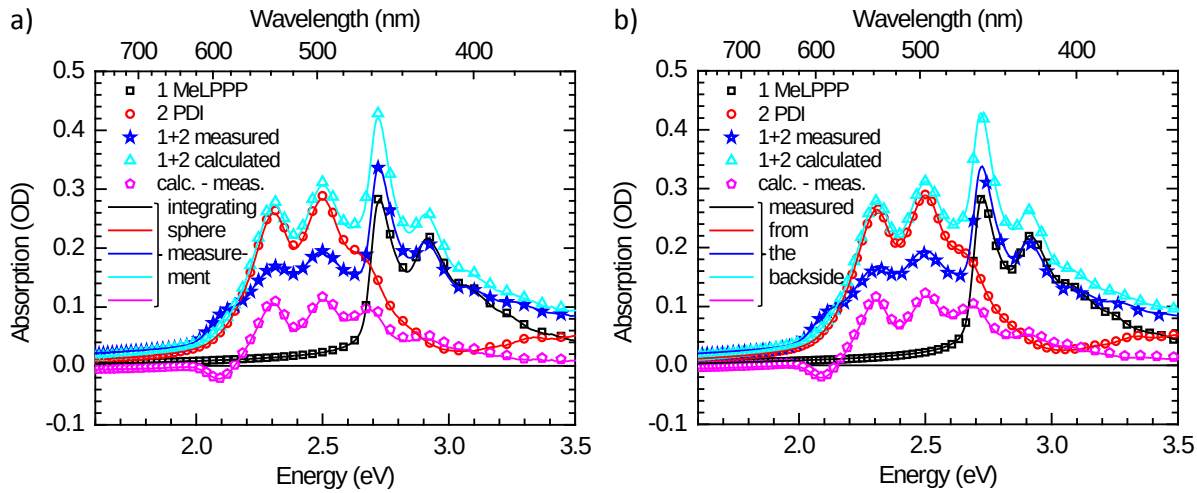

Figure S2: Absorption spectra (small symbols) of a single MeLPPP layer (41 nm) and an evaporated PDI derivative (42 nm), as well as the bilayer of both, measured in the geometry of Figure 1 Configuration I, as presented in the main article . a) The lines indicate the absorption of the similar films measured in an integrating sphere to check for the effects of scattering and reflection. b) The lines indicate the absorption the similar films when the samples are measured from the backside of the substrate to check whether the spectra are independent on the direction of the light path.

In both auxiliary experiments we found no significant changes, thus excluding optical and scattering effects.

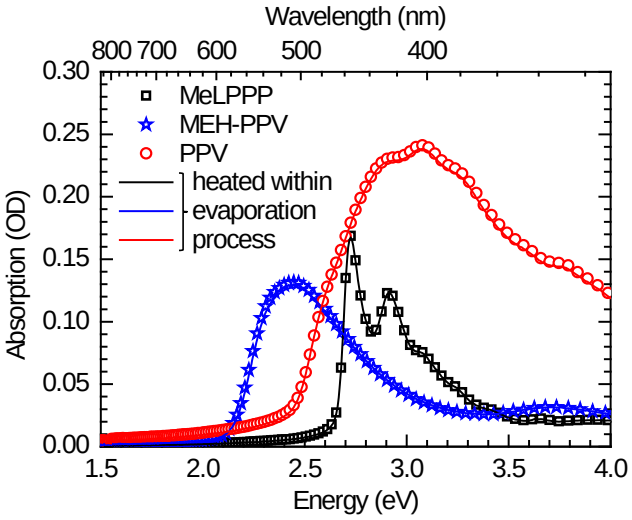

Figure S3: Absorption spectra of thin films of MeLPPP, MEH-PPV and PPV in the pristine form (small symbols) and after the heat treatment of the thermal radiation within an evaporation process (lines).

We found the polymer absorption to be unaltered by this process.

Danksagung

Annähernd drei Jahre sind nun bis zum Abschluss der Doktorarbeit vergangen. Damit ist es nun an der Zeit, mich bei denjenigen zu bedanken, die mich in dieser spannenden Phase meiner akademischen Laufbahn begleitet haben.

Vielen Dank an Prof. Anna Köhler für die Betreuung der Doktorarbeit, meine durchgehende Finanzierung und den Gestaltungsfreiraum, den ich, zum einen die Arbeit selbst betreffend hatte und der mir zum anderen bei der Betreuungsarbeit der Studenten individuelle Anpassungen ermöglichte.

Vielen Dank auch an Prof. Heinz Bässler, der für physikalische Probleme immer ein offenes Ohr hatte und sich, besonders bei der theoretischen Modellbildung, sehr engagierte.

Vielen Dank an Prof. Mukundan Thelakkat und Prof. Peter Strohriegl, die mir bei meiner Mitgliedschaft im GRK 1640 als Mentoren beratend zur Seite standen.

Ein ganz spezieller Dank geht an meine Studenten, die ich während ihrer Teamprojekt-, Bachelor-, Master- oder Diplomarbeiten unterstützt habe. Mir hat die Zusammenarbeit mit Euch immer gefallen und ich habe während dieser Zeit viele Sachen gelernt. Vielen Dank an Markus Reichenberger, Steffen Tscheuschner, Johannes Büttner, Tobias Hahn, Julian Kahle, Johannes Geiger, Jakob Gleissl, Eray Ulcay und Alexander Moser. Durch Euch ist der Lehrstuhl gewachsen und ich wünsche Euch viel Erfolg und Glück bei Euren weiteren Arbeiten! Nicht aufgeben, wenn mal Schwierigkeiten auftreten!

Vielen Dank an unsere Techniker. An meinen Freund Jürgen Gmeiner, der trotz Ruhestand bei „kleinen Problemen“ stets erreichbar war und immer weitergeholfen hat. Vielen Dank an Frank Schirmer. Dein Einsatz war und ist ausgezeichnet und ich hoffe, dass Du dem Lehrstuhl noch lange erhalten bleibst. Vielen Dank auch an Irene Bauer für die synthetisierten Materialien und die Mithilfe im Labor.

Ich danke allen Kollegen des GRK 1640 für die gute Zusammenarbeit und dem GRK 1640 selbst für die finanzielle Unterstützung während der vergangen drei Jahre.

Vielen Dank auch an meine Projektpartner, die mit mir zusammengearbeitet haben oder mich durch Materialsendungen unterstützt haben.

Vielen Dank an meine weiteren Kollegen am Lehrstuhl für die Zusammenarbeit und die schöne Zeit.

Abschließend noch ein großer Dank an meine Familie für die Unterstützung seit Beginn der Studienzeit. Hierbei geht ein spezieller Dank an meinen Vater, mit dem ich täglich zur Uni und wieder nach Hause fahren konnte, was mir erlaubte, über viele Fragestellungen nachzudenken und mit ihm darüber zu diskutieren. Vielen Dank an meine Mutter, die sich um alle nicht-physikalischen Probleme gekümmert hat. Vielen Dank auch an meine Freundin, die mich in hektischen Zeiten verstanden hat und bei der ich mich sehr wohl fühle.

Erklärung

Hiermit erkläre ich, dass ich die vorliegende Arbeit selbstständig verfasst und keine anderen, als die von mir angegebenen Quellen und Hilfsmittel verwendet habe.

Ferner erkläre ich, dass ich weder anderweitig mit oder ohne Erfolg versucht habe, diese Dissertation einzureichen, noch eine gleichartige Doktorprüfung an einer anderen Hochschule endgültig nicht bestanden habe.

Berndorf, den

Christian Schwarz